Studies towards understanding the biological roles of TH2BS11ph histone mark and H1t linker histone variant in mammalian spermatogenesis

A Thesis Submitted for the Degree of

Doctor of Philosophy

By

Iyer Aditya Mahadevan

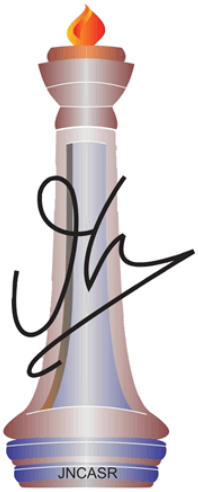

Molecular Biology and Genetics Unit

Jawaharlal Nehru Centre for Advanced Scientific Research

(*A Deemed University*)

Bangalore, India.

February 2020

DECLARATION

I hereby declare that the matter embodied in the thesis titled "**Studies towards understanding the biological roles of TH2BS11ph histone mark and H1t linker histone variant in mammalian spermatogenesis**" is an authentic record of research work carried out by me under the guidance of **Prof. M.R.S Rao** at Chromatin Biology Laboratory, Molecular Biology and Genetics Unit (MBGU), Jawaharlal Nehru Centre for Advanced Scientific Research (JNCASR), Bangalore, India and that it has not been submitted elsewhere for the award of any degree or diploma.

In keeping with the norm of reporting scientific observations, due acknowledgement has been made whenever work described here has been based on findings of other investigators. Any omission due to oversight or misjudgement is regretted.

_____

Iyer Aditya Mahadevan

Bangalore, India

Date:

CERTIFICATE

I hereby certify that the matter embodied in the thesis titled "**Studies towards understanding the role of TH2BS11ph histone mark and H1t linker histone variant in mammalian spermatogenesis**" has been carried out by **Iyer Aditya Mahadevan** under my supervision at Chromatin Biology Laboratory, Molecular Biology and Genetics Unit, Jawaharlal Nehru Centre for Advanced Scientific Research, Bangalore, India and that it has not been submitted elsewhere for any degree or diploma to any other institution.

Prof. M.R.S Rao

Bangalore, India

Date:

ACKNOWLEDGMENTS

At the outset, I would like to thank Prof. M.R.S Rao for this providing me with an opportunity to work on testicular histone variants under his guidance. I gained a lot from his knowledge, constant support, and encouragement during my Ph.D. He has always inspired me to try something new and novel, which has also taught me how to brave all odds and become independent in my scientific journey. I have gained a lot, both personally and professionally, under his tutelage.

I want to thank all the MBGU and NSU faculty members for the coursework and constructive criticism during the work presentations. A special thanks to Prof. Kaustuv Sanyal and Prof. Ganesh Nagaraju for their inputs during my comprehensive examination. I would also like to acknowledge Prof. Anuranjan Anand, Prof. Udaykumar Ranga, Prof. Namita Surolia, Prof. Hemalatha Balaram, Prof. Tapas Kundu, Prof. Maneesha Inamdar, Prof. Sheeba Vasu, Dr. Ravi Manjithaya, Dr. James Chelliah, and Dr. Kushagra Bansal their help and guidance during my doctoral studies. This work would have been incomplete without the support of the scientific facilities of JNCASR. I want to thank Dr. Prakash of the Animal facility, Suma and Sunil of the Confocal facility, and Ross of Taplin for their help with the generation of data.

I would to specially thank the lab members Zenia, Bhavana, Anjhana, Anusha, Dr. Shalini, Dr. Sangeeta, Sunita, Veena, and Muniraju for their unconditional support and keeping the lively atmosphere in the lab. I want to thank the co-authors of my publications Dr. Satyakrishna, Raktim Roy, Utsa, Sanjeev for their immense help during my Ph.D. I would also like to acknowledge past lab members Dr. Vijay (and Ajay), Shrinivas, Neha, Dr. Deboshree, Dr. Laxmi Narayan Mishra, Dr. Nikhil, Dr. Sai Nitin, Dr. Arun, and others for the excellent training and support that helped the initial years of my Ph.D.

I would like to thank my friends at JNCASR Manjeet, Raaghesh, Shivram, Achal, Gaurav, Pavan, Anand, Rafi, Praveen, Rajaji, Shivram, Asutosh, Anshul, Pramoda, Lakshmeesha, Arnab, Vishwa, Anshul, Greg, Vijay, Sreedevi, Veena, Aditya, Ranbhir for standing by my side, for being supportive and caring throughout my Ph.D. Without the support of my batchmates KD, Suchismita, Rima, Praveen, and Aparna, the stay at JNCASR would have been challenging to say the least. I would like to thank members

of my so-called second lab Vascular Biology Lab Rohan, Ronak, Divyesh, Diana, Payel, Saloni, Arindham, Preeti, Aksa, Rajarshi, Kaustubh, Deeti, for always being part of my Ph.D, for always extending a helping hand and for creating a pleasant atmosphere at MBGU.

Special thanks to my MSU batchmates (Khattarnaak 20), seniors and juniors, especially Dr. Hashim, Madhulika, Prashish, Terence, Abhijit, Ashok, Nitin, Renu, Yash, Phani, Praveen, Dhanashree, Abhik Paul and others for pleasant company and get-togethers in Bangalore. A special thanks to Nitin, Dr. Sai Nitin and Aparna, for organizing and managing the Bavarian state tour. I want to thank various facilities like JNC Sports Facilities, Security, Mess, Admin, Accounts, Chandraya, Dhavantari, Hostel, & others for creating a setup for a comfortable stay at JNCASR. I would like to immensely thank Department of Biotechnology (DBT), JNCASR and DBT-travel grant for extending the financial support during the various stages of my Ph.D.

Finally, a special thanks to my Dad, Mom, Anand, and Nitya for their unconditional love and support during my Ph.D. Despite missing various family functions, their guidance also made me stay focussed during my graduate study. This thesis would have been nowhere without their blessings. A special thanks to my uncles Vasan and Naresh, who have also lent support and motivation for my academic career.

Abbreviations

ac: Acetylation

ATM: Ataxia-telangiectasia-mutated

ATR: Ataxia-telangiectasia and Rad3-related

Bp: Base pair

Brdt: Bromodomain, Testis-specific

Cbx1: Chromobox protein homolog 1

cDNA: complimentary DNA

ChIP: Chromatin immunoprecipitation

DAPI: 4', 6- Diamidino-2-phenylindole

DDR: DNA damage response

DNA: Deoxyribonucleic acid

DNaseI: Deoxyribonuclease I

DTT: Diothiothreitol

E. coli: *Escherischia coli*

EDTA: Ethylenediaminetetraacetate

ES: Embryonic stem

HAT: Histone acetylatransferase

HDAC: Histone deacetylase

HORMAD1: HORMA (Hop1, Rev7 and Mad2)-domain containing protein 1

HRP: Horse radish peroxidise

kb: Kilobase

kDa: Kilodalton

mESC: Mouse embryonic stem cell

mRNA: Messenger RNA

Mre11: Meiotic recombination 11

mM: millimolar

MNase: Micrococcal nuclease

M.W.: Molecular weight

nm: Nanometer

O.D: Optical Density

PBS: Phosphate buffer saline

PCR: Polymerase chain reaction

ph: Phosphorylation

PMSF: Phenyl methyl sulfonyl fluoride

PRDM9: PR domain-containing 9

PTM: Post-translational modification

RNA: Ribonucleic acid

RNA pol II: RNA polymerase II

RNase- Ribonuclease

RT-PCR: Reverse transcriptase polymerase chain reaction

SDS-PAGE: Sodium Dodecyl Sulphate- polyacrylamide gel electrophoresis

Smarca5: SWI/SNF Related, Matrix Associated, Actin Dependent Regulator of Chromatin, Subfamily A, Member 5

Scml2: Sex comb on midleg- like protein 2

TCA: Trichloroacetic acid

TF: Transcription factor

TSS: Transcription start site

Tris: Tris(hydroxymethyl)aminoethane

UV: Ultraviolet

µg: Microgram

µl: Microlitre

List of Figures

List of Tables

Table of Contents

Chapter 1

Introduction

1.1 Structure of Chromatin

Almost all eukaryotes package DNA in the form of nucleosomes. A high-resolution X-ray crystal structure of the nucleosome core particle was first solved in 1997 (Luger et al., 1997). Each nucleosome core particle comprises of approximately 147 bp of double-stranded DNA wrapped around a histone octamer, composed of a single tetramer $(H3\text{-}H4)_2$ and two (H2A-H2B) dimers (Kornberg, 1974). The basic structure of histones that contains the histone fold domain (HFD) and N-terminal tail is highly conserved across eukaryotic species. Each HFD contains three alpha-helices (α1, α2, and α3) separated by two loops (L1 and L2). Each of HFDs is associated in an anti-parallel fashion- H3 with H4 and H2A with H2B. On the other hand, the N-terminal tails of H2B and H3 pass through the gyres of the DNA helix. The N-terminal tails of histones are disordered and are subject to many post-translational modifications (PTMs), which is essential for various chromatin-templated events.

A groundbreaking study had shown that chromatin is organized into 30nm wide filaments (Finch and Klug, 1976). Electron microscopy and X-ray crystallographic studies provide *in vitro* evidence for the occurrence of two forms of 30nm *in vitro*, referred as solenoidal and zig-zag models (Robinson et al., 2006; Schalch et al., 2005; Song et al., 2014). However, there has been a growing debate on the existence and formation of 30nm fibers *in vivo*. It is only clear that chromatin indeed exists as a 10nm fiber state (beads on a string structure) (Bian and Belmont, 2012; Eltsov et al., 2008; Fussner et al., 2011; Joti et al., 2012).

Each nucleosome is connected to adjacent nucleosomes by a stretch of linker DNA, the length of which differs between cell types and organisms. Linker histone H1 binds to this DNA and promotes higher-order chromatin organization. The chromatosome is a higher-order structure, consisting of about 166 bp DNA wrapped around the histone octamer with histone H1 (Bharath et al., 2003; Simpson, 1978). H1s contain the N-terminal domain, conserved trypsin-resistant globular domain, and C-terminal domain (Bradbury et al., 1975; Hartman et al., 1977). The N and C-terminal domains of H1 are divergent and mostly unstructured in solution (Aviles et al., 1979; Rattle et al., 1977; Roque et al., 2016). Its globular domain is the nucleosome binding domain that protects a 20-bp of nucleosomal DNA, just like the full-length H1. This protection is due to the direct interaction between the globular domain and the entry-exit sites of the nucleosomal DNA. On the other hand, the C-terminal domain of H1 is the primary determinant of DNA binding in cells (Hendzel et al.,

2004). Further, the DNA-nucleosome polymers fold progressively to form higher-order chromatin structures like 120 nm chromonema, 300-700 nm chromatid ultimately, giving rise to condensed mitotic chromosomes (Figure 1.1, left panel)(Belmont et al., 1987; Dehghani et al., 2005; Kireeva et al., 2004; Rattner and Lin, 1985; Sedat and Manuelidis, 1978). Rather than chromatin being a homogenous entity, it is segregated into functionally important chromatin domains that regulate the transcriptional activity of the associated DNA (Li et al., 2007).

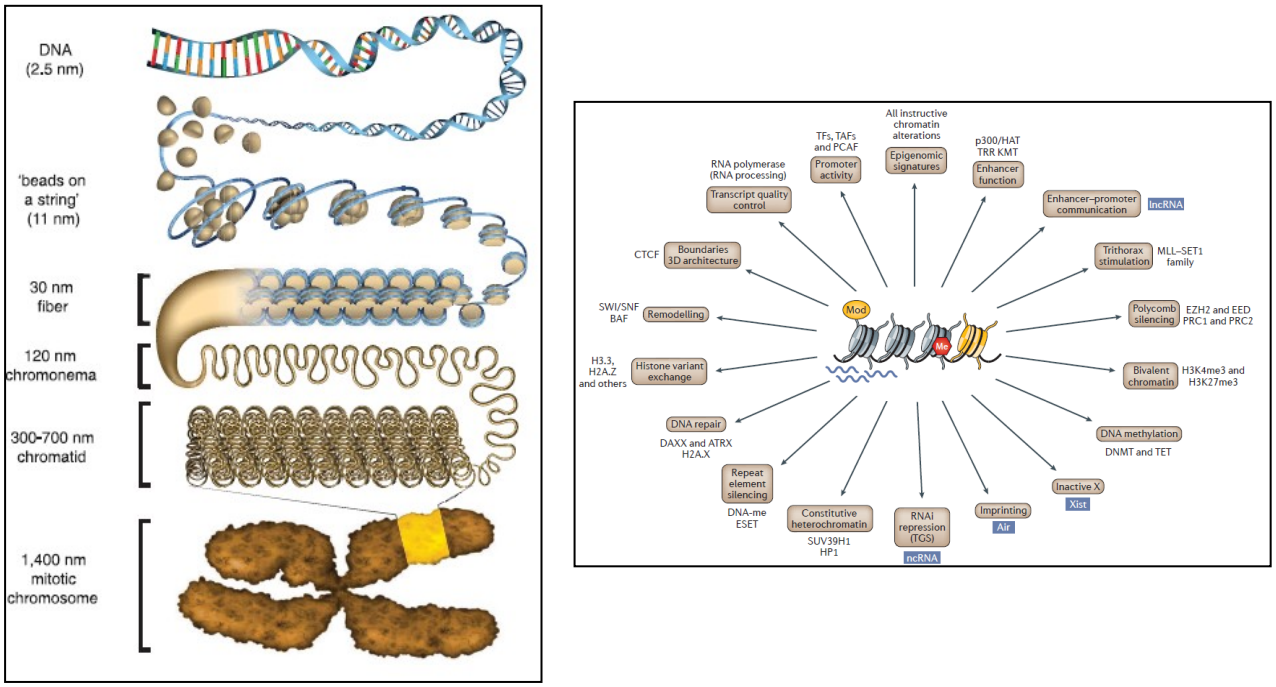

Figure 1.1- Left Panel- Folding of chromatin at various length scales*- DNA is organized as a double helical structure as determined by Watson and Crick. 147 bp of DNA is wrapped around the histone octamer to give rise to the nucleosome. These DNA-nucleosome polymers further fold onto form higher-order chromatin structures like 120 nm chromonema, 300-700 nm chromatid and finally, the condensed mitotic chromosomes (Taken with permission from the publication 'ChromEMT: Visualizing 3D chromatin structure and compaction in interphase and mitotic cells' (Ou et al., 2017).*

Right panel- Epigenetic factors involved in chromatin organization and function*- There are various epigenetic factors like histone variant exchange, ncRNAs, chromatin remodeling, DNA methylation, imprinting, etc that are important in various development processes. Their misregulation are implicated in various diseases. The figure is taken with permission from the review "The molecular hallmarks of epigenetic control" (Allis and Jenuwein, 2016).*

The previous understanding that histones compact the DNA indiscriminately has now changed and demonstrated to be associated with a plethora of regulatory functions related to gene regulation, DNA repair, centromere formation, etc. It is known that archaeal histones do not function as packaging molecules, suggesting a possibility of evolution of histones to regulate DNA transaction processes (Dekker, 2008; Malik and Henikoff, 2003).

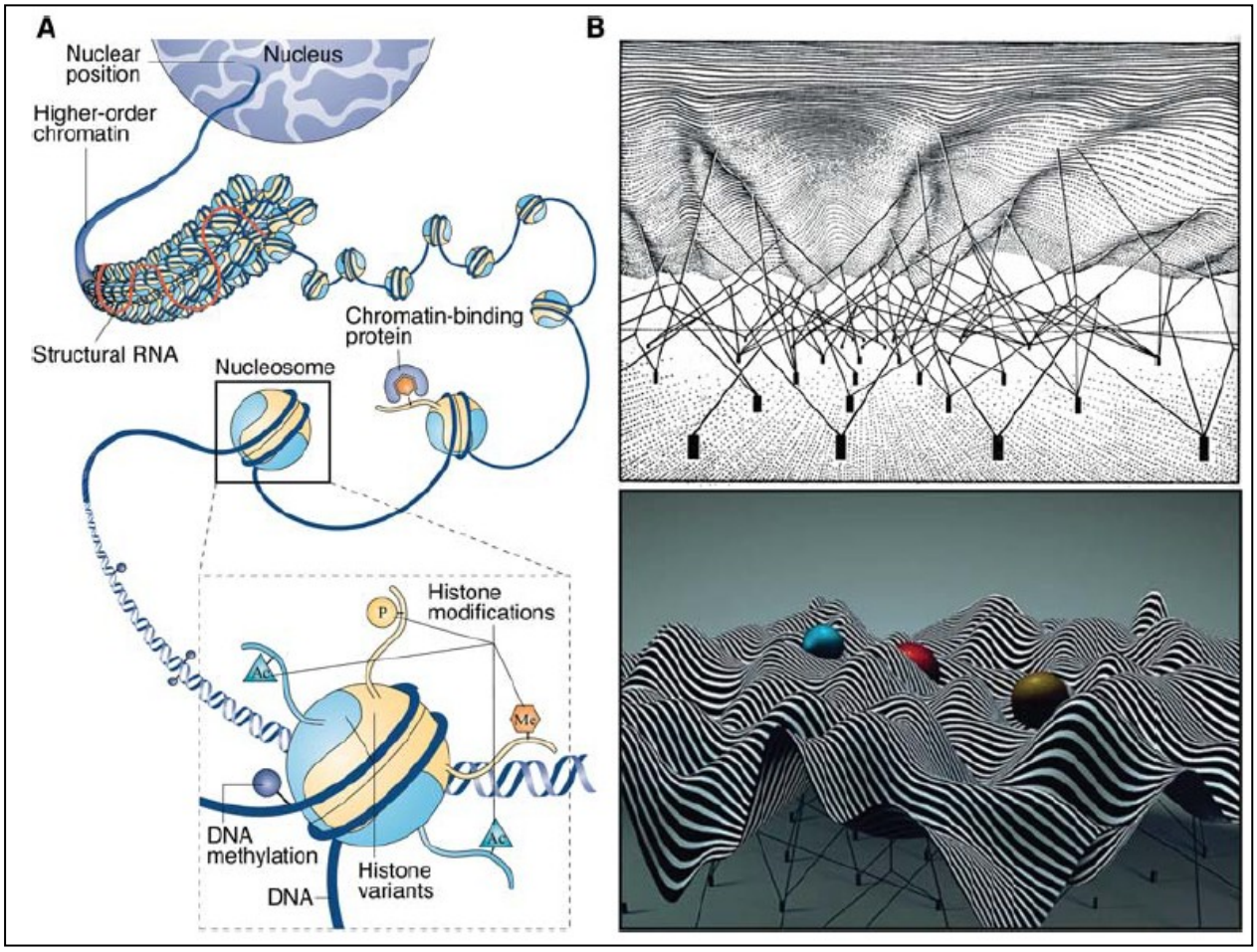

Figure 1.2- A. *Histone variants along with other chromatin-associated factors like histone modifications, DNA methylation, are important players in chromatin dynamics and functions.* ***B.*** *The network of genetic (represented as blubs) and epigenetic interactions (represented as strings) play a significant role in cell fate decision events in the cells (represents by troughs) as represented by the modern interpretation of the Waddington landscape.*
The entire figure is taken with permission from the review "Shaping Chromatin in the Nucleus: The Bricks and the Architects" (Sitbon et al., 2017).

1.2 Histone variants

Histone variants are non-allelic forms of the conventional histones deposited on DNA in specific biological contexts, and within defined chromatin domains, to fulfill distinct functions (Figure 1.1 right panel, Figure 1.2A). The sequences of histone variants differ at the level of primary sequence that can range from a few amino acids to broader domains, further contributing to distinct biophysical and biochemical properties to the variant-containing nucleosomes. There are two major classes of histone variants based on their expression pattern: replicative and replacement variants. Replicative variants are synthesized during the S-phase and are replication coupled, e.g., H3.1, H3.2, etc. Replacement variants are synthesized constitutively or outside the S-phase of the cell cycle. Examples of replacement variants are H3.3, TH2B, MacroH2A, CenH3, etc., Major developmental transitions are linked to chromatin remodeling and concomitant replacement of histones with histone variants (Figure 1.2B). Due to the positive selection of certain histone sequences, some of the histone variants like CenH3, H2AZ, H3.3, macroH2A, etc have evolved to replace the canonical core histones in specialized regions of the genome in a wide variety of species (Figure 1.3, left panel). How specific histones (variant) mark specific chromatin states has been a subject of intense investigation.

The biochemical properties and biological functions of the nucleosomes containing histone variants CenH3, H3.3, and macroH2A, with their importance in processes related to mammalian development are reviewed below.

1.3 CenH3

CenH3 (also referred to as CENPA) is a replacement H3 variant that is highly enriched at centromeres. This histone variant is sufficient for centromere formation and function in *Drosophila melanogaster* (Mendiburo et al., 2011). CENPA shares about 50% sequence similarity with the parent histone H3.1 and the majority of sequence conservation is found in the histone fold domain (HFD). The N-terminal sequence is highly divergent and has been suggested to be required for the recruitment of kinetochore proteins. The short stretch of amino acids, termed as the CENPA targeting domain (CATD), is required for efficient targeting at the centromeres (Okamoto et al., 2007; Sullivan, 2001). CenH3 gene is essential, as knockout mice die before conception. Various mitotic defects like lagging chromosomes and macronuclei due to failed chromosome segregation are observed in these knockout mice (Howman et al., 2000).

1.4 H3.3

H3.3 differs from the canonical histone H3 in just four-five amino acids depending on the organism. The bulk of nucleosome assembly occurs during the S-phase. The replacement histone variant H3.3 replaces H3 as differentiating cells exit the cell cycle and also during histone to protamine transition. In *Tetrahymena*, the constitutive synthesis of H3, not the particular variant, is critical for S-phase independent functions (Cui et al., 2006; Yu and Gorovsky, 1997). However, in the case of *Drosophila*, H3.3 is involved in replication-independent nucleosome assembly and is targeted to transcriptionally active loci. This suggests that H3.3 might be necessary for replacing H3-nucleosomes and heritable gene activation. The critical residues in H3.3 (S87, V89, M90) have proved to be critical for H3.3 S-phase independent deposition to chromatin and differential localization (Ahmad and Henikoff, 2002).

Nucleosomes containing H3.3 are less stable compared to canonical H3 containing nucleosomes (Jin and Felsenfeld, 2007). Due to this unique property, H3.3 is associated with transcriptionally active loci (Chen et al., 2013). H3.3-containing nucleosomes possess unique biochemical and functional properties highlighted by the fact that HP1 is relatively depleted from H3.3-containing nucleosomes (Loyola et al., 2006). Also, H3.3 inhibits the association of linker histone H1 *in vivo*, highlighting their involvement in transcriptional initiation (Braunschweig et al., 2009; Jin et al., 2009). It has been proposed that H3.3 and H2AZ also influence nucleosome dynamics at active gene regulatory regions causing nucleosome repositioning or disassembly, influencing access to transcription factors and chromatin remodelers (Thakar et al., 2009). In the context of developmental processes, H3.3 is a dominant histone H3 variant in adult mouse neurons. The turnover and dynamics of H3.3 assembly have been implicated in neural plasticity and memory formation in mice (Maze et al., 2015; Zovkic and Sweatt, 2015). During spermatocyte differentiation, H3.3 replaces canonical H3 nucleosomes in the unsynapsed chromatin during the induction of MSCI (van der Heijden et al., 2007).

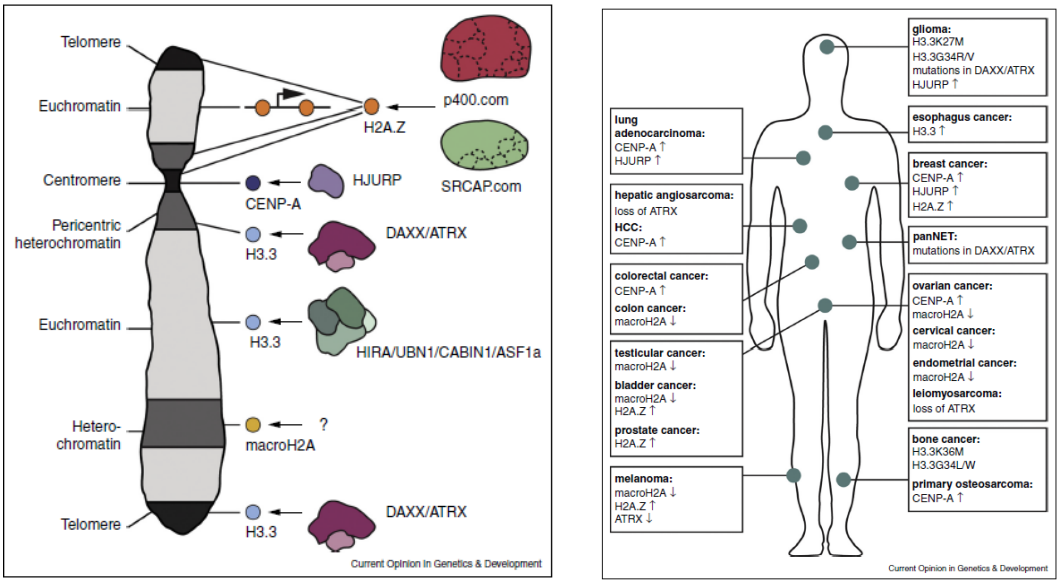

Figure 1.3- Left Panel- *Histone variants are deposited and replace core histone variants in specialized regions of the genome in a context-dependent manner. E.g., CENP-A is known H3 variant present at centromeres, H3.3 at transcriptionally active or euchromatic regions, macroH2A with the heterochromatin regions, etc. Their recruitment imparts the specificity of localization by specific histone remodeler proteins like HIRA, DAXX, etc. Adapted with permission from the review 'Histone variants: nuclear function and disease' (Zink and Hake, 2016).*

Right panel- *Mutation or misexpression of various histone variants are implicated in various diseases like cancer — a table showing the association of misregulation of histone variants in various cancers of the human body. The entire figure is taken with permission from the review article "Histone variants: nuclear function and disease" (Zink and Hake, 2016).*

1.5 MacroH2A

MacroH2A is the largest histone variant known in mammals (Pehrson and Fried, 1992). It contains an N-terminal domain (called the histone H2A resembling domain) that is connected to a non-histone macro-domain by a lysine-rich linker sequence. *In vitro* assays have shed light on the unique property of macroH2A, where they have been shown to repress biochemical interactions with transcription factor and nucleosome remodeling factors (Angelov et al., 2003). Due to this unique property, macroH2A is enriched in the inactive X-chromosome of male meiotic nuclei (Hoyer-Fender et al., 2000; Richler et al., 2000).

Various *in vitro* studies have also shed light on the influence of macroH2A in affecting the stability of nucleosome and higher-order chromatin fibers. Macro-linker, a basic region present between N and C terminal domains, has been shown to promote condensation of

chromatin fibers (Muthurajan et al., 2011). The linker is positioned at the entry-exit site of the nucleosome, useful in stabilization and increased protection of DNA from the exonuclease III digestion (Chakravarthy et al., 2012; Muthurajan et al., 2011). MacroH2A also displays a higher affinity for chromatin than its counterpart histone H2A. This affinity is independent of core histone acetylation status in the nucleosomes (Abbott et al., 2004; Chakravarthy et al., 2005).

Ser 137 phosphorylation of macroH2A, which occurs in the macro-linker, has been shown to remove macroH2A from the inactive X chromosome in mammals (Bernstein et al., 2008). In the avian system, macroH2A-containing genomic regions are devoid of linker histone H1 suggesting the role of macroH2A in H1-like condensation properties. In macroH2A containing nucleosome core particle (NCP), the L1-L1' interface is less flexible due to high hydrophobic interactions compared to the canonical NCP. L1-L1 interface may render macroH2A containing nucleosome refractory to transcriptional initiation (Angelov et al., 2003). The extended C-terminal region exhibits a alpha-beta fold that may be involved in HDAC recruitment, thus establishing a unique condensed chromatin domain (Chakravarthy et al., 2005). MacroH2As are required for pre and postnatal growth, the loss of which affects reproductive efficiency and liver metabolism (Pehrson et al., 2014).

We can thus appreciate the unique roles played by these histone variants in the context of mammalian differentiation and development. The mutations or misexpression of histone variants are implicated in various diseases like cancer, inflammation, etc (Summarised in Figure 1.3, right panel).

1.6 Mammalian Spermatogenesis

Mammalian spermatogenesis offers an excellent model system to study the biological functions of histone variants as the testis expresses various core and linker histones in a stage-specific manner. Spermatogenesis, the process of differentiation of male germinal cells, can be characterized into three major phases: pre-meiotic phase, meiotic phase and post-meiotic phase (Figure 1.4, Figure 1.5). During the pre-meiotic phase, the diploid spermatogonia divide by mitosis. There are three types of spermatogonia, the A-type, In-type (intermediate) and the B-type. A-type spermatogonia undergo four successive divisions giving rise to A1 to A4 in rodents. The A4 cells undergo several rounds of cell division resulting in the formation of A0 or A1 and In type cells. In type cells further differentiate into B-type spermatogonia. They undergo mitotic division and then enter the meiotic phase through the formation of pre-leptotene spermatocytes. These differentiate through meiotic

prophase I division consisting of leptotene, zygotene, pachytene, and diplotene intervals to give rise to secondary spermatocytes. The diplotene spermatocytes rapidly go through the meiotic II division to form round spermatids. The differentiation process from round spermatids to mature spermatozoa is termed as post-meiotic phase or spermiogenesis. The beginning of spermiogenesis results in a change in the nuclear shape from round to an elongated structure. The process of spermiogenesis is further divided into sixteen steps in the mouse and nineteen steps in the rat. These steps are as follows: round spermatids (steps 1-8), early elongating (steps 9-12), mid elongating (steps 13-15) and elongating/condensing spermatids (steps 16-19). The histones are removed and replaced first by transition proteins, ultimately replaced by protamines to form the condensed toroidal structure found in the mature spermatozoan.

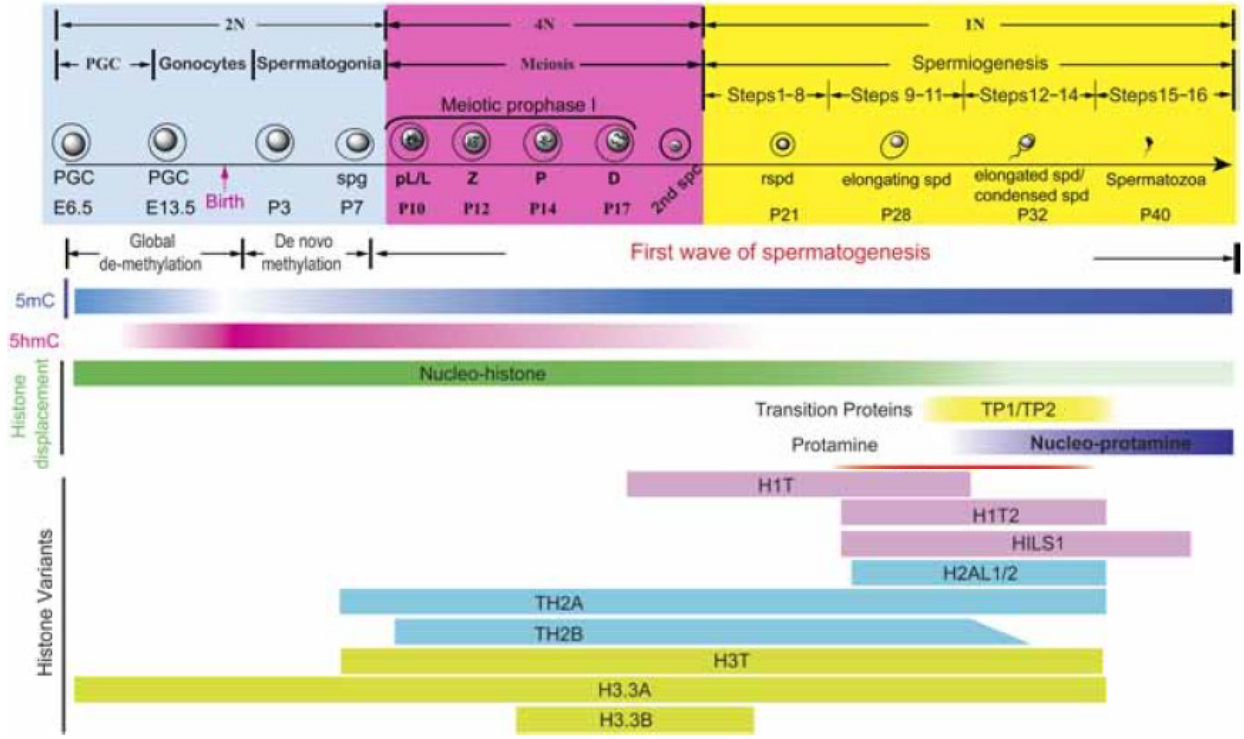

Figure 1.4– *Process of mammalian spermatogenesis from primordial germ cells till the formation of mature spermatozoa in the mouse- This process is divided into three major phases- the pre-meiotic phase (diploid phase), meiotic phase (tetraploid phase) and the post-meiotic phase or spermiogenesis (haploid phase). Various core (TH2A, TH2B, H3T, H3.3A, H3.3B) and linker histone (H1T, H1T2, HILS1) variants are expressed in a stage-specific manner during various stages of spermatogenesis (Modified and adapted from the review "Epigenetic regulation of the histone-to-protamine transition during spermiogenesis" (Bao and Bedford, 2016).*

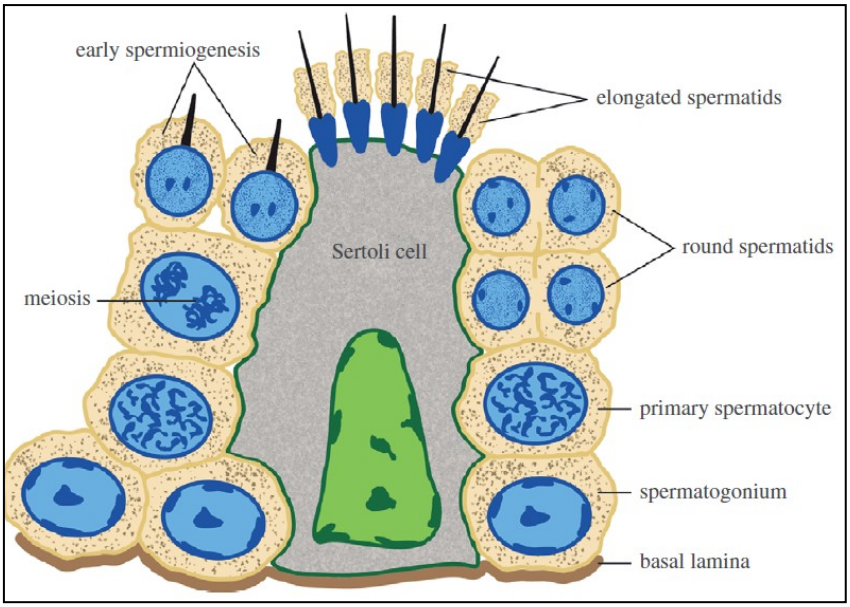

Figure 1.5- Schematic representation of the different cell types associated with mammalian spermatogenesis in contact with the Sertoli cell in the seminiferous tubule.

Spermatogonia undergo various mitotic divisions to give rise to meiotic spermatocytes. The preleptotene spermatocytes undergo DNA replication and reductional divisions by meiosis to form round spermatids. The round spermatids undergo a series of differentiation involving chromatin remodeling events, ultimately giving rise to mature spermatozoa. These mature spermatozoa detach from the Sertoli cell, travel down the seminiferous tubule to reach the epididymis. Sertoli cells provide the contact and milieu for the development of germ cells (Adapted with permission from the review "Transcription and post-transcriptional regulation of spermatogenesis" (Bettegowda and Wilkinson, 2010).

There are various processes characteristic to each of these phases. Homologous recombination, chromosome pairing, and active transcription are the major processes characteristic of the meiotic phase. During the post-meiotic or spermiogenesis phase, transcriptional shutoff, nuclear remodeling, and chromatin compaction are the major biological events to be taking place. Histones are eventually replaced, first by transition proteins TP1 and TP2 and ultimately by protamines. A small amount of histones along with their post-translational modifications is retained in the mature sperm (about 1% in rodents and about 10% in humans) and they have been shown to mark the genes necessary for early embryonic development (Brykczynska et al., 2010; Carone et al., 2014; Erkek et al., 2013; Samans et al., 2014; Xue et al., 2013).

1.7 Meiotic Recombination

One of the major processes that occur during spermatocyte differentiation is meiotic recombination and homologous chromosome pairing. Meiotic recombination is critical for the generation of diversity in the offspring. The homologous chromosomes undergo synapsis and recombination at defined chromosomal loci. Meiotic prophase I can be characterized into leptotene, zygotene, pachytene and diplotene intervals (Figures 1.6 and 1.7).

During the leptotene interval, homologous recombination is initiated by programmed DNA double-strand breaks (DSBs) (Lam and Keeney, 2014). DSBs are actively catalyzed by topoisomerase family member Spo11 at selected genomic locations termed as recombination hotspots (Boateng et al., 2013; Neale et al., 2005). Spo11 is recruited to genomic regions containing histone marks H3K4me3 and H3K36me3 (Grey et al., 2017; Yamada et al., 2017). Prdm9 is involved in trimethylation of histone H3 at K4 and K36 positions at hotspots, thus creating a nucleosome depleted region important for Spo11-mediated DSB formation (Powers et al., 2016). Single strand DNA ends that are created at DSB locations, invade the homologous double-stranded DNA and new Watson Crick base pairs are formed. This homology-directed strand invasion is mediated by two recombinases Rad51 and Dmc1 (Kobayashi et al., 2016; Tarsounas et al., 1999). The end resection and strand invasion activities mediated by Rad51, Dmc1 and MRN complex are characteristic of the zygotene interval (Cloud et al., 2012; Czornak et al., 2008; Neale and Keeney, 2006).

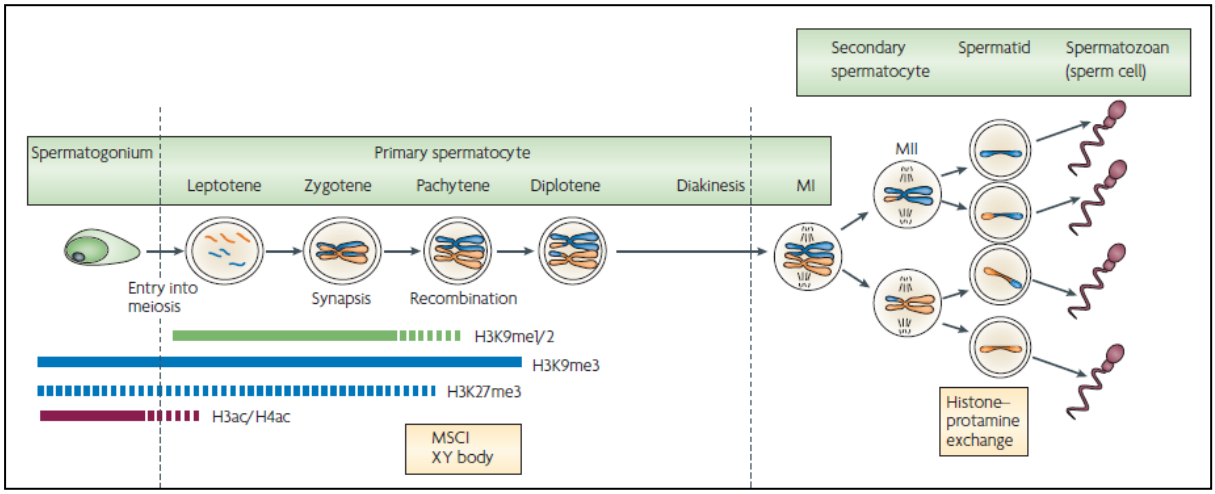

Figure 1.6- Epigenetic changes that occur during male spermatogenesis

There are dynamic changes in levels of histone modifications that occur during various phases of male gametogenesis. The dashed lines indicate that the level of histone modifications are lower in the stages unless during the differentiation time-period

represented by solid lines. Adapted with permission from the review article "Epigenetic events in mammalian germ-cell development: reprogramming and beyond."

During pachytene interval, the homologous chromosomes are already synapsed, because of which the central portion of the synaptonemal complex is apparent. Due to less or non-homology between chromosomes X and Y, there is delayed DNA repair and recombination during the pachytene interval. BRCA1 is involved in sensing of asynapsis, recruits specialized enzyme ATR, to mediate γH2AX formation (Broering et al., 2014; Royo et al., 2013). A specialized structure called the XY body is formed during the pachytene stage (Figure 1.6). The region of homology between the X and Y chromosomes is termed as the pseudoautosomal region (PAR) of the XY body. An increased DSB density is found in the PAR compared to the autosomes to ensure chromosome segregation with at least one crossover in the PAR (Baudat et al., 2013). The higher DSB density in the PAR is due to specialized chromatin configuration wherein DNA is organized into longer axes and shorter loops compared to the autosomes (Kauppi et al., 2011; Lange et al., 2016). The non-PAR regions are transcriptionally silenced by the process of meiotic sex chromosome inactivation (MSCI) (Cloutier and Turner, 2010; Turner et al., 2005). The crossover and non-crossover products are generated at the end of the pachytene interval (Guillon et al., 2005; Guillon and de Massy, 2002).

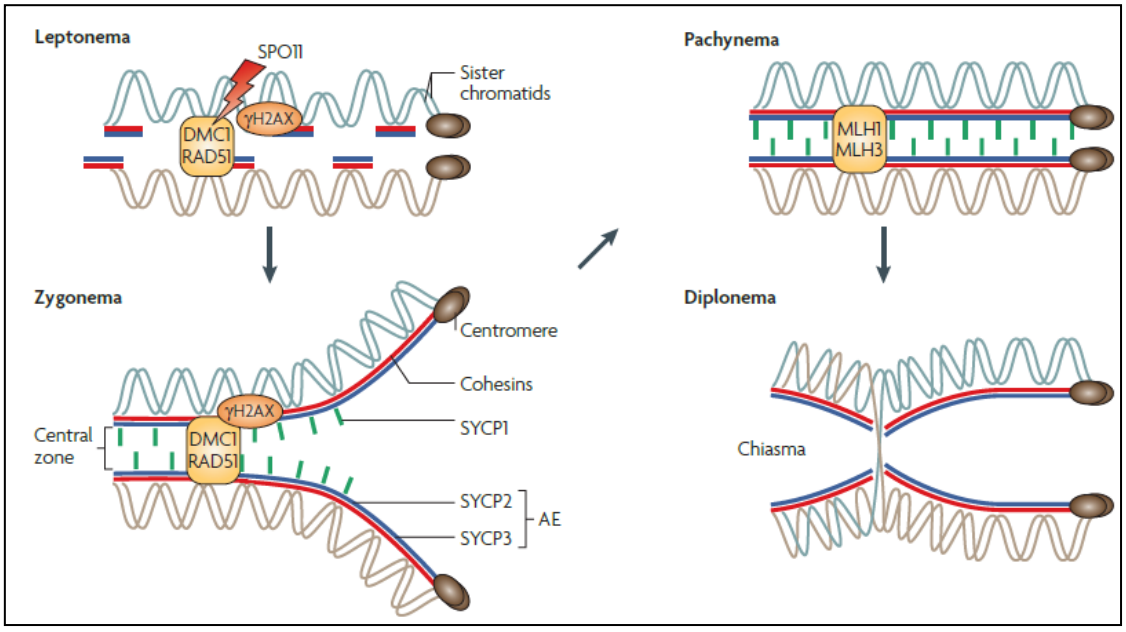

Figure 1.7- Substages of meiotic prophase I- *Meiotic prophase I is divided into four intervals- leptotene, zygotene, pachytene and diplotene. Adapted with permission from the*

review "Genetics of mammalian meiosis: regulation, dynamics and impact on fertility"(Handel and Schimenti, 2010).

1.8 Testis-specific histone variants in development

One of the important characteristics of chromatin remodeling during mammalian spermatogenesis is the expression of a large number of core and linker histone variants. The contribution of testis-specific histone variants to mammalian spermatogenesis is interesting to consider, as their differential timing of expression and influence on chromatin structure offers control over numerous genomic functions. Several non-canonical histone variants have been discovered in testis for histones H1, H2A, H2B, and H3. Histone H4 is one of the most conserved proteins with no variants identified in mammals till date. Understanding how each variant influences chromatin structure and function is a real challenge.

Core Histone Variants-

1.9 TH2A

TH2A, a testicular variant of histone H2A, was discovered in rat testis in 1982. TH2A shares 87% sequence similarity with core histone H2A, with major amino acid residue differences in the C-terminal tail (Figure 1.8A). Its expression begins in 16-day old rats corresponding to primary spermatocytes and increases with progression of spermatogenesis (Trostle-Weige et al., 1982). Interestingly, TH2A is also detected in spermatogonia of neonatal mouse testis (Beedle et al., 2019). TH2A and TH2B share a bidirectional promoter, indicating to their possible common biological functions (Huh et al., 1991b). Their common functions can be related by the fact that loss of both TH2A and TH2B genes cause male infertility with major spermatogenic defects in cohesin release and histone to protamine replacement (Shinagawa et al., 2015). TH2A/TH2B nucleosomes exhibit lower stability due to fewer histone-DNA contacts compared to canonical histone-containing NCP (Padavattan et al., 2015b). Apart from the expression of TH2A in testes, it is also expressed in early embryos and contributes to paternal genome activation along with TH2B (Figure 1.8B) (Shinagawa et al., 2014). The combination of histone variants TH2A and TH2B with histone chaperone Npm2 enhance reprogramming of somatic cells like fibroblasts to iPSCs in mouse and human model systems (Huynh et al., 2016a; Shinagawa et al., 2014).

TH2A threonine phosphorylation (specifically TH2AT127ph) has been detected in metaphase I spermatocytes, oocytes, condensed spermatids and mitotic preimplantation embryos (Hada et al., 2017a; Hada et al., 2017b). Haspin kinase mediates phosphorylation of this threonine residue in oocytes and spermatocytes (Hada et al., 2017a). In the sperm genome, this histone mark is localized to transcription start sites of the sperm chromatin, as demonstrated by ChIP-sequencing assays (Hada et al., 2017b).

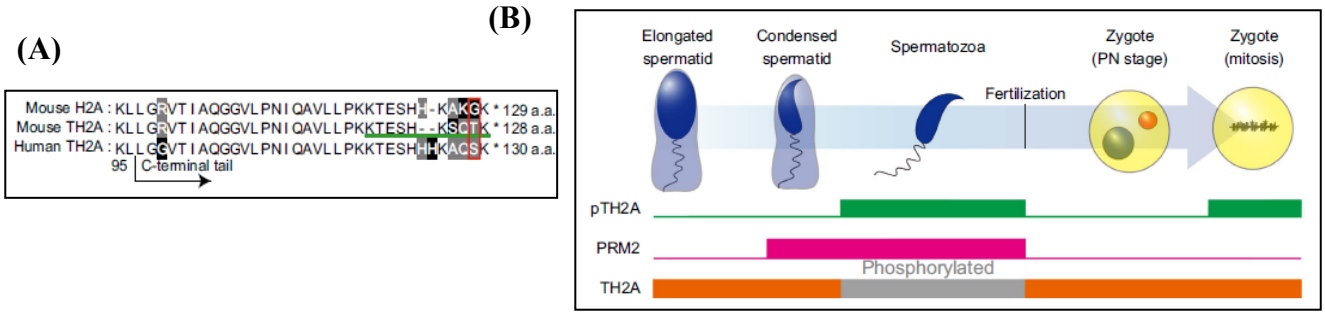

Figure 1.8- A*. Alignment of amino acid sequences of the C-terminal end between mouse H2A, mouse TH2A and human TH2A. The black arrow indicates the start of C-terminal tails, red box indicates the phosphorylated threonine residue, and the number of amino acids are indicated in the right-hand side.*

B. Schematic summary of dynamics of pTH2A (TH2AT127) histone mark across mammalian spermiogenesis and 1-cell stage. pTH2A is observed in condensed spermatids where transcription is shut down.

The images have been taken with permission from the publication "Identification of variant-specific phosphorylation of TH2A during spermiogenesis" (Hada et al., 2017b).

Histone Variants	Biological Functions
H2A Variants	
H2AX	DNA repair and recombination
H2AZ	Gene Expression, chromosome segregation
macroH2A	Transcriptional repression, X-chromosome inactivation
H2ABBD	Transcriptional activation
H2B Variants	
TH2B	Histone to protamine replacement
H3 Variants	
H3.3	Transcriptional regulation

CENPA H3T	Kinetochore assembly Spermatogonial differentiation and meiosis initiation
H1 variants HILS1 H1T2 H1t	 Regulation of LINE L1 repeats Histone to protamine replacement Unknown
Histone modifications	**Biological Functions**
H3K4me3, H4K5ac, H4K9ac, H4K8ac,H4K12ac, H3K79me2	Transcriptional activation Transcriptional reactivation
H3K9me3, H2Aub	Transcriptional repression
H3K27me3	Synapsis and pericentric heterochromatin formation
H3K4me3, H3K9ac, H3K36me3	Meiotic recombination
Epigenetic modifiers	**Biological Functions**
H3K9 trimethyltransferases Suv39h1, Suv39h2	Synapsis and pericentric heterochromatin formation
H3K9 mono- and dimethyltransferase Ehmt2	Chromosome synapsis and gene regulation
H3K4 and K6 trimethyltranferase Prdm9	Chromosome synapsis, meiotic recombination, XY body formation
Regulation of DNA methylation Dnmt3L	Chromosome synapsis, Repression of retrotransposons
Polycomb protein Scml2	Regulator of chromatin modifications in the XY body
PIWI family protein Mili	Repression of retrotransposons

Table 1.1- Table of key histone variants, histone modifications and epigenetic modifiers with their associated biological functions during mammalian spermatogenesis.

1.10 H2AL.2

Several histone variants have been identified during the process of histone to protamine transition during mouse spermiogenesis. Histone variant H2A.L.2 is detected in spermatids coinciding with the appearance of transition proteins. *In vitro* studies have shown that

H2A.L.2 is present in MNase-sensitive nucleosome particles of elongating spermatids, which means that they can drastically destabilize the NCP. From the H2A.L.2 knockout mouse model, their functional relevance has been understood in that H2A.L.2 possibly aids the process of loading of transition proteins onto the chromatin. In the absence of H2A.L.2, transition proteins are expressed but remain non-functional. These observations point to the fact that H2A.L.2 aids in nucleosomal disassembly allowing for chromatin loading of transition proteins, in turn facilitating the preprocessing and the final assembly of protamine within the chromatin. Histone variant TH2B may aid H2A.L.2 in the formation of 'loose' NCPs during histone to protamine replacement (Figure 1.9) (Barral et al., 2017).

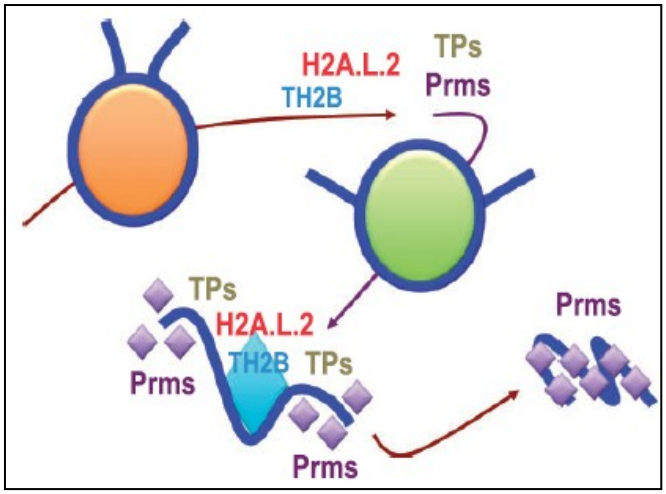

Figure 1.9- Coordinated functions of histone variants, transition protein and protamines during the process of histone to protamine replacement

The unstable TH2B-H2A.L.2 nucleosomes allow the loading of transition proteins. In turn, H2A.L.2 controls the histone removal, preprocessing of protamines and assembly of protamines to mediate genome compaction in late spermatids. This figure has been adapted with permission from the review titled "Histone variants: essential actors in male genome programming" (Hoghoughi et al., 2018).

1.11 H3t

A non-allelic variant of histone H3, H3t was reported in 1977 (Albig et al., 1996; Franklin and Zweidler, 1977; Witt et al., 1996). This variant differs from core histone H3 in few amino acids (Figure 1.10, H3t, red letters). This protein is actively synthesized in A and B type spermatogonia (Ueda et al., 2017b). Cell fusion studies have demonstrated that H3t is recruited to chromatin in a replication-dependent manner. The crystal structure of H3t-containing nucleosome has shed light on two critical residues essential for the structural

integrity of the H3t-nucleosome. H3t-containing nucleosomes form open chromatin configuration as compared to the nucleosomes containing the canonical histone counterparts, as demonstrated by both *in vitro* and *in vivo* studies (Tachiwana et al., 2010; Tachiwana et al., 2011).

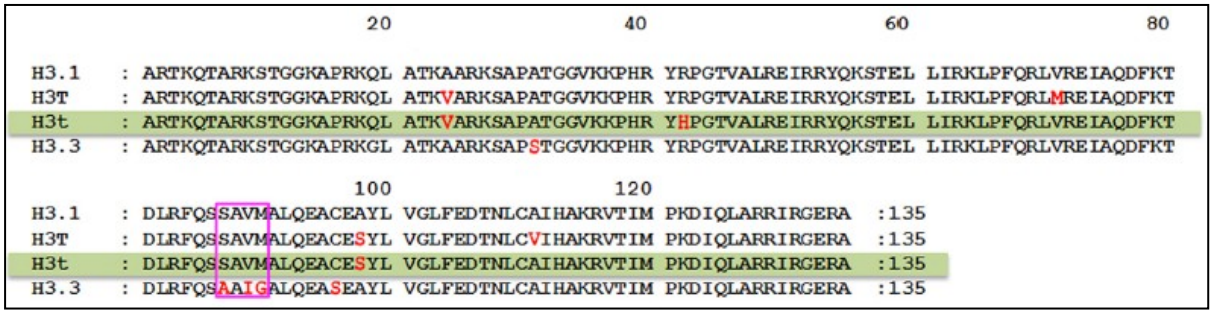

Figure 1.10- Alignment of protein sequences of histone H3 with variants H3T, H3t and H3.3

The unique amino acids of each of the variants are highlighted in red and the chaperone recognition motif is given in a pink box. This figure has been taken with permission from the publication "Testis-specific histone variant H3t gene is essential for entry into spermatogenesis" (Ueda et al., 2017a).

Conflicting reports exist regarding the interaction of H3t-containing NCP with DNA. The human testis-specific H3T has been shown to affect nucleosome stability, due to the weaker association of the (H3T-H4)2 tetramer with the H2A-H2B dimer. This unique property is due to a residue located in the DNA entry-exit site of the nucleosome, critical for weakened interaction between H3t and DNA (Tachiwana et al., 2008a). Importantly, the deficiency of H3t causes male sterility in mice due to defects in premeiotic processes required for entry into meiosis (Ueda et al., 2017a). This report highlights that a histone variant by itself can dictate cell fate during mammalian spermatogenesis.

Different chaperone pathways have been reported to facililate incorporation of H3t into testis chromatin analogous to Nap1-mediated incorporation of H3 and other histones (Okuwaki et al., 2005; Tachiwana et al., 2008b). Apart from its high expression in the testes, H3t is also detected in somatic cells in low abundance (Andersen et al., 2005; Govin et al., 2005; Govin et al., 2007). However, the function of H3t in somatic cells is still unknown.

Linker histone variants-

1.12 HILS1

Linker histone variant HILS1 is expressed during steps 9-15 of mouse spermiogenesis (elongating and condensing spermatids), coinciding with histone to protamine transition. The-C terminal domain is highly divergent in relation to other linker histones (Figure 1.11). Through various biochemical assays, it has been shown that HILS1 acts as a linker histone *in vitro* and is a poor condenser of chromatin (Mishra et al., 2015; Yan et al., 2003).

HILS1 occupy LINE-L1 element containing chromatin domains of the rat spermatid genome. These HILS1-containing chromatin domains are associated with heterochromatin specific modifications like H3K9me3 and H4K20me3 in rat spermatids (Mishra et al., 2018b). These histone modifications are known to be transmitted from the sperm to the embryo. As repetitive elements like LINE are reactivated shortly after fertilization in zygotes, HILS1 may shape the chromatin landscape in the broad context of chromatin remodeling of the paternal genome during spermiogenesis. The loss of HILS1 causes defects in DNA condensation but does not lead to male infertility. On the other hand, the genetic interaction of HILS1 with TP1 but not TP2 is critical for sperm production and male fertility (Wu et al., 2009). It is quite possible that compensatory pathways could operate to overcome the loss of HILS1 in spermatids in these HILS1 null mice.

Post-translational modifications have been mapped on spermatid HILS1 (Mishra et al., 2015); however, their biological functions have not been deciphered in great detail.

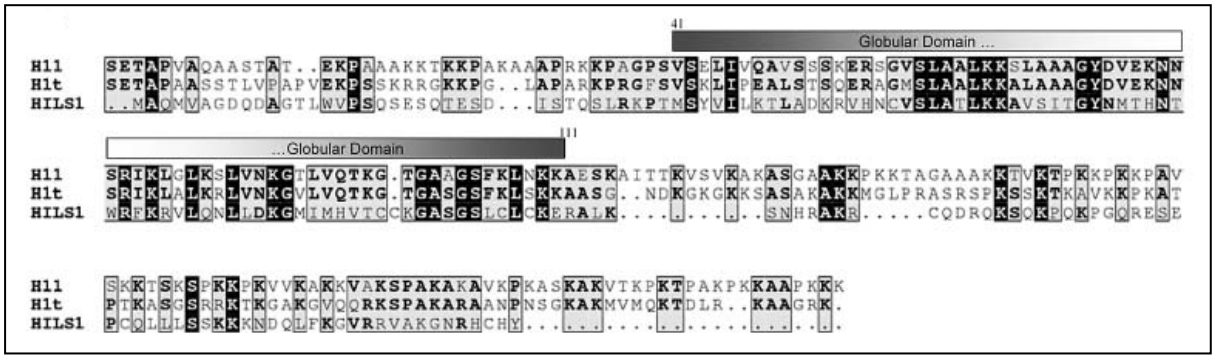

Figure 1.11- Sequence of conventional linker histone H1.1 aligned against testicular linker histone variants H1t and HILS1.

This figure has been adapted with permission from the review titled "The role of histones in chromatin remodeling during mammalian spermiogenesis" (Govin et al., 2004).

1.13 H1T2

Another important linker histone variant is H1T2, whose expression begins in late spermatids in the mouse. Its expression coincides with replacement stages concerning histone

replacement first to transition proteins, then to protamines (Martianov et al., 2005; Tanaka et al., 2005). H1T2 protein has an extended C-terminal domain in comparison with the somatic H1, which is rich in acidic amino acid residues and contains a high number of potential sites for phosphorylation. H1T2 shows an asymmetric localization pattern in that it is principally localized towards the apical pole in round spermatocytes and spermatids. This localization pattern of H1T2 is dependent on the expression of proteins HMGB2 and TRF2 (Catena et al., 2006; Martianov et al., 2005). The inherent property of H1T2 or the role of adaptor proteins in inducing polarity and localization of H1T2 in the spermatid nucleus remains to be delineated. The functional importance of H1T2 in germ cells can be explained by the fact that the loss of H1T2 causes male infertility with major defects in chromatin condensation and abnormal nuclear elongation (Martianov et al., 2005; Tanaka et al., 2005).

Thus, these histone variants contribute to specific pathways of differentiation during spermatogenesis, e.g., H3t during spermatogonial differentiation, and H2A.L.2, H1T2, HILS1 during histone to protamine transition.

1.14 Histone modifications

Development from a single cell into a complex multicellular organism requires thousands of cell-fate decisions, and failure to recapitulate these decisions can result in a broad spectrum of diseases. The major mechanism by which the cell remembers these decisions are histone modifications that function as epigenetic cellular memory. Histones are highly basic proteins, rich in lysine and arginine residues. Histone proteins are subject to various post-translational modifications like acetylation, phosphorylation, methylation, etc. Acetylation neutralizes the positive charge of lysines, thus increasing the accessibility of nucleosomal DNA. Phosphorylation of histones causes repulsion with the negatively charged DNA backbone, thus disrupting histone-histone interactions. The addition of methyl group on histones leads to an increase in hydrophobicity that mediate effector functions based on the specificity of the residue that is modified. Apart from the consequence of charge in influencing histone-histone and histone-DNA contacts, these PTMs can also act as potential sites to recruit specialized effector and reader molecules to mediate various chromatin-based transactions like kinetochore assembly, DNA replication, DNA repair, etc (Figure 1.12). These reader proteins possess distinct domains for recognition of these histone marks, e.g., the bromodomain domain for recognition of acetylation marks. Post-translational modifications (PTMs) allow for the functional flexibility of a protein in the cell. The PTM modified protein could also localize to certain regions of the genome to influence specific biological output.

Kenneth Murray showed for the first time that histones are substrates of methylation modification (Murray, 1964). Vincent Allfrey's pathbreaking study first showed that histones are also acetylated (Allfrey et al., 1964; Pogo et al., 1966). Since then, many studies have been carried out to understand and unravel the repertoire of the histone-associated post-translational modifications and biological functions of these modifications (Figure 1.13, left panel). Histone PTMs alone do not contribute to epigenetic output in the cell. Combinations of histone PTMs called the 'Histone Code' determine the recruitment of specialized molecular machinery necessary to mediate chromatin-templated events (Figure 1.13, right panel) (Kouzarides, 2007; Strahl and Allis, 2000).

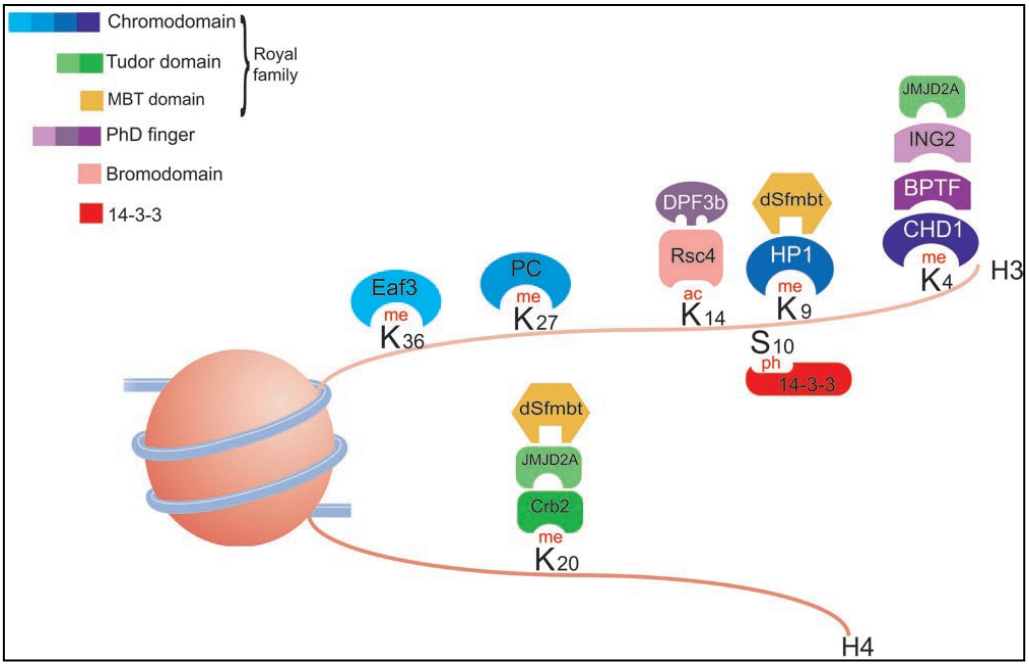

Figure 1.12- *Histone marks recruit specialized effector molecules to perform various DNA mediated transactions in cells- For e.g., bromodomain and chromodomain containing proteins are normally recruited to the chromatin template containing acetylation and methylation marks respectively (Adapted with permission from the review" Regulation of chromatin by histone modifications" (Bannister and Kouzarides, 2011).*

Thus, the diversity of nucleosome composition, with the combination of histone modifications and the introduction of specific histone variants, provides a layer of information beyond the genomic DNA sequence.

The search for post-translational modifications requires the extraction of protein of interest from the homogenous population of cells. Various techniques can be employed to purify specific cell types. Elutriation based on density gradient centrifugation method, had been

widely used before, to isolate spermatogonia, spermatocyte and spermatid populations (Gupta et al., 2017; Pivot-Pajot et al., 2003). Recently, FACS is widely used for isolation of specific cell types (Bastos et al., 2005; Getun et al., 2011; Lassalle et al., 1999; Romer et al., 2018). This technique is useful to purify even specific cell types of meiotic prophase I: leptotene, zygotene, pachytene and diplotene cells and different stages of spermiogenesis like round, elongating and mature spermatids. Apart from various cell isolation protocols, the unraveling of PTMs requires purified protein as a source of sample for mass spectrometry. Our laboratory has recently published a book chapter that highlights the workflow required for HPLC based purification of endogenous proteins from various testicular types required for mass spectrometry (Gupta et al., 2017).

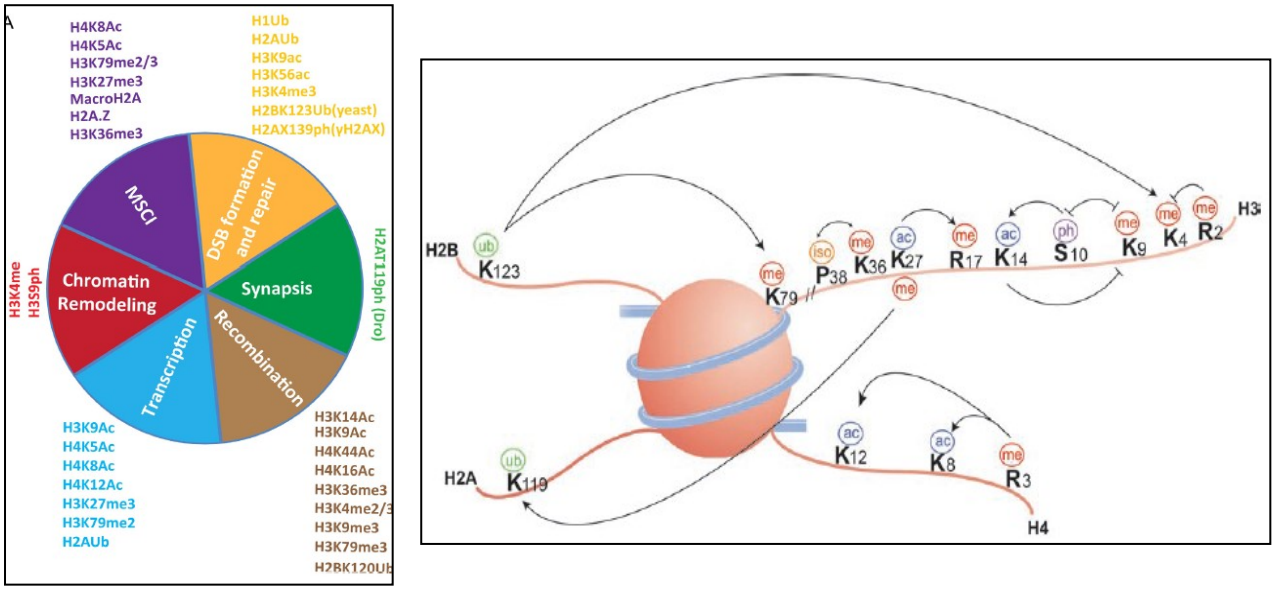

Figure 1.13- Right panel- *Summary of histone modifications during male meiosis (Adapted with permission from the review "The histone codes for meiosis" (Wang et al., 2017).*
Left panel- *Crosstalk between histone modifications- These histone modifications can also modulate the formation or erasure of other histone modifications by crosstalk with other epigenetic factors. (Adapted with permission from the review "Regulation of chromatin by histone modifications" (Bannister and Kouzarides, 2011).*

PTMs can also be characterized without the purification of the specific testicular protein. However, this method affects the coverage of low abundant PTMs in the process. Recently, a nano LC-MS/MS analyses revealed an entire repertoire of PTMs on histone and histone variants derived from meiotic, round spermatid, elongating spermatid, mature sperm, and human sperm samples (Luense et al., 2016). It is important to characterize PTMs of low

abundant histone variants by extraction of particular protein before mass spectrometry. Apart from covering important PTMs on testicular proteins, the determination of the abundance of those PTMs becomes necessary. The stage-specific PTMs along with quantitation could give an indication of the importance of that PTM in that stage. For example, TH2B acetylation increases from spermatocyte to the spermatid stages (Pentakota et al., 2014). These observations suggest that TH2B, in addition to acetylation, along with protein effectors, could contribute to the destabilization of nucleosomes required for histone to protamine replacement.

Various approaches are being used for the identification of PTMs on cellular proteins. The top-down approach deals with the identification of PTMs on whole proteins, whereas the bottom-up approach uses single or multi-enzyme digestions to catalogue various PTMs. The middle-out approaches makes use of digestion of proteins into large peptides (Mw range of 3 to 9 kDa) which can also be used to address combinatorial PTMs in proteins like histones, closely approaching the sensitivity of bottom-up workflow. The top-down strategy is typically used for the identification of combinatorial PTMs in a particular protein. Each approach has its own advantages and disadvantages and requires an understanding of specific questions to be addressed. Apart from the characterization of PTMs on testis-specific histone variants, the associated protein effectors and enzyme(s) involved in the function of that PTM are not clearly understood.

1.15 Histone modifications in spermatocytes

It is reasonably clear that PTMs modulate the function of histones in a context-dependent manner. Various efforts have focused on understanding the repertoire and biological functions of PTMs on testis-specific histone variants like TP1 (Gupta et al., 2015), TP2 (Gupta et al., 2015), TH2B (Lu et al., 2009; Pentakota et al., 2014), HILS1 (Mishra et al., 2015), etc. The important testis-specific histone marks like γH2AX and H4K5/K8 acetylation marks have been further explained in detail for their importance during spermatocyte differentiation.

1.16 γH2AX

The involvement of H2AX in DSB repair is well documented in the context of somatic cells and testes. H2AX is a crucial factor involved in the recruitment of various DSB associated factors to the DSB foci. The phosphorylation of H2AX mediated by ATM or ATR kinases is an important marker of DSBs. There are two waves of H2AX phosphorylation involved in

different repair pathways of meiotic recombination- ATM-mediated phosphorylation in autosomal DSB formation and ATR mediated formation of γH2AX in XY body DSB formation. Male mice deficient in histone H2AX are sterile with defects in the inactivation of sex chromosomes and crossover formation. In H2AX-deficient mice, various proteins usually associated with XY body like macroH2A and XMR do not localize to the XY body, suggesting that this variant is involved in chromatin remodeling in the XY body (Fernandez-Capetillo et al., 2003).

A high-resolution map of genome-wide occupancy of γH2AX has provided insights into mechanisms into the functions of recombination machinery (Iacovoni et al., 2010). Mapping of γH2AX genomic occupancy have been carried out in a human cell line where the γH2AX distribution was found to be discontinuous and spread around large chromatin domains around the DSBs. However, transcription start sites seem to be resistant to γH2AX spreading (Iacovoni et al., 2010).

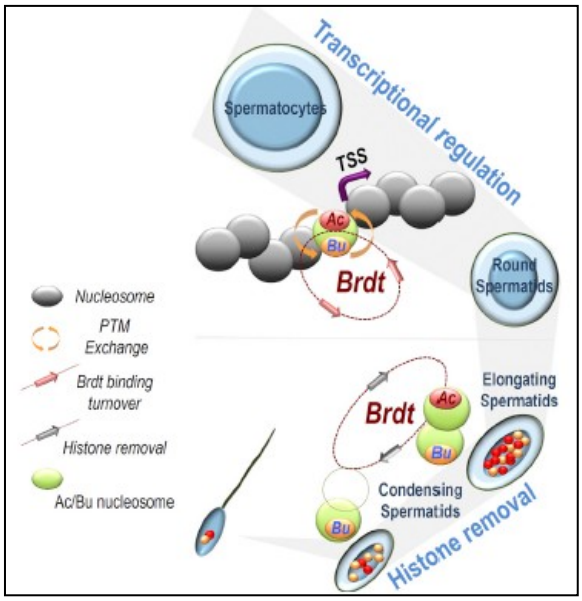

Figure 1.14- Association of H4K5/K8 acetylation and butyrylation marks with active gene promoters in mouse spermatocytes- *These acetylated marks attract bromodomain-containing protein Brdt to activate transcription during the meiotic phase. However, during spermiogenesis, the histone hyperacetylation signal leads to the recruitment of Brdt, aiding in the process of histone to protamine replacement (Taken with permission from the publication "Dynamic Competing Histone H4 K5K8 Acetylation and Butyrylation Are Hallmarks of Highly Active Gene Promoters" (Goudarzi et al., 2016).*

1.17 H4K5/K8 acetylation marks

H4K5/K8 acetylation and butyrylation marks are present in active TSS in spermatocytes (Goudarzi et al., 2016). H4K5/K8 acetylation mediates the recruitment of a testis-specific chromatin remodeler Brdt. Brdt activated genes are functionally essential in spermatocytes and spermatids. At the same time, Brdt also represses non-spermatogenesis related genes. Brdt has two bromodomain modules called BD1 and BD2 in its N-terminal region. These bromodomain modules remodel chromatin in an acetylation-dependent manner involving association with Smarce1 protein (Dhar et al., 2012; Gaucher et al., 2012). Therefore, Brdt is an essential gene for spermatocyte survival. Concerning its role in post-meiotic genome organization, Brdt binds to histone hyperacetylated chromatin, further facilitating histone removal and replacement by transition proteins (Goudarzi et al., 2014; Govin et al., 2006; Shang et al., 2007). Because Brdt is involved in critical functions involving stage-specific gene expression and post-meiotic genome organization (Figure 1.14), it has become a popular target for male contraception. Bromodomain inhibitor JQ1 has been used to block Brdt function in spermatogenic cells (Matzuk et al., 2012).

1.18 Histone variant TH2B

TH2B (a synonym of germ-cell specific H2B.1 or TS H2B.1) (Talbert et al., 2012) was discovered in testicular histone extracts in 1975 (Kumaroo et al., 1975; Meistrich et al., 1985). TH2B is expressed in meiotic and post-meiotic cells. Recently, it is shown to be expressed in spermatogonia too (Beedle et al., 2019). It is the dominant histone variant in spermatocyte and spermatids that replaces 80-85% of H2B in these cells (Montellier et al., 2013). As mentioned earlier, TH2A and TH2B, the two germ cell histone variants share a bidirectional promoter in the genome (Huh et al., 1991a). Apart from expression in testes, TH2B is expressed in early embryos and is involved in paternal genome activation after fertilization (Shinagawa et al., 2014). Recently, TH2A and TH2B have been shown to improve the reprogramming efficiency of somatic cells (fibroblasts) into induced pluripotent stem cells (Huynh et al., 2016b; Padavattan et al., 2015a; Shinagawa et al., 2014).

Figure 1.15- Alignment of proteins sequences of TH2B from rat and mouse with H2B from the rat. *The majority of amino acid residue differences between TH2B and H2B occur in the amino-terminal tail. The curved lines in the sequences indicate the helical structures in these histones (Pentakota et al., 2014).*

With respect to the protein sequence, TH2B differs from H2B with major amino acid differences being present in the amino-terminal tail (Figure 1.15). Most of the residues are, however, conserved in the central helical and C terminal portions between the two proteins. It was shown earlier that TH2B-containing pachytene chromatin is more susceptible to DNase I digestion compared to H2B-containing liver chromatin. Circular dichroism (CD) and thermal denaturation studies also revealed a decreased compaction of TH2B-containing pachytene NCPs in comparison to liver NCPs (Rao et al., 1983). The pachytene chromatin exhibit higher MNase sensitivity due to weakened histone-DNA interactions at the TH2B-interacting sites (Rao and Rao, 1987). In short, the pachytene NCP harboring TH2B is less compact compared to H2B-containing liver NCP (Rao et al., 1983; Rao and Rao, 1987). Nucleosome reconstitution studies have also confirmed these observations wherein hsTH2B-containing histone octamer exhibit lower stability than H2B-containing histone octamer (Li et al., 2005). The nucleosome models have been derived computationally with TH2B and TH2A replacing H2B and H2A, respectively (Padavattan et al., 2015a; Pentakota et al., 2014). The overall quaternary structure of TH2B-containing nucleosome is unchanged compared to H2B-containing nucleosome. The residue differences of TH2B compared to H2B contribute to loosened nucleosome structure as the number of overall contacts (hydrogen bonds and salt bridges) across all interfaces was reduced in the TH2B-containing nucleosome model (Padavattan et al., 2017; Pentakota et al., 2014). Therefore, the computational studies with

nucleosome models become useful to study the effect of residue substitutions on the overall nucleosome structure. Some of these models can also be generated with other histone variants with their associated PTMs to understand the loci-specific functions of these PTMs of such histone variants.

The functions of histones are modulated by post-translational modifications through the reader and effector molecules that catalyze the chromatin-templated processes. The first study involving the characterization of PTMs on TH2B was reported by Lu and others (Lu et al., 2009). In this study, acetylation of TH2B at residues K13, K16, K17 and K21 were discovered in spermatogonia and spermatocyte cell populations. Apart from acetylation modification, TH2B is also post-translationally modified by phosphorylation (T116) and methylation (K117). The dominant histone variant TH2B bearing few PTMs was surprising. However, with the use of the latest mass spectrometry technologies and multi-enzyme digestion approaches, Pentakota et al. characterized the post-translational modifications extensively that occur on TH2B isolated from tetraploid spermatocytes and haploid spermatids (Pentakota et al., 2014). The use of a multi-enzyme approach in this mass spectrometric study led to an improvement in the overall coverage of analyses. Residue substitutions and PTMs harbored by some residues were found to contribute to loosened nucleosome structure involving the TH2B molecule. This analysis also revealed many important PTMs like acetylation, methylation and phosphorylation on TH2B, the biological functions of which remain to be understood. Recently, a comprehensive analysis of PTMs on testis-specific histone variants has identified the TH2B PTMs repertoire in spermatocytes, round and elongating spermatids (Luense et al., 2016). This study revealed for the first time the repertoire of PTMs on TH2B extracted from elongating stages of spermiogenesis.

Furthermore, the biological role(s) of TH2B in spermatogenesis have been previously addressed by two systems- knockout mice and C-terminal tagged knock-in mice (Figure 1.16)(Montellier et al., 2013). The loss of TH2B does not cause male sterility and is compensated by H2B upregulation and additional PTMs on core histones H2B, H3 and H4. The two main specialized PTMs observed were H4K77 and H3K122 crotonylation marks. These PTMs were mapped to histone-histone and histone-DNA interaction sites thus creating nucleosomal instability. The genome-wide incorporation of TH2B replacing H2B during spermatocytes and spermatids suggested an important TH2B-specific function. However, no meiotic arrest or meiosis related defects were observed in the TH2B-null testes. The knock-in of the C-terminal tagged version of TH2B caused male sterility due to defective histone replacement. On the other hand, the tag did not cause aberrations during spermatocyte

processes like sex chromosome inactivation, γH2AX incorporation etc. The tag caused a dominant-negative phenotype that resulted in defective histone replacement during late spermatid stages. Histone variants TH2B and H2A.L.2 have been postulated to create destabilized nucleosomes required for histone replacement to transition proteins, and then subsequently to protamines (Barral et al., 2017).

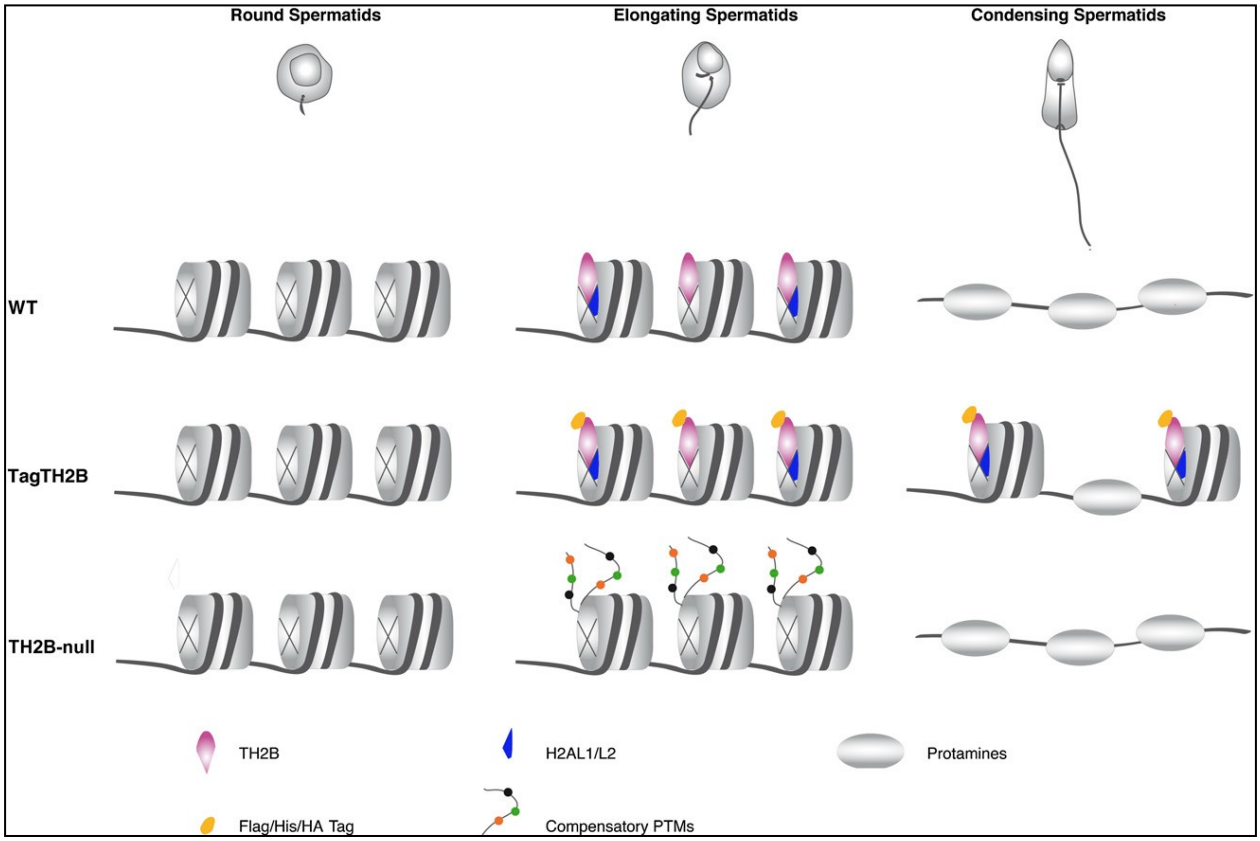

Figure 1.16- Biological functions of TH2B as determined by tag-TH2B and TH2B knockout models. *In the tagged-TH2B expressing mice, the tag created a dominant-negative phenotype, interfered with the function of TH2B during histone replacement, ultimately resulted in male infertility. However, in the TH2B knockout mice, the loss of TH2B is compensated by H2B overexpression and compensatory histone modifications in the histones H2B, H3 and H4. The specialized histone modification found in these knockout mice were lysine crotonylation. This figure is adapted from the review "How mammals pack their sperm: a variant matter" (Boskovic and Torres-Padilla, 2013).*

TH2A and TH2B double knockout males are infertile, suggesting the importance of these two testis-specific histone variants in the success of spermatogenesis (Shinagawa et al., 2015).

However, detailed studies have not been carried out to determine the functions of TH2B or its PTMs because of the difficulty in raising PTM-specific antibodies.

The genome-wide occupancy of TH2B has revealed its exclusion from H2AZ-containing TSS sites (Montellier et al., 2013). There was no specific enrichment of TH2B at specific gene regulatory regions as revealed by ChIP-sequencing studies. This leads us to the question of how post-translationally modified TH2B generate chromatin domains to influence local chromatin dynamics and function. What are the important roles of post-translationally modified TH2B in spermatocytes and spermatids? A long-standing question remains as to why TH2B has evolved to replace H2B on a genome-wide scale in spermatocytes and spermatids.

With the combination of histones, histone variants, histone modifications and the involvement of specific epigenetic players at particular genomic locations, loci-specific genome programming exists in spermatogenic cells. As mentioned before, the histone code hypothesis states that histone modifications could act in concert to mediate DNA-based transactions in cells. In the context of mammalian spermatogenesis, little or no studies have been carried out to understand the influence of histone variants associated with their PTMs and their crosstalk in influencing genomic functions like transcription, meiotic recombination, histone-protamine replacement, etc.

1.19 Linker histone variant H1t

The germ cell-specific linker histone variant H1t is expressed from preleptotene spermatocytes till early round spermatids (in mouse) or till late-round spermatids (in humans) (Figure 1.17) (Drabent et al., 1996; Drabent et al., 1998; Lennox and Cohen, 1984; Steger et al., 1998). Even though H1t mRNA is detected in spermatogonia, the protein is absent. H1t accounts for about 50% of the total H1 in these cell types (Bucci et al., 1982; Govin et al., 2004; Grimes et al., 2003).

H1t gene shares several proximal regulatory elements with the somatic H1s. A testis-specific regulatory element drives the expression of H1t in spermatocytes and early spermatids (Figure 1.18). This element contains two inverted repeat sequences, TE1 and TE2 boxes, and a GC-box between the two inverted repeat elements (Wolfe et al., 1995). TE boxes are the binding sites for Sp family of transcription factors (Sp1 and Sp3), and RFX proteins (RFX2) that drive their specific expression in spermatocytes and early spermatids (Grimes et al., 2005; Horvath et al., 2004; Wilkerson et al., 2002a, b; Wolfe et al., 2004). Replacement of this regulatory element with a heterologous DNA has been shown to abolish H1t expression

(VanWert et al., 2008). TE boxes are methylated in tissues where H1t is not expressed (Clare et al., 1997a; Clare et al., 1997b). Brdt binds to a distal silencer region in the H1t gene (-948 to -780) and represses H1t expression in late spermatids (Shang et al., 2007; Wolfe and Grimes, 1999).

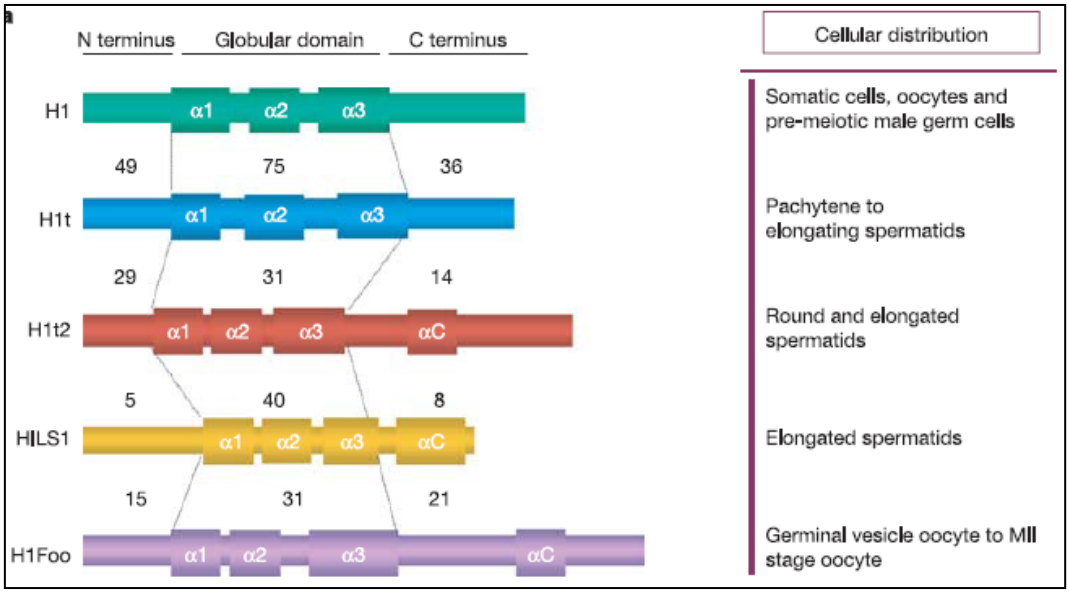

Figure 1.17- Germ cell-specific linker histone variants and their expression during various stages of male and female germ cell development. *The linker histone variant of interest, H1t is expressed from pre-leptotene stages, with its maximal expression during pachytene and is expressed till elongating spermatids in humans. These germ cell linker histone variants have a characteristic tripartite structure- unstructured N and C terminal ends, and the conserved central globular domain. Adapted with permission from the review "Chromatin remodelling and epigenetic features of germ cells" (Kimmins and Sassone-Corsi, 2005).*

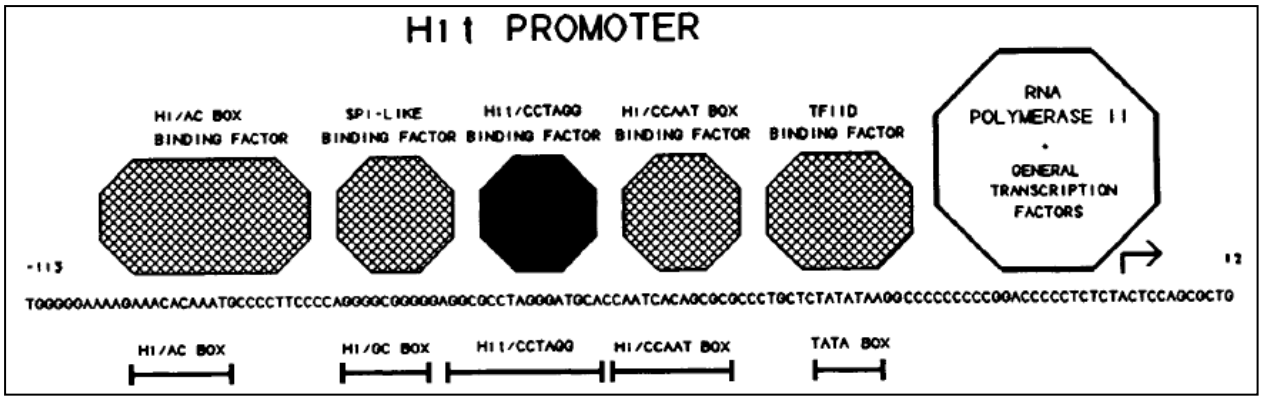

Figure 1.18- Hypothetical model of the H1t promoter- *The promoter is made up of two TE boxes important for the binding of the Sp and RFX group of transcription factors. H1/AC box (AAACACA) is a highly conserved sequence, has been shown to be required for synthesis of histone H1 genes during S phase. The unique element called the H1t box or CCTAGG*

element is the binding site for testis-specific transcription factors required for the optimal expression in spermatocytes and spermatids (Taken with permission from the publication "Histone H1t: A tissue-specific model used to study transcriptional control and nuclear function during cellular differentiation" (Wolfe and Grimes, 1993).

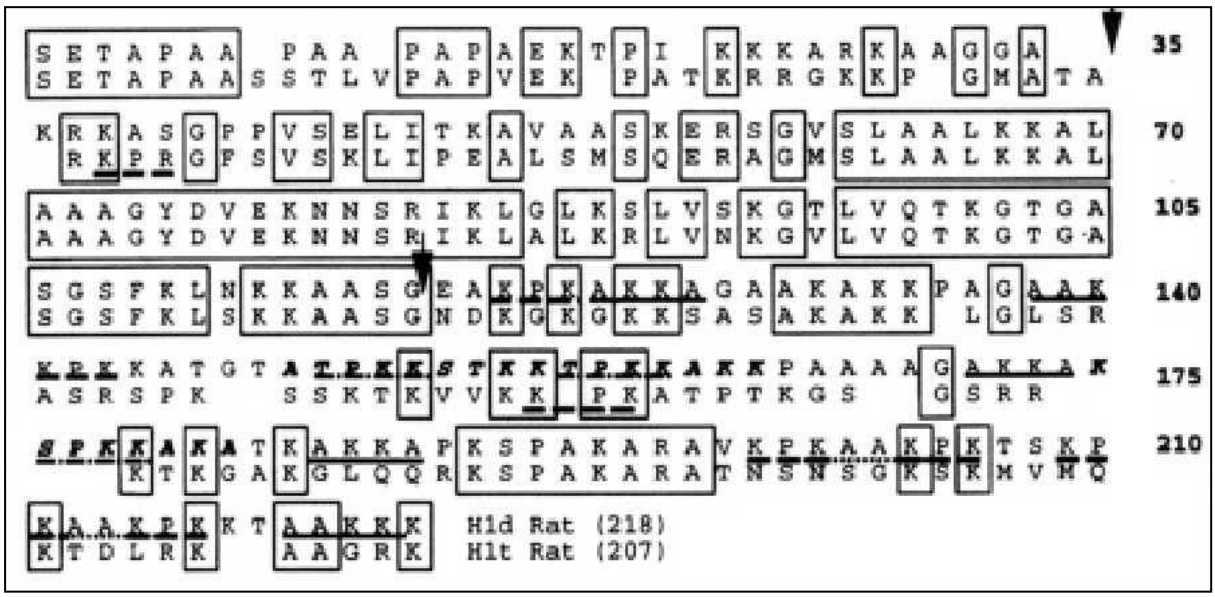

Figure 1.19- Sequence comparison of amino acids of rat histones H1d and variant H1t. *The boxed regions indicate the identity between the two proteins. The region between the two downward-facing arrows is the globular domain. The major amino acid differences can be seen in the C-terminal domain of H1t, also where most of the DNA binding motifs like SPKK are absent (Khadake and Rao, 1995).*

H1t differs from the somatic H1 with amino acid residue differences observed in the C-terminus (Figure 1.19). H1t is a poor condenser of chromatin as demonstrated by *in vitro* CD (Circular dichroism) spectroscopic studies (De Lucia et al., 1994; Khadake and Rao, 1995). This property is attributed to a lack of DNA binding motifs like SPKK in the C-terminal domain of H1t (Bharath et al., 2002; Drabent et al., 1991; Khadake and Rao, 1997; Suzuki, 1989). SPKK and other motifs are responsible for DNA condensation property in histone H1d. A K52Q substitution in the globular domain of histone H1t causes a reduction in its DNA-binding affinity (Ramesh et al., 2006).

The loss of H1t causes no detectable defects during spermatogenesis in mice. There are conflicting reports on the phenotypes observed in H1t-null mice. Other H1s compensate for the loss of H1t (Lin et al., 2000). In another study, H1t-deficient chromatin was shown to be

H1 free (Drabent et al., 2003; Fantz et al., 2001). *In vitro* studies have demonstrated that H1t can be poly ADP-ribosylated (PAR) and PAR modified H1t promotes chromatin compaction (Faraone-Mennella et al., 1999). Disturbance in PAR metabolism causes retention of H1t, HILS1 and core histones in the mature spermatozoan (Meyer-Ficca et al., 2011). Recently, various post-translational modifications have been characterized on H1t obtained from spermatocyte and round spermatocyte cell populations by mass spectrometry (Luense et al., 2016). The biological functions of these PTMs would be interesting to address in future.

H1s are known to condense chromatin structure and repress gene expression (Bustin et al., 2005; Woodcock et al., 2006). However, the biological functions of linker histone variant H1t in terms of its genome-wide occupancy and associated protein effectors remain to be further determined and are the subject of the present study.

1.17 Aims and scope of the study

As discussed above, histone variants and their post-translational modifications are essential for various developmental pathways during mammalian development. The model system like mammalian spermatogenesis is interesting due to the fact that the testis expresses a wide variety of somatic and linker histone variants in a stage-specific manner. Loci specific genome reprogramming and extensive chromatin remodeling involving histone variants are the main features of mammalian spermatogenesis. Therefore, it becomes important to understand the functions of dominant histone variants TH2B and H1t in the context of mammalian spermatogenesis with respect to their chromatin-associated functions.

TH2B differs from H2B amino sequence in its amino-terminal tail and replaces 80-85% H2B in spermatocytes and spermatids. To determine the unique functions of TH2B compared to H2B, our study is focused on understanding the biological role of TH2B Serine 11 phosphorylation histone mark (TH2BS11ph; Brno system of nomenclature for histone modifications) in the context of processes related to mammalian spermatocyte differentiation.

H1t is the dominant H1 in pachytene spermatocytes. H1t was reported to be associated with nucleolus in spermatocytes (Tani et al., 2016). Apart from its nucleolar localization, we would like to determine the extra-nucleolar localization regarding its genome-wide occupancy and associated protein partners in mammalian spermatocytes.

With this background, following are the primary objectives defined for the present investigation,

1. Determination of the unique functions of TH2B with respect to post-translational modifications on residues of the TH2B N terminal tail.
2. Understanding the biological function of N-terminal modification TH2B Serine 11 phosphorylation (TH2BS11ph) histone mark in mammalian spermatocytes with respect to its genome-wide occupancy and associated protein players in mammalian spermatocytes.
3. Understanding the genome-wide occupancy of linker histone variant H1t to get a deeper understanding of the extra-nucleolar localization of H1t in mammalian spermatocytes.
4. Determination of H1t-containing chromatin domains with respect to associated protein players.

Chapter 2

Genome-wide occupancy of TH2BS11ph histone mark in mammalian spermatocytes

2.1 Introduction

As explained earlier, TH2B differs from H2B protein with the major amino acid residue differences found in the N-terminal end. It has been shown that these amino acid residue differences and PTMs on some of these residues contribute to destabilization of TH2B-containing nucleosomes (Pentakota et al., 2014). In order to understand the unique functions of TH2B, we went ahead in determining the various post-translational modifications on TH2B particularly on the N-terminal tail. Understanding the unique functions of TH2B with respect to post-translationally modified TH2B, could help us understand as to why TH2B has replaced H2B on a genome-wide scale in mammalian spermatocytes and spermatids.

Pentakota et al. had characterized the PTMs associated with TH2B isolated from both spermatocyte and spermatid stages (Pentakota et al., 2014). We were interested in exploring whether we could characterize any additional PTMs on TH2B by employing different sets of procedures routinely used in the literature. After unraveling the PTMs on TH2B derived from spermatocyte TH2B, our main aim was to determine the biological role(s) of post-translationally modified TH2B using biochemical, genomics and cell biology approaches. Our efforts were thus directed towards characterizing the PTMs on TH2B and understanding its biological functions in processes related to mammalian spermatocyte differentiation model system. To understand the biological functions of TH2B further, raising specific antibodies and performing rigorous characterization of its specificity is a prerequisite.

As explained earlier, an important event during the process of meiotic recombination is the formation of a condensed XY body during the pachytene interval. XY body harbors various proteins related to meiotic recombination, heterochromatin formation, etc. Different staining patterns are observed for proteins localized in the XY body (Figure 2.1) (Lu et al., 2013). E.g., pATM, ATR, BRCA1 proteins are localized in the unsynapsed axes. Rad51 is located as foci along the unsynapsed axes, whereas γH2AX and Mdc1 proteins are spread along the entire XY body (axes plus loops).

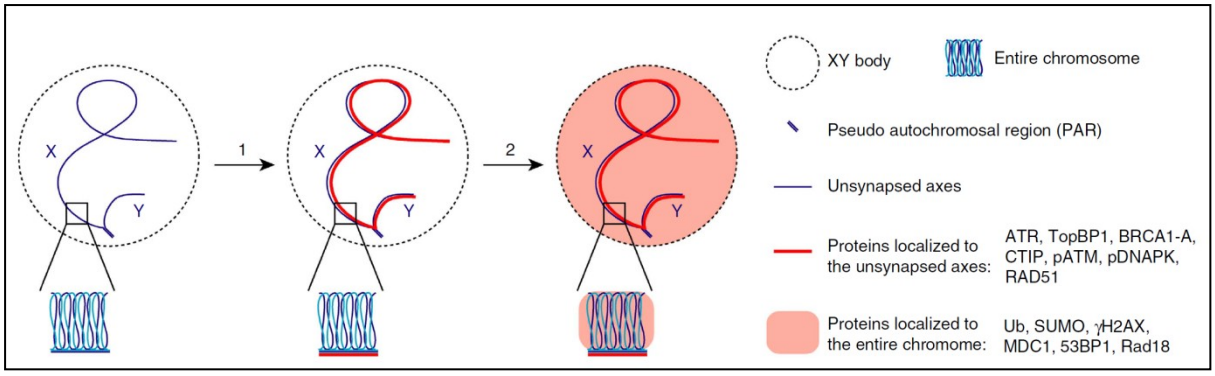

Figure 2.1- Immunostaining patterns of different proteins related to meiotic recombination and heterochromatin observed in the XY body- *Taken from the publication 'Regulation of the DNA damage response on male meiotic sex chromosomes' (Lu et al., 2013).*

2.2 Materials and Methods

2.2.1 Alignment of the amino acid sequences

Multiple sequence alignment (MSA) was performed for TH2B of selected mammals to examine the sequence conservation across species.

2.2.2 Extraction of histones

Histones were extracted from rat testicular cells using the acid extraction method (Shechter et al., 2007). Briefly, the testes were homogenized in hypotonic lysis buffer (10mM Tris-Cl pH 8.0, 1mM KCl, 1.5mM $MgCl_2$ and 1mM DTT), incubated at 4^{o}C for 30 minutes. The nuclei were resuspended in 0.4N H_2SO_4, and TCA precipitation of histones was carried out on ice for 30 min. The histones were pelleted, washed with ice-cold acetone, air dried and resuspended in water to obtain the histone preparation.

2.2.3 Purification of *in vivo* TH2B

TH2B was purified from the total testicular histones by reverse phase HPLC technique using the published protocol (Pentakota et al., 2014).

2.2.4 Mass spectrometric identification of TH2B serine 11 phosphorylation (TH2BS11ph) histone mark in mammalian spermatocytes

(i) In-Gel Digestion

Gel bands were cut into one mm^3 pieces and washed twice with MilliQ water. The gel was destained using 1:1 methanol:50 mM ammonium bicarbonate for 1 min, twice, then were dehydrated for 5 min using 1:1 acetonitrile: 50 mM ammonium bicarbonate followed by acetonitrile for 30 seconds. The gel pieces were dried in a speed-vac (Thermo Savant) for 10 min. They were rehydrated in 25 mM dithiothreitol, 50 mM ammonium bicarbonate and incubated at 56^{o}C for 20 minutes. After discarding the supernatant, the gel pieces were incubated in 55 mM iodoacetamide at RT for 20 min in the dark and subsequently were washed twice with water, dehydrated and dried as before. They were rehydrated in 50 mM ammonium bicarbonate containing 250 ng of mass spectrometry grade trypsin (Promega) and incubated overnight at 37^{o}C. Following digestion, the reaction mixture was acidified with 1% acetic acid and dried in a speed-vac to reduce the volume to 5 µL, to which 10 µL of mobile phase A was added and directly processed for LC-MS/MS analysis. Mobile phase A was 94.5% MilliQ water, 5% acetonitrile, 0.5% acetic acid.

(ii) Liquid Chromatography-Tandem Mass Spectrometry

Each reaction mixture was analyzed by LC-MS/MS. LC was performed on a Easy nanoLC II HPLC system (Thermo Fisher Scientific). Mobile phase A was 94.5% MilliQ water, 5% acetonitrile, 0.5% acetic acid. Mobile phase B was 80% acetonitrile, 19.5% MilliQ water, 0.5% acetic acid. The 120 min LC gradient ran from 2% B to 35% B over 90 min, with the remaining time used for sample loading and column regeneration. Samples were loaded onto a 2 cm x 100 um I.D. trap column positioned on an actuated valve (Rheodyne). The column was 13 cm x 100 um I.D. fused silica with a pulled tip emitter. Both trap and analytical columns were packed with 3.5 µm C18 resin (Zorbax SB, Agilent). The LC was interfaced to a dual pressure linear ion trap mass spectrometer (LTQ Velos, Thermo Fisher) via nano-electrospray ionization. An electrospray voltage of 1.8 kV was applied to a pre-column tee. The mass spectrometer was programmed to acquire, by data-dependent acquisition, tandem mass spectra from the top 15 ions in the full scan from 400 - 1400 m/z. Dynamic exclusion was set to 30 s.

(iii) Data Processing and Library Searching

Mass spectrometer RAW data files were converted to MGF format using msconvert. Briefly, all searches required strict tryptic cleavage, 0 or 1 missed cleavages, fixed modification of cysteine alkylation, variable modification of methionine oxidation and expectation value scores of 0.01 or lower. MGF files were searched using X! Hunter against the latest library

available on the GPM at the time. Other searches used the cRAP contaminant library from the GPM and libraries constructed from the most recent ENSEMBL release available at the time. MGF files were searched using X!!Tandem using both the native and k-score5 scoring algorithms and by OMSSA. All searches were performed on Amazon Web Services-based cluster compute instances using the Proteome Cluster interface. XML output files were parsed, and non-redundant protein sets were determined using in-house scripts. Proteins were required to have 2 or unique peptides with E-value scores of 0.01 or less, 0.001 for X!Hunter and protein E-value scores of 0.0001 or less.

2.2.5 Generation of TH2BS11ph specific antibodies in rabbits

Peptides corresponding to TH2BS11ph modification (CKGTTI(pS)KKGFK) and H2B(KSRPAPKKGSK) were injected into rabbits, and the 14-day cycle of antibody generation was followed. Immunoglobulins were purified by caprylic acid based purification method. Peptide-affinity based purification with the Sulfolink columns containing immobilized peptides, was used to purify the TH2BS11ph and H2B specific antibodies. The TH2BS11ph antibody was outsourced from Abgenex company (Bhubaneshwar, India).

2.2.6 Preparation of testicular nuclear lysates

Nuclear lysates were prepared by the method described previously with modifications (Somyajit et al., 2013). Briefly, testes were dissected in cytoplasmic lysis buffer (10mM HEPES pH 7.5, 50mM NaCl, 0.5M sucrose, 0.5% Triton-X-100, 0.1mM EDTA, 1mM DTT, protease inhibitor cocktail), incubated on ice for 15 minutes and centrifuged at 1500g for 7 minutes. The nuclear pellet was resuspended in Buffer B1 (10mM HEPES pH 7.5, 500mM NaCl, 0.1mM EDTA, 1mM DTT, 0.5% NP-40, protease inhibitor cocktail) to obtain nuclear lysates or Buffer B2 (10mM HEPES, 200mM NaCl, 1mM EDTA, 0.5% NP-40, protease inhibitor cocktail) for isolation of chromatin. The nuclear lysates were clarified by centrifugation at 15100 X g for 10 minutes.

2.2.7 ELISA

Peptides were used at 200 ng per well. The pre-bleed and immune sera were used at 1:5000 dilution. Goat anti-rabbit HRP were used as the secondary antibody at 1:5000 dilution. TMB (3, 3', 5, 5'- Tetramethylbenzidine) was used as the substrate for the reaction. After three minutes of enzyme-substrate reaction, the plate was read at 450 nm.

2.2.8 Dot Blot

Two µg of peptides corresponding to TH2B (CKGTTISKKGFK), TH2BS11ph (CKGTTI(pS)KKGFK), H2B(KSRPAPKKGSK) and H2BS14P (SRPAPKKG(pS)KKC) were applied as separate spots on the nitrocellulose membrane. After drying, the blot was subjected to steps of western blotting with the TH2BS11ph antibody.

2.2.9 Western Blot and peptide competition assays

For western blot, proteins were resolved by SDS-PAGE gel electrophoresis and then transferred onto a nitrocellulose membrane using the semi-dry transfer technique. The membrane was blocked using 5% skimmed milk or 3% BSA (diluted in TBS) for 1 hr at room temperature, then incubated with the specific primary antibody for 1 hr at room temperature or overnight at $4^{O}C$. The blots were given multiple washes with 0.1% PBST or TBST for 10 min each. Next, the blot was incubated with the secondary antibody (anti-rabbit /anti-mouse) for 1 hr at room temperature. The blots were washed extensively with 0.1% PBST or TBST and developed using the ECL kit (Thermo Scientific). For the peptide competition assay, fifty fold molar excess of the modified and unmodified peptides were added to the antibody solution and mixed for 3 hrs at $4^{o}C$ before addition to the blot.

2.2.10 Preparation of meiotic spreads from testicular cells

Meiotic spreads were prepared using the published protocol (Peters et al., 1997). Briefly, testes were decapsulated and chopped in PBS solution (pH 7.4). The cell pellet was resuspended in hypotonic buffer (30mM Tris, 17mM sodium citrate, 50mM sucrose, 5mM EDTA, 0.5mM DTT, protease inhibitor cocktail) and incubated for 30 minutes. The pellet was then resuspended in 100mM sucrose solution, and the nuclei were spread onto PFA-coated slides. The slides were kept for drying at room temperature for 2 hours and proceeded for immunofluorescence studies.

2.2.11 Immunofluorescence studies and Colocalization analyses

The slides were kept in blocking solution (3% BSA solution in PBS) for 1 hour at room temperature. The slides were then treated with primary antibody overnight in the cold room, washed with 0.1% PBST solution and then incubated with secondary antibody for 1 hr at room temperature. Next, washes were given with 0.1% PBST solution and the smears were mounted using DAPI solution (prepared in 80% glycerol). Images were acquired by Zeiss

confocal laser scanning microscope (LSM880 or LSM510). Zen software was used for preparation of figures.

Pearson Correlation Coefficient was computed to determine the overlap between the two channels. To evaluate specific colocalization, using ImageJ (Fiji) software, we rotated the red channel in the images by 90 degrees in the anticlockwise direction in the XY plane (Dunn et al., 2011; Parvanov et al., 2017). Pearson Correlation Coefficient was computed to evaluate colocalization percentages upon rotation of images captured in the red channel. Colocalization percentages were calculated multiplying the Pearson Correlation Coefficient by 100. All data were confirmed with at least three independent meiotic spread preparations from mice and rats.

2.2.12 Isolation of mononucleosomes

Immunoprecipitation using mononucleosomes were carried out as described (Montellier et al., 2013). Briefly, mouse testes were dissected and homogenised in lysis buffer (60mM KCl, 15mM NaCl, 15mM Tris-HCl, 0.03% Triton-X-100, 0.34M Sucrose, 2mM EDTA, 0.5mM EGTA, 0.65mM spermidine, 1mM DTT, 1% glycerol, protease and phosphatase inhibitor cocktail), centrifuged at 650 X g for 10 min at 4^{O}C. The pellet was washed with wash buffer containing 60mM KCl, 15mM NaCl, 15mM Tris-HCl, 0.34M Sucrose, 0.5mM EGTA, 1mM DTT, 0.5mM PMSF and protease and phosphatase inhibitor cocktail. The pellet was resuspended in MNase buffer (10mM Tris-HCl, 10mM KCl, and 2mM $CaCl_2$). MNase enzyme digestion was carried out for 20 min to obtain homogenous preparation of mononucleosomes. The nucleosome fraction was isolated by centrifugation at 650 X g for 10 min at 4^{o}C, mixed with LSDB250 buffer (20% glycerol, 50mM HEPES, 3mM $MgCl_2$, 250mM KCl, protease and phosphatase inhibitor cocktail) and proceeded with the immunoprecipitation protocol.

2.2.13 ChIP-sequencing of TH2BS11ph-associated chromatin in P20 and P12 mouse testicular cells

DNA was isolated from the immunoprecipitated TH2BS11ph-mononucleosomes by the phenol-chloroform method. The quality control of the DNA samples was checked by using the Qubit and Tapestation methods. The libraries were prepared using the NEBNext Ultra DNA Library prep kit. The libraries were subjected for 40 million depth paired-end (100 bp x 2) sequencing that was carried using Illumina HiSeq 2500. FASTQ files were obtained and data analyses were carried out further.

2.2.14 Data Analysis

FASTQ files were aligned to mm10 genome assembly using Bowtie2 (Langmead and Salzberg, 2012). While aligning, unpaired and discordant reads were removed. The aligned files were sorted and indexed accordingly, and also made free from PCR duplicates. On average for all samples read-alignment rate appeared to be higher than 70%. Principal Component Analysis (PCA) was performed to evaluate the correlation between the aligned samples of each condition. The sorted aligned replicates of background TH2B and antibody treated (IP) TH2BS11ph IP were merged respectively using Samtools Merge (Powers et al., 2016). Unique peaks were obtained by performing the peak calling of TH2BS11ph data against the published TH2B ChIP seq data. The peaks were called between the control and IP files using SICER 1.1 Version (Xu et al., 2014) with the following parameters- Redundancy threshold: 1; Window size: 200bp; Fragment size: 150bp; Gap size: 600bp; FDR: 0.01. The final peaks were shortlisted giving the cutoff of >1.5 fold change. The ChIP-sequencing dataset containing the raw and processed files have been deposited in the Gene Expression Omnibus (Accession Number- GSE135209) (Annexure 1 and Annexure 2).

2.2.15 Aggregation plot

ngs.plot.r was used to plot read count per million mapped reads for each ChIP samples (P20 TH2BS11ph, background TH2B, P12 TH2BS11ph) individually against the genome-wide coordinates of the following datasets – Total H3K4me3, common H3K4me3, transcription specific H3K4me3, TSS, and Total hotspots (Table 2.2). Furthermore, ngs.plot.r was also used to plot $\log_2$(Fold change vs. Control) of in-house ChIP-seq sample (P20 TH2BS11ph) over the TH2B dataset for each of the following genome-wide coordinates of Total H3K4me3, common H3K4me3, transcription specific H3K4me3 (H3K4me3 common), TSS, and Total DSB hotspots.

2.2.16 Primer design for ChIP-PCR studies

Peak summits corresponding to high TH2BS11ph occupancy were chosen for experimental validation using ChIP-PCR. In order to maintain the rigour of primer design, primers were designed using the Primer BLAST and primer 3 tools. These primers were also verified computationally using NCBI Primer Blast and UCSC In-silico PCR tools. Verification of primer-dimer formation were also considered during the design. Primers used for ChIP-PCR are listed in Annexure 3.

2.2.17 Immunoprecipitation and Quantitative PCR

The mononucleosome fraction was incubated with either anti-γH2AX (Upsate, 05-636) or anti-H3K4me3(Abcam, ab12209) or anti-TH2BS11ph for overnight at 4^{o}C. Protein A or Protein G dynabeads were added the next day and washed with Buffer C (with 150mM NaCl) for ChIP. LSDB250 buffer was used as the wash buffer for immunoprecipitation studies with mononucleosomes. After the washes, the beads were either proceeded with DNA extraction for PCR analysis or boiled in 5X SDS dye for western blotting. After washing of beads, DNA was eluted from the beads as follows- 210 µl of the elution buffer was added and incubated at 65^{o}C overnight for de-crosslinking. 200 µl of TE buffer was added the next day, subjected for RNase (Final; 40µg/ml) and proteinase K (Final; 100µg/ml) treatment and DNA were extracted by the phenol-chloroform method. DNA that was purified from TH2BS11ph ChIP were proceeded for ChIP-seq analyses. SYBR kit from TAKARA was used to set up quantitative PCR reactions. PCR was carried out for 40 cycles and was followed by melt curve analyses before recording the raw Ct values. The fold enrichment values were calculated over input taking the percentage of input used for the ChIP procedure and the Ct values obtained for the target genomic region from Input and ChIP DNA. PCR was carried out in duplicates for each of the three biological replicates.

Fold Enrichment over Input = % of Input X 2^{Ct (Input)- Ct (ChIP)}

Reagents				
Antibodies-	**Host**	**Company Name**	**Cat number**	**Application**
Scp3	Mouse	Abcam	ab97672	IF
γH2AX	Mouse	Upstate (Millipore)	05-636	IF, ChIP, WB
H2BS14P	Rabbit	Scbt	sc31671	WB
pATM	Mouse	Upstate (Millipore)	05-740	IF
ATR	Mouse	Abcam	ab54793	IF
H3K4me3	Mouse	Abcam	ab12209	ChIP, WB
TH2B	Rabbit	Generated in house		IF, WB

Rad51	Mouse	Abcam	ab1837	IF
Spo11	Goat	Santa Cruz	sc22476	IF

IF immunofluorescence; *ChIP* chromatin immunoprecipitation, *WB* western blotting

Table 2.1- List of antibodies used in the present study

2.2.18 Mass spectrometric identification of proteins associated with TH2BS11ph-containing mononucleosomes

Immunoprecipitation of TH2BS11ph-containing proteins was carried out and the proteins were extracted from the beads using the elution buffer of the Pierce co-IP kit. The eluted proteins were resolved on 15% SDS gel and the gel was subjected to Coomassie staining. The stained gel pieces corresponding to the IgG and IP lanes (2 samples each of IgG and ChIP) were outsourced for mass spectrometry to identify the associated proteins.

(i) Methods for Protein Sequence Analysis by LC-MS/MS

Excised gel bands were cut into approximately 1 mm^3 pieces. Gel pieces were then subjected to a modified in-gel trypsin digestion procedure (Shevchenko et al., 1996). Gel pieces were washed and dehydrated with acetonitrile for 10 min. followed by removal of acetonitrile. Gel pieces were then completely dried in a speed-vac. Rehydration was done with 50 mM ammonium bicarbonate solution containing 12.5 ng/µl modified sequencing-grade trypsin (Promega, Madison, WI) at 4ºC. After 45 min., the excess trypsin solution was removed and replaced with 50 mM ammonium bicarbonate solution to just cover the gel pieces. Samples were then placed in 37ºC overnight. Peptides were later extracted by removing the ammonium bicarbonate solution, followed by one wash with a solution containing 50% acetonitrile and 1% formic acid. The extracts were then dried in a speed-vac (~1 hr). The samples were then stored at 4ºC until analysis.

On the day of analysis, the samples were reconstituted in 5 - 10 µl of HPLC solvent A (2.5% acetonitrile, 0.1% formic acid). A nano-scale reverse-phase HPLC capillary column was created by packing 2.6 µm C18 spherical silica beads into a fused silica capillary (100 µm inner diameter x ~30 cm length) with a flame-drawn tip (Peng and Gygi, 2001). After equilibrating the column each sample was loaded via a Famos auto sampler (LC Packings, San Francisco CA) onto the column. A gradient was formed and peptides were eluted with increasing concentrations of solvent B (97.5% acetonitrile, 0.1% formic acid).

As peptides eluted, they were subjected to electrospray ionization and then entered into an LTQ Orbitrap Velos Pro ion-trap mass spectrometer (Thermo Fisher Scientific, Waltham, MA). Peptides were detected, isolated, and fragmented to produce a tandem mass spectrum of specific fragment ions for each peptide. Peptide sequences (and hence protein identity) were determined by matching protein databases with the acquired fragmentation pattern by the software program, Sequest (Thermo Fisher Scientific, Waltham, MA) (Eng et al., 1994). All databases include a reversed version of all the sequences and the data was filtered to between a one and two percent peptide false discovery rate along with filter to being set to at least 1 unique peptide per protein. The table of proteins obtained in the mass spectrometry dataset are given in Annexure 4.

2.3 Results

2.3.1 Mass spectrometry and discovery of TH2BS11ph modification

By employing a different set of procedures that include single-enzyme digestion and post mass spectrometry analyses, we discovered Serine 11 phosphorylation on TH2B (TH2BS11ph according to Brno system for histone modifications) (Fig 2.2B, 2.2D). We observed the abundance of the TH2BS11ph modification to be 6.73% in spermatocyte TH2B. We also observed this specific serine residue to be solvent-exposed in the TH2B-containing nucleosome model as the case with N-terminal tails of core histones (Fig 2.2B). This serine residue is conserved across rodents and humans (Fig 2.2C), indicating that this modification might have an important function(s) in germ cells. The representative MS/MS plot is given in Fig 2.2D. TH2BS11ph modification was earlier identified on TH2B derived from round spermatid cell populations (Luense et al., 2016). We have detected this modification for the first time on spermatocyte TH2B. The somatic H2BS14ph has been shown to be involved in DNA repair in somatic cells (Fernandez-Capetillo et al., 2004). Histone phosphorylation has been linked to various biological processes like DDR response, meiosis/mitosis, apoptosis, transcription etc (Loury and Sassone-Corsi, 2003). Therefore, we were interested in ascertaining the biological function of the TH2BS11ph histone mark in the context of processes related to spermatocyte biology.

2.3.2 Validation of TH2BS11ph antibodies

To determine the biological functions of the TH2BS11ph histone mark, we first generated TH2BS11ph-specific antibodies in rabbits. We validated the reactivity of TH2BS11ph antibodies by multiple assays: ELISA, dot-blot, western blotting, and peptide competition

assays. By use of ELISA assays, we demonstrate that TH2BS11ph antibodies showed specific reactivity towards TH2B Serine 11 phosphopeptide but did not crossreact with the TH2B or H2B unmodified peptides (Figure 2.2E). The antibodies showed specific reactivity with TH2B-containing testis nuclear lysate but did not react with the H2B-containing liver nuclear lysate or the recombinant TH2B (Figure 2.2F). Further, the reactivity of the antibodies was specifically blocked with the prior addition of TH2B Serine 11 phosphopeptide but not with the addition of no peptide or TH2B unmodified peptide (Figure 2.2G). By all these assays, we demonstrate the specificity of TH2BS11ph antibodies towards TH2BS11ph modification.

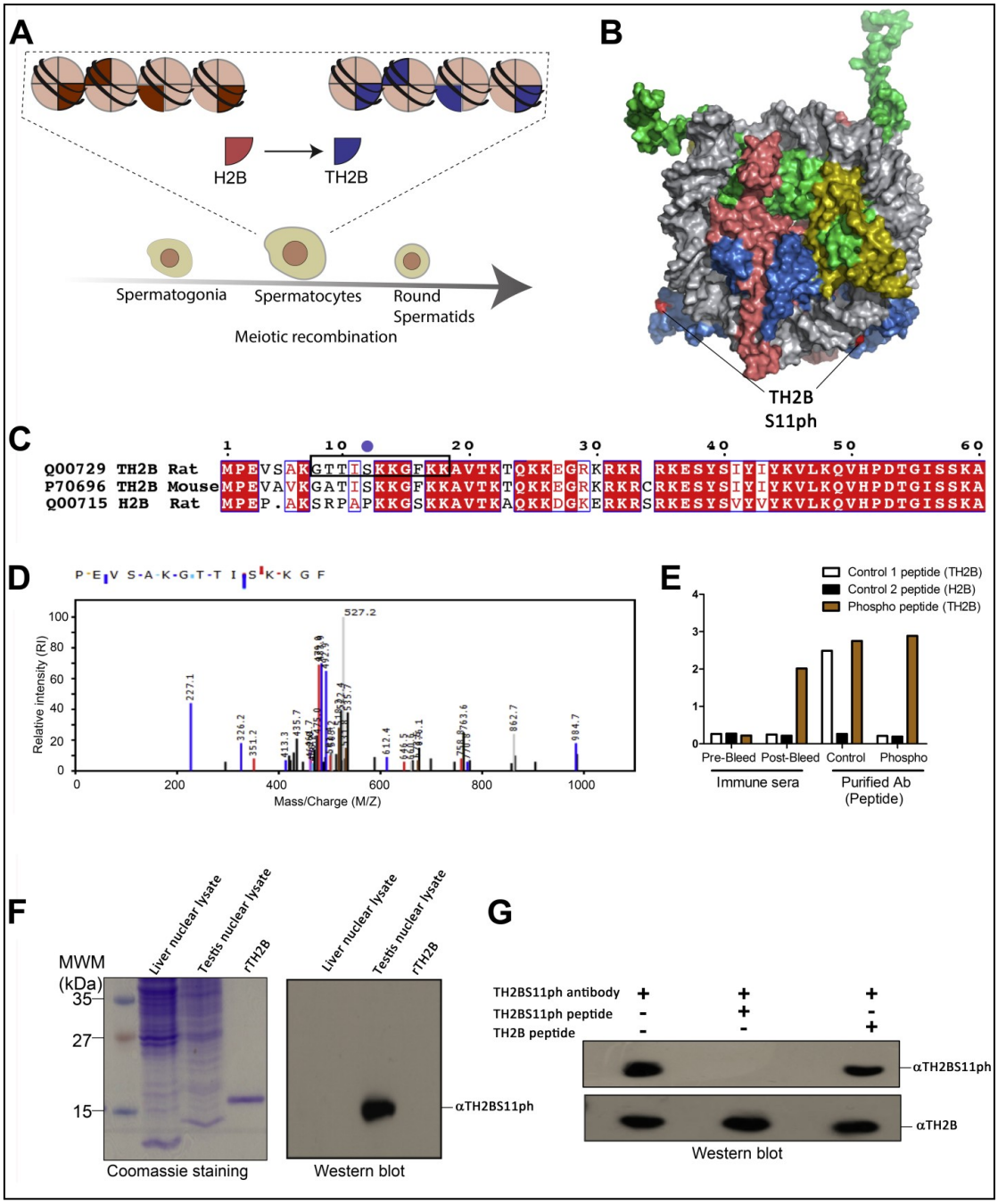

Figure 2.2- Identification of TH2BS11ph modification by mass spectrometry and validation of TH2BS11ph antibody

***A**- Genome-wide replacement of H2B by TH2B in mammalian spermatocytes and spermatids (Montellier et al., 2013).*

***B**- Model of TH2B-containing nucleosome highlighting the solvent-exposed serine 11 residue.*

***D**- Identification of TH2BS11ph modification by LC-MS/MS technique. The y-axis depicts the relative intensity of MS/MS spectra and the x-axis indicates the e/m ratio (mass to charge ratio). The phosphorylated serine residue of the TH2B containing peptide is highlighted in red.*

***E**- ELISA assay- The backbone TH2B antibody reacts with both the TH2B and TH2B serine 11 phosphopeptides, whereas the TH2BS11ph antibody reacts with only TH2B serine 11 phosphopeptide. The white bars represent the reactivity of mentioned sera or antibody with the TH2B backbone peptide; the black bars represent the reactivity with the H2B peptide, whereas the orange bars represent the reactivity with the TH2B serine 11 phosphopeptide. The data plotted is the average of the two experiments.*

***F**- Immunoblotting of the purified TH2BS11ph antibody showing the reactivity with only TH2B containing testis nuclear lysate, Western blotting was performed with anti-TH2BS11ph antibody against liver nuclear lysates, testis nuclear lysates and recombinant TH2B (rTH2B). Coomassie blue-stained gel is given on the left for reference.*

***G**- Peptide competition assay- The reactivity of the TH2BS11ph antibody is blocked by the addition of TH2B serine 11 phosphopeptide, but not with the addition of TH2B backbone peptide or addition of no peptide. The first lane represents no peptide control, the second lane TH2BS11ph antibody preincubated with TH2B serine 11 phosphopeptide, third lane TH2BS11ph antibody preincubated with the backbone TH2B peptide.*

2.3.3 Immunostaining pattern of TH2BS11ph across leptotene, zygotene and pachytene intervals of meiotic prophase I

To understand the biological functions of TH2BS11ph modification, we first determined the localization pattern of TH2BS11ph and TH2B during leptotene, zygotene and pachytene intervals of meiotic prophase I. As explained earlier, TH2B is the dominant histone variant in spermatocytes and spermatids. We have used Scp3 and γH2AX as markers to distinguish various stages of meiotic prophase I (Chi et al., 2009). It is interesting to note that backbone TH2B is detected all over the nucleus (Fig 2.3a), while TH2BS11ph signal was more

distributed as specific loci (Fig 2.3b). This suggests that TH2BS11ph may have a locus-dependent function. An interesting observation that was apparent from the staining pattern of TH2BS11ph histone mark in pachytene spermatocytes was that TH2BS11ph was found to be enriched in the axes of the XY body (Fig 2.3b, pachytene). This was further corroborated by colocalization analysis as represented in Fig 2.4, Scp3, which revealed that TH2BS11ph colocalizes with the Scp3 in the XY body. We found a higher colocalization percentage of TH2BS11ph and Scp3 of about 47% in the XY body compared to 14% in the whole pachytene spermatocyte (Fig 2.4, Scp3, pachytene wo rotation, XY body wo rotation). To evaluate the specificity of colocalization and to ensure that the observed signal is not a result of random overlap, we performed colocalization analysis after rotating images captured in the red channel by 90 degrees in the anticlockwise direction. A significant decrease in colocalization percentages with usage of rotated images in comparison to non-rotated images would mean specific colocalization between the two channels (Dunn et al., 2011; Parvanov et al., 2017). On rotation of the TH2BS11ph images captured in the red channel, we found that the colocalization percentage between TH2BS11ph and Scp3 decreased significantly in the XY body (Fig 2.4, Scp3, pachytene w rotation, XY body w rotation). This indicates that TH2BS11ph is highly enriched in the axes of the XY body of the pachytene spermatocyte. Therefore we conjectured that this modification may have a XY body-specific function in spermatocytes.

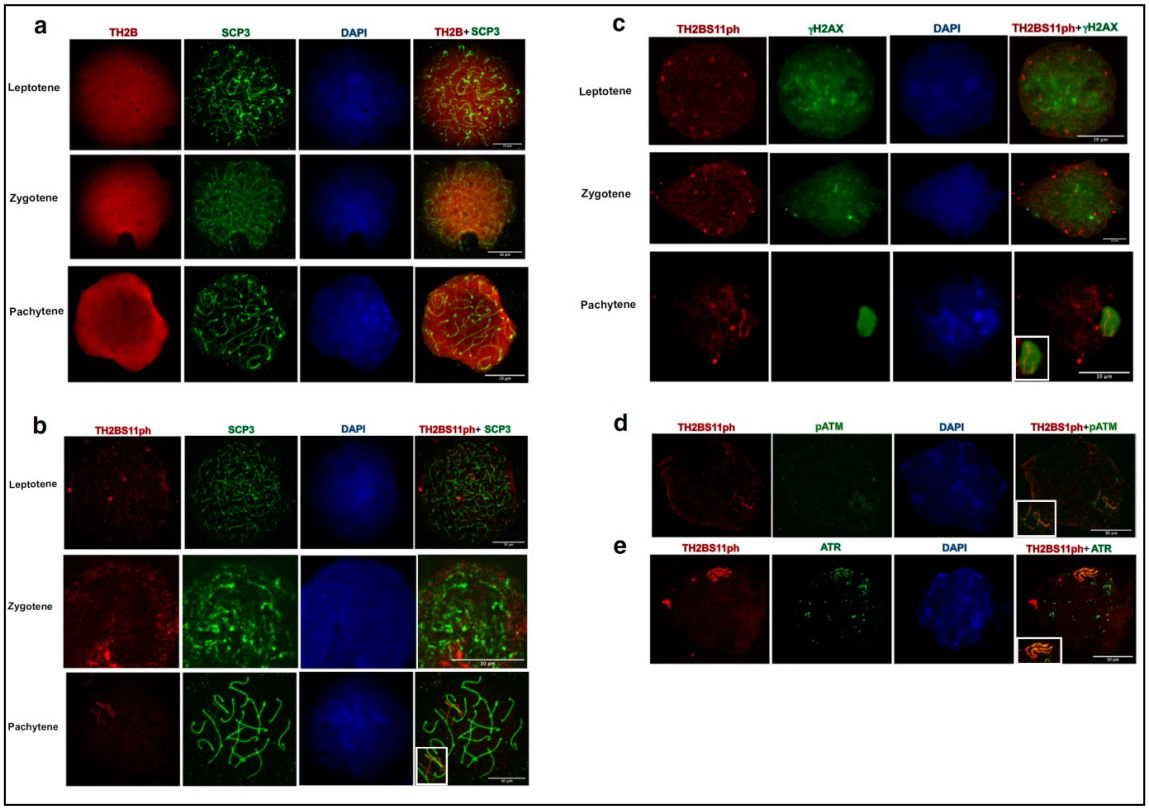

Figure 2.3- TH2BS11ph modification is densely localized in the unsynapsed axes of the XY body

***a**- Immunostaining pattern of backbone TH2B across leptotene (1st panel), zygotene (2nd panel) and pachytene (3rd panel) intervals of meiotic prophase I.*

***b**- Colocalization studies of TH2BS11ph modification with synaptonemal complex protein Scp3 in leptotene (1st panel), zygotene (2nd panel) and pachytene (3rd panel) intervals of meiotic prophase I.*

***c**- Colocalization studies of TH2BS11ph modification with sex body marker γH2AX in leptotene (1st panel), zygotene (2nd panel) and pachytene (3rd panel) intervals of meiotic prophase I.*

*Immunofluorescence studies of TH2BS11ph with **d-** pATM and **e-** ATR in pachytene spermatocytes. The inset shows the XY body.*

*Data information in **(a-e)**- All data was confirmed with at least three independent mice. Nuclei were visualized by DAPI staining. Scale bars, 10μm.*

To further substantiate whether the observed enrichment was in the XY body, we performed colocalization studies with XY body-specific marker γH2AX across stages of meiotic prophase I. H2AX is required for chromatin remodeling and sex chromosome inactivation in male meiosis (Fernandez-Capetillo et al., 2003). We confirmed the enrichment and localization of TH2BS11ph histone mark in the XY body of the pachytene nucleus using the sex body-specific marker γH2AX. We observed that TH2BS11ph colocalizes with γH2AX corresponding to the axes of the XY body as can be seen in Fig 2.3c. The percentage of colocalization of TH2BS11ph with γH2AX was found to be 21% in the XY body as opposed ~11% in the whole pachytene spermatocyte (Fig 2.4, γH2AX, pachytene wo rotation and XY body wo rotation). It is to be noted from Fig 2.1, that γH2AX has a different staining pattern compared to TH2BS11ph. γH2AX is localised in the axes plus loops of the XY body, whereas TH2BS11ph immunostains only the axes of the XY body. This might be the reason for lower colocalization percentages between TH2BS11ph and γH2AX in the XY body. On rotation of TH2BS11ph images captured in the red channel, we found colocalization percentages to decrease significantly in comparison with the non-rotated images (Fig 2.4, γH2AX, XY body w rotation, pachytene w rotation). Based on colocalization observed with Scp3 and γH2AX, we conclude that TH2BS11ph is densely localised in the axes of the XY body.

2.3.4 Colocalization studies of TH2BS11ph with Scp3, γH2AX, pATM and ATR

Immunofluorescence studies established the fact that TH2BS11ph is enriched in the axes of the XY body of pachytene spermatocyte. To examine the specific localized association of this modification within the XY body, we performed colocalization studies with kinases pATM and ATR, both of which are markers of unsynapsed axes of the XY body (Already explained in Figure 2.1).

Colocalization studies were carried out to determine the association of unsynapsed axis marker pATM kinase with TH2BS11ph histone mark. There was a distinct colocalization seen specifically in the axes of the XY body as seen in Fig 2.3d. We also quantified the colocalization percentages between TH2BS11ph and pATM, where we found a high colocalization percentage of about 35% in the XY body (Fig 2.4, XY body wo rotation). The colocalization percentages decreased significantly on rotation of the TH2BS11ph images captured in the red channel (Fig 2.4, pATM, pachytene w rotation, XY body w rotation).

In the mid-zygotene interval, unsynapsed chromosomes are marked by ATR, where the latter carries out the second level of H2AX phosphorylation (Royo et al., 2013). We observe colocalization with XY body specific kinase ATR in axes of the XY body as can be seen in Fig 2.3e. Upon further quantitative analyses, we observe colocalization with ATR of about 43% corresponding to the axes of the XY body, as indicated in Fig 2.4, ATR, XY body wo rotation. On rotation of the TH2BS11ph images captured in the red channel, the colocalization percentage decreased significantly suggesting the specific overlap of TH2BS11ph and ATR in the axes of the XY body in the non-rotated images (Fig 2.4, ATR, XY w rotation).

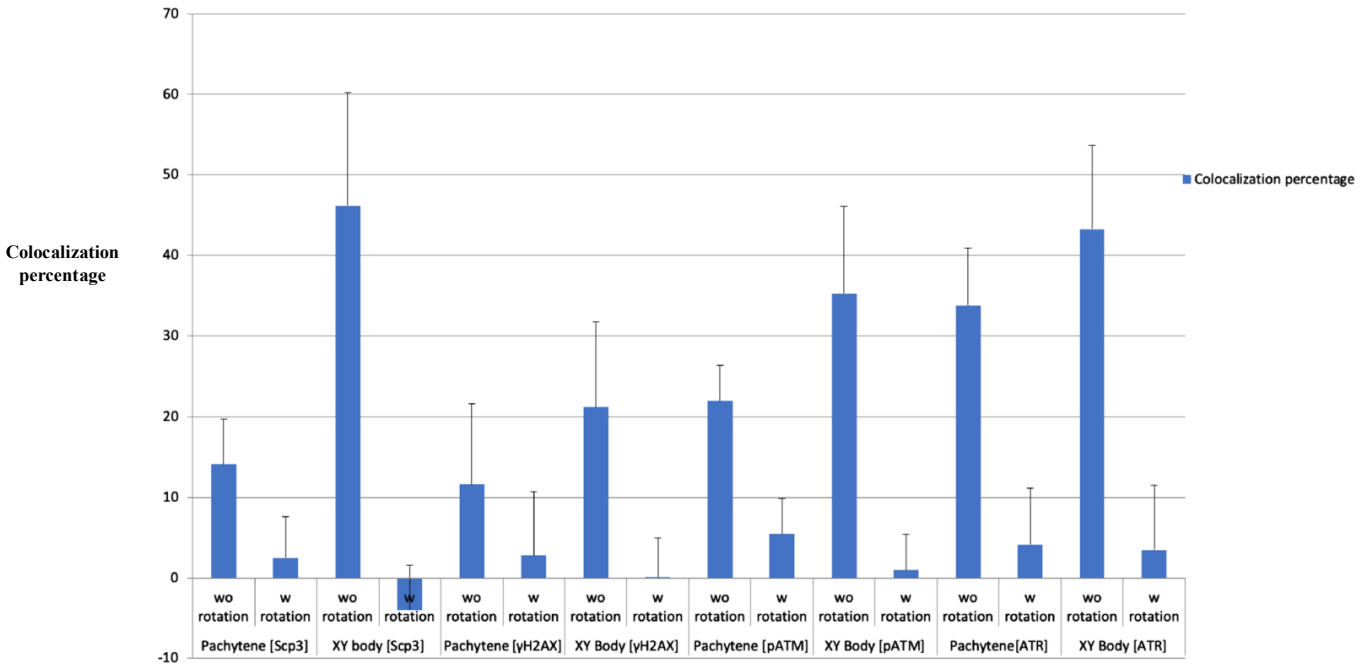

Figure 2.4- Colocalization percentages of TH2BS11ph with proteins Scp3, H2AX, pATM and ATR in XY body and whole pachytene spermatocytes

*The colocalization percentages were evaluated with (w rotation) and without (wo rotation) image rotation. Pearson correlation coefficients were calculated to determine the significance of colocalization. For calculation of colocalization percentages, the TH2BS11ph images captured in the red channel were rotated by 90^{o} in the anticlockwise direction in the XY plane. The number of nuclei analysed are Scp3 (n=10), γH2AX (n=15), pATM (n=15) and ATR (n=15). w rotation- with image rotation; wo rotation- without image rotation. The data are plotted in terms of mean +/- SD. ***P<=0.0005; P<=0.005; P<=0.05.*

2.3.5 Characterization of commercial H2BS14ph and in-house H2B antibodies

H2BS14ph modification was previously reported to be localized in the XY body of pachytene spermatocyte (Fernandez-Capetillo et al., 2004). Since these results were contrasting with our result of enriched localization of TH2BS11ph in the XY body, we wanted to first determine the staining pattern of H2B/H2BS14ph during the stages of meiotic prophase I. Dot-blot experiments further showed that the TH2BS11ph antibody specifically reacted with the TH2B serine 11 phosphopeptide but not with TH2B, H2B or H2BS14P specific peptides (Figure 2.5a), strongly supporting our earlier observations.

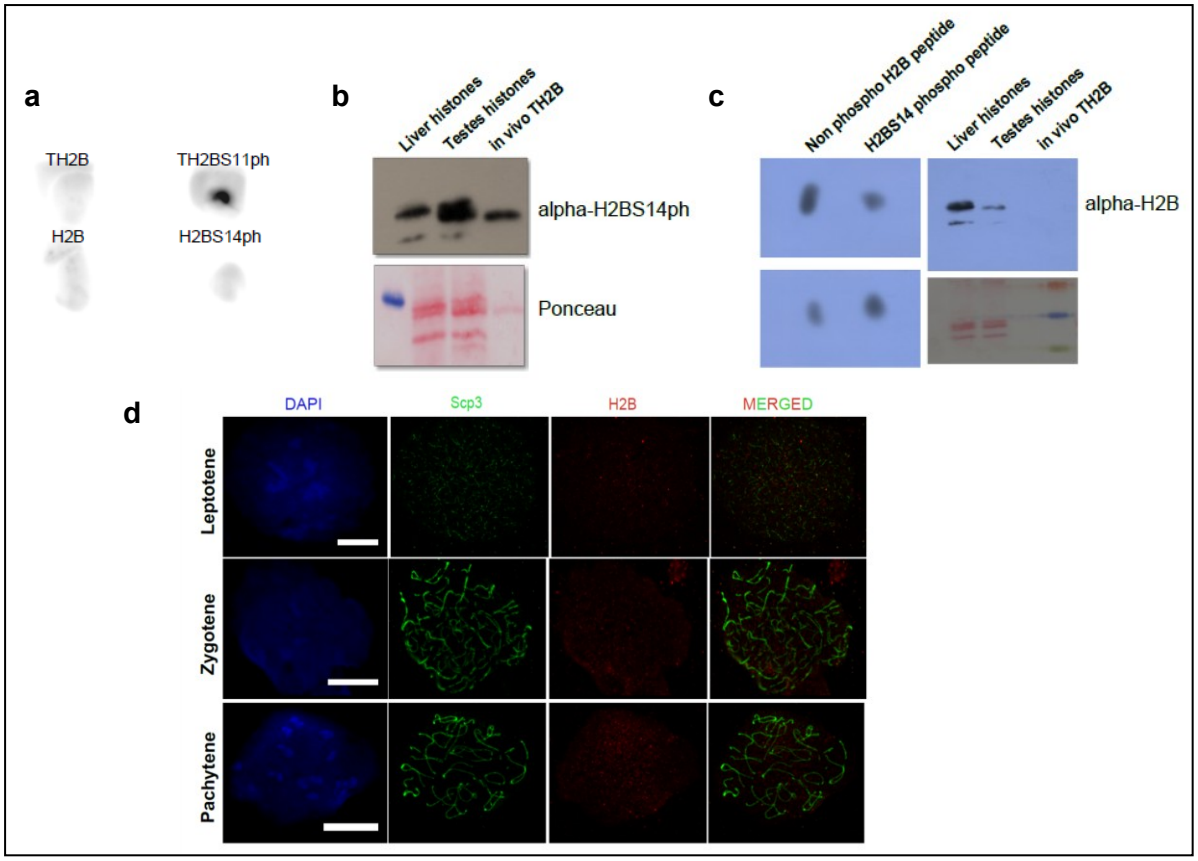

Figure 2.5- a- *Dot blot assay showing the specificity of TH2BS11ph antibody towards the TH2B serine 11 phosphopeptide, but the antibody does not crossreact with the TH2B backbone, H2B backbone and H2B serine 14 phosphopeptides.*

b- *Specificity of the commercial H2BS14ph antibody- The first lane represents the reactivity with liver histones, second lane testis histones and the third lane purified in vivo TH2B. This antibody cross-reacts with TH2B as can be seen by its reactivity against testis histones and in vivo TH2B.*

c- *First panel- Immunoblotting of the in house generated H2B antibody as shown by dot blot against backbone H2B and H2B serine 14 phosphorylated peptides- The antibody reacts to both H2B and H2B phosphopeptides.*

Second panel- Immunoblotting against liver histones, testis histones and recombinant TH2B.

First, we validated the reactivity of commercial H2BS14ph antibody used in the previous publication, and found that the antibody cross-reacts with TH2B (Fig 2.5b, *in vivo* TH2B). The antibody has been withdrawn from the company and no more available. This prompted us to generate a H2B-specific antibody in the laboratory. We validated the reactivity of the antibody and observed specific reactivity to H2B-containing liver nuclear lysate (Fig 2.5c, second panel). The levels of H2B are lower in P20 testis that are enriched in spermatocyte

populations, which might be the cause of their low reactivity against testis histones. When we determined the staining pattern of H2B, we observed H2B to not stain the XY body (Fig 2.5d, pachytene). Apart from this, the staining pattern was found to be not dense as previously reported. Therefore, the reported staining pattern of H2BS14ph to be localized in the XY body is possibly an artifact and a result of cross-reactivity with TH2B. These observations are in good agreement with data from Montellier *et al* (Montellier et al., 2013), where they observed levels of H2B to drop from 16 dpp onwards, which corresponds to the onset of differentiation to pachytene spermatocytes. Nevertheless, the combination of Western blotting with peptide competition, and ELISA assays prove that the TH2BS11ph antibody does not cross-react with H2B, further negating the previous report where H2BS14P was shown to localize to the XY body.

2.3.6 Colocalization studies of TH2BS11ph with Scp3, γH2AX, pATM, Spo11 and Rad51 in rat spermatocytes

The above data suggested TH2BS11ph modification is densely localized in the unsynapsed axes of the XY body. These observations were also reproducible in meiotic spreads made from rat testicular cells, where we observed enriched localization of this modification in the XY body of rat pachytene spermatocytes. We observed colocalization with XY body proteins Scp3, γH2AX, pATM, Spo11, and Rad51 as can be seen in Figure 2.6 A-E, respectively.

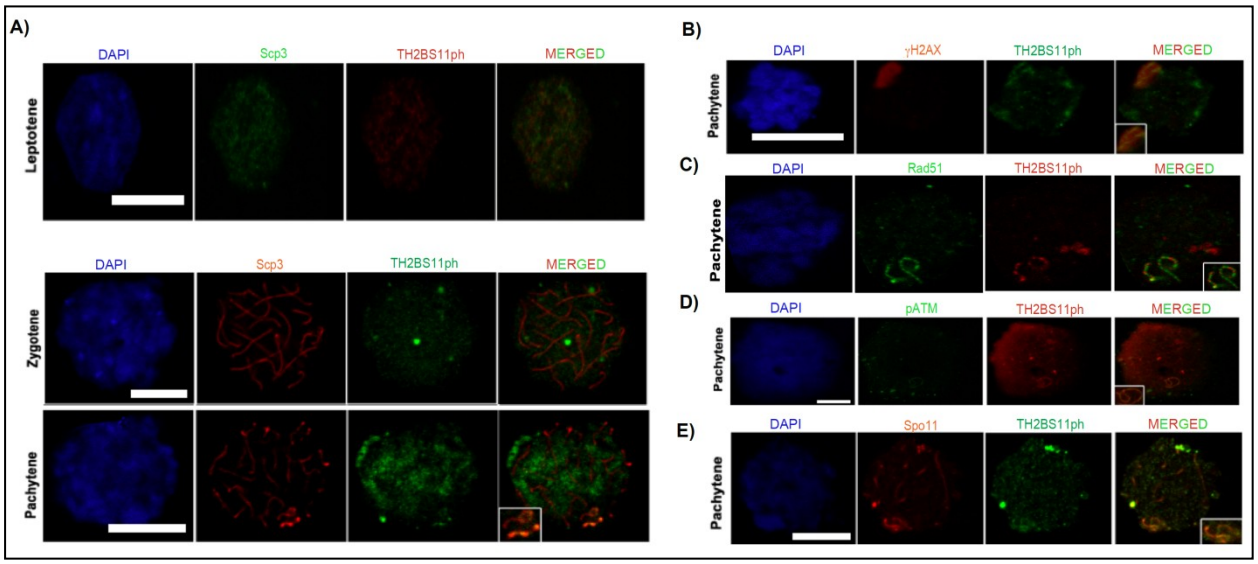

Figure 2.6- Immunofluorescence studies of TH2BS11ph modification with proteins Scp3, γH2AX, Rad51, pATM and Spo11 in meiotic spreads made from rat testicular cells

A) *Immunofluorescence studies of TH2BS11ph modification with Scp3 across leptotene (1st panel), zygotene (2nd panel) and pachytene intervals (3rd panel) in rat spermatocytes. Colocalization studies of TH2BS11ph histone mark with* ***B)*** *Scp3,* ***C)*** *Rad51,* ***D)*** *pATM and* ***E)*** *Spo11, a clear colocalization observed in the axes of the XY body.*
(A-E) *The inset in all the pachytene images shows the XY body. All data were confirmed with at least three independent rats. Nuclei were visualized by DAPI staining. Scale bars, 10 µm.*

2.3.7 Co-association of TH2BS11ph and γH2AX

We observed that TH2BS11ph is associated with sex body proteins γH2AX, pATM and ATR as demonstrated by immunofluorescence studies. We were interested in supporting the cytological data further by performing biochemical assays like co-IP, to determine whether TH2BS11ph and γH2AX co-associate in mononucleosomes. We performed micrococcal nuclease (MNase) digestion followed by immunoprecipitation assays to determine whether these two histone marks coexist *in vivo*.

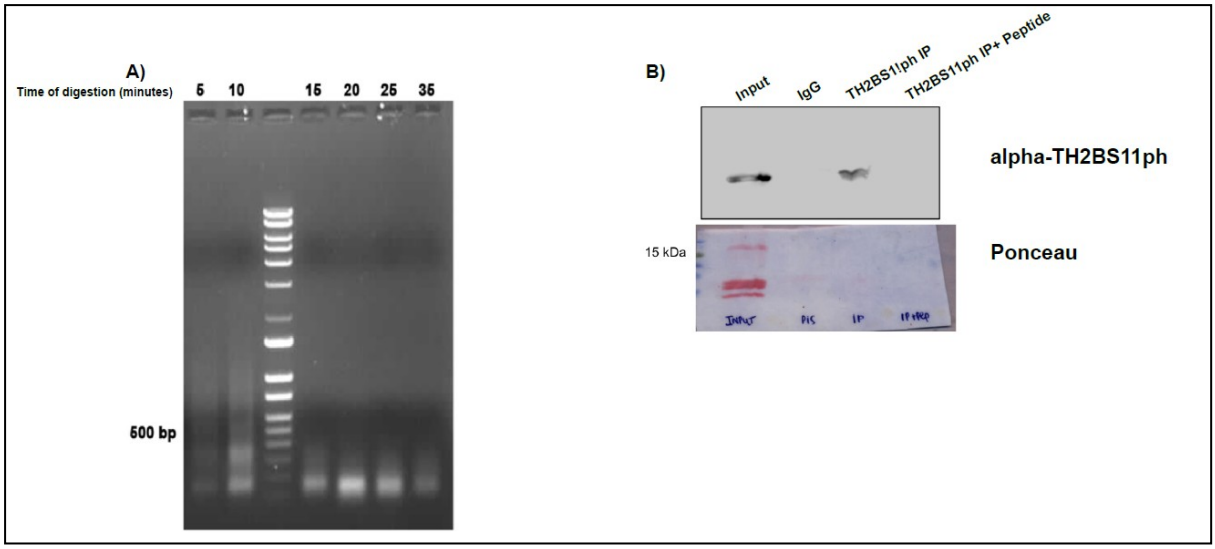

Figure 2.7- A. *Profile of DNA fragments obtained after various time points of MNase digestion of chromatin of mouse testicular cells*
B. *Specificity of TH2BS11ph antibody in the immunoprecipitation reaction- the first lane refers to the input fraction, second lane IP with the non-specific rabbit IgG; the third lane refers to the TH2BS11ph ChIP fraction whereas the fourth lane refers to TH2BS11ph ChIP carried out along with the addition of competing TH2B serine 11 phosphopeptide.*

We first isolated mononucleosomes by performing MNase digestion for 20 min to obtain homogenous preparation of mononucleosomes (Fig 2.7A). We have again revalidated the specificity of the TH2BS11ph antibody, wherein we observed that the TH2B serine 11 phosphopeptide competes with the antibody in the immunoprecipitation reaction (Fig 2.7B). We find that γH2AX is associated with TH2BS11ph IP elute fraction (Figure 2.8a, left panel). By reverse IP assays, we observed that TH2BS11ph is associated with γH2AX-containing mononucleosomes Figure 2.8a, right panel). These forward and reciprocal IP assays suggested that TH2BS11ph and γH2AX histone marks coexist in nucleosome core particles *in vivo*. This biochemical evidence supported by colocalization assays provides strong evidence to the fact that TH2BS11ph is associated with DNA repair domains of the XY body. This suggests that TH2BS11ph and γH2AX co-associate possibly to recruit similar set of proteins in turn to facilitate DSB processes in the XY body.

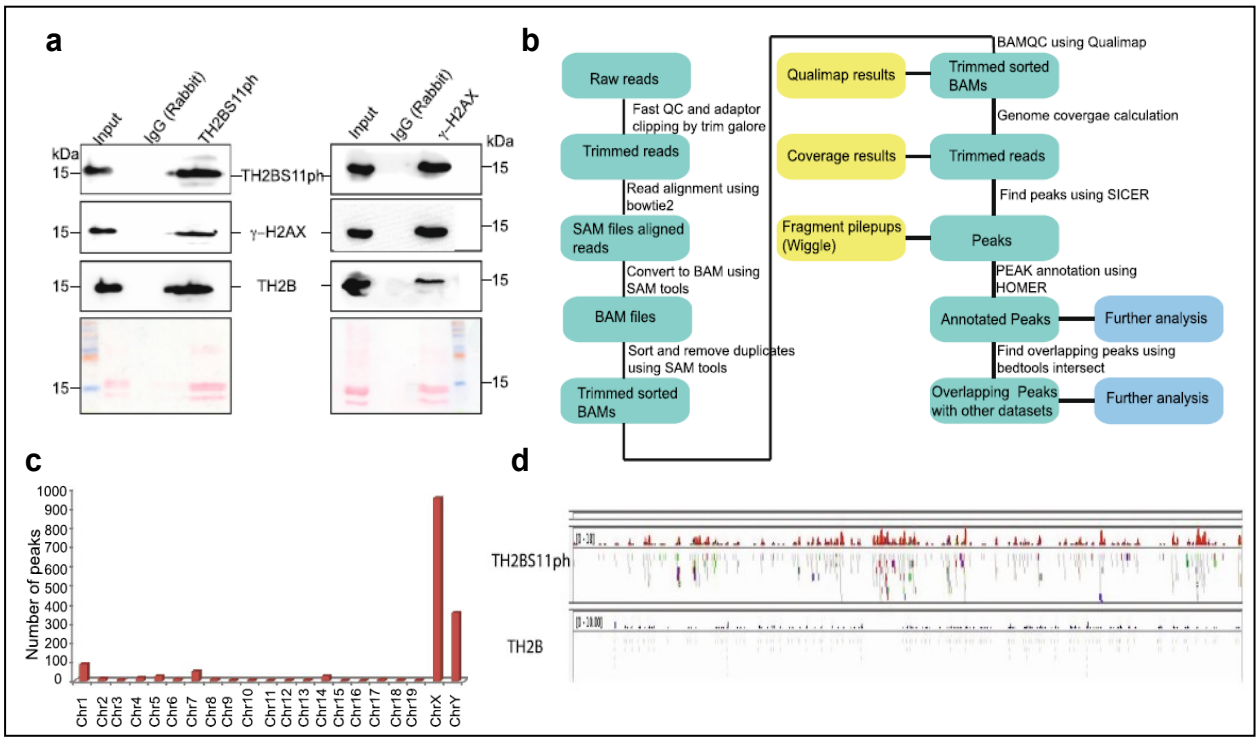

Figure 2.8- Association of TH2BS11ph modification with DNA repair domains of the XY body

a- *Co-association of TH2BS11ph with γH2AX histone mark in mononucleosomes*

Right panel- IP was carried out using the anti-TH2BS11ph antibody where γH2AX, TH2BS11ph and TH2B were probed by western blotting.

Left panel- Reciprocal IP was carried out using the γH2AX antibodies and the proteins TH2BS11ph, γH2AX, TH2B were scored by western blotting.

***b**- Workflow of the ChIP-sequencing analysis carried out for TH2BS11ph histone mark in P20 testicular cells*

***c**- Chromosome wise distribution of unique peaks of TH2BS11ph occupancy- the distribution of peaks were plotted after peak calling was performed for TH2BS11ph ChIP seq dataset against the published TH2B dataset.*

***d**- Distribution of TH2BS11ph and TH2B reads across the X-chromosome as observed in the IGV genome browser- The upper track represent the read distribution of the peaks corresponding to the TH2BS11ph IP, whereas the bottom track represents the read distribution of the TH2B IP. Below each of these tracks, the raw reads have also been shown in the figure. The read distribution have been plotted on the same scale for comparison.*

2.3.8 Genome-wide occupancy of TH2BS11ph modification in mouse P20 testicular cells

Our cytological and biochemical assays gave a clear indication of the association of TH2BS11ph modification with the DNA repair domains of the XY body. To obtain a comprehensive picture of the association of TH2BS11ph with genomic regions, we performed ChIP-sequencing to determine the genome-wide occupancy sites of TH2BS11ph in P20 mouse testicular cells that are enriched in pachytene cells. The workflow of the ChIP-sequencing protocol and computational analysis are given in Fig 2.8b. We used the already published TH2B ChIP seq dataset for comparison that was carried out in elutriation-purified spermatocyte populations representative of TH2B occupancy in pachytene cells (Montellier et al., 2013) (Table 2.2, TH2B). An important aim was to determine the unique peaks of TH2BS11ph occupancy compared to backbone TH2B occupancy. To address this, we performed peak calling of TH2BS11ph ChIP seq data against the backbone TH2B data to obtain the unique peaks of TH2BS11ph occupancy. The backbone TH2B hence referred to in the entire chapter represent the non-phosphorylated or unmodified TH2B serine 11 protein. As further support of increased staining of TH2BS11ph in the XY body, we also observed higher number of peaks in chromosomes X and Y (Fig 2.8c). As can be seen in Fig 2.8d, we observed higher number of reads of TH2BS11ph IP in chromosome X compared to backbone TH2B reads. These results provide additional support to the immunofluorescence data, wherein TH2BS11ph modification was found to be enriched over unmodified TH2B in the XY body.

To identify the important features of the genomic regions bound by TH2BS11ph histone mark, we next investigated the overlap of TH2BS11ph with characteristic histone mark signatures related to meiotic recombination and transcription processes. To address the

overlap between various datasets, we generated aggregation plots and heat maps to determine the localization of the reads with respect to the centre of the binding sites of the total H3K4me3 marks, recombination hotspot associated H3K4me3 (B6 specific H3K4me3) and transcription-associated H3K4me3 marks (common H3K4me3) (Table 2.2). Aggregation plots provide a visual representation of the read distribution at the respective genomic coordinates, for e.g., TSS, etc. Heat maps are generated for the corresponding aggregation plots, that address the spatial distribution of the reads within the region of interest.

Dataset	Geo Accession IDs
DSB Hotspots	GSE93955
TSS (of mouse)	GENCODE
H3K4me3	GSE35498
H3K4me3 common	GSE93955
H3K4me3 (B6 specific)	GSE93955
TH2B	GSE45915

Table 2.2- List of datasets used for computational data analyses

The table contains the list of ChIP-sequencing datasets along with their GEO (Gene Expression Omnibus) accession IDs used for analysis of overlap with TH2BS11ph ChIP-sequencing dataset.

All the analyses carried out as shown in Fig 2.9, have been generated for TH2BS11ph ChIP-seq dataset that has been compared against the backbone TH2B ChIP-seq dataset. Aggregation plot as given in Fig 2.9a, shows the majority of reads to be concentrated within 1kb from the centre of occupancy of total H3K4me3 marks (Table 2.2, H3K4me3). The heat maps corroborate with the fact that majority of TH2BS11ph reads were enriched over TH2B reads at the total H3K4me3-containing genomic regions. It is to be pointed out that H3K4me3 marks are present at both meiotic recombination hotspots and transcription start sites (TSS), both of which are catalyzed by different enzymes. Also, hotspots and TSS are distinctly located in the mouse genome (Brick et al., 2012). Therefore, we were interested in delineating whether TH2BS11ph histone mark is linked to hotspot-specific H3K4me3 or

TSS-specific H3K4me3 or both. With respect to DSB hotspots represented by C57BL6 mouse species-specific H3K4me3 marks (Table 2.2, DSB hotspots), we observed no significant overlap of TH2BS11ph reads at hotspots (Fig 2.9b). Further, this analysis revealed a close association of TH2BS11ph with TSS-associated H3K4me3 marks represented by common H3K4me3 (Table 2.2, H3K4me3 common) (Fig 2.9c). It is to be pointed out that H3K4me3 is a hallmark histone modification of active promoters, enhancers, etc. This was further supported wherein we observed close association of TH2BS11ph with TSS (Table 2.2, TSS (of mouse)) (Fig 2.9d). Therefore, the overlap of TH2BS11ph was specific to TSS and TSS-associated H3K4me3 marks.

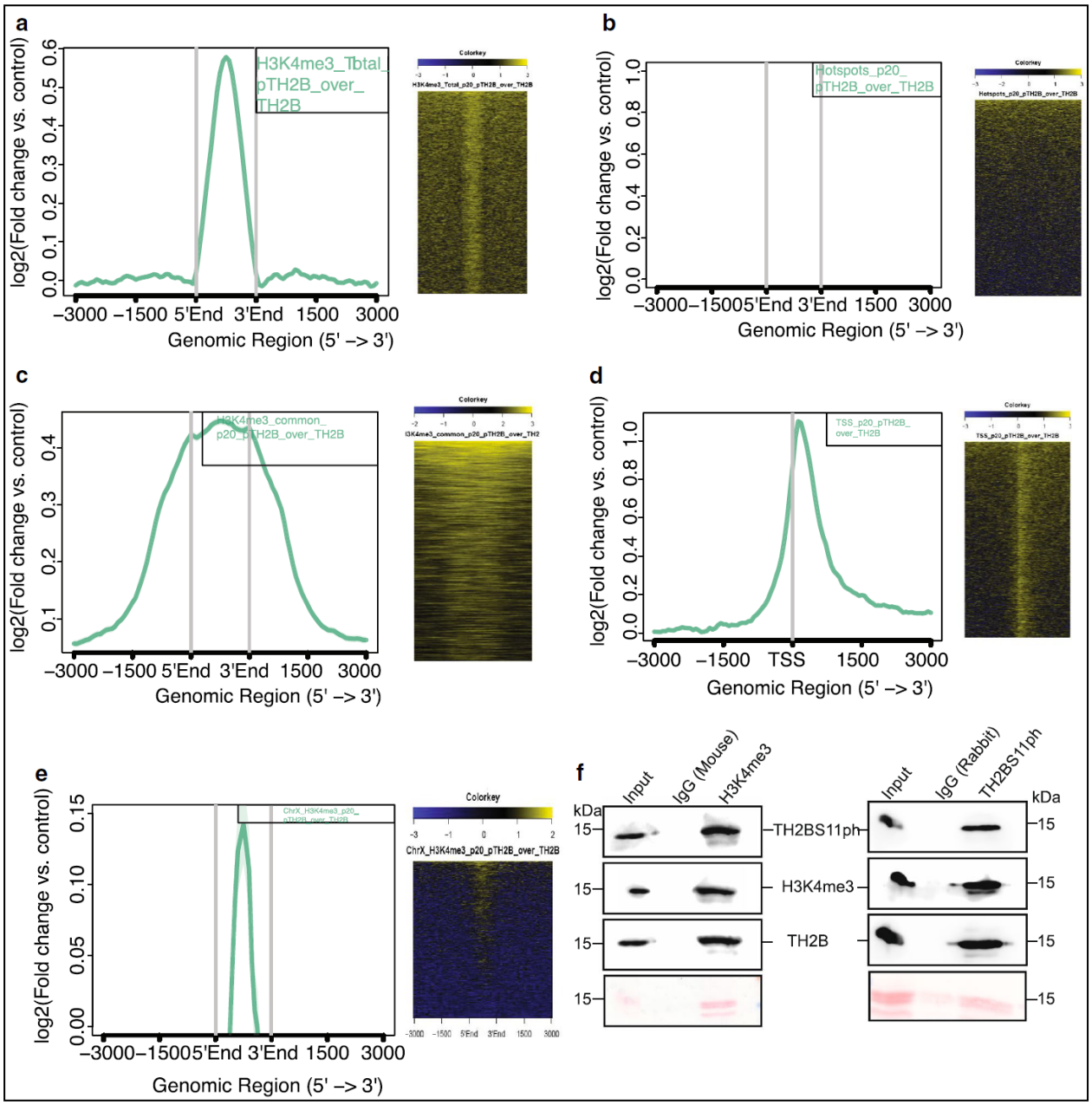

Figure 2.9- Localization of TH2BS11ph modification at TSS and recombination hotspots with respect to TH2B occupancy

a- *Analysis of overlap of TH2BS11ph with total H3K4me3 marks.*

b- *Analysis of overlap of TH2BS11ph with DSB hotspots*

c- *Overlap of TH2BS11ph with common H3K4me3 marks representing the TSS-associated H3K4me3 marks*

d- *Localization of TH2BS11ph at TSS*

e- *Localization of TH2BS11ph at chromosome X related H3K4me3 marks*

f- *Co-association of TH2BS11ph and H3K4me3 histone marks in mononucleosomes. IP were carried out using mononucleosomes to determine the coexistence of histone marks TH2BS11ph and H3K4me3 by forward (left panel) and reciprocal IP (right panel) assays. The first lane in all the blots represent the input fraction, the second lane represent the IP carried out with the non specific IgG antibody and the third lane represents the IP carried out with the relevant antibody (anti-TH2BS11ph/anti-H3K4me3). The antibodies labeled alongside the blot refers to the antibodies used for western blotting. Ponceau stained blots are given for reference.*

Cytological and biochemical assays provided enough evidence for the association of TH2BS11ph with DNA repair domains of the XY body. Since the H3K4me3 mark is linked to DSB activity in the PAR of the X-chromosome (Brick et al., 2012), we were interested in determining the overlap between TH2BS11ph and chromosome X-specific H3K4me3 mark. As can be seen in Fig 2.9e, the majority of TH2BS11ph reads are concentrated at the centre of chromosome X specific H3K4me3 marks.

Aggregation plots established the close association of TH2BS11ph with H3K4me3 histone mark related to both transcription and DNA repair chromatin domains of the XY body. To verify this further, we carried out immunoprecipitation assays to determine whether TH2BS11ph and H3K4me3 histone marks coexist in the context of mononucleosomes. From Fig 2.9f (left panel), we observe that TH2BS11ph is associated with H3K4me3-containing nucleosomes. Also, H3K4me3 histone mark is found in TH2BS11ph-containing mononucleosomes (Fig 2.9f, right panel). These data collectively indicate the co-association between TH2BS11ph and H3K4me3 in nucleosome core particles (NCPs).

2.3.9 Read distribution of TH2BS11ph (compared against background input) at recombination hotspots and TSS

Next, we investigated whether TH2BS11ph is significantly associated with the H3K4me3-containing transcription and chromosome X-associated genomic regions. For this, we compared the occupancy of TH2BS11ph at candidate genomic regions and plotted the TH2BS11ph read distribution enriched over background input. We obtained similar results in that when we plotted the read distribution of TH2BS11ph enriched over backbone TH2B, wherein we observed the close association of TH2BS11ph with TSS and chromosome X related H3K4me3 marks (Fig 2.10A,C,D,E). Further, we did not observe significant TH2BS11ph localization at DSB hotspots, as can be seen in Fig 2.10B.

2.3.10 ChIP-sequencing in mouse P12 testicular cells

ChIP-seq results in P20 mouse testicular cells gave a strong indication of the association of TH2BS11ph with chromatin domains related to XY body DSB repair and transcription. Our next aim was to determine whether the association of TH2BS11ph is specific to late recombination events in the XY body or whether TH2BS11ph is also localized at initiation sites of meiotic autosomal recombination. For this, we performed ChIP-sequencing studies in mouse P12 testicular cells that are enriched in leptotene cells, where initiation of meiotic recombination takes place. Aggregation plots derived from TH2BS11ph ChIP-seq data of mouse P12 testicular cells showed the specific association of TH2BS11ph with TSS and TSS-associated H3K4me3 marks (Fig 2.11 a,c,d), but not with the hotspot genomic regions (Fig 2.11b).

These data suggest that TH2BS11ph histone mark is associated with TSS and specifically with DNA repair domains of the XY body but not with autosomal recombination hotspots.

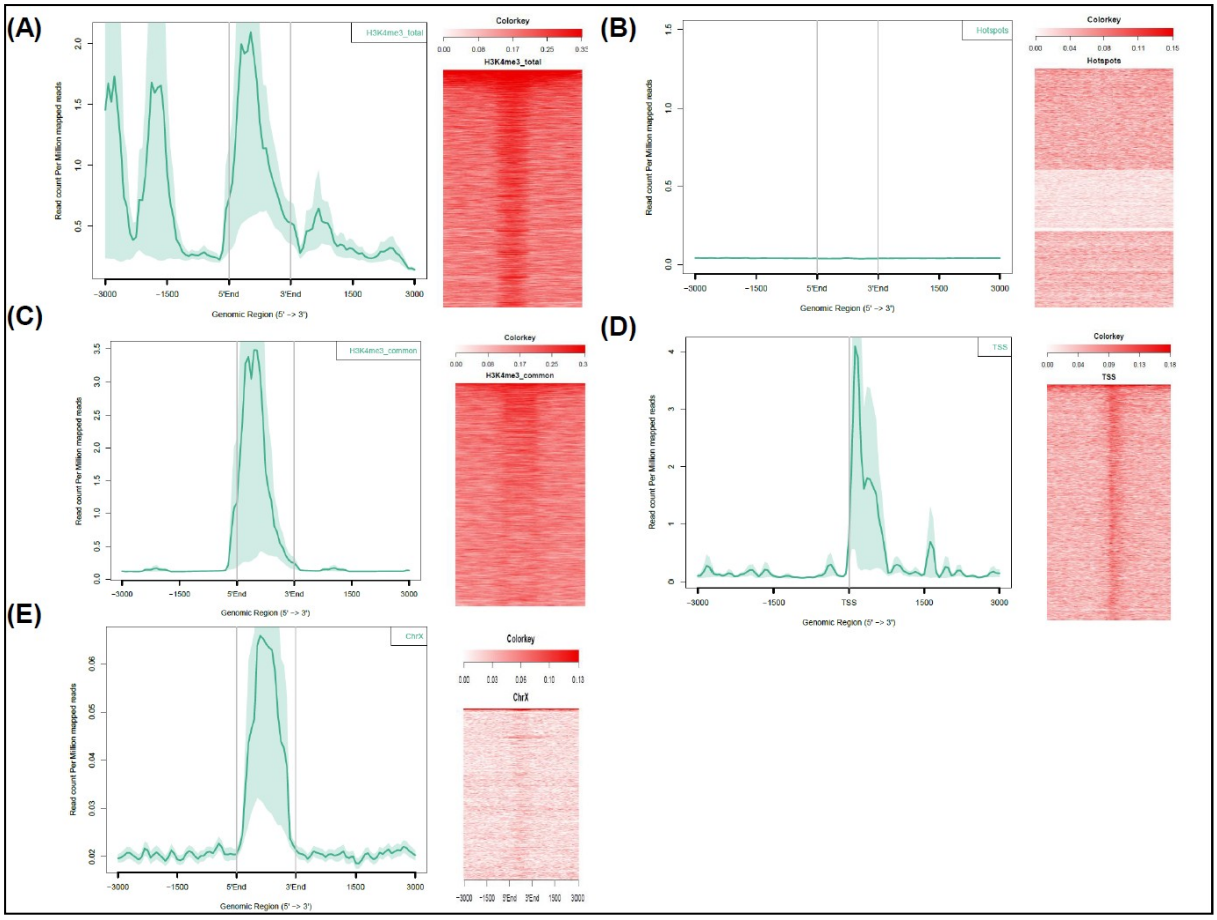

Figure 2.10- Read distribution of TH2BS11ph at TSS and recombination hotspots in P20 mouse testicular cells.

*Profile of read distribution of TH2BS11ph with respect to the centre of occupancy of **A**. Total H3K4me3 marks, **B**. DSB hotspots, **C**. TSS-associated H3K4me3 (common H3K4me3), **D**. TSS of mouse, **E**. Chromosome X-specific H3K4me3 marks.*

*The read distribution were plotted in terms of aggregation plots (left panels in figures **A-E**) and heat maps (right panels in figures **A-E**). The X-axis in the aggregation plots represent read per million mapped reads whereas the Y-axis represent the distance from the centre of reference peak in kilobase pairs (kb).*

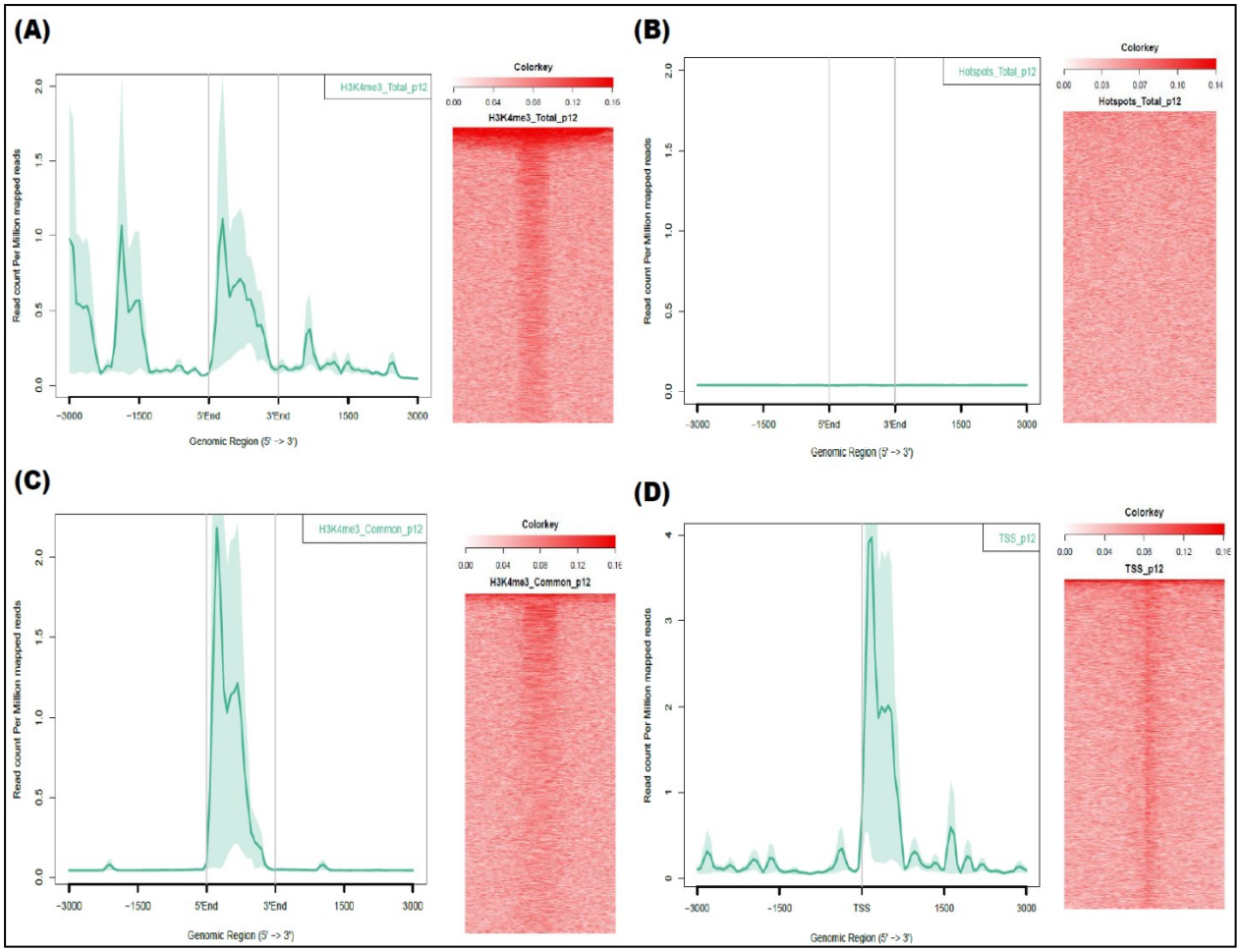

Figure 2.11- Genome-wide occupancy of TH2BS11ph modification in P12 mouse testicular cells

*Read distribution of TH2BS11ph histone mark at TSS and recombination hotspots in P12 mouse testicular cells- Analysis of occupancy of TH2BS11ph histone mark at **A**. Total H3K4me3 mark, **B**. DSB hotspots, **C**. TSS-associated H3K4me3 (common H3K4me3), **D**. Transcription start sites of mouse. The overlap were determined by aggregation plots (left panels in all figures **A-D**) and heat maps (right panels in all figures **A-D**). The X-axis in all the aggregation plots represent the read count per million mapped reads whereas the Y-axis represent the distance from the centre of reference peak in kilobase pairs (kb).*

2.3.11 Level of backbone TH2B at TSS and meiotic recombination hotspots

Since we have consistently demonstrated the close association of TH2BS11ph with H3K4me3 marks of the XY body and TSS, it became important to determine the levels of backbone TH2B at these characteristic genomic loci. The backbone TH2B here is referred to the non-phosphorylated or unmodified TH2B serine 11 protein. We observed that TH2B is

present at background levels at TSS and recombination hotspots (Fig 2.12a,b,c). We reconfirmed the published dataset wherein TH2B was found to be depleted from TSS (Montellier et al., 2013). We did not observe significant enrichment of TH2B at the centre of transcription-associated genomic regions (Fig 2.12d). The important point to be noted here is that the read count per million mapped reads was plotted on the same scale as the observed TH2BS11ph levels. Hence, we provide additional evidence to the fact that TH2BS11ph is preferentially enriched over non-phosphorylated TH2B at H3K4me3-positive TSS and XY body genomic regions.

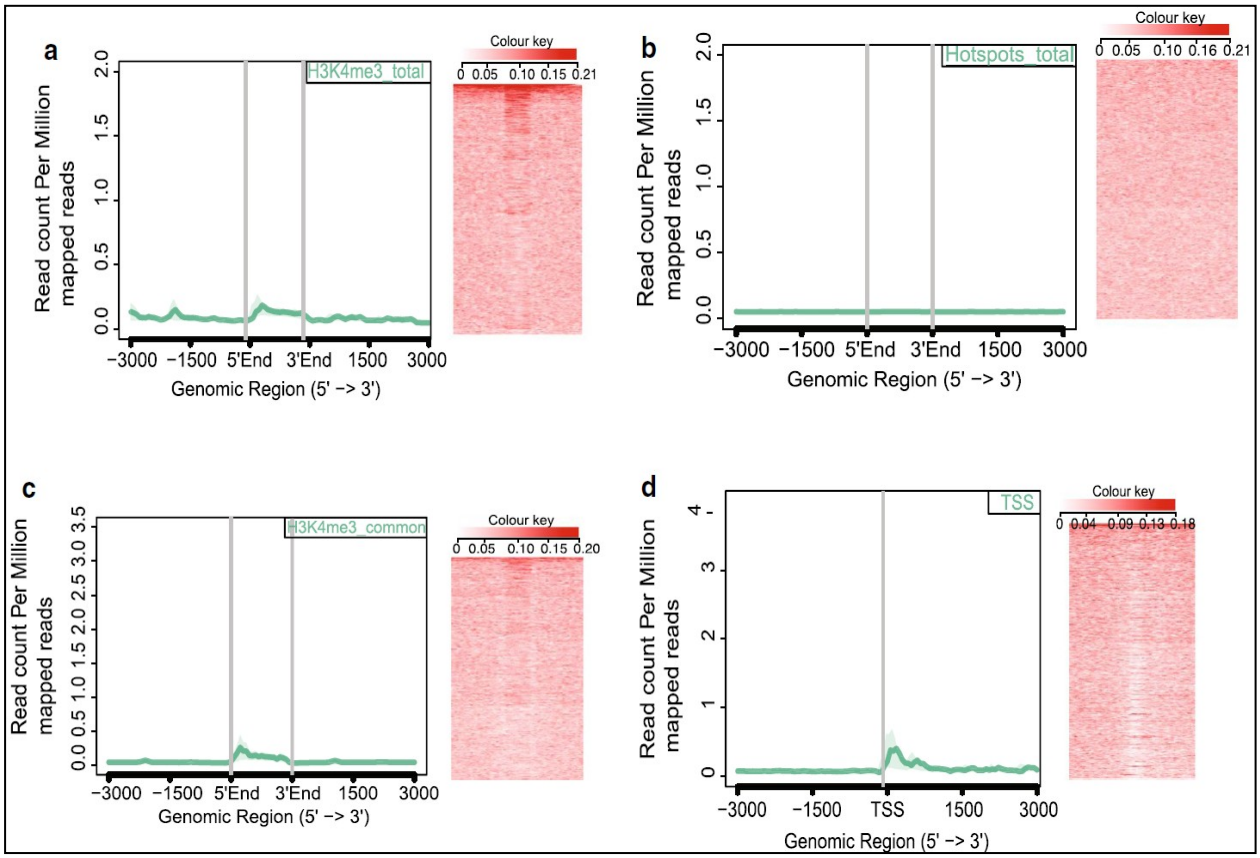

Figure 2.12- Localization of backbone or non-phosphorylated TH2B at recombination hotspots and TSS

*Analysis of overlap between TH2BS11ph and **a**. Total H3K4me3, **b**. DSB hotspots, **c**. common H3K4me3 representing the TSS-associated H3K4me3 marks, **d**. TSS of mouse.*

*TH2B were observed to depleted at TSS regions (Montellier et al., 2013). In each figure from **a-d**, the overlap has been determined using aggregation plots (left panels) and heat maps (right panels).*

2.3.12 Validation of TH2BS11ph bound genomic regions by ChIP-PCR

For confirmation of the ChIP-seq results, we designed primers for the various chromosomal loci across the mouse genome. The list of primer sequences for these selected genomic loci are given in Annexure 3. We were interested in determining the genomic regions unique for TH2BS11ph enrichment, not for unmodified TH2B occupancy. The genomic regions with the TH2BS11ph and TH2B IP tracks used for experimental validation by ChIP-PCR are given in Fig 2.13a. We have chosen two peaks from chromosome X, one from chromosome Y and two from autosomal regions. By ChIP-PCR in P20 mouse testicular cells, we show the occupancy of TH2BS11ph at all the selected genomic loci, further validating the ChIP-seq dataset (Fig 2.13b, chrX1, chrX2, chrY, Auto1, Auto2). We observe the specific enrichment of TH2BS11ph over TH2B at these genomic regions (Fig 2.13b, chrX1, chrX2, chrY, Auto1, Auto2). There was no significant enrichment of TH2BS11ph over TH2B control at selected negative control regions (Fig 2.13b, Neg Ctrl1, Neg Ctrl2).

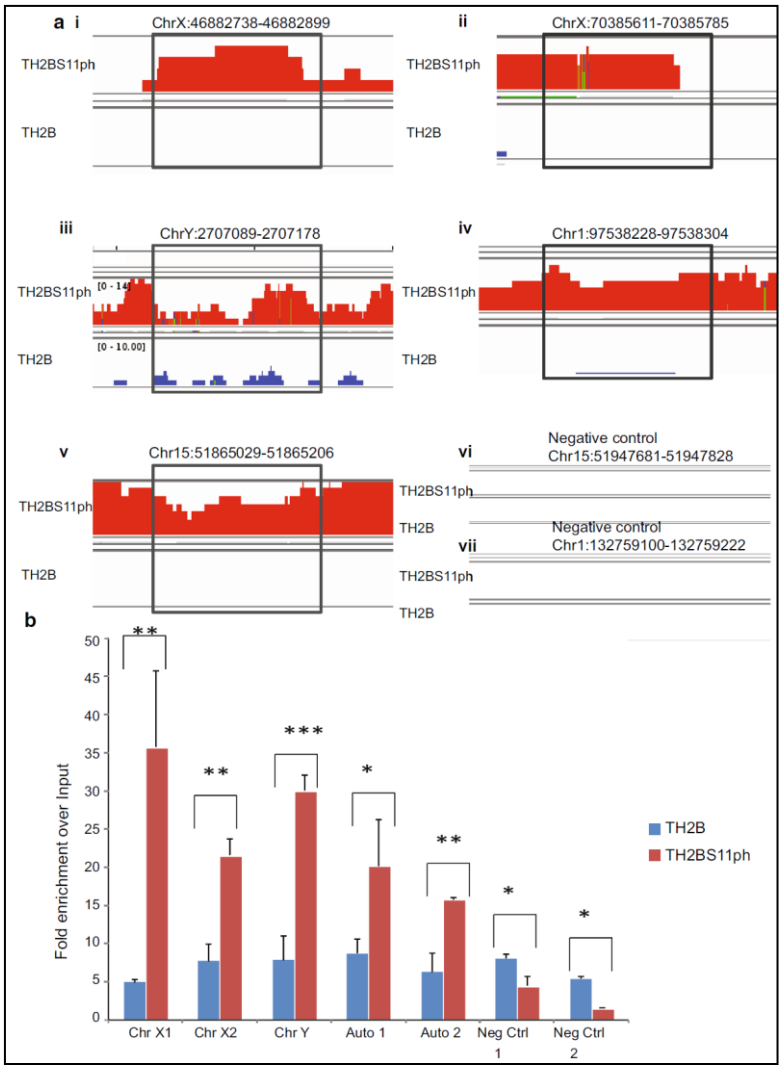

Figure 2.13- Validation of ChIP-sequencing dataset by ChIP-PCR carried out in P20 mouse testicular cells.

a. *Genomic regions used to design primers required to confirm the ChIP-sequencing dataset by ChIP-PCR technique. The top panel in figures (i-vii) represent the TH2BS11ph IP, bottom panel in (i-vii) represents the TH2B IP.*

b. *Validation of TH2BS11ph ChIP-sequencing data by ChIP-PCR using TH2BS11ph and TH2B antibodies. TH2BS11ph is enriched over backbone TH2B and background input at the selected genomic regions, two from chromosome X (i,ii), one from chromosome Y (iii), two from autosomal regions (iv,v). TH2BS11ph is not significantly enriched over TH2B at two regions (vi,vii) that were used as negative controls. The values of fold enrichment were plotted against input control. ChIP-PCR experiments were carried out for three biological replicates including technical replicates for a single biological replicate. The data were plotted in terms of mean +/- S.D, ***P<=0.0005; P<=0.005; P<=0.05.*

2.3.13 Mass spectrometry analysis of proteins associated with TH2BS11ph-containing mononucleosomes

Since TH2BS11ph is a nucleosomal histone protein, we were interested in determining the proteins associated with TH2BS11ph-bound mononucleosomes. To address this, we performed mass spectrometry to determine the proteins that are associated with TH2BS11ph-containing mononucleosomes. The proteins were identified based on enrichment observed for immunoprecipitated proteins compared to that of non-specific rabbit IgG lane (Fig 2.14a). Mass spectrometry analyses revealed key proteins belonging to the functions of XY body and transcription to be associated with TH2BS11ph-mononucleosomes (Fig 2.14b). The list of proteins identified to be associated with TH2BS11ph-containing mononucleosomes are given in Annexure 4.

Smarca5 is known to regulate phosphorylation of histone variant H2AX (Broering et al., 2015). Scml2, a germ-cell specific subunit of the polycomb repressive complex, is involved in epigenetic silencing and reprogramming of the sex chromosomes (Hasegawa et al., 2015; Maezawa et al., 2018). Remodeling of the sex chromosome is also mediated by replacement of histone H3 by variant H3.3 wherein remodeling and DNA repair proteins act in sync to bring about meiotic sex chromosome inactivation (MSCI) in the XY body (van der Heijden et al., 2007). Mre11 is a part of MRN complex associated with DNA repair events of the XY body (Handel, 2004). It is known that Cbx1 and macroH2A are co-associated in the PAR region of the XY body (Turner et al., 2001). Since both Cbx1 and macroH2A were found to

be associated with TH2BS11ph-mononucleosmes, this further supports the conclusion of TH2BS11ph to be associated with DNA repair domains of the XY body.

The proteins indicated in red are the proteins that are common to both TH2BS11ph and previously reported γH2AX IP (Broering et al., 2015) (Fig 2.15b). Proteins that are known in XY body related functions like Scml2 (Hasegawa et al., 2015), Cbx1 (Metzler-Guillemain et al., 2003), macroH2A (Richler et al., 2000), H2AX (Fernandez-Capetillo et al., 2003), H3.3 (van der Heijden et al., 2007) and common protein effectors between TH2BS11ph and γH2AX that were identified in the mass spectrometric analysis, reconfirms the association of TH2BS11ph with the DNA repair domains of the XY body.

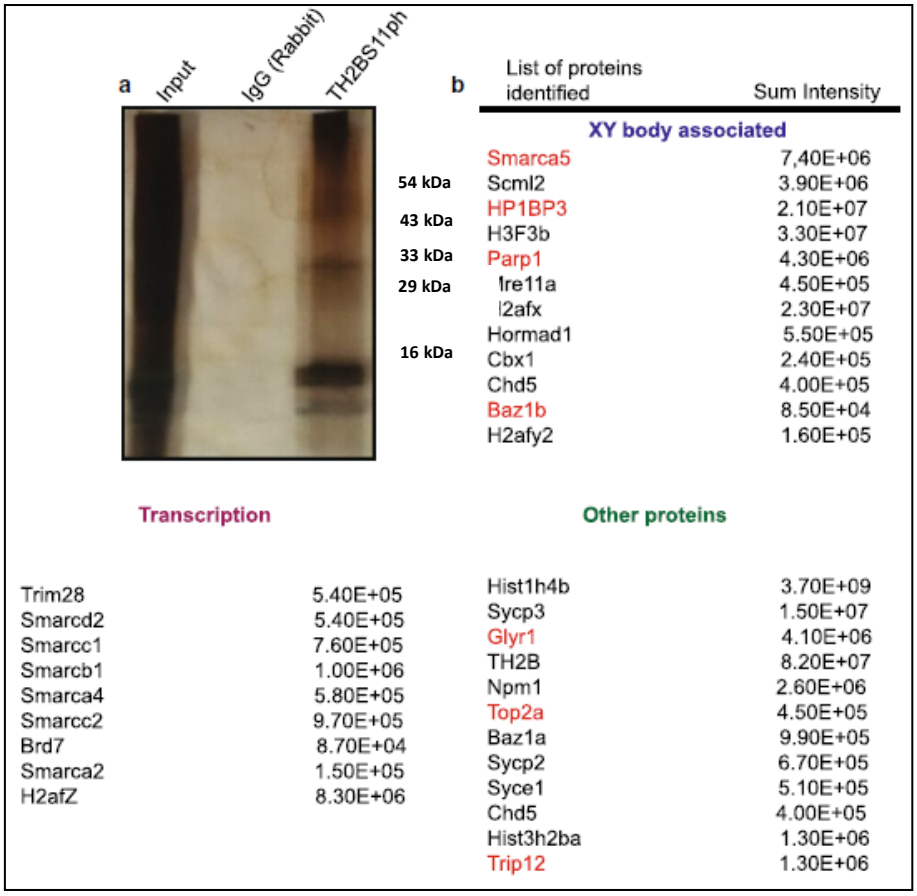

Figure 2.14- Determination of protein partners associated with TH2BS11ph-containing mononucleosomes as determined by mass spectrometry in rat testicular cells

a*- Silver stained image of the TH2BS11ph ChIP- input lane refers to 5% input, IgG lane refers to IP carried out with non-specific rabbit IgG control, TH2BS11ph refers to TH2BS11ph IP lane.*

b*- The interacting proteins of TH2BS11ph-positive mononucleosomes as determined by mass spectrometry were classified based on their known biological functions- XY body, Transcription, and other important proteins. The first row is the gene/protein name; the*

second row refers to the sum intensity that refers to the peak intensity values for all the peptides matched to a particular protein. The proteins highlighted in red refer to common proteins identified between TH2BS11ph IP and γH2AX IP (Broering et al., 2014).

Apart from the XY body related proteins, TH2BS11ph associates with proteins related to transcriptional regulation as determined by mass spectrometry. H2AZ-containing nucleosomes are sites of transcriptional activation (Soboleva et al., 2011). The fact that TH2BS11ph associates with proteins like H2AZ, Trim28 (Wang and Wolgemuth, 2016), H3.3, members of the SWI/SNF complex, establish that TH2BS11ph-containing nucleosomes are TSS-associated. In the list of interacting proteins, we also obtained core nucleosomal histones, thus serving as internal control for the isolation of mononucleosomes.

We would like to point out that mass spectrometric analysis reflects the average picture of protein complexes associated with all TH2BS11ph-containing mononucleosomes. The important point to be stressed here is that TH2BS11ph associates with different set of proteins machineries in turn regulating different loci in a context-dependent manner. A recurrent theme that emerges is that TH2BS11ph histone mark is densely localized in the unsynapsed axes of the XY body and associates with H3K4me3-containing genomic regions in mammalian spermatocytes.

2.4 Discussion

Chromatin is a dynamic structure and changes in chromatin structure are linked to cell fate decisions during development (Bonev et al., 2017; Dixon et al., 2015; Rennie et al., 2018). This dynamicity is regulated by a combination of post-translational modifications that are widespread on histone and DNA. The major PTMs that occur on histones are acetylation, methylation, ubiquitination, and phosphorylation, among others (Tan et al., 2011). PTMs on histones can modulate nucleosome dynamics by either modulating histone-DNA interactions or by creating docking sites for various chromatin-modifying complexes.

Meiosis is a specialized process that produces haploid spermatids from diploid cells, resulting from one round of DNA replication followed by two rounds of successive cell divisions. The events such as active transcription, programmed DSB formation, homologous recombination, crossover formation, crossover resolution are characteristic of this tetraploid phase. These events are mediated by dynamic chromatin transactions like transcription, chromatin remodeling events influenced by histone modifications etc. Histone PTMs have also been implicated in various processes during meiosis (Wang et al., 2017). Efforts have been made

to characterize novel histone PTMs that are important for modulation of epigenetic networks during meiosis.

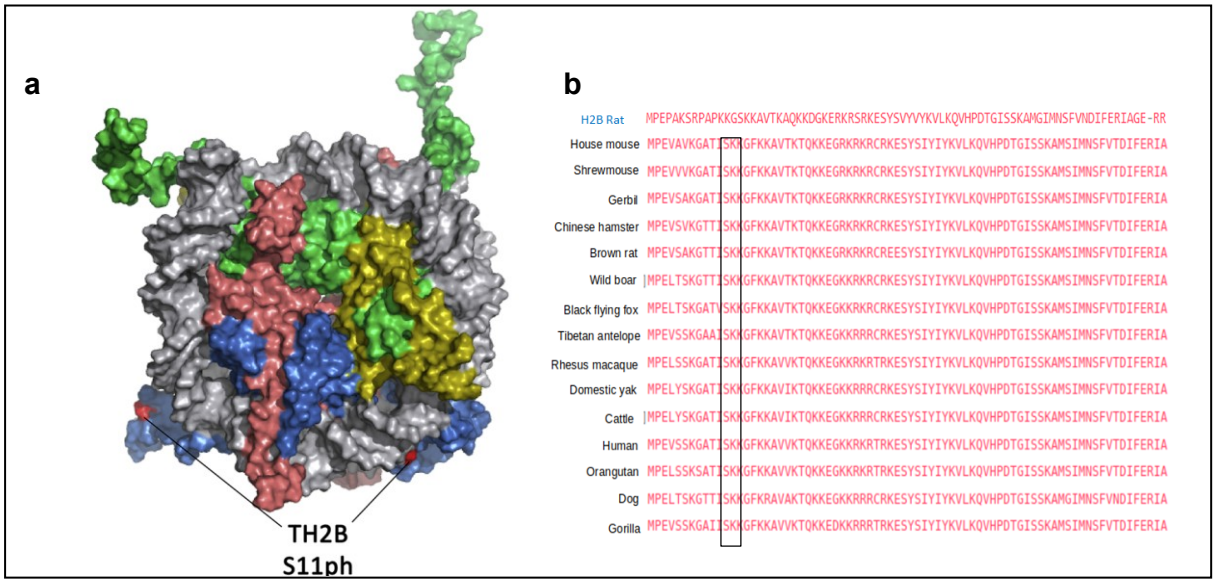

Figure 2.15- a*. Model of TH2B-containing nucleosome core particle highlighting the exposed serine 11 residue.*

b*. Alignment of protein sequences of TH2B from different species. The boxed region shows the conserved serine 11 residue across various mammalian species. The sequence of rat H2B has been given for reference on top. A similar residue on H2B, H2BS14ph is involved in DNA repair in somatic cells.*

Although, the biological function of TH2B has been delineated in spermatids in the context of histone to protamine transition (Montellier et al., 2013), very little is known about its role during meiotic prophase I. The present study was initiated to explore the possible biological function(s) of N-terminus of TH2B particularly with respect to PTMs and their role(s) in biological events specific to mammalian spermatocytes. The identification of histone variant-specific PTMs is a challenging task due to the high similarity of the amino acid sequences between the canonical and variant histones. Recently, PTMs have been successfully characterized on TH2B isolated from spermatocytes and spermatids (Luense et al., 2016; Pentakota et al., 2014). By revisiting the mass spectrometry procedures and post-mass spectrometry analyses, we discovered the histone mark TH2B serine 11 phosphorylation (TH2BS11ph) in spermatocytes. This residue phosphorylation has been already reported by (Luense et al., 2016) but in round spermatids. We report this histone mark for the first time in spermatocytes. Since the N-terminal tails are disordered and highly exposed in solution, the role of the phosphorylated TH2B might lie in recruitment of effectors than modulating

histone-histone and histone-DNA contacts per se (Fig 2.15a). Also, TH2B serine 11 residue is conserved in mammals as shown in Fig 2.15b; this suggests an important function in germ cells. Further, to study the *in vivo* functions, we first generated a TH2BS11ph specific antibody and validated its reactivity, showed that the antibody did not crossreact with its somatic counterpart H2B/H2BS14ph and backbone TH2B by multiple assays like ELISA, western blotting, peptide competition assay, etc.

2.4.1 TH2BS11ph and XY body

One of the major observations made in this study is the enrichment of TH2BS11ph modification in the unsynapsed axes of the XY body, as evidenced by cytological assays. The important biological events that occur in the XY body are DNA repair and heterochromatin formation. Based on the co-association with DSB marker γH2AX, we provide further evidence to the fact that TH2BS11ph is associated with DNA repair domains of the XY body. Another interesting result from the ChIP-sequencing assays is that the highest number of TH2BS11ph peaks were found in chromosomes X and Y compared to autosomes. This might mean the XY body-related association of TH2BS11ph histone mark might be the major function of this histone mark in spermatocytes. A similar residue phosphorylation, H2BS14ph is associated with DNA repair in somatic cells (Fernandez-Capetillo et al., 2004). The involvement of H2BS14ph in DNA repair and serine 11 residue of TH2B being highly conserved provides additional support to the fact that TH2B serine 11 phosphorylation might have a major role in XY body DSB repair in spermatocytes. The intense staining of TH2BS11ph modification in the XY body could be due to increased DSB density that is found in the PAR compared to the autosomal DSBs. A unique chromatin organization is found in the PAR wherein chromatin is organized into larger axes and shorter loops promoting high DSB density (Kauppi et al., 2011). TH2BS11ph, along with histone marks like γH2AX might be important for recombination repair and subsequent heterochromatinization in the XY body (Fig 2.16a). It is pertinent to point out that TH2BS11ph is associated explicitly with H3K4me3 genomic regions of the XY body, the formation of which are not catalyzed by PRDM9 (Brick et al., 2012; Powers et al., 2016). Therefore, the association of TH2BS11ph was specific to late recombination events in the XY body, but not with the initiation sites of meiotic recombination that occurs in leptotene spermatocytes (P12 testicular cells).

On the other hand, H2B ubiquitination mediated by RNF20 has been shown to regulate meiotic recombination in mice (Xu et al., 2016). Since we demonstrate the specific

association of TH2BS11ph with XY body-related histones/histone marks like macroH2A, γH2AX, H3K4me3, etc, there could be plethora of other combinations of histone/histone PTMs or 'histone code' in the context of autosomal and XY body hotspot nucleosomes, that need to characterized. An interesting question awaiting further investigation is which methyltransferase enzyme mediates methylation of histone H3 at the fourth lysine position in the context of XY body DNA repair domains. Another important fact to be established is whether TH2B is phosphorylated at the serine 11 position before incorporation into the chromatin, or the chromatin-bound TH2B is then phosphorylated for the setting of this unique chromatin template. Based on the colocalization observed with pATM and ATR kinases, it is tempting to speculate whether either of these kinases catalyze the TH2B phosphorylation at the serine 11 position, however, this has to be addressed further. Also, much of the TH2BS11ph puncta are also observed on the periphery in leptotene and zygotene cells which provides further support to the association with heterochromatin domains in these cells, but this has to be investigated further. Apart from the XY body of pachytene cells, we observed many foci outside the sex body suggesting the association of TH2BS11ph might not be just restricted to XY body-specific functions.

2.4.2 TH2BS11ph and Transcription

Another observation made in this study is that TH2BS11ph modification is associated with genomic regions containing the H3K4me3 histone mark. H3K4me3 is present at enhancers, promoters, and meiotic recombination hotspots. Since H3K4me3 marks that are present at promoters, enhancers, and meiotic recombination hotspots are distinctly located in the mouse genome and are catalyzed by different enzymes, it became important to delineate the association of TH2BS11ph with specific H3K4me3 datasets. Overlap studies by the use of aggregation plots and heat maps resulting from ChIP-seq studies carried out in P20 mouse testicular cells demonstrated the specific association of TH2BS11ph with transcription-associated H3K4me3 marks. This was further proven by forward and reciprocal immunoprecipitation assays showing TH2BS11ph and H3K4me3 to coexist in the context of mononucleosomes. This co-association was also found to be true in P12 mouse testicular cells (leptotene). It is quite likely that punctuate staining observed outside the XY body might correspond to the transcription domains in pachytene spermatocytes.

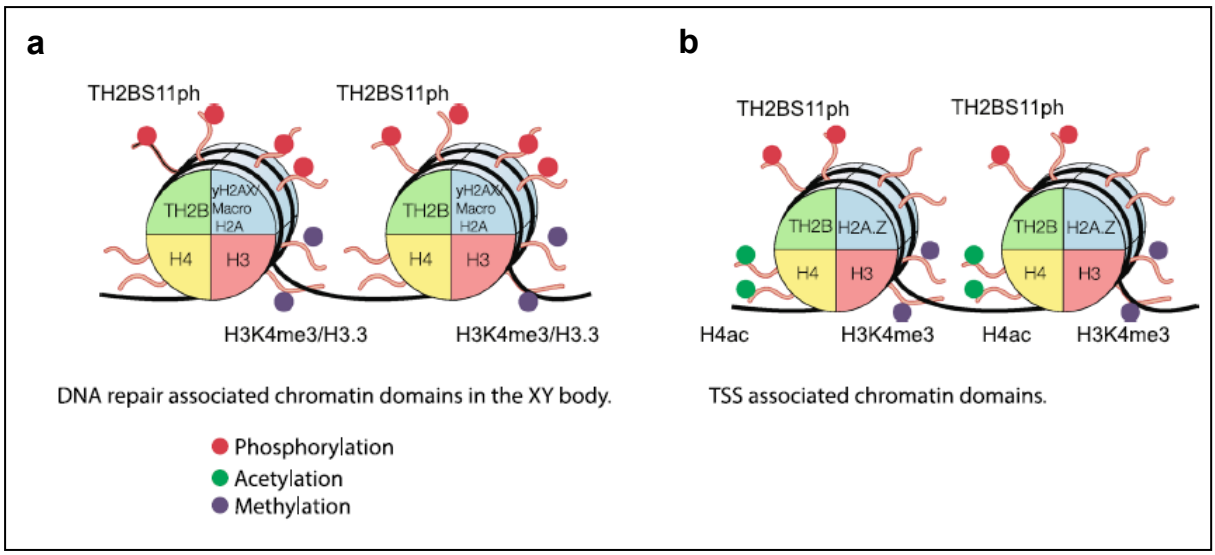

Figure 2.16- a. *Model of TH2BS11ph-containing nucleosomes showing the association with XY body-related histone marks. TH2BS11ph could function along with γH2AX and H3K4me3 histone marks to mediate DNA repair in the XY body.*

b*. Model of TH2BS11ph-containing nucleosomes showing the association of this histone mark with transcription start sites. TH2BS11P could associate with H3K4me3, H2AZ and transcription-associated H4 acetylated marks to mediate transcription in pachytene cells. TH2BS11ph could function in association with the specific repertoire of histone marks to mediate chromatin-templated events like DNA repair in the XY body or TSS activation*

As explained earlier, histone PTMs also function in concert with various chromatin-modifying complexes. These complexes are very critical during development, as their mutations result in various developmental disorders or cancer (Chen et al., 2016; Sheikh, 2014). Genomic accessibility is controlled by combination of factors like histone modifications, chromatin remodelers, DNA sequence, etc (Bell et al., 2011; Lai and Pugh, 2017). In this study, we also observe the specific association of TH2BS11ph with chromatin remodeler complexes like SWI/SNF, histone PTMs like H3K4me3, H2AZ, H3.3 all being colocated at TSS (Fig 2.14b). Taken together, we demonstrate the specific association of TH2BS11ph with proteins and histone marks related to transcription *in vivo*. Also, H3K4me3 is a PTM found in active gene promoters highly conserved from yeast to mammals (Schneider et al., 2004). This begs for the question of whether the association of TH2B serine 11 phosphorylation with TSS is conserved across germ cells of rodents to humans. Also, whether the similar H2B residue phosphorylation is a conserved histone PTM like H3K4me3 for transcriptional activation in various species. It would be interesting to decode the

repertoire of histone TH2B/H2B PTMs responsible for TSS activation in spermatocytes of higher eukaryotes.

Many studies have demonstrated the influence of histone variant H2AZ in transcription in *S. cerevisiae* (Guillemette et al., 2005; Raisner et al., 2005; Zhang et al., 2005), plants (Zilberman et al., 2008) and mammals (Barski et al., 2007). H2AZ is localized to either side of the TSS (+1 or -2 nucleosome) of a poised or an active RNA polymerase II promoter (Barski et al., 2007; Conerly et al., 2010; Henikoff et al., 2009; Schones et al., 2008). Also, in mouse spermatocytes, H2AZ histone variant is localized to active promoters (Soboleva et al., 2011). At human TSS, H3.3/H2AZ double-positive nucleosomes causes destabilization of nucleosomes, important for access to transcription factors and chromatin regulators to mediate gene activation (Jin et al., 2009). Since we observe both H3.3 and H2AZ to be associated with TH2BS11ph-containing mononucleosomes, their coexistence could cause open chromatin configuration important for the access of transcription factors, thus influencing transcriptional output in spermatocytes. Interestingly, the acidic patch of H2AZ also interacts with histone H4 tail, wherein PTMs on H4 can modulate chromatin interactions, thus determining specific biological functions (Dorigo et al., 2004; Kan et al., 2009; Li and Reinberg, 2011; Roussel et al., 2008; Sinha and Shogren-Knaak, 2010). As explained earlier, H4K5/K8 acetylation marks are found on active gene promoters in spermatocytes (Goudarzi et al., 2016). The interactions between acidic patch of H2AZ and acetylated H4 tail may be influenced by TH2BS11ph association with histone variants H2AZ and H3.3, further causing interactions with chromatin remodeler complexes at these TSS nucleosomes (Fig 2.16b).

HBR domain of H2B (30-37 amino acid residues) has been well studied and has been shown to be involved in transcriptional repression in yeast (Parra et al., 2006). Acetylation of the HBR domain relieves repression to facilitate transcriptional activation. Our present study shows for the first time, the involvement of serine phosphorylation on TH2B to be localized at transcription chromatin domains *in vivo*. It remains to be seen whether TH2B serine 11 phosphorylation influences nucleosome dynamics by modulation of the function of the HBR domain. It will also be interesting to determine whether the involvement of serine phosphorylation is unique to spermatocyte transcription or whether analogous H2B serine phosphorylation is also involved in transcription processes in somatic cells. The mechanism behind the steps where TH2BS11ph can be involved at the TSS nucleosome towards polymerase recruitment or towards recruitment of coactivators or transcriptional elongation factors etc, remains to be further decoded.

Recently, TH2A-Thr127 phosphorylation (TH2AT127ph) was shown to co-associate with H3.3-containing TSS in the sperm chromatin (Hada et al., 2017b). Since TH2BS11ph modification occurs during spermatid stages (Luense et al., 2016), it would be interesting to determine whether TH2AT127ph co-associates with TH2BS11ph at TSS regions of sperm chromatin. Even though histone-associated genomic regions are not well characterized in the mature sperm, enrichment of histones at TSS might be a general property to utilize accessible chromatin structure during embryogenesis (Johnson et al., 2016; Saitou and Kurimoto, 2014). Since histone variant TH2B is present in the early embryos (Shinagawa et al., 2014) and also associates with H3.3 in spermatocytes, a burning question is whether TH2BS11ph is also involved in marking TSS in the sperm chromatin required for the establishment of the epigenome during early embryonic development.

In conclusion, we observed TH2B serine 11 phosphorylation (TH2BS11ph) to be associated with two primary functionally important chromatin domains in spermatocytes- (i) TH2BS11ph is located at DNA repair domains of the XY body that are positive for proteins and histone marks like γH2AX, H3K4me3, etc (Fig 2.16a), (ii) TH2BS11ph could function with H3K4me3/H2AZ mediated recruitment of effectors to mediate transcription in spermatocytes (Fig 2.16b). As explained earlier, multiple histone PTMs called the 'histone code' act in concert to signal the functionality of the specific chromatin region (Linggi et al., 2005; Strahl and Allis, 2000). What is the mechanism underlying the crosstalk between TH2BS11ph and these specific PTMs like H3K4me3, γH2AX, H2AZ, H3.3 in the context of XY body DNA repair or TSS activation? Recent evidence has implicated the role of histone modifications in the regulation of chromatin compartmentalization by phase separation mechanism (Wang et al., 2019). It would be interesting to determine whether TH2BS11ph regulates these biological events through such mechanisms.

It is interesting to point out that TH2BS11ph associates with both condensed (XY body) and relaxed chromatin domains (like TSS) in pachytene spermatocytes. The differences in the functional outcome of the chromatin structure are probably brought about by the combination of the associated histone PTMs and chromatin regulators *in vivo*. More work is needed to elucidate the mechanism(s) by which TH2BS11ph influences transcription and also DNA repair, and whether co-association of TH2BS11ph with the specific histone marks and protein effectors is essential for the success of these biological events. Besides, H3K4me3 and TH2BS11ph do not have the propensity to interact directly in a nucleosome core particle; therefore recruitment of appropriate protein machinery via formation of signature nucleosomes might be the major mechanism underlying XY body and TSS related functions.

Further, the steps from either setting of the chromatin template to the recruitment of specialized effectors in the biological events related to XY body and TSS activation remain to be delineated.

The higher-order chromatin structure of pachytene spermatocytes is characterized by attenuated TAD structures, weak genome compartmentalization and increased local interactions compared to the chromatin structures that of post-meiotic spermatids and mature sperm (Alavattam et al., 2019). Whether the role of TH2BS11ph in modulating three-dimensional chromatin structure by regulation of the formation of specific chromosome territories is an interesting question that may be addressed in future. Recently, Hi-C analysis of chromatin structure has been carried out for pachytene, round spermatids and mature sperm (Alavattam et al., 2019). It would be interesting to correlate the TH2BS11ph ChIP-seq data with the available Hi-C maps to further understand the genomic and chromatin architectural features associated with TH2BS11ph-containing nucleosomes in pachytene spermatocytes.

Still, the question remains of how the loss of TH2B allele can be compensated by the upregulation of H2B and compensatory histone PTMs on H2B, H3, and H4 (Montellier et al., 2013). What H2B PTM(s) complement TH2BS11ph function in the case of TH2B deficiency, will be an interesting avenue to explore. If TH2B deficiency can be compensated by H2B, the important question is why TH2B has evolved to replace H2B on a genome-wide scale in mammalian spermatocytes and spermatids. Nevertheless, in summary, we have documented for the first time the genome-wide localization of a PTM on a germ cell-specific histone variant in meiotic prophase I related events (Mahadevan et al., 2019).

Chapter 3

Genome-wide occupancy of linker histone variant H1t in mouse pachytene spermatocytes

3.1 Introduction

Despite their significant roles in various chromatin-templated biological events, linker histones have not been studied in great detail as much as core histones. Along with core histones, the linker histone (H1) is one of the five major histone families associated with the eukaryotic chromatin. In mice and humans, eleven H1 variants have been identified to date that includes seven somatic subtypes (H1.0, H1.1-H1.5, and H1x), three testis-specific variants (H1t, HILS1, and H1T2) and one oocyte-specific variant (H1oo).

Tremendous progress has been made only recently towards understanding the molecular functions of H1 action in developmental processes beyond their architectural roles in chromatin (Summarised in Table 3.1). Bednar *et al* reported the first X-ray structure of the chromatosome core particle (linker histone complex containing a nucleosome) at 5.5Å resolution (Bednar et al., 2017). A high-resolution crystal structure of a linker histone-nucleosome complex (Fig 3.1A) along with 11Å structure cryo-electron microscopy derived structure of the 30nm fiber has been solved (Ozturk et al., 2018; Song et al., 2014; Zhou et al., 2015). Many studies have shed light on how linker histone interacts with the nucleosome core particle and organize higher-order chromatin structures.

H1s are preferentially associated with repetitive sequences in various functional regions of the genome like TSS, heterochromatin domains etc (Summarised in Table 3.1). The lack of studies on H1 function can be largely attributed to technical difficulties involving reduced protein coverage of H1 obtained during the use of mass spectrometry approaches and also the generation of subtype-specific antibodies.

Linker histone	Cell Type	Localisation at specific genomic regions
H1.0	Breast Cancer Cells (T47D)	Nucleolus associated domains (NADs-inner part of nucleus); CpG islands; high GC content regions
H1.X	Breast Cancer Cells (T47D)	RNA polymerase II enriched regions; hypomethylated CpG islands; high GC content regions
H1.c (H1.2)	Breast Cancer Cells (T47D)	intergenic + distal promoter regions of repressed genes; Overlap with LADs (nuclear periphery);regions of low GC content
H1.4	Breast Cancer Cells (T47D)	Overrepresented in genes, exons and downstream regulatory regions, less at CpG islands
H1		H1s are usually enriched in intergenic regions and introns; H1 histone associates with high GC content regions
H1d (H1.3)	mouse ESCs	GC rich and LINE elements; high GC content regions compared to H1c
H1.c (H1.2)	mouse ESCs	AT rich, Giemsa positive regions and satellite DNA [Heterochromatin regions]
H1.1	Human fibroblasts IMR90 cells	Transcription associated; localised at subset of promoters (slightly); preferentially localised in H3K7me3, transcrip repressed
H1.2.	Human fibroblasts IMR90 cells	Depleted from CpG dense regions and active regulatory elements; enriched in HP1 and null domains (no histone mark)
H1.3	Human fibroblasts IMR90 cells	Depleted from CpG dense regions and active regulatory elements; enriched in HP1 and null domains (no histone mark)
H1.4	Human fibroblasts IMR90 cells	Depleted from CpG dense regions and active regulatory elements; enriched in HP1 and null domains (no histone mark)
H1.5	Human fibroblasts IMR90 cells	Depleted from CpG dense regions and active regulatory elements; enriched in HP1 and null domains (no histone mark)
HILS1	Elongating and Condensing Spermatids	LINE L1 elements

Table 3.1- Characteristic features of genome-wide occupancies of linker histones and their variants with in human and mouse cells.

Summary of the genome-wide distribution of linker histones and their variants in various cell types related to humans and mice. The genomic distributions of H1.0 and H1.x in human breast cancer cell lines (Mayor et al., 2015), H1.2, H1.4 and H1 in human breast cancer cell lines (Millan-Arino et al., 2014), H1.2 and H1.3 in mouse ESCs (Cao et al., 2013), H1.1-H1.5 in human fibroblasts (Izzo et al., 2013) and HILS1 in rat spermatids (Mishra et al., 2018a) with their characteristic features have been reviewed in this table.

(A)

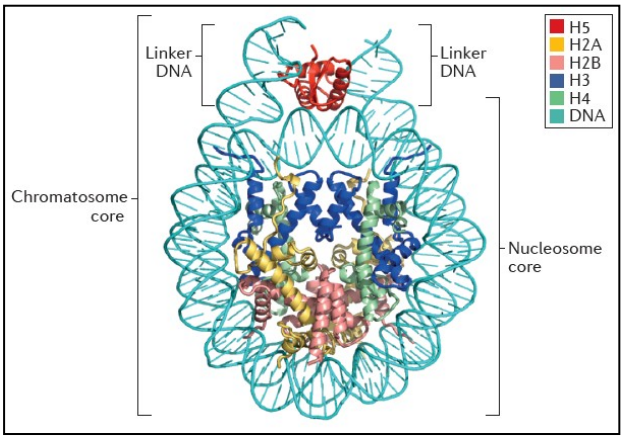

(B)

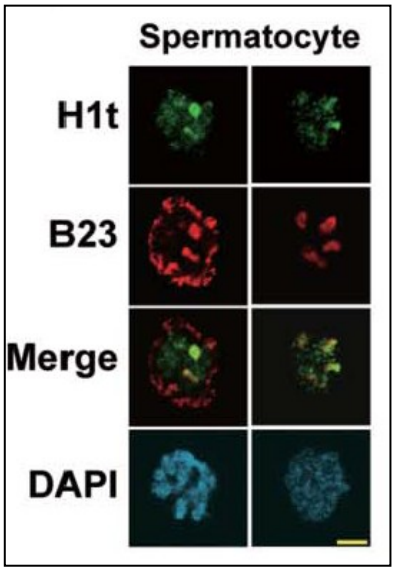

Figure 3.1- A. *Crystal structure of the chromatosome core particle. Taken with permission from the publication "Structural Mechanisms of Nucleosome Recognition by Linker Histones" (Zhou et al., 2015).*
B*. Colocalization of linker histone variant H1t with nucleolar marker B23 (or NPM1) in mouse spermatocytes. Taken with permission from the publication "Linker histone variant H1T targets rDNA repeats" (Tani et al., 2016).*

Our main aim was to determine the genome-wide occupancy of linker histone variant H1t in pachytene spermatocytes, which would give an idea about its association with specific chromatin domains and consequent biological functions. H1t is not exclusively expressed in testis but also expressed in various cancer cells and mouse embryonic stem cells (Tani et al., 2016). Recently, H1t ChIP-sequencing was carried out in human cancer cell lines and mouse ESCs. H1t was found to be majorly associated with the rDNA element of the nucleolus in these cells (Tani et al., 2016). Also, in the same study, various extra-nucleolar foci of H1t were observed in spermatocytes (Fig 3.1B). This provided major inspiration for our study to characterize the genomic occupancy of the linker histone variant H1t in spermatocytes. It is essential to characterize the binding sites of H1t in the pachytene genome, as H1t is the dominant H1 in pachytene spermatocytes, constituting about 50-60% of total H1 content in these cells (Bucci et al., 1982; Govin et al., 2004; Grimes et al., 2003). This would give us information about the unique role(s) of H1t due to which they have primarily replaced somatic H1s in the germ cells.

Maintaining genomic stability and diversity through multiple generations is critical for the survival of various species. Retrotransposons form about 40% of the mouse genome and are characterised into three classes: long interspersed nuclear element (LINE), short interspersed nuclear element (SINE), and long terminal repeat (LTR) retrotransposons (Fig 3.2A). They contribute to genomic instability by acting as sites for chromosomal deletions and rearrangements, by influencing the expression of neighboring genes or by causing mutations at sites of new retrotransposition events. LINE-1 elements are active in mammals wherein their integration has been reported to cause phenotypic changes and diseases in mammals (Hancks and Kazazian, 2012; Maksakova et al., 2006; Shukla et al., 2013).

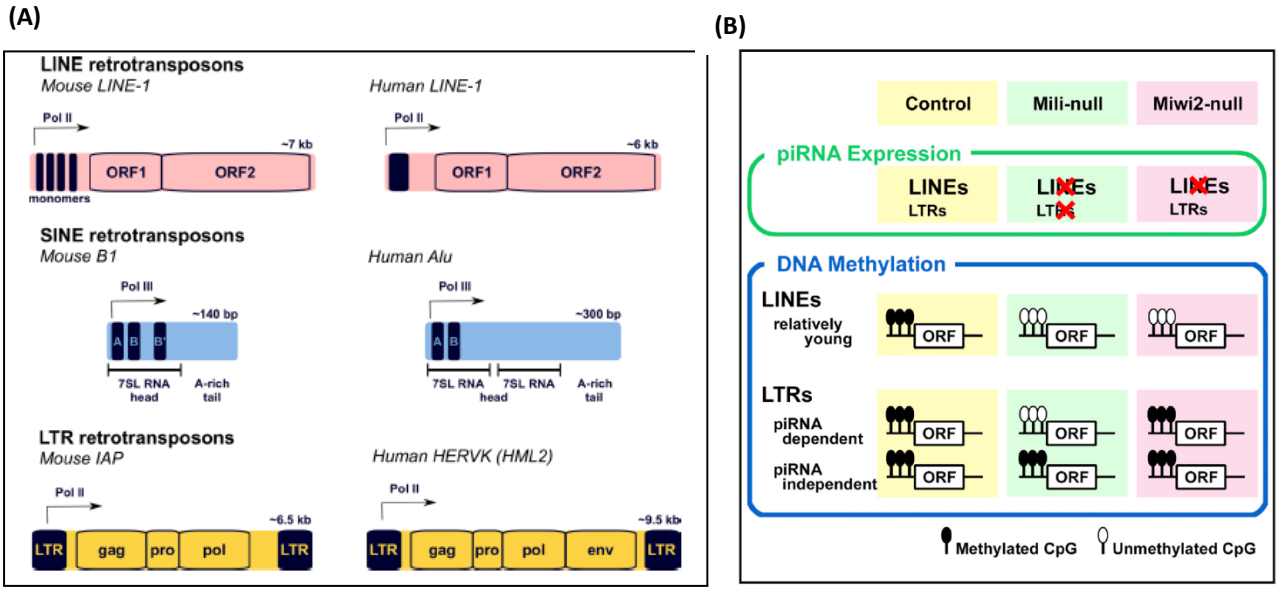

Figure 3.2- Structure of the major classes of retrotransposable elements in the mouse and human genome

A. *Retrotransposon elements can be characterized in LINE, SINE and LTR elements. LINE elements constitute about 17%, LTR about 9%, SINE about 10% of the total sequenced mammalian genomes. The filled rectangles represent the transcription regulatory regions, whereas the open rectangles represent the protein-coding regions. Transcription start sites are indicated with an arrow. Some of the classes have lost specific genes to constitute new subclasses of these major retrotransposable elements. Adapted with permission from the review "Defending the genome from the enemy within: mechanisms of retrotransposon suppression in the mouse germline" (Crichton et al., 2014).*

B. *Patterns of DNA methylation observed in WT, Mili-null and MIWI2-null germ cells (Nagamori et al., 2015). DNA methylation of LINE elements, but not LTR, is dependent on piRNAs. A subset of LTRs displays MIWI2-independent and Mili-dependent DNA methylation. Mili and MIWI2 are RNaseH enzymes belonging to the PIWI family of proteins, the loss of which results in male infertility (Aravin et al., 2008; Carmell et al., 2007). Adapted with permission from the publication "Comprehensive DNA Methylation Analysis of Retrotransposons in Male Germ Cells" (Nagamori et al., 2015).*

Various defense mechanisms have evolved in germ cells of various species to prevent the expression of these retrotransposable elements, thus limiting their mutagenic potential. DNA methylation at LINE and LTR retrotransposable elements can be dependent on piRNA expression or not, also termed as piRNA-dependent and piRNA-independent respectively (Fig 3.2B) (Nagamori et al., 2015).

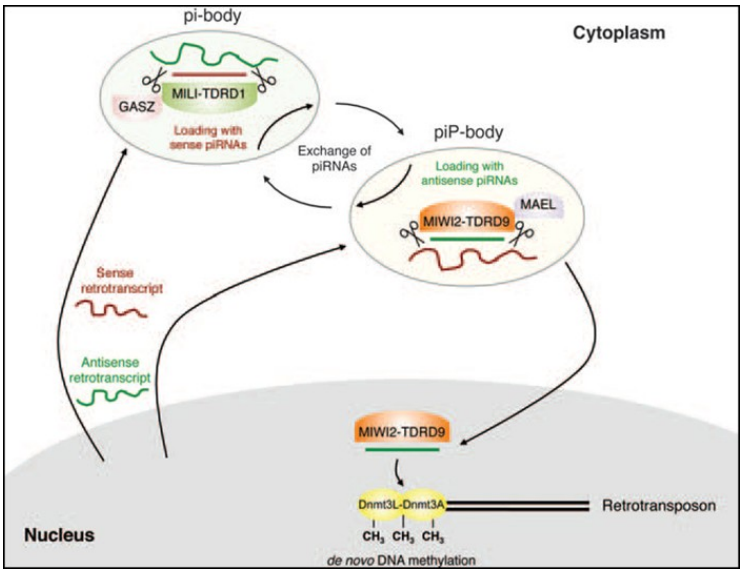

Figure 3.3- Interaction of piRNA pathway and DNA methylation machinery in the male germline

piRNA pathway is also called a major fertility protector by virtue of its dual role in restricting TE expression through post-transcriptional degrdation of target RNAs and DNA methylation-dependent transcriptional silencing. The sense and antisense transcripts originating from the TE sequences have been given in red and green lines respectively. Adapted with permission from the review "Transposable elements in the mammalian germline: a comfortable niche or a deadly trap?"(Zamudio and Bourc'his, 2010).

Retrotranscripts originating from TE sequences in the nucleus are cleaved into sense and antisense piRNAs (Fig 3.3). The sense RNAs associate with GasZ containing MILI-TDRD1 complexes within pi-bodies (Ma et al., 2009). On the other hand, the antisense RNAs associate with MIWI2-TDRD9 complexes and then localize to MAEL-containing piP bodies (Kojima et al., 2009; Reuter et al., 2009). Degradation of retrotranscripts occurs by the exchange of sense and antisense transcripts in the cytoplasmic compartments. MIWI2-TDRD9 complexes can also induce feedback signaling into the nucleus to facilitate the recruitment of Dnmt3L/3A machinery to induce *de novo* DNA methylation at the target TE loci. Some of the important proteins like MIWI, MAEL, GasZ related to TE repression are also expressed during later stages of spermatogenesis (Fig 3.4). Mutations in these genes result in pachytene arrest and male infertility.

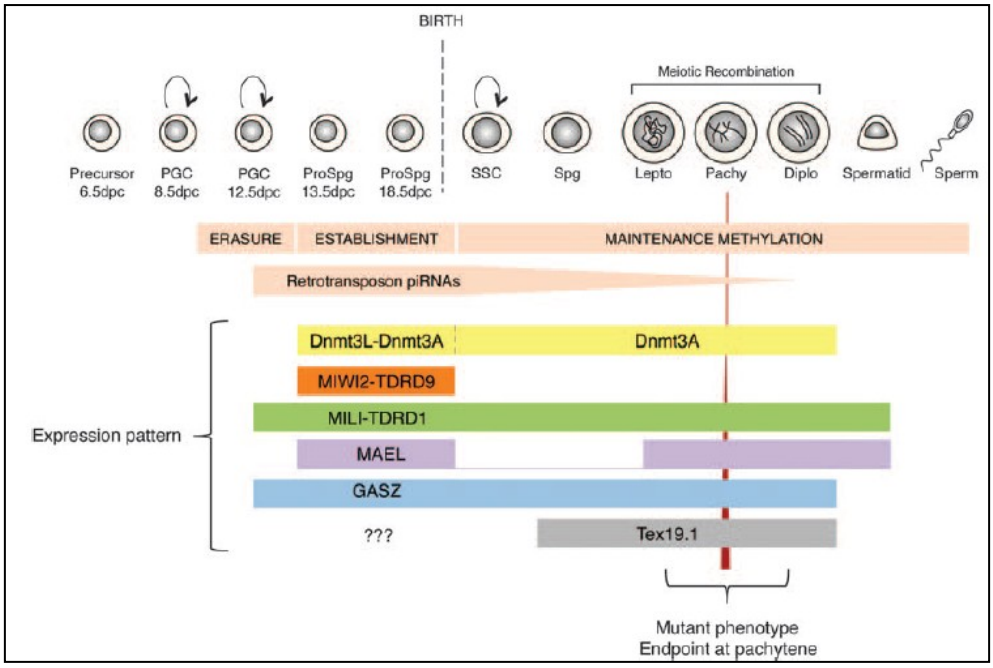

Figure 3.4- Expression pattern of proteins involved in TE repression in the developing germ cells of mouse

The germline genome gets demethylated as primordial germ cells (PGCs) colonize the genital ridges (10.5 dpc). After sex determination, male PGCs differentiate to form prospermatogonia (ProSpg). The genome is remethylated at 13.5 dpc till birth, at the formation of spermatogonial stem cells (SSCs). This time period is associated with the expression of TE-derived piRNAs, DNA methyltransferases (Dnmt3L and Dnmt3A) and PIWI proteins (Mili and MIWI2). Some of the proteins are expressed until the adult stages of spermatogenesis. Mutations in some of these genes result in arrest at the pachytene stage. Adapted with permission from the review "Transposable elements in the mammalian germline: a comfortable niche or a deadly trap?"(Zamudio and Bourc'his, 2010).

DNA methylation at LINE retrotransposons are piRNA-dependent (Nagamori et al., 2015). Orchestration of LINE silencing occurs by three cooperative and stage-dependent epigenetic mechanisms (Di Giacomo et al., 2013): a. CpG methylation and H3K9me2/3 transcriptionally repress LINE elements until the late zygotene stage; b, H3K9me2/3 is sufficient for repression at certain LINE elements, even with defects in LINE CpG methylation and c. Loss of H3K9 methylation results in the pachytene arrest, even without LINE deregulation (Tachibana et al., 2007). Silencing of LINE retrotransposons by DNA methylation can be piRNA-dependent or independent whereas DNA methylation at most of LTRs is piRNA-independent. Another set of transposable elements like SINE does not exhibit piRNA-

dependent repression (Shoji et al., 2009). This suggests that retrotransposon inactivation in germ cells is more complex and their mechanism by the action of important players is currently being investigated in great detail.

3.2 Materials and Methods

3.2.1 Cloning and expression of C-terminal protein fragment of H1t

The coding sequence (CDS) corresponding to 112-207 amino acid residues of H1t protein was cloned using specific primers into the pET22b(+) vector using HindIII and NotI restriction sites. The primer sequences are given in Annexure 3. The expression vector was transformed in Rosetta strain of E.coli, and His-tagged proteins was purified using Ni-NTA purification method.

3.2.2 Antibody generation

The recombinant protein (C terminal fragment of H1t) was injected into rabbits, and the 14-day cycle of antibody generation was followed. Immunoglobulins were purified by caprylic acid-based purification method. Antigen-affinity based purification with the Sulfolink columns containing immobilized protein was used to purify the H1t-specific antibodies. The H1t antibody was outsourced from the Abgenex company (Bhubaneshwar, India).

3.2.3 ELISA

The recombinant proteins were used at 200 ng per well. The pre-bleed and immune sera were used at 1:5000 dilution. Goat anti-rabbit HRP was used as the secondary antibody at 1:5000 dilution. TMB (3, 3', 5, 5'- Tetramethylbenzidine) was used as the substrate for color development. After three minutes of enzyme-substrate reaction, the plate was read at 450 nm.

3.2.4 Extraction of linker histones from mouse testes

Linker histones along with other acid-soluble nuclear proteins were extracted from mouse testes by the perchloric acid method (Burston et al., 1963; Gupta et al., 2017). Briefly, the purified nuclei were resuspended in 10% perchloric acid, homogenized and kept on ice for 30 minutes. The sample was centrifuged for 10000g for 10 min at 4^{o}C to pellet the residual chromatin. The proteins were precipitated from the supernatant using 30% trichloroacetic acid (TCA). After incubation on ice for 30 minutes, the proteins were recovered by centrifugation at 12000g at 4^{o}C for 10 min. The protein pellet was sequentially washed once

with cold acetone containing 0.05% HCl and twice with ice-cold acetone. The pellet obtained was dried, dissolved in water and stored in aliquots at -20^{o}C.

3.2.5 Extraction of histones from mouse testes

Histones were extracted from the mouse testes using the published protocol (Shechter et al., 2007). Briefly, the cell pellet was resuspended in hypotonic lysis buffer (10mM Tris-Cl pH 8.0, 1mM KCl, 1.5mM $MgCl_2$ and 1mM DTT, 1X protease inhibitor cocktail) and then incubated on a rotator for 30 min at 4^{o}C. The nuclei were pelleted by centrifugation at 10000g, 10 min, 4^{o}C. The pellet was resuspended in 0.4N H_2S0_4 and then incubated on a rotator for 30 min at 4^{o}C. Histones were then precipitated using 33% TCA (final concentration) and the histone pellet was then washed with ice-cold acetone two times before resuspending in appropriate volume of water.

3.2.6 Preparation of meiotic spreads from testicular cells

Meiotic spreads were prepared according to the published protocol (Peters et al., 1997). All the experimental details regarding the preparation of meiotic spreads are given in the Materials and Methods section of the previous chapter (Under the heading “Preparation of testicular meiotic spreads”- Page number 36).

3.2.7 ChIP-sequencing of linker histone variant H1t in P20 mouse testicular cells

Chromatin immunoprecipitation (ChIP) was carried out using the published protocol (Tardat et al., 2010). Briefly, P20 mice testes were dissected in 1X PBS (with 1% formaldehyde), incubated for 10 min on a rotating wheel at room temperature. Quenching to remove formaldehyde was done using glycine (250mM final concentration). The pellet was washed with 1X PBS multiple times. The suspension was filtered using a 40µm filter and then centrifuged at 500g for 5 min at 4^{o}C. The pellet was resuspended in Buffer A (10mM Tris pH 8.0; 10mM KCl; 0.25% Triton-X-100; 1mM EDTA; 0.5mM EGTA; 1X protease inhibitor cocktail from Roche), and incubated on ice for 5 minutes. Again, the contents were centrifuged at 500g for 5 min at 4^{o}C. The pellet was then resuspended in Buffer B (10mM Tris pH 8.0; 200mM NaCl; 1mM EDTA, 0.5mM EGTA; 1X protease inhibitor cocktail), incubated on ice for 10 min, centrifuged again at 500g for 5 min at 4^{o}C. Finally, the pellet was resuspended in SDS lysis buffer (1% SDS, 10mM EDTA, 50mM Tris pH 8.0, 1X protease inhibitor cocktail). The contents were incubated on a rotating wheel for 30 min at

4°C. Sonication was carried out 40 cycles, and chromatin fractions were diluted 1/10 times with the dilution buffer (5mM Tris PH 8.0, 140mM NaCl, 0.5% TritonX-100, 0.05% sodium deoxycholate, 0.5mM EGTA) before subjecting it to antibody binding overnight at 4°C on a rotating wheel. Dynabeads were added the next day, washes were given with W1 (10mM Tris pH 8.0, 150mM KCl, 0.50% NP-40, 1mM EDTA), W2 (10mM Tris pH 8.0, 100mM NaCl, 0.10% sodium deoxycholate, 0.50% Triton-X-100), W3a (10mM Tris pH 8.0, 400mM NaCl, 0.10% sodium deoxycholate, 0.50% Triton-X-100), W3b (10mM Tris pH 8.0, 500mM NaCl, 0.10% sodium deoxycholate, 0.50% Triton-X-100), W4 (10mM Tris pH 8.0, 250mM LiCl, 0.50% sodium deoxycholate, 0.50% NP-40, 1mM EDTA), W5 (10mM Tris pH 8.0, 1mM EDTA) wash buffers. The complexes were eluted from input, rabbit IgG control ChIP, and H1t ChIP samples using elution buffer (50mM Tris pH 8.0, 1% SDS, 1mM EDTA) and then incubated at 65°C overnight with intermittent shaking. The supernatants recovered from the tubes were subjected to RNase A and proteinase K digestions at 37°C. DNA was then extracted from the elute fractions using the phenol-chloroform method. The input and ChIP DNA libraries were prepared using the NEBNext Ultra II DNA library preparation kit. The resulting libraries were quantified before getting sequenced on the Illumina HiSeqX system to generate read depth of 40 million reads (2X150 bp paired-end sequencing).

3.2.8 Computational data analysis

The quality control of FASTQ files was carried out using Tapestation. Further, the reads were aligned to the mm10 reference assembly (mouse genome) using Bowtie2 (Langmead and Salzberg, 2012) using default parameters. Peaks were called from the aligned reads using the MACS2.0 peak caller (Feng et al., 2012) using the p=0.05 setting. The ChIP-sequencing dataset is given in Annexure 5.

The read concentration of H1t peaks was compared against the already published datasets of active gene promoters (GSE93955), TSS (GENCODE), DSB hotspots (GSE93955) and ATAC sequencing data (GSE102954) using ngsplot.r. Annotation of H1t-bound genomic regions was carried out using HOMER.

FASTA sequences corresponding to the rDNA element were obtained from NCBI (Grozdanov et al., 2003). The peak files FASTAQ were generated from these FASTA sequences. After the peaks were mapped to the rDNA element using the rDNA annotation file, the tag densities were then computed on the various regions of the rDNA element.

The raw bisulfite sequencing data for P20 mouse testicular cells were obtained from the Sequence Read Archive (SRA) database. The reads were aligned using Bowtie2, and the

methylated markers were isolated after the mapping of the reads to the reference mouse. The methylation analysis was done using bismark_v0.22.1 (Krueger and Andrews, 2011). The comparison of the bisulfite sequencing dataset with the H1t dataset was carried out using ngsplot.r, after peak extension and splitting of the regions into genomic and non-genomic locations.

Motif analysis was carried out using MEME software (Bailey et al., 2006).

3.2.9 Mass spectrometric identification of proteins associated with H1t-containing chromatin fragments

All the experimental details regarding the mass spectrometry protocol are given in the Materials and Methods section of the previous chapter (Page Number 80). The list of H1t-associated proteins is given in Annexure 6.

3.3 Results

3.3.1 Validation of the specificity of H1t antibodies

As mentioned earlier, our main aim was to determine the genome-wide localization of linker histone variant in pachytene spermatocytes, for which we required to generate an H1t-specific antibody. Since the C-terminal region of H1t is highly divergent between H1t and somatic H1s, we first cloned and purified the C-terminal protein fragment of H1t and then used as an antigen to generate polyclonal antibodies in rabbits (Fig 3.5a, 3.5b). We determined the specificity of H1t antibodies by ELISA and western blotting assays. By ELISA assays, we found that the sera, as well as purified antibody, reacted to the recombinant H1t C-terminal protein fragment (Fig 3.5c, 3.5d). Western blotting also showed specific reactivity with the protein corresponding to H1t in the perchloric acid testicular extracts (Fig 3.6A, α-H1t lane). Also, we observe a different band when H1.2 antibodies were used for immunoblotting (Fig 3.6A, α-H1.2 lane), suggesting that the molecular weights of the bands were specific to these variants and the antibodies did not crossreact with other variants. Additionally, we observed, after preincubation with the H1t C-terminal antigen, the reactivity of H1t antibodies was abolished, thereby demonstrating the specificity towards the H1t linker histone variant (Fig 3.6A, protein competition, α-H1t lane). However, as can be seen in Fig 3.6A (protein competition, α-H1.2 lane) the reaction to H1.2 was not competed out with the after preincubation with the H1t C-terminal antigen. We obtained similar results with immunoblotting using H1t and H1.2 antibodies against acid extracts (0.4N H_2S0_4)

derived from P20 mouse testicular cells, wherein we observed specific reactivity of the antibodies towards the variant histones (Fig 3.6B, α-H1t and α-H1.2 lanes). The C-terminal antigen blocked the specific reactivity of H1t antibodies (Fig 3.6B, protein competition, α-H1t lane) but not the H1.2 antibodies (Fig 3.6B, protein competition, α-H1t lane) against acid extracted nuclear proteins.

The specificity of H1t antibodies was additionally confirmed by mass spectrometry, as H1t was the only variant to be associated with the immunopurified H1t-containing oligonucleosomes (See later). We further determined the staining pattern of H1t across the various stages of meiotic prophase I. We observed uniform distribution of H1t protein across the leptotene, zygotene and pachytene cells (Fig 3.7a), consistent with being the dominant H1 in spermatocytes.

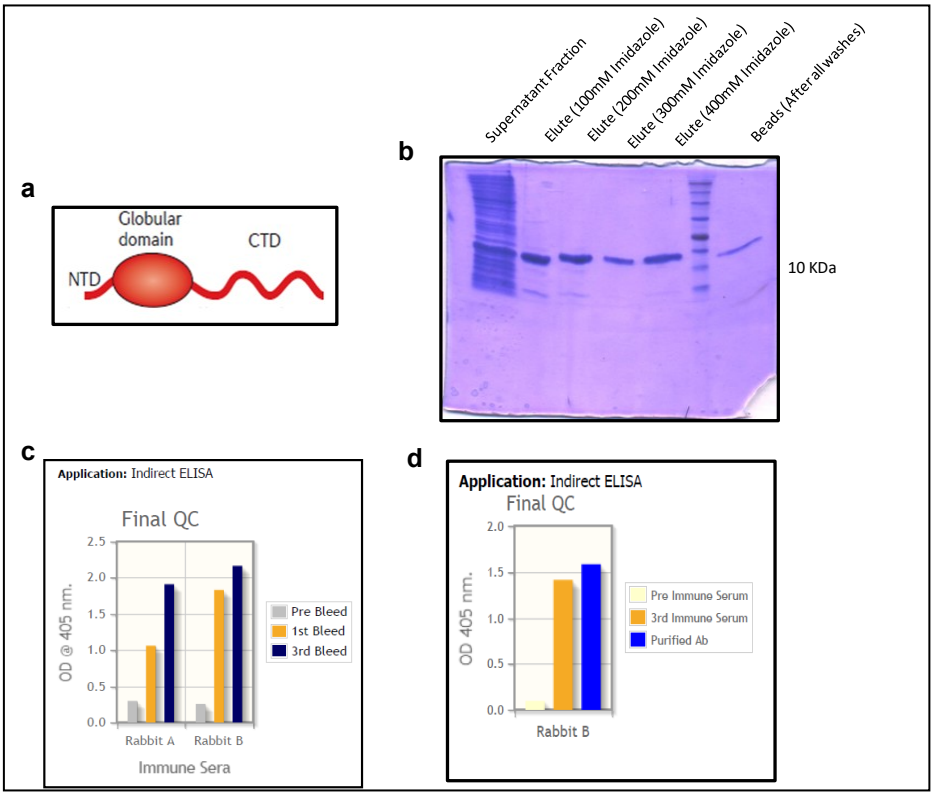

Figure 3.5- a. *The tripartite structure of linker histones- the linker histones possess three major domains: N-terminal domain, globular domain, and the C-terminal domain. Since the C-terminal of H1t protein is highly divergent in comparison with other variants, we used 112-207 amino acid residues as protein fragment for the generation of H1t-specific antibodies in rabbits.*

b. *Coomassie-stained gel showing the successful purification of His tagged C-terminal fragment of H1t. The purity of proteins was determined after elution using 100mM, 200mM,*

300mM, and 400mM imidazole, wherein pure proteins were obtained after elution using 300/400mM concentration of imidazole.

Validation of specificity of H1t antibody towards the H1t C-terminal protein fragment by ELISA using ***c.*** *Immune sera and* ***d.*** *Purified antibody. The sera, as well as purified antibodies, showed reactivity against the protein fragment. Information in* ***(c-d)*** *The color code schemes are indicated to the right of the figures. The data plotted is the average of the two experiments.*

3.3.2 Genome-wide occupancy of linker histone variant H1t in pachytene spermatocytes

Since H1t is a linker histone and a component of chromatin, we carried out ChIP-sequencing with the crosslinked chromatin to determine the occupancy sites of H1t in the pachytene chromatin of mouse. We chose mouse testis as the model system for the study, since various datasets related to biological processes like meiotic recombination, transcription have been well characterized in the mouse species.

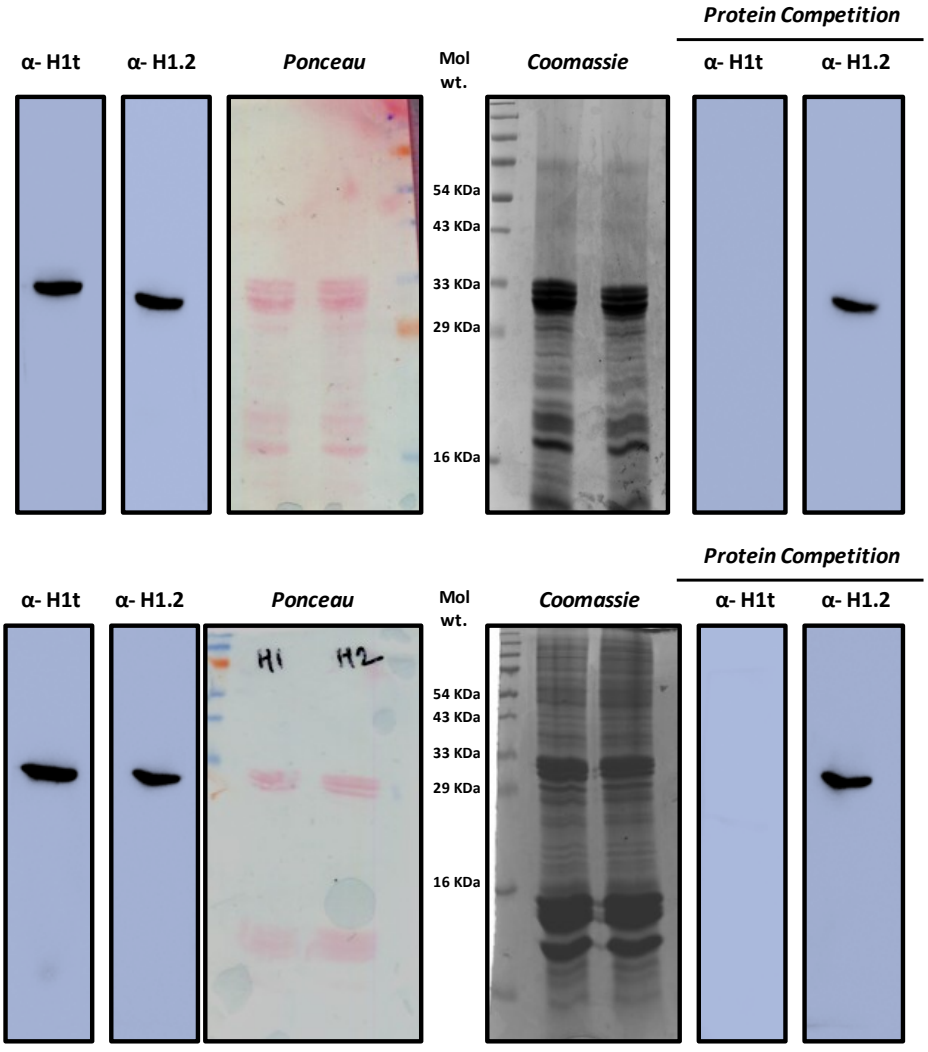

***Figure 3.6- A**. Western blotting of H1t and H1.2 antibodies against perchloric acid extracts prepared from P20 mouse testicular cells. The anti-H1t and anti-H1.2 antibodies showed reactivity to the specific linker histones, as seen in the blot images on the left, where bands corresponding to molecular weights of H1t and H1.2 were obtained. The blots on the right indicate the immunoblotting performed with the H1t and H1.2 antibodies after preincubation with the recombinant H1t C-terminal protein fragment, before their addition to the blot. Ponceau and Coomassie-stained images are given for reference.*

***B**. Immunoblotting using H1t and H1.2 antibodies against 0.4N H_2SO_4 acid extracted histones prepared from P20 mouse testicular cells. The blots on the left show the western blotting data performed using H1t and H1.2 antibodies against the acid extracted histones. The blots on the right indicate the western blotting data performed using H1t and H1.2 antibodies after preincubation with the 10µg recombinant H1t C-terminal protein fragment. Ponceau and Coomassie-stained images are given for reference.*

We obtained 48681 peaks of H1t occupancy after performing the ChIP-sequencing analysis. The chromosome-wide distribution of H1t peaks is given in Figure 3.7b. As can be seen in Fig 3.7b, linker histone variant H1t is depleted from the XY body relative to the autosomes (224 peaks in chromosome X and 89 peaks in chromosome Y). This corroborates with previously published data wherein H1t was found to be depleted from the XY body and is associated with autosomal chromatin domains in pachytene spermatocytes (Hu et al., 2018), highlighting the robustness of our ChIP-sequencing data.

To reiterate, linker histones are known to be generally depleted from active TSS, open chromatin structures *in vivo*, except some variants like H1x, H1.1 (Izzo et al., 2013)(See Table 3.1). We wanted to determine whether the variant H1t is associated with genomic regions related to transcription, meiotic recombination, etc. We performed overlap analysis of H1t genomic peaks with other ChIP-sequencing datasets and the results are represented as aggregation plots and heat maps. Both these methods show the spatial distribution of reads within the target genomic regions (34).

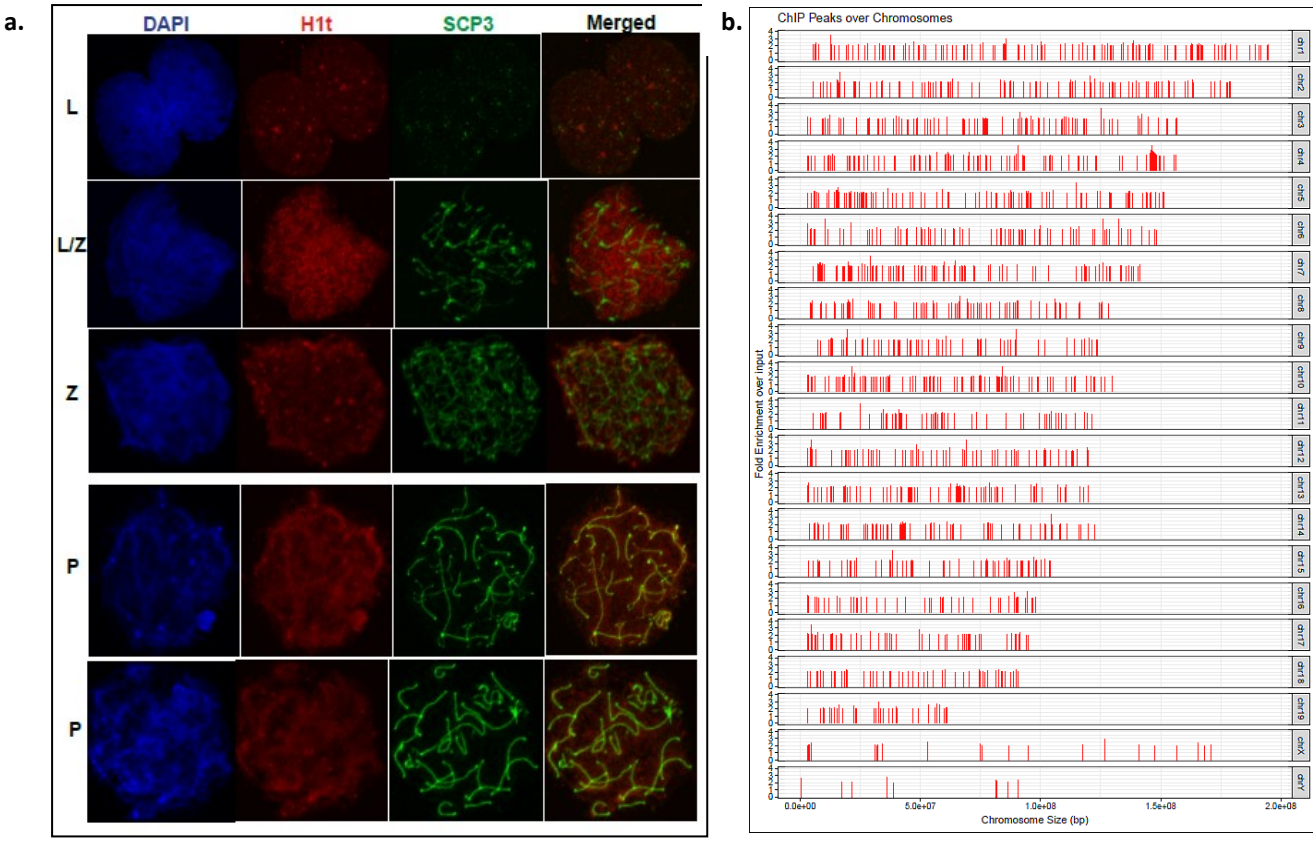

Figure 3.7- a. *Immunostaining pattern of linker his tone variant H1t across various stages of meiotic prophase I. Staining of anti-H1t and anti-Scp3 across leptotene (L, first panel), leptotene-zygotene (L/Z, second panel), zygotene (Z, third panel), and pachytene (P, fourth and fifth panels).*

b. *Chromosome-wise distribution of H1t peaks in the pachytene genome. The y-axis represents the fold enrichment over background input, and the x-axis is the various locations along the length of each chromosome. The normalisation of high fold enriched peaks has been done to 3.5 fold change and the lower threshold has been maintained for fold change=2.*

We observe H1t to be not significantly associated with active gene promoters, DSB hotspots and transcription start sites (Fig 3.8 a,b,c, respectively). Also, when performing the overlap analysis of the H1t ChIP-seq dataset with ATAC-sequencing dataset available for pachytene spermatocytes, we observed that H1t is not majorly associated with open chromatin regions (ATAC-seq positive genomic regions) in the pachytene genome (Fig 3.8d). These observations suggested that H1t might be associated with chromatin regions whose functional consequence would be to ultimately form condensed structures *in vivo*.

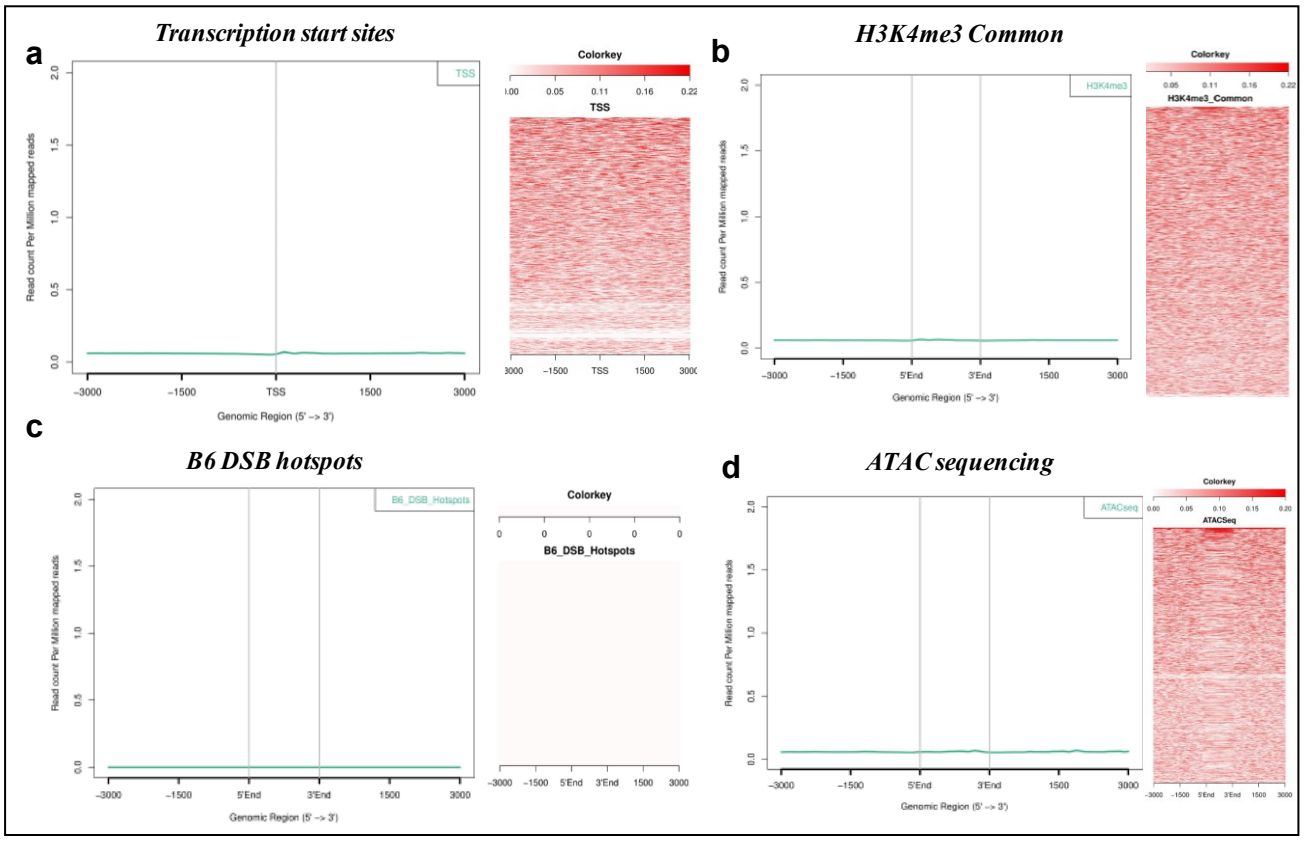

Figure 3.8- Localization of linker histone variant H1t at TSS, active gene promoters, recombination hotspots and open chromatin regions (ATAC seq positive regions)

Analysis of overlap between TH2BS11ph and ***a****. H3K4me3 common representing the TSS-associated H3K4me3 marks,* ***b*** *TSS of the mouse,* ***c****. DSB hotspots,* ***d****. open chromatin regions of pachytene spermatocytes. H1t were observed to depleted at active gene promoters, TSS regions. In each figure from* ***a-d****, the overlap has been determined using aggregation plots (left panels) and heat maps (right panels).*

3.3.3 Localization of linker histone variant H1t at repetitive elements

Since H1t is not associated with TSS, active gene promoters, DSB hotspots, and ATAC-seq positive regions, the primary question remained to what genomic regions are H1t localized at. We observed that H1t is majorly associated with intergenic and intronic regions (Fig 3.9a). On further annotation of the H1t-bound genomic regions, we observed that the majority of the H1t-peaks were closely associated with LINE and LTR classes of repetitive elements, and SINE to a lesser extent (Fig 3.9b). We conclude that H1t is localized to retrotransposable elements LINE, LTR and SINE *in vivo*. These retrotransposable elements are repressed in the germ cells by the action of RNA interference machinery and small RNAs. Despite millions of

years of divergence, the machinery involving RNAi machinery and piRNAs in preventing transposable element (TE) expression have been conserved in fungi, plants, and animals. piRNAs are essential for de novo DNA methylation at these TE loci crucial for silencing of LINE and LTR elements in embryonic male germ cells. DNA methylation is carried out the methyltransferase Dnmt3L in early germ cells, the loss of which results in male infertility due to meiotic failure (Bourc'his and Bestor, 2004). Therefore, DNA methylation of repeat elements is a major mechanism for preventing TE expression and is critical for success of productive spermatogenesis.

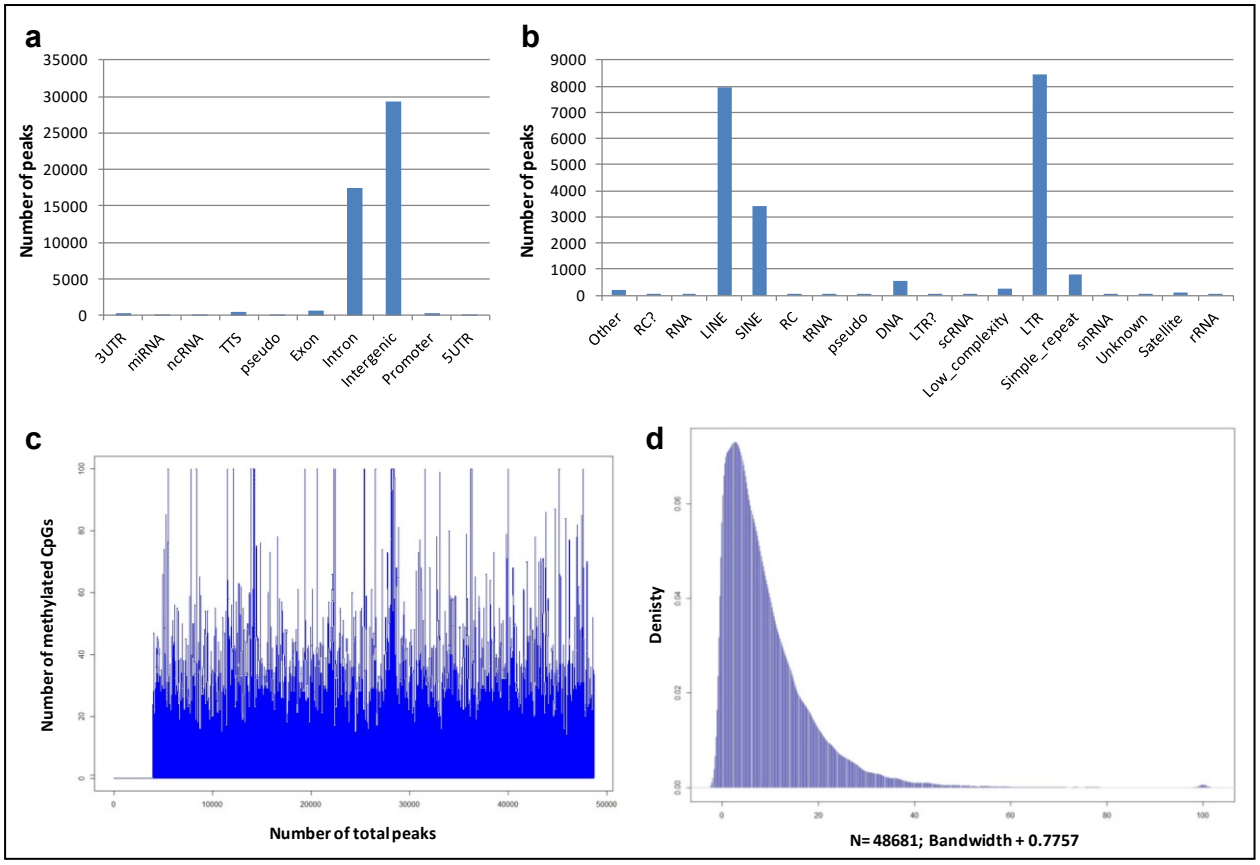

Figure 3.9- Localization of linker histone H1t at CpG methylated repeat elements

a. *Annotation of H1t-bound genomic regions using HOMER*

b. *Annotation of H1t peaks at repeat elements showing its predominant association with LINE and LTR subclasses of retrotransposable elements.*

c. *Profile of methylated cytosines across all the H1t peaks. More than 90% of the H1t peaks overlap with methylated CpGs. The y-axis is the count of methylated CpG positions at each peak. Some peaks with more than 100 methylated cytosines have been truncated to 100 for better visualization of the overall plot.*

d. *Density plot of H1t peaks overlapping with methylated CpGs. The y-axis represents the density function and the x-axis represents the bandwidth parameter. N represents the number of observations.*

Since the piRNA pathway machinery repress TE by DNA methylation, our next question was to determine whether H1t-associated genomic regions are associated with DNA methylation. We determined the overlap of H1t ChIP-sequencing data with the already published bisulfite sequencing dataset available for P20 mouse testicular cells. As can be seen in Fig 3.9c and Fig 3.9d, we observed more than 90% (44720 peaks) of H1t peaks were associated with methylated CpGs at these repetitive elements. These observations gave a major indication that H1t, apart from its major association with classes of repetitive elements LINE and LTR, are methylated in pachytene-enriched mouse P20 testicular cells.

3.3.4 Localization of linker histone variant H1t in the rDNA element of pachytene spermatocytes

Linker histone variant H1t was previously demonstrated to be localized to the rDNA element of the nucleoli in spermatocytes, human cancer cell lines, and mouse ESCs (Tani et al., 2016). We confirmed the association of H1t in the rDNA element of pachytene spermatocytes (Fig 3.10a), wherein we observed 13008 peaks to be localized at the known mouse rDNA element. The majority of the H1t peaks are localized in the intergenic spacer of the rDNA element (Fig 3.10b).

The rDNA element harbors many repetitive elements, the major element being SINE (Grozdanov et al., 2003). SINE elements constitute about 20% of the total rDNA element in the mouse. We observed that H1t peaks are located at or close to the vicinity of the predominant SINE elements (marked in green) in the rDNA element of the pachytene spermatocyte (Fig 3.10c). We also wondered whether the H1t peaks localized at the repetitive elements of the rDNA element are associated with DNA methylation. True to our intuition, we observed more than 95% (12550 peaks) of H1t peaks are indeed associated with methylated CpGs in the rDNA element (Fig 3.10d). In addition to the extra-nucleolar localization of H1t at the retrotransposon classes LINE and LTR, we also observe a significant overlap of H1t at the repetitive elements of the rDNA element, characterized by the occupancy of methylated CpGs. Thus, in both nucleolar and extranucleolar mouse genome of P20 testicular cells, linker histone variant H1t occupy methylated CpG repeat-associated chromatin domains.

3.3.5 Combinatorial histone marks at H1t-bound genomic regions

In addition to DNA methylation, repressive histone modifications like H3K9me3 (Pezic et al., 2014) and H4K20me3 (Delaval et al., 2007) are deposited for silencing of the retrotransposable elements. The characteristic histone marks of these major classes of retrotransposable elements are indicated in Fig 3.11a. H3K9me3 histone mark is present on LINE and LTR repeat elements in germ cells and is dependent on the function of the piRNA pathway (Pezic et al., 2014). H3K9 methylation is an important epigenetic mark involved in transcriptional silencing and heterochromatin formation. The formation of H3K9me3 histone mark is mediated by histone methyltransferases (HMTs) Suv39h1 and Suv39h2 in germ cells (Grewal and Jia, 2007; Peters et al., 2001; Peters and Schubeler, 2005).

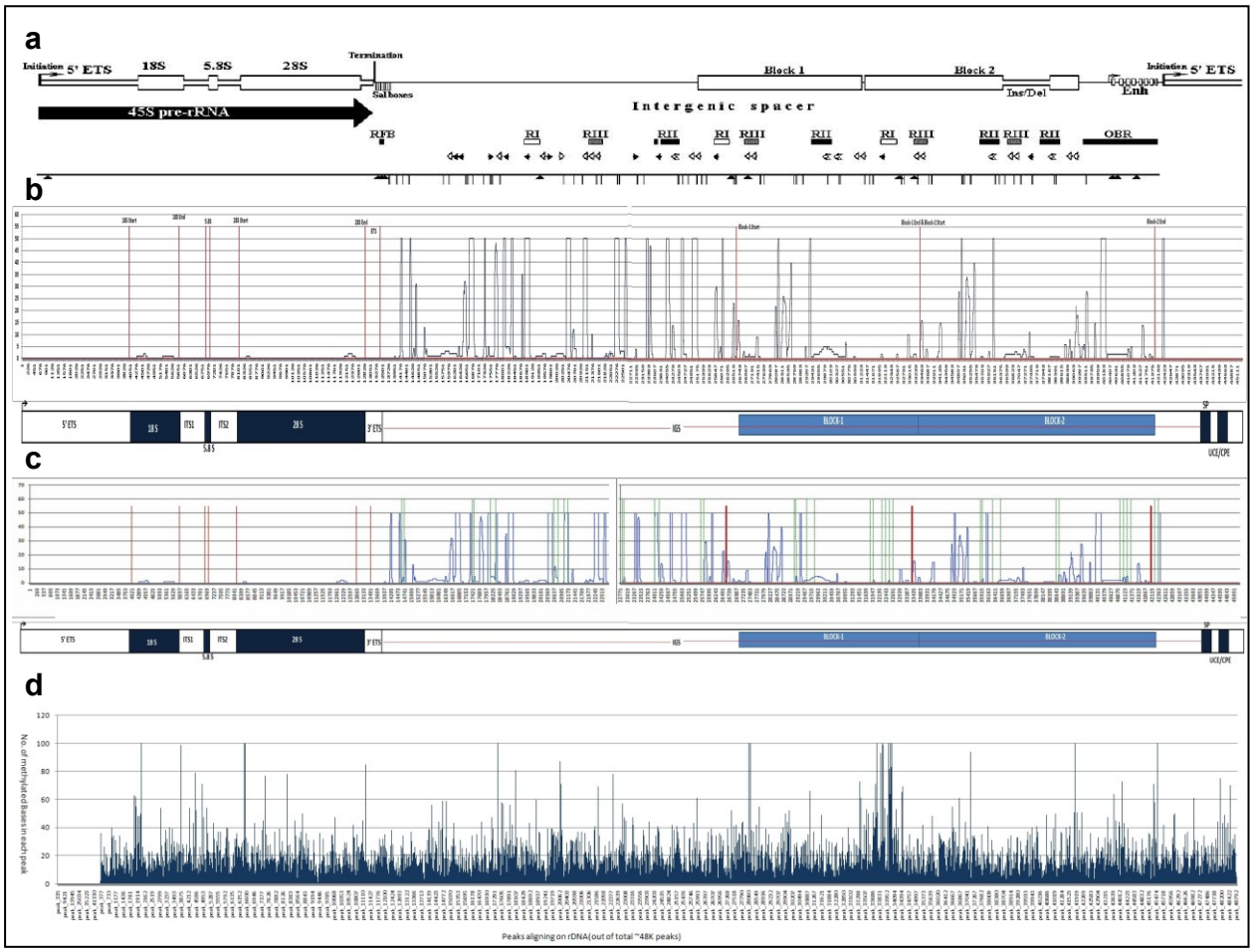

Figure 3.10- Localization of linker histone H1t in the mouse rDNA element

a. *The complete sequence of the 45kb rDNA element showing both the coding and intergenic spacer regions (Grozdanov et al., 2003).*

b*. Peak distribution of H1t across various regions of the rDNA element.*

c*. Peak distribution of H1t with respect to SINE elements (green lines) localized in the rDNA element.*

*Information in (**b-c**) The red lines demarcate various regions of the rDNA element, blue lines are the H1t peaks, and the regions have been labeled below the peak distribution maps.*

***d**. Distribution of methylated CpGs across all the H1t peaks in the rDNA element. More than 99% of the H1t peaks overlap with methylated CpGs in the rDNA element. The y-axis represents the number of methylated CpGs and the x-axis represents the individual H1t peaks that are localized in the rDNA element.*

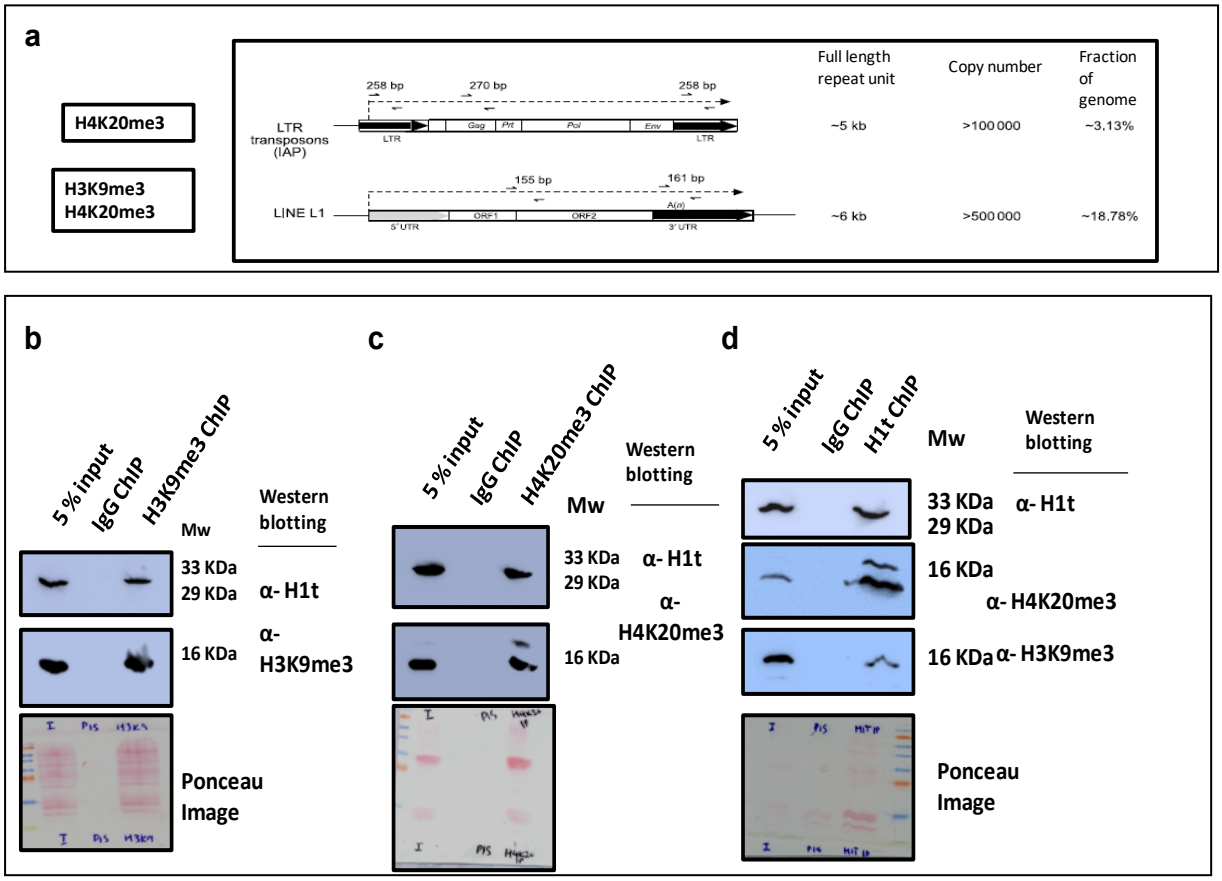

***Figure 3.11- a.** Characteristic histone modifications at LINE and LTR elements (Martens et al., 2005).*

Co-immunoprecipitation assays showing the coexistence of H1t-containing oligonucleosomes with histone marks H3K9me3 and H4K20me3.

***b**. Coassociation of H3K9me3 with H1t*

***c.** H1t is associated with H4K20me3 ChIP elute fraction*

***d**. H1t-containing chromatin domains are associated with histone marks H3K9me3 and H4K20me3 in vivo.*

*Information in **(b-d)** The first lane is the input fraction, the second lane is the IP using the non-specific IgG isotype control and the third lane is the IP with the mentioned antibodies (anti-anti-H3K9me3/anti-H4K20me3/anti-H1t). The antibodies labeled alongside the blot*

refers to the antibodies used for western blotting. Ponceau stained blots are given for reference.

Next, we went ahead to determine whether H1t-containing oligonucleosomes are associated with repressive histone marks like H3K9me3 and H4K20me3 *in vivo*. By the use of oligonucleosome IP assays, we found that H3K9me3 and H4K20me3 pulled down H1t protein (Fig 3.11b, 3.11c, respectively). Also, by reciprocal IP assays, we observed H1t-associated oligonucleosomes to be positive for H3K9me3 and H4K20me3 histone marks *in vivo* (Fig 3.11d). These biochemical assays demonstrate the interaction of repressive histone marks H3K9me3 and H4K20me3 with H1t-containing chromatin fragments in pachytene-enriched P20 testicular cells. Thus, we provide strong support to the fact that H1t-containing genomic regions are associated with DNA methylation and repressive histone modifications H3K9me3 and H4K20me3 in pachytene-enriched P20 testicular cells.

Nucleolar Associated Proteins	No. of unique peptides	No. of total peptides
Ncl	16	25
Numa1	9	10
Npm1	3	4
Rps9	3	3
Rpl23a	3	5
Rpl5	1	1
H2afy2	1	2

Heterochromatin and Repeat-associated Proteins	No. of unique peptides	No. of total peptides
Top2a	18	25
Scml2	9	20
Fyttd1	7	15
H2afx	6	19
H3f3b	5	15
Hormad1	4	6
Chd4	3	4
Cenpv	3	4
Cbx1	3	3
Cbx5	2	4
Sin3a	2	2
Piwil1	2	2
Hspa2	2	2
Trim28	1	1
Hdac1	1	1
Mael	1	1
Baz2a	1	1
H2afy2	1	2
Mre11a	1	1

MIWI Associated proteins	No. of unique peptides	No. of unique peptides
Myh11	2	2
Myh10	2	2
Myh9	7	9
Other Important Proteins		
Sycp3		
Sycp2	7	17
Hist1h1t	6	25
Parp1	6	9
Syce1	4	7
Smarcc1	4	5
Smarcd2	4	5
Baz1b	3	4
Rad50	3	3
Smarca4	1	1

Figure 3.12- List of key proteins associated with H1t-positive chromatin fragments in pachytene spermatocytes as determined by mass spectrometry

The key proteins that are associated with H1t-containing oligonucleosomes can be divided into four major classes: Nucleolar function, heterochromatin and repeat-associated proteins,

MIWI associated proteins and Other important proteins. The proteins indicated in red color have been selected for further validation by co-IP assays.

3.3.6 Mass spectrometric based identification of proteins associated with H1t-bound chromatin fragments

H1t being the major linker histone component of pachytene chromatin, we wanted to identify the proteins that co-associate with H1t-containing chromatin fragments. For this purpose, after carrying out the H1t ChIP, we performed mass spectrometric analysis of the eluted proteins to identify the H1t-associated proteins in the chromatin context. The proteins were identified based on the enrichment of proteins observed in the H1t ChIP fraction compared to preimmune rabbit IgG ChIP fraction. Interestingly, we observed H1t be the only linker histone variant associated with the H1t ChIP fraction. This provides additional strength for our studies regarding the specificity of the H1t antibody, highlighting the robustness of our observations.

Further, we observed that the H1t-associated proteins could be identified into three classes-nucleolar-associated, repeat element and heterochromatin-associated and other important proteins (Fig 3.12). We expected association with nucleolus related proteins as H1t is known to be localized at the rDNA element (Fig 3.12, nucleolar proteins) (Tani et al., 2016). Importantly, we observed various PIWI-piRNA pathway proteins such as Piwil1(MIWI) and its associated proteins (Myh9, Myh10, Myh11), HSPA2, MAEL to be associated with H1t-oligonucleosomes (Fig 3.12, repeat-associated and heterochromatin proteins, MIWI associated proteins). Piwil1 protein is a bonafide slicer (small-RNA-directed endonuclease) in postnatal germ cells wherein the loss of Piwil1 has been shown to cause male fertility due to the upregulation of LINE1 retrotransposon transcripts (Reuter et al., 2011). Also, Tdkrh1 is known to interact with PIWI proteins and is an essential factor implicated in piRNA biogenesis (Saxe et al., 2013). These results provide additional evidence for the association of H1t with proteins related to TE silencing in pachytene spermatocytes.

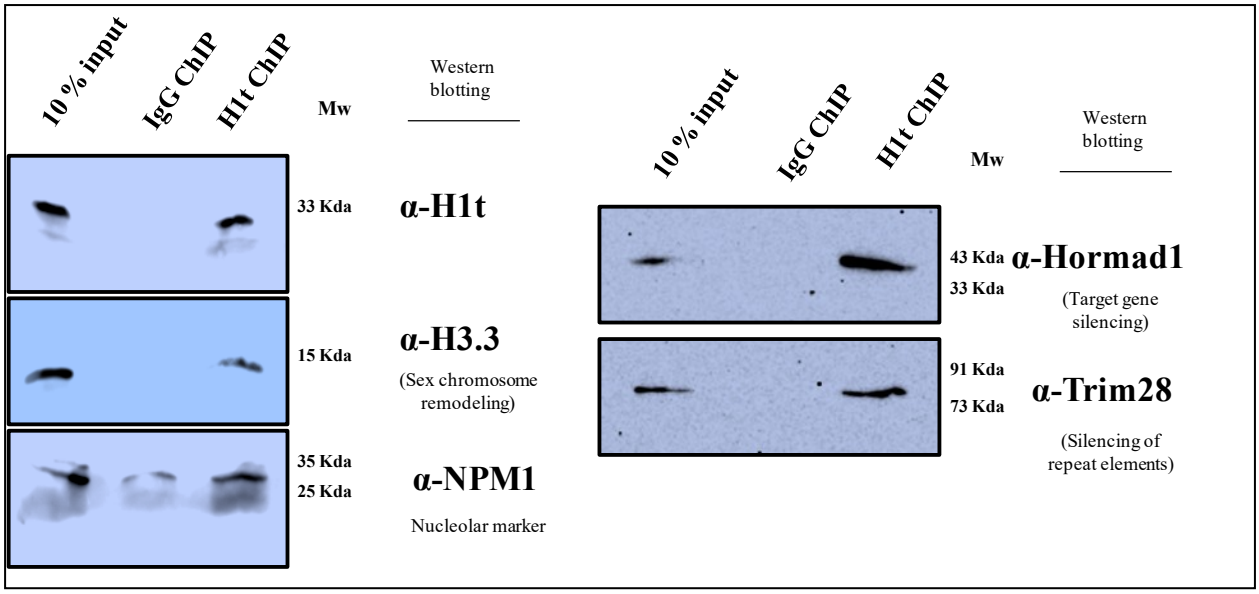

Figure 3.13- Validation of H1t-associated proteins by ChIP-western blotting technique

To validate further the association of some of these important proteins with H1t-associated chromatin, we carried out western blot analysis of the H1t-containing ChIP fraction. We observe proteins related to the nucleolus (NPM1), MSCI (H3.3), heterochromatin related (Hormad1, Trim28) are associated with H1t-containing chromatin fragments. The first lane in all the blots represents the 10% input fraction, second lane ChIP with the non-specific isotype control, and the third lane ChIP with the H1t antibody. The antibodies labeled in alpha alongside the blot represent the antibodies used for western blotting.

Also, we have validated the association of H1t with key set of proteins by IP assays followed by western blotting and observed that H1t is associated with proteins related to nucleolar function (Npm1), repeat-repression and heterochromatinization (Hormad1, Trim28) *in vivo* (Fig 3.13). These observations demonstrate the association of linker histone H1t with repressed repeat-chromatin domains in pachytene spermatocytes. We wish to validate the association of H1t with more proteins belonging to the PIWI pathway and repeat-repression related proteins in the future.

Table 3.2- Table of motifs identified of H1t bound genomic regions in pachytene spermatocytes using MEME software.

Motif Serial no	MEME Motif ID	Motif Sequence	E value	Motif Width	Total Occurrences
Motif-1	MEME-8	ARGRRRRRRRRRRARRRRRRRARRVAGVM	3E-17	29	16607
Motif-2	MEME-6	TTTTTTTTTTTWWTTNTTTWTTTTTTTWT	3.9E-29	29	16215
Motif-3	MEME-9	SCBGGSMGTGGTGGCRCACGCCTTTAATCCCAGCACTYGGGAGGCAGAGG	4.5E-24	50	14623
Motif-4	MEME-10	CAAGGAGCTRAAGGGRTYTGCAACCCTATAGGWGGAACAAC	3.3E-10	41	13824
Motif-5	MEME-5	GCTGGAGAGATGGCTCAGYGGTTAAGAGC	1.9E-36	29	13553
Motif-6	MEME-4	TGAGTTCGAGGCCAGCCTGGTCTACARAGTGAGTTCC	1.4E-39	37	12466
Motif-7	MEME-11	ATGRGATCTGAYGCCCTCTTCTGGTGT	0.000000053	27	11117
Motif-8	MEME-3	ATGGTTGTGAGCCACCATGTGGTTGCTGG	2.2E-36	29	10716
Motif-9	MEME-12	GGGATCCATCCCATAWKCAGMCACCAAACCCAGACACTATTGCWKATGCC	0.000035	50	9593
Motif-10	MEME-7	TTGGCCCTGGCRTTCCCCTGTACTGGGGCATATAAAGTTTGCAAGWCCAA	1.1E-17	50	9481
Motif-11	MEME-1	CACACACACACACACACACACACACAC	3.7E-52	29	4058
Motif-12	MEME-2	YTCTYTCTYTYTYTCTYTYTYTYTYTCTYTYTYTYTYTYTY	1.9E-71	41	3646

3.3.7 Motif Analysis

To further determine the characteristics of H1t-bound genomic regions, we used the MEME suite to identify the characteristic DNA motifs enriched in the H1t peaks. We observed a combination of twelve significant motifs bound by 86% of the total H1t peaks in the mouse genome (Table 3.2). It remains to be determined whether the DNA motifs are sufficient for H1t binding, or whether adaptor proteins mediate the binding of H1t in pachytene spermatocytes.

3.4 Discussion

Various studies reported in the literature have shed light on the *in vitro* biochemical characterization of the H1t-containing nucleosomes. H1t-containing nucleosomes form relaxed chromatin structures due to a lack of DNA binding motifs in the C-terminal region (Bharath et al., 2002; De Lucia et al., 1994; Drabent et al., 1991; Khadake and Rao, 1995, 1997; Suzuki, 1989). Also, H1t has been shown to weakly suppress Rad51/Rad54 mediated homologous pairing in comparison with H1.2 (Machida et al., 2016), suggesting their contribution towards generating a relaxed chromatin template. We observe the general

property of linker histones to be true for H1t in that it was found to be not enriched in active gene promoters and TSS. Further, they were found to be not closely associated with DSB hotspots and open chromatin regions.

However, studies involving the biological roles of linker histone variant H1t are few and lacking in the context of pachytene spermatocytes. H1t has been observed to be localized to the nucleolus in spermatocytes (Tani et al., 2016). Various foci of H1t also exist outside the nucleolus of spermatocytes, and determining the H1t extra-nucleolar chromatin domains was the main focus of the present investigation. Our study is focussed on understanding the genome-wide occupancy and associated chromatin-templated functions of dominant linker histone variant H1t in pachytene spermatocytes.

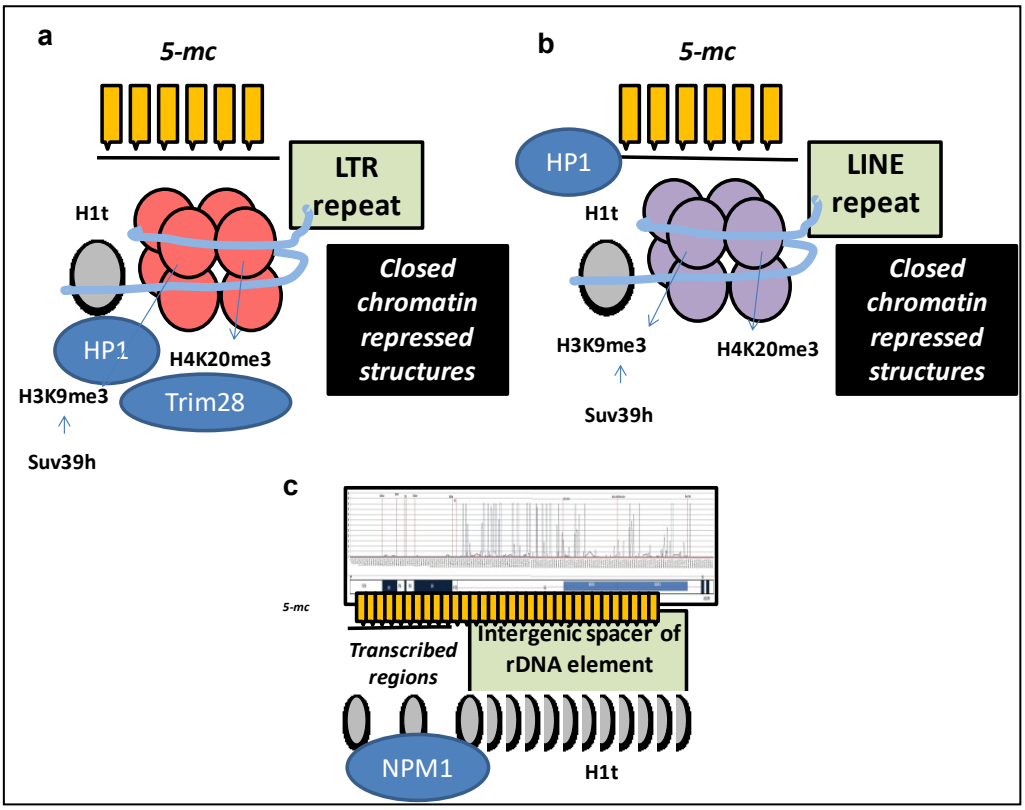

Figure 3.14- Model of H1t-positive chromatin domains in pachytene spermatocytes

Extra-nucleolar localization of linker histone variant H1t is related to ***a.*** *LINE and* ***b.*** *LTR repeat-element chromatin domains. This forms a chromatin template for binding of PIWI proteins, DNA methylation machinery (forming methylated CpGs), repressive histone modifications like H3K9me3 and H4K20me3 in pachytene spermatocytes. H3K9me3 nucleosomes are binding sites for HP1 proteins to mediate heterochromatinization at these target loci.*

***c**. Predominant association of linker histone variant with the intergenic spacer of the rDNA element. H1t co-associates with methylated CpGs and nucleolar proteins like Npm1 at nucleolar domains in pachytene spermatocytes.*

3.4.1 Extranucleolar localization of linker histone variant H1t in pachytene spermatocytes

An important observation from the present study is the localization of linker histone variant H1t at repeat elements belonging to LINE and LTR. The repeat elements need to be repressed to prevent mutagenesis and genome instability in mammalian spermatocytes. Even though the expression of proteins like Dnmt3A does not occur in spermatocytes, the defects in establishing methylation patterns in prespermatogonia become very important in spermatocytes, because the defects are inherited during the pachytene interval (Fig 3.4). The loss of Dnmt3A leads to the upregulation of LINE and LTR transcripts in spermatogonia and spermatocytes, suggesting its role in TE repression in the premeiotic germ cells. These epigenetic processes involving TE repression are important especially during pachytene interval, where scanning and apoptotic checkpoint mechanisms are in place (Fig 3.4). Importantly, defects in DNA methylation at TE elements results in shifting of recombination hotspots to non-canonical genomic sites, ultimately resulting in male infertility. Based on the observation of the H1t-occupied repeat elements coinciding with occupancy of methylated CpGs, it is tempting to say that these repeat elements are repressed *in vivo*. H1 has been shown to contribute to the establishment of DNA methylation patterns in mESCs (Fan et al., 2005). This provides additional support for the importance of H1t and its association with DNA methylation regions in pachytene spermatocytes. The association of H1t with repressed repeat-element chromatin domains is further supported by the fact that H1t is co-associated with repressive histone modifications like H3K9me3 and H4K20me3 in P20 mouse testicular cells.

On the other hand, dysfunction of the piRNA pathway results in loss of DNA methylation and H3K9me3 marks at repeat elements in germ cells, suggesting their important in TE repression in germ cells. Mass spectrometric identification of H1t-bound chromatin proteins also revealed piRNA-PIWI pathway proteins to be associated with these chromatin domains, supporting the conclusion that these repeat elements are indeed repressed *in vivo*. Even piRNA independent mechanisms do exist in catalyzing CpG methylation at repeat elements in germ cells (Nagamori et al., 2015). It will be interesting to decipher whether the association of H1t with methylated CpGs in the repeat elements is dependent on the piRNA-

PIWI pathway or not. It is tempting to speculate that the DNA methylation at H1t peaks is piRNA-PIWI dependent based on the chromatin interaction observed for H1t with various PIWI proteins. However, this has to be investigated in great detail. Despite ongoing efforts to characterize in-detail the mechanisms of TE repression in germ cells, the crosstalk between epigenetic pathways involving repressive histone modifications, DNA methylation, and piRNAs/PIWI proteins have not been delineated in great detail. We suspect H1t along with repressive histone H4K20me3 and H3K9me3 might set the template for TE repression in germ cells.

H3K9me3 formation is mediated by histone methyltransferases (HMTs) Suv39h1 and Suv39h2 in germ cells (Grewal and Jia, 2007; Peters et al., 2001; Peters and Schubeler, 2005). H3K9me3-positive nucleosomes become the docking sites for the binding of HP1 proteins establishing the chromatin condensed structure. This chromatin template has been proven for transcriptional repression and setting of 'chromatin state' that is epigenetically heritable in mammalian embryos. The fact that H1t-containing nucleosomes associate with H3K9me3, HP1α, HP1β gives a strong indication for the localization of linker histone H1t at repressed repeat-element chromatin domains. Repression of repeat elements is also critical in ES cells, wherein SETDB1-mediated H3K9me3 formation plays a major role in TE silencing. Is the repeat repression phenomena conserved in all the cells? This might not be true because the expression of piRNA-PIWI pathway components is specifically restricted to germ cells. Also, the enzyme mediating H3K9 methylation at repeat elements are different, SETDB1 in ES cells and Suv39h in germ cells. In summary, H1t containing nucleosomes are associated with repeat elements LINE and LTR in pachytene spermatocytes, which are positive for repressive signatures like histone marks and methylated CpGs (Fig 3.14a, 3.14b). H1t might generate a relaxed chromatin template to recruit effectors like PIWI proteins, heterochromatin proteins, ultimately leading to the formation of repressed chromatin structures *in vivo*.

In addition to H3K9me3 and H4K20me3, there could be other histone marks that could be signatures of repeat element nucleosomes. Uhrf1 has been shown to interact with PRMT5 (arginine methyltransferase) to catalyze the formation of H4R3me2s and H3R2me2s. These histone marks also act together with PIWI proteins to retrotransposon silencing in the germline (Dong et al., 2019). We found that H1t-oligonucleosomes associate with Tdkrh, a known interacting protein partner with Uhrf1 and PIWI proteins, further supporting our observations of association of H1t with repressed-repeat element chromatin domains in pachytene spermatocytes. This is additionally supported by the overlap analysis of H1t ChIP-sequencing data with ATAC sequencing data (specific for pachytene spermatocytes), wherein

we observed H1t-containing genomic regions to be predominantly condensed chromatin structures. Crosstalk between H1t and repressive histone modifications could occur, working with conjunction with piRNA-PIWI pathway and heterochromatin proteins leading to the formation of repressed chromatin structures *in vivo*. Still, the molecular mechanism of how piRNA-dependent or piRNA-independent pathways act in conjunction with DNA methylation machinery and repressive histone modifications leading to the final TE repression remains to be understood. We hypothesise that H1t might set a relaxed chromatin template for recruitment of effectors leading to formation of repressed chromatin structures *in vivo* (Figure 3.14a, 3.14b).

3.4.2 H1t and nucleolus

As explained earlier, H1t has been previously shown to be localized to the nucleolus in mouse spermatocytes and human cancer cell lines (Tani et al., 2016). We found H1t-containing oligonucleosomes to be associated with nucleolar proteins such as Npm1, Numa1, Ncl corroborating with the previous results. An interesting observation made in the present study is the predominant association of H1t peaks with the intergenic spacer of the rDNA element. There have been numerous reports of the role of the intergenic spacer in modulating rDNA transcription (Ghosh et al., 1993; Zentner et al., 2014). macroH2A has been shown to repress rDNA transcription in human HeLa and mouse ES cells (Cong et al., 2014). Since we observed macroH2A to be associated with H1t ChIP fraction as determined by mass spectrometry, this suggests that H1t could function with macroH2A to modulate rDNA transcription in germ cells, providing further support to the possible role of H1t in rDNA transcriptional dynamics. The rDNA element is a host to repetitive elements of various classes, SINE being the predominant class (Grozdanov et al., 2003). Since we observed H1t to be closely associated with SINE elements of the rDNA, this provides strong support to the association of H1t with repetitive elements of the rDNA. Both the nucleolar and extra-nucleolar localization of H1t occurs in the repetitive regions of the mouse pachytene genome.
In mammalian cells, chromatin is organized into structural and functional compartments like TADs (topologically associated domains), LADs (lamin associated domains) etc (Belmont, 2014; Bickmore, 2013; Bickmore and van Steensel, 2013; Dekker et al., 2013; Pombo and Dillon, 2015; Sexton and Cavalli, 2015). Recently, nucleolus associated domains (NADs) have been discovered in HeLa cervical carcinoma and HT1080 fibrosarcoma cells (Nemeth et al., 2010; van Koningsbruggen et al., 2010). Various repeat elements like LTR are enriched in NADs and inter NADs (Dillinger et al., 2017). It would be interesting to see whether this

kind of nucleolar organization exists in pachytene spermatocytes, if yes, then does H1t influence structure of NADs and inter NADs via its association with repeat elements. We demonstrate that H1t is predominantly localized at the intergenic spacer of the rDNA element, setting the chromatin template for further association with methylated CpGs and nucleolar proteins (Fig 3.14c).

What determines the localization of H1t to these specific genomic loci? We observed a combination of twelve motifs to be significant in the total H1t peaks, as identified through motif analysis using MEME (Table 3.2). Whether the motif information of the target DNA sequence is sufficient for H1t binding in the pachytene spermatocyte genome remains to be further examined. Since we observed that the occupancy of the repeat elements is characteristic of linker histone H1t in pachytene spermatocytes, it could be possible that the unique C-terminus of H1t carries information to localize at repetitive elements. It is also possible that adaptor proteins might recruit histone H1t to these specific genomic loci. In this context, we would like to mention that PIWI proteins recruit H1 to TE loci to repress these chromatin domains in ovarian somatic cells (OSC) of Drosophila (Iwasaki et al., 2016). Therefore, proteins belonging to the PIWI pathway might regulate H1t localization at repeat elements in pachytene spermatocytes. This presumption is additionally supported by the fact that various proteins belonging to the PIWI pathway like PIWIL1, Hspa2, Uhrf1, Trim28 are associated with H1t-containing chromatin domains. It is also known that the C-terminal domain of H1 is required for the recruitment of Piwi and TE silencing in Drosophila (Iwasaki et al., 2016). We were surprised to see that the Drosophila H1 and H1t protein sequences are similar in the C-terminal regions being devoid of various DNA binding motifs like S/TPKK. It would be interesting to see whether PTMs on H1t mark specific repeat element subclasses. H1t PTMs have been characterized in spermatocytes and round spermatids (Luense et al., 2016). It will be exciting to determine the loci-specific functions of H1t PTMs in repeat repression phenomena.

Nucleosomal retention occurs in repetitive sequences associated with intergenic and intronic regions in mammalian sperm (Carone et al., 2014; Samans et al., 2014). This epigenetic landscape sets up an important marker for paternally derived nucleosomes in preimplantation embryos. Since H1t has been demonstrated to occur at repeat sequences associated with intergenic and intronic regions, this begs for the question of which linker histone variants/PTMs mark these functionally important genomic regions in the mature sperm. Since H1t is associated with important proteins that are related to TE repression and nucleolar function, this leads to the question of why H1t knockout mice are fertile. Since H1t-deficient

chromatin remains H1 free, does this mean H1t remains a silent 'passenger' during these processes? It is worth mentioning here that TH2B knockout mice are also fertile, but in these mice, the somatic histones H2B, H3 and H4 acquire compensatory histone PTMs that could substitute the role of TH2B during spermatogenesis. Thus, a more detailed investigation of chromatin modifications in histone H1t null mice is necessary to understand the biological function and relevance of histone H1t in mammalian spermatogenesis.

Another important point to be noted is that H1t expression is restricted till early round spermatids in mouse, other linker variants could replace H1t at the repeat elements during spermiogenesis. One candidate variant, HILS1, is also enriched at the LINE1 elements in rat spermatids (Mishra et al., 2018a). This begs for the question of how the information of silencing of repeat elements is transmitted from germ cells to the embryo. Specific marking of chromatin territories might occur in various stages of germ cell development, wherein different histone variants with their PTMs might contribute to unique functions in shaping the epigenetic landscape important for male fertility and transgenerational inheritance.

Chapter 4
General Summary and Perspectives

Almost all eukaryotes wrap their DNA around histones to form nucleosomes. Each nucleosome comprises of a single tetramer of $(H3\text{-}H4)_2$ and two (H2A-H2B) dimers. Histone H1 interacts with the nucleosome near the entry/exit site of linker DNA. There is enough evidence in the literature to demonstrate the involvement of non-canonical histone variants in a wide variety of processes such as DNA repair, recombination, chromosome segregation, sperm chromatin packing, etc. The functions that are associated with histone variants are due to either change in the amino acid sequences or structural changes that alter the nucleosomal dynamics. Given the fact that these histone variants modulate a variety of functions, their role in understanding the developmental processes becomes important. Mammalian spermatogenesis offers an excellent model system for the fact that the testis is known to express various core and linker histone variants in a stage-specific manner. The present study sheds light on understanding the chromatin-templated functions of TH2B Serine 11 phosphorylation (TH2BS11ph) histone mark and linker histone variant H1t concerning the biological events occurring in mammalian spermatocytes.

4.1.1 Insights into the role of TH2BS11ph modification in mammalian spermatocytes

One of the major testicular histone variants known to replace a core histone on a genome-wide scale is TH2B (a variant of H2B). Earlier studies from our laboratory have demonstrated that the TH2B-containing pachytene nucleosome core particle (NCP) is less compact compared to the liver NCP (Rao et al., 1983; Rao and Rao, 1987). TH2B has 85% sequence conservation with its somatic histone counterpart H2B, with a majority of amino acid differences occurring in the N-terminal end. We surmised that the amino-terminal residues or post-translational modifications acquired by some of the residues could contribute to the unique functions of TH2B compared to H2B. We have recently identified various post-translational modifications on TH2B across the tetraploid and haploid stages of spermatogenesis. By computational analysis, it was also shown that the amino acid differences in the N-terminal tail and the post-translational modifications acquired by some of the residues could cause the destabilization of the nucleosomes (Pentakota et al., 2014). In our attempt to decipher the unique functions of histone variant TH2B, we discovered a histone modification Serine 11 phosphorylation on TH2B (TH2BS11ph) in spermatocytes.

Our present study is aimed at understanding the function of the TH2BS11ph modification in the context of processes that occur during meiotic prophase I.

The immuno-staining of TH2BS11ph in the pachytene spermatocyte revealed an interesting phenomenon in that this modification was highly enriched in the axes of the XY body. Immunofluorescence studies further revealed that TH2BS11ph histone mark is enriched in the unsynapsed axes of the sex body and is associated with XY body axes-associated proteins like Scp3, γH2AX, ATR, pATM, etc. This enriched staining could be due to the unique structure of the XY body chromatin, wherein the chromatin is organized into larger axes and shorter loops (Kauppi et al., 2011). The association of TH2BS11ph with the XY body was additionally supported by immunoprecipitation assays, where we observed the association of TH2BS11ph and γH2AX in the context of mononucleosomes in pachytene spermatocytes. Genome-wide occupancy studies, as determined by ChIP-sequencing experiments in P20 mouse testicular cells, revealed that majority of TH2BS11ph peaks lie in chromosomes X and Y. Further, ChIP-seq analysis revealed that TH2BS11ph is not associated with meiotic recombination hotspots, but majorly associated with H3K4me3-containing genomic regions of the XY body and active gene promoters in both P12 (leptotene) and P20 (pachytene) mouse testicular cells. Mass spectrometric analysis of proteins that bind to TH2BS11ph-containing mononucleosomes revealed key protein effectors associated with the functions of XY body and transcription related functions. TH2BS11ph is associated with proteins that are linked to XY body DNA repair and transcription chromatin domains in pachytene spermatocytes.

Combinations of histone PTMs called the ‘Histone Code’ determine the recruitment of specialized molecular machinery necessary to mediate chromatin-templated events. This modification was also found to associate with TSS-related histone mark H3K4me3 in the context of mononucleosomes. TH2BS11ph might associate with H2AZ, H3K4me3 marks to create a TSS nucleosom necessary for transcriptional activation in mammalian spermatocytes. Also, TH2BS11ph along with γH2AX, H3K4me3 marks might generate a chromatin platform for the recruitment of DSB repair proteins to the XY body. We propose that TH2BS11ph modification could act alone or in conjunction with specific histone marks to create a chromatin template for the recruitment of either XY body DNA repair or transcription protein machinery at specific genomic loci. This is the first study documenting the role of a post-translational modification of a germ cell-specific histone variant in meiotic prophase I related events. It will be interesting to characterize the ‘histone code’ of TH2BS11ph-containing mononucleosomes that will shed light on repertoire of histone marks

associated with transcription and XY body functions in pachytene spermatocytes. Future studies are required for the characterization of the in-detailed mechanism of TH2BS11ph in XY body DSB repair and transcription-related processes in mammalian spermatocytes. Whether TH2BS11ph is required for the success of XY body DSB repair and transcription processes remain to be further determined. Another important question to be answered is what compensatory histone/histone PTMs complement TH2BS11ph function in the case of TH2B-deficient testicular cells.

4.1.2 Insights into the genome-wide occupancy of linker histone variant H1t in pachytene spermatocytes

H1t is the major linker histone variant in pachytene spermatocytes and constitutes about 50-60% of total H1 content in these cell types (Bucci et al., 1982; Govin et al., 2004; Grimes et al., 2003). Our lab had proven previously that H1t-containing chromatin are relaxed chromatin structures compared to somatic H1.d containing chromatin based on *in vitro* biochemical assays (Khadake and Rao, 1995, 1997). H1t, by immunofluorescence studies, has been shown to localize to the rDNA element in human cancer cell lines and mouse ES cells. We also confirmed the same wherein in our ChIP-sequencing analysis in P20 mouse testicular cells; we found H1t to be predominantly associated with intergenic spacer of the rDNA element. The association of linker histone variant with the rDNA occurs at the repeat regions that coincide occupancy of methylated CpGs. There have been numerous reports implicating the role of intergenic spacer in modulation of rDNA transcription (Ghosh et al., 1993; Zentner et al., 2014). We hypothesize that H1t, due to its localization at CpG methylated repeat regions, could modulate transcription in the rDNA element. However, apart from its localization in the nucleolus, its extra-nucleolar localization of this linker histone variant had to be determined and is the main aim of our present study.

Genome-wide occupancy studies, as determined by ChIP-sequencing in P20 mouse testicular cells revealed that H1t did not closely associate with active gene promoters and open chromatin regions (ATAC-seq positive regions). Annotation of H1t bound genomic regions revealed that H1t is depleted from DSB hotspots and TSS, but are highly associated with retrotransposable repeat elements like LINE and LTR in pachytene spermatocytes. Repression of transposable elements like LINE, LTR is critical for the prevention of mutagenesis and genomic instability. Despite millions of years of species divergence, the common pathway involved in transposable element (TE) repression is the RNAi pathway. The major mechanism by which repeat regions (LTR and LINEs) are repressed by piRNA is

by deposition of DNA methylation machinery at these target elements. In the germ cells, transposable element mRNAs are cleaved into PIWI-interacting RNAs (piRNAs) by MILI and MIWI in mouse. TE-associated genes are silenced by deposition of proteins like MIWI2 that further deposit DNA methylation machinery onto those regions to repress those regions. Any defects in piRNA pathway/DNA methylation components cause excessive DNA damage in spermatocytes resulting in pachytene arrest and ultimately male sterility.

Since H1t is predominantly associated with repeat regions (apart from the already known rDNA localization), we speculated that repeat-associated H1t-bound regions might be repressed by DNA methylation. More than 90% of the total H1t peaks overlap with methylated CpGs, suggesting that these repeat elements bound by H1t are repressed by DNA methylation. In addition to DNA methylation, repressive histone modifications like H3K9me3 and H4K20me3 are deposited at TE elements (Martens et al., 2005). We demonstrate by coimmunoprecipitation assays that H1t were found to associate with these two histone marks H3K9me3 and H4K20me3 *in vivo*. These results were corroborated by mass spectrometric analysis wherein we found piRNA-PIWI pathway proteins, repeat repression associated proteins and heterochromatin proteins to be interacting with H1t-bound chromatin fragments. Apart from localisation of H1t at the rDNA element, we demonstrate close association of this linker histone variant at repeat-associated chromatin domains in pachytene spermatocytes. We hypothesize that H1t might induce local chromatin relaxation to recruit heterochromatin and repeat repression-associated protein factors necessary for TE repression. It would be interesting to determine whether silencing of H1t-associated chromatin is dependent on piRNA expression or not. Is the localization of linker histone variant H1t at repeat elements dependent on the unique C-terminal domain of H1t? The factors and mechanisms that regulate the deposition of H1t to TE chromatin domains need to be understood in great detail. PTMs on H1t could also regulate the localization at the unique subclasses of the retrotransposable elements. Even though H1t is not expressed until the later stages of spermiogenesis, which histone variants/PTMs replace H1t-associated functions in elongating spermatids would be an exciting avenue to explore.

In summary, we have mapped the genome-wide occupancies of TH2BS11ph histone mark and H1t linker histone variant in pachytene spermatocytes, wherein we observe the association of these proteins with unique functional chromatin domains. The present study is a small step carried out towards understanding the role of testicular histone variants and their PTMs in processes related to meiotic prophase I. Despite the localization of TH2BS11ph and H1t at functionally important chromatin domains in pachytene spermatocytes; the major

question remains as how TH2B/H1t knockout mice are fertile. If they are not essential for these processes, why TH2B and H1t are the dominant histone variants in pachytene spermatocytes? Future work is required to understand these important histone variants and their PTMs in the context of higher-order genome organization in mammalian germ cells.

Annexure 1

Chromosome	Start	End	Fold Change
chr1	12575500	12579500	1.741191962
chr1	41843100	41847100	1.935552662
chr1	67952700	67956700	1.902466228
chr1	80231900	80235900	3.035623197
chr1	114419400	114423400	1.640204526
chr1	149782600	149786600	1.631602092
chr1	167154400	167158400	12.37364072
chr1	180667500	180671500	1.608198373
chr1	183244400	183248400	1.517254436
chr1	187646600	187650600	1.587716286
chr1	191952100	191956100	1.148295769
chr1	193737500	193741500	1.854435344
chr10	5299200	5303200	1.841637104
chr10	32718000	32722000	1.938374554
chr10	70036500	70040500	1.738778895
chr10	81806300	81810300	1.727256835
chr10	92998900	93002900	1.45990316
chr10	117393500	117397500	1.941879622
chr11	15464500	15468500	1.791700581
chr11	31209700	31213700	1.69611985
chr11	61335800	61339800	2.32874745
chr11	105151900	105155900	1.873756253
chr12	29043400	29047400	1.173746325
chr12	71447900	71451900	1.682104832
chr12	98563200	98567200	4.493647392
chr12	112533300	112537300	1.009370679
chr12	117721100	117725100	1.161258216
chr13	12944500	12948500	1.132218202
chr13	45442200	45446200	1.879000385
chr13	93737300	93741300	2.325232245
chr13	119719600	119723600	1.016386391
chr13	119926900	119930900	1.516328707
chr13	120031700	120035700	23.39185517
chr13	120213100	120217100	1.066642426
chr14	3173200	3177200	4.198836453
chr14	3558000	3562000	1.408414948
chr14	3623900	3627900	2.599418227
chr14	4204400	4208400	1.799183335
chr14	4880100	4884100	1.422669081
chr14	5238400	5242400	3.843410181
chr14	5382100	5386100	1.17030359
chr14	5497900	5501900	2.711369674
chr14	5586900	5590900	1.472482829
chr14	5712400	5716400	1.775680493
chr14	6488800	6492800	23.74728144
chr14	13307100	13311100	3.487983908
chr14	22065400	22069400	15.2170509
chr14	25294100	25298100	4.198836453
chr14	25989000	25993000	1.679066456
chr14	34018300	34022300	7.042246634
chr14	41883300	41887300	4.554262726
chr14	42397300	42401300	14.15077209
chr14	43195600	43199600	1.98441679

chr14	48148000	48152000	2.07870631
chr14	52863700	52867700	3.7775905
chr14	52955900	52959900	39.87474856
chr14	53098100	53102100	2.42170509
chr14	61286700	61290700	2.777131363
chr14	97244500	97248500	2.167829181
chr15	6100500	6104500	2.500688706
chr15	23998600	24002600	2.542701268
chr15	71396600	71400600	12.37364072
chr15	103827800	103831800	3.023195705
chr16	3014600	3018600	4.952340151
chr16	3127400	3131400	18.06046108
chr16	10607100	10611100	2.879810064
chr16	58298400	58302400	1.751588414
chr17	5233600	5237600	1.848668127
chr17	10385800	10389800	1.826972428
chr17	13446800	13450800	1.796069368
chr17	26777000	26781000	1.886936726
chr17	39973900	39977900	1.789394236
chr17	40063400	40067400	1.878044959
chr17	40138500	40142500	2.329048774
chr17	47432300	47436300	2.296503176
chr17	75315900	75319900	2.065479625
chr18	7116900	7120900	4.909688998
chr18	43968800	43972800	1.892664447
chr18	77205300	77209300	1.813065122
chr18	80050100	80054100	1.779953963
chr18	84994500	84998500	2.274780957
chr18	89216800	89220800	12.37364072
chr19	3545000	3549000	1.859883969
chr19	5220000	5224000	1.877384312
chr19	22006300	22010300	1.888846538
chr19	46990300	46994300	2.022798045
chr19	58929900	58933900	2.133435055
chr2	12734700	12738700	2.490763067
chr2	40796800	40800800	2.526752795
chr2	71532800	71536800	1.947943909
chr2	86596900	86600900	1.982778012
chr2	89704100	89708100	2.512677599
chr2	90275500	90279500	1.807174573
chr2	90619900	90623900	1.746663863
chr2	95747400	95751400	2.008731809
chr2	111667000	111671000	1.81810351
chr2	148948800	148952800	1.58679078
chr2	176766200	176770200	1.236613792
chr2	177323100	177327100	2.184256446
chr2	179862400	179866400	1.406290795
chr3	9303000	9307000	1.479648977
chr3	28248000	28252000	1.234683376
chr3	45701900	45705900	15.2170509
chr3	74633100	74637100	1.517379989
chr3	105941500	105945500	1.413638911
chr3	122450200	122454200	1.257286182
chr3	145701400	145705400	1.153841222
chr4	22451000	22455000	13.79534581
chr4	51531200	51535200	2.777131363

chr4	60586000	60590000	1.072907953
chr4	60806300	60810300	1.874620661
chr4	91663800	91667800	1.795979062
chr4	121923600	121927600	2.038417152
chr4	122079700	122083700	2.821353335
chr4	122192900	122196900	2.350619836
chr4	122399100	122403100	1.928861179
chr4	126422100	126426100	1.540866067
chr4	136981000	136985000	1.439873142
chr4	144739400	144743400	1.676242306
chr4	146167400	146171400	1.856898779
chr4	146535900	146539900	3.843410181
chr4	146729000	146733000	2.42170509
chr4	151571800	151575800	1.411525987
chr4	156331600	156335600	2.127044992
chr5	7030600	7034600	1.76539756
chr5	11183700	11187700	1.821129631
chr5	11325900	11329900	1.813631488
chr5	11474700	11478700	2.068563144
chr5	11617100	11621100	1.711894414
chr5	11711600	11715600	10.06336995
chr5	11774900	11778900	1.432851412
chr5	13455400	13459400	2.118801451
chr5	22960500	22964500	1.809579235
chr5	61906200	61910200	2.083713303
chr5	93654900	93658900	2.136687702
chr5	94029400	94033400	2.2401382
chr5	94201300	94205300	2.471147728
chr5	94357900	94361900	1.352860018
chr5	94704900	94708900	1.335588527
chr5	94988700	94992700	2.599418227
chr5	95393000	95397000	2.020880995
chr5	95591100	95595100	1.906016577
chr5	95688100	95692100	1.903659318
chr5	110226600	110230600	1.859668532
chr5	127249900	127253900	2.475025815
chr5	130582500	130586500	2.038195065
chr5	134880300	134884300	1.865452618
chr5	140539900	140543900	1.680030163
chr5	147800800	147804800	3.004277703
chr6	16899100	16903100	3.453763895
chr6	39241500	39245500	1.865636066
chr6	60014700	60018700	2.079066183
chr6	97219500	97223500	2.067348305
chr6	122089600	122093600	1.791094356
chr6	122796600	122800600	2.042091449
chr6	128304900	128308900	1.833951961
chr6	136340100	136344100	1.710768843
chr6	142867700	142871700	1.653126598
chr6	147826700	147830700	1.703772341
chr7	3492000	3496000	2.221984705
chr7	3703700	3707700	5.391082451
chr7	4770400	4774400	1.872055971
chr7	6810300	6814300	2.123589834
chr7	7835100	7839100	1.533897786
chr7	7969300	7973300	1.547703414

chr7	8115400	8119400	2.655610783
chr7	8392400	8396400	1.780297276
chr7	8784700	8788700	1.779069062
chr7	8917800	8921800	1.69356292
chr7	9139200	9143200	1.861580423
chr7	9355900	9359900	1.949371665
chr7	12544000	12548000	1.772557352
chr7	17710500	17714500	1.777446437
chr7	20196100	20200100	1.748441061
chr7	20272700	20276700	2.003419598
chr7	20338700	20342700	1.277439537
chr7	20397500	20401500	1.460215743
chr7	20561100	20565100	1.829530388
chr7	20655300	20659300	1.161557397
chr7	20704500	20708500	2.303229666
chr7	20820400	20824400	1.307311799
chr7	21180500	21184500	3.843410181
chr7	22059300	22063300	2.765864964
chr7	22180900	22184900	3.348381458
chr7	22259700	22263700	1.782203127
chr7	22331500	22335500	1.584646555
chr7	22419800	22423800	1.755447727
chr7	22507700	22511700	1.884008934
chr7	22550100	22554100	2.901370172
chr7	22598900	22602900	1.591733233
chr7	22811500	22815500	1.76024503
chr7	23179200	23183200	1.651738761
chr7	27806700	27810700	1.252382521
chr7	32406300	32410300	1.500287053
chr7	32528900	32532900	18.06046108
chr7	32594400	32598400	1.203957692
chr7	33094200	33098200	3.843410181
chr7	35868500	35872500	1.689797013
chr7	38780500	38784500	1.945612914
chr7	38978100	38982100	1.834545949
chr7	39180900	39184900	1.289471984
chr7	49571900	49575900	1.087846834
chr7	82847400	82851400	1.317001811
chr7	105882300	105886300	1.428554825
chr7	106067200	106071200	1.234513854
chr7	106142900	106146900	1.17665532
chr7	122582000	122586000	1.32568111
chr7	140524000	140528000	1.710852545
chr7	143561700	143565700	1.128072595
chr8	11403900	11407900	2.449097154
chr8	20028300	20032300	2.429165003
chr8	20348100	20352100	2.234726139
chr8	20597800	20601800	2.563416985
chr8	21112100	21116100	2.838757569
chr8	27727400	27731400	2.348385275
chr8	44582800	44586800	1.71870585
chr8	63007000	63011000	1.844170278
chr8	71717000	71721000	1.848099158
chr8	100970200	100974200	1.938616243
chr9	8158200	8162200	1.791726197
chr9	61096400	61100400	2.01323012

chr9	116410200	116414200	2.003181674
chr9	124039800	124043800	1.884919734
chr9	124256700	124260700	1.971549204
chr9	124483000	124487000	1.934247386
chrM	6100	10100	2.029568123
chrX	3064500	3068500	1.984227243
chrX	3219200	3223200	2.166694427
chrX	3310700	3314700	1.877142298
chrX	3461200	3465200	12.37364072
chrX	3782200	3786200	1.247920795
chrX	3843100	3847100	1.222021019
chrX	4101600	4105600	1.401380907
chrX	4373700	4377700	16.63875599
chrX	4556200	4560200	1.120619776
chrX	4882000	4886000	1.306836352
chrX	4931300	4935300	1.368754758
chrX	5141300	5145300	1.761019491
chrX	5337300	5341300	2.326054732
chrX	5515900	5519900	12.37364072
chrX	5747500	5751500	3.487983908
chrX	6083700	6087700	3.843410181
chrX	6379600	6383600	15.2170509
chrX	6507300	6511300	6.331394089
chrX	6604500	6608500	12.37364072
chrX	6738000	6742000	2.42170509
chrX	6863900	6867900	1.384182443
chrX	7043600	7047600	1.459476545
chrX	7218500	7222500	2.599418227
chrX	8025800	8029800	1.059705994
chrX	8817100	8821100	4.198836453
chrX	8965400	8969400	20.90387126
chrX	9123300	9127300	1.101422143
chrX	9226100	9230100	5.975967816
chrX	9588900	9592900	5.265115271
chrX	9908600	9912600	1.947803394
chrX	9965600	9969600	1.59777231
chrX	10007500	10011500	1.328031757
chrX	10070500	10074500	2.49493274
chrX	10123200	10127200	1.165213436
chrX	10173500	10177500	4.554262726
chrX	10218600	10222600	1.340919078
chrX	10321500	10325500	1.533139409
chrX	10442200	10446200	2.287992687
chrX	10567700	10571700	1.459379496
chrX	10683600	10687600	12.37364072
chrX	10796000	10800000	1.829116028
chrX	10872100	10876100	1.923484804
chrX	10970200	10974200	1.921515835
chrX	11126100	11130100	12.37364072
chrX	11272500	11276500	1.372906253
chrX	11352200	11356200	1.710852545
chrX	11479400	11483400	2.1518352
chrX	11983400	11987400	2.669970461
chrX	12545200	12549200	2.834739251
chrX	12928000	12932000	1.991575515
chrX	13225600	13229600	1.464102769

chrX	13412600	13416600	1.273627212
chrX	13573900	13577900	1.532829573
chrX	13677500	13681500	1.58802537
chrX	13876500	13880500	1.891507717
chrX	14056000	14060000	1.771938817
chrX	14388500	14392500	1.782717381
chrX	14684600	14688600	2.640952837
chrX	14885700	14889700	2.140875379
chrX	15066700	15070700	1.946803293
chrX	15123800	15127800	2.009408645
chrX	15283600	15287600	2.288277451
chrX	15830800	15834800	1.687022475
chrX	16484700	16488700	1.409455304
chrX	16735200	16739200	2.221777812
chrX	16815500	16819500	7.543488813
chrX	16924900	16928900	1.678294413
chrX	17088300	17092300	2.19956367
chrX	17251300	17255300	1.267057035
chrX	17449200	17453200	1.286074805
chrX	17620300	17624300	1.376751849
chrX	17940800	17944800	1.283441205
chrX	18313900	18317900	1.373479671
chrX	18507300	18511300	13.79534581
chrX	18637400	18641400	1.454155793
chrX	18752600	18756600	1.633585964
chrX	18816600	18820600	5.265115271
chrX	18919300	18923300	1.457181375
chrX	18993300	18997300	1.592377121
chrX	19104300	19108300	1.532043381
chrX	19307700	19311700	1.649438754
chrX	19950100	19954100	1.548353756
chrX	20727900	20731900	1.567797157
chrX	21043100	21047100	2.377276806
chrX	21214000	21218000	1.464686942
chrX	21440300	21444300	1.527094744
chrX	21704800	21708800	18.06046108
chrX	21790400	21794400	1.572162875
chrX	21952300	21956300	3.843410181
chrX	22114900	22118900	1.798380733
chrX	22184700	22188700	15.2170509
chrX	22278100	22282100	1.509546165
chrX	22430400	22434400	1.608489779
chrX	22593700	22597700	1.601224312
chrX	22786300	22790300	1.521015157
chrX	22873300	22877300	1.438487847
chrX	22930000	22934000	1.900413224
chrX	23017300	23021300	4.198836453
chrX	23096600	23100600	1.605972661
chrX	23209200	23213200	1.607530954
chrX	23327300	23331300	12.37364072
chrX	23462700	23466700	1.888565681
chrX	23622000	23626000	1.468396333
chrX	23822300	23826300	1.625423678
chrX	23884500	23888500	1.491723212
chrX	24182500	24186500	1.629104502
chrX	24458100	24462100	1.355426273

chrX	24524000	24528000	1.429647641
chrX	24688800	24692800	1.59492498
chrX	25270300	25274300	1.647133638
chrX	25466500	25470500	1.77725086
chrX	25754300	25758300	1.629612254
chrX	25949500	25953500	2.041035474
chrX	26154300	26158300	2.0952129
chrX	26323400	26327400	1.819806408
chrX	26411400	26415400	1.71050814
chrX	26515300	26519300	2.152733857
chrX	26629600	26633600	1.721807465
chrX	26728500	26732500	4.198836453
chrX	26833900	26837900	1.570484923
chrX	27249000	27253000	1.505409003
chrX	28061100	28065100	1.505606388
chrX	28711500	28715500	1.507313069
chrX	28774500	28778500	1.524825344
chrX	28865500	28869500	1.529638362
chrX	28911300	28915300	1.585702449
chrX	29624200	29628200	1.680387436
chrX	29971900	29975900	1.586226757
chrX	30243300	30247300	1.514232066
chrX	30285300	30289300	1.496081526
chrX	30411700	30415700	1.446561214
chrX	30935000	30939000	2.041766661
chrX	31235300	31239300	1.494686859
chrX	31697000	31701000	1.502273443
chrX	32009300	32013300	1.477579426
chrX	32148900	32152900	1.507963381
chrX	32305700	32309700	1.506020846
chrX	32476800	32480800	1.55480096
chrX	32651800	32655800	1.44807017
chrX	32872500	32876500	1.530399338
chrX	33004100	33008100	1.402192887
chrX	33090900	33094900	2.015503636
chrX	33186900	33190900	1.491065981
chrX	33308100	33312100	1.412530771
chrX	33434300	33438300	4.554262726
chrX	33563100	33567100	1.524802249
chrX	33643100	33647100	1.525872329
chrX	33823600	33827600	1.523273182
chrX	33968700	33972700	1.796411149
chrX	34141100	34145100	1.624104438
chrX	34273500	34277500	1.577184218
chrX	34465100	34469100	1.546957971
chrX	34516500	34520500	1.488222902
chrX	34566700	34570700	1.623761339
chrX	35324000	35328000	1.489575488
chrX	35545600	35549600	12.37364072
chrX	35859700	35863700	13.79534581
chrX	36113200	36117200	1.537902854
chrX	36183800	36187800	1.582084432
chrX	36331800	36335800	1.440480737
chrX	36428000	36432000	1.53540039
chrX	36738100	36742100	1.947803394
chrX	37126300	37130300	1.543012361

chrX	37458700	37462700	1.424807429
chrX	37626300	37630300	1.642501339
chrX	38105600	38109600	1.54856788
chrX	38340800	38344800	4.198836453
chrX	38481400	38485400	12.37364072
chrX	38955700	38959700	1.459992984
chrX	39420500	39424500	1.929247002
chrX	39529200	39533200	4.554262726
chrX	39677100	39681100	1.498127646
chrX	39778100	39782100	1.32808579
chrX	39884700	39888700	1.600720461
chrX	40061800	40065800	1.510751912
chrX	40234600	40238600	1.895147649
chrX	40368900	40372900	1.586155809
chrX	40441100	40445100	1.531558331
chrX	40610000	40614000	1.266651299
chrX	40735700	40739700	1.419006016
chrX	40803900	40807900	1.369874495
chrX	40891100	40895100	1.630822788
chrX	40982700	40986700	1.564239208
chrX	41101500	41105500	1.600926894
chrX	41290300	41294300	1.39169426
chrX	41404500	41408500	1.655368691
chrX	41491100	41495100	1.112239876
chrX	41735100	41739100	1.888565681
chrX	41984700	41988700	1.153697848
chrX	42158100	42162100	15.2170509
chrX	42379400	42383400	15.2170509
chrX	42607400	42611400	2.777131363
chrX	42774500	42778500	1.462918413
chrX	42832700	42836700	1.07917912
chrX	42880300	42884300	1.473901697
chrX	43015300	43019300	2.599418227
chrX	43100100	43104100	1.568682036
chrX	43227200	43231200	1.06313493
chrX	43410800	43414800	1.797758171
chrX	43480200	43484200	1.439114357
chrX	43727600	43731600	1.144580179
chrX	43943700	43947700	1.323986767
chrX	44153300	44157300	1.803940378
chrX	44337900	44341900	1.339307167
chrX	44518600	44522600	1.464680457
chrX	44717500	44721500	1.655564014
chrX	44923900	44927900	12.37364072
chrX	45075700	45079700	1.808838213
chrX	45272600	45276600	2.777131363
chrX	45581800	45585800	5.265115271
chrX	45836700	45840700	1.300178665
chrX	46004200	46008200	12.37364072
chrX	46149500	46153500	2.42170509
chrX	46311300	46315300	1.365914261
chrX	46400700	46404700	1.313221062
chrX	46528400	46532400	1.441071158
chrX	46677100	46681100	1.360357042
chrX	46856000	46860000	1.628831098
chrX	46990100	46994100	2.42170509

chrX	47166900	47170900	5.975967816
chrX	47416400	47420400	1.355426273
chrX	47531900	47535900	1.525147019
chrX	47672200	47676200	1.522052718
chrX	47805200	47809200	1.570335182
chrX	47988200	47992200	1.659019547
chrX	48321600	48325600	1.781267184
chrX	48535500	48539500	1.597368325
chrX	48732800	48736800	1.674185968
chrX	48963500	48967500	1.855788619
chrX	49073100	49077100	1.404480262
chrX	49124200	49128200	1.430273481
chrX	49261000	49265000	1.69234076
chrX	49365500	49369500	1.630121504
chrX	49561700	49565700	2.761678047
chrX	49771900	49775900	1.515520982
chrX	49993500	49997500	1.520261645
chrX	50217000	50221000	1.617098371
chrX	50366200	50370200	1.603398091
chrX	50482000	50486000	1.619774563
chrX	50710100	50714100	1.590776102
chrX	50915200	50919200	1.516763113
chrX	50996000	51000000	1.559586287
chrX	51094300	51098300	6.686820361
chrX	51161100	51165100	1.591726157
chrX	51242600	51246600	1.469798079
chrX	51327300	51331300	15.2170509
chrX	51432900	51436900	1.452510301
chrX	51564100	51568100	1.431048884
chrX	51615500	51619500	12.37364072
chrX	51876900	51880900	1.407736053
chrX	52190400	52194400	1.439055984
chrX	52343500	52347500	3.843410181
chrX	52422300	52426300	1.443947533
chrX	52509300	52513300	1.507079641
chrX	52563500	52567500	1.668035111
chrX	52788900	52792900	1.737134065
chrX	52980500	52984500	1.529707181
chrX	53043500	53047500	1.449001777
chrX	53141100	53145100	1.385045129
chrX	53235300	53239300	4.554262726
chrX	53376000	53380000	2.954844499
chrX	53706600	53710600	1.547293552
chrX	54040100	54044100	2.232144412
chrX	54236500	54240500	1.476908687
chrX	54766400	54770400	1.625238917
chrX	55260100	55264100	1.947803394
chrX	55303300	55307300	1.551445507
chrX	55360000	55364000	2.831812328
chrX	55572400	55576400	1.549025886
chrX	55934300	55938300	3.843410181
chrX	56202200	56206200	1.502570677
chrX	56392400	56396400	1.60008284
chrX	56461200	56465200	1.61157956
chrX	56583000	56587000	15.2170509
chrX	56774900	56778900	1.574498536

chrX	57204200	57208200	1.593770949
chrX	57478700	57482700	1.625059997
chrX	57668700	57672700	1.502577277
chrX	57833400	57837400	1.620822601
chrX	57895300	57899300	1.6246886
chrX	57984300	57988300	1.592377121
chrX	58093100	58097100	1.550660422
chrX	58164000	58168000	1.527071155
chrX	58256700	58260700	1.478117904
chrX	58365200	58369200	1.432692854
chrX	58498200	58502200	1.49979478
chrX	58615300	58619300	1.42186109
chrX	58715000	58719000	1.533139409
chrX	58796700	58800700	1.561227009
chrX	58845100	58849100	3.221414204
chrX	58964700	58968700	1.675770017
chrX	59089900	59093900	1.981537391
chrX	59132700	59136700	1.755280829
chrX	59207800	59211800	1.556288415
chrX	59305000	59309000	1.830323561
chrX	59434200	59438200	12.37364072
chrX	59582000	59586000	1.561802818
chrX	59669800	59673800	1.444417676
chrX	59758000	59762000	2.42170509
chrX	60015200	60019200	1.513606284
chrX	60254200	60258200	1.637134503
chrX	60784600	60788600	1.466040243
chrX	60947700	60951700	1.470019802
chrX	61121100	61125100	1.547685324
chrX	61310300	61314300	1.496020029
chrX	61427700	61431700	1.561765319
chrX	61550000	61554000	1.710852545
chrX	61704300	61708300	1.530405361
chrX	62045800	62049800	5.265115271
chrX	62356300	62360300	1.466666556
chrX	62439700	62443700	1.964728454
chrX	62513900	62517900	1.947803394
chrX	62687400	62691400	1.505538186
chrX	63203800	63207800	2.066278818
chrX	63647900	63651900	2.42170509
chrX	63729900	63733900	1.583543427
chrX	63868700	63872700	1.66134302
chrX	64006300	64010300	1.475869727
chrX	64172900	64176900	1.97742225
chrX	64360900	64364900	16.63875599
chrX	64492300	64496300	13.79534581
chrX	64717500	64721500	1.589586067
chrX	64846700	64850700	1.729893238
chrX	64919700	64923700	15.2170509
chrX	65212800	65216800	1.679274029
chrX	65646700	65650700	12.37364072
chrX	66085000	66089000	1.670871674
chrX	66527100	66531100	1.668623681
chrX	66868500	66872500	1.592721026
chrX	67005500	67009500	3.843410181
chrX	67190600	67194600	1.254050394

chrX	67342800	67346800	2.777131363
chrX	67509500	67513500	3.843410181
chrX	67693700	67697700	1.698871884
chrX	67794900	67798900	1.568592282
chrX	67960800	67964800	1.581606628
chrX	68151700	68155700	1.506482438
chrX	68271700	68275700	1.80846962
chrX	68404800	68408800	1.767896268
chrX	68661700	68665700	1.632358902
chrX	68981700	68985700	1.596552466
chrX	69210900	69214900	1.6161881
chrX	69345300	69349300	5.975967816
chrX	69412600	69416600	1.519068281
chrX	69491000	69495000	1.838583862
chrX	69562900	69566900	2.688274795
chrX	69664800	69668800	1.770522649
chrX	69781900	69785900	12.37364072
chrX	69991900	69995900	1.620585555
chrX	70158700	70162700	1.360894369
chrX	70476900	70480900	1.346333973
chrX	70823100	70827100	1.528618331
chrX	70911200	70915200	1.496286454
chrX	71011000	71015000	1.534712091
chrX	71146600	71150600	2.184754242
chrX	71299800	71303800	3.003311718
chrX	71424900	71428900	1.543346791
chrX	71531800	71535800	12.37364072
chrX	71650700	71654700	13.79534581
chrX	71721700	71725700	1.534934491
chrX	71797000	71801000	1.432692854
chrX	71864500	71868500	1.459698014
chrX	71947600	71951600	1.590634835
chrX	72025900	72029900	1.21114432
chrX	72262400	72266400	1.540281544
chrX	72531200	72535200	1.573943343
chrX	72620700	72624700	1.533139409
chrX	72668300	72672300	1.597373073
chrX	72751700	72755700	1.655207529
chrX	72868500	72872500	1.536645131
chrX	73029000	73033000	1.540950975
chrX	73191300	73195300	12.37364072
chrX	73689400	73693400	1.542245371
chrX	74295000	74299000	1.666864145
chrX	74557300	74561300	1.54591002
chrX	74738900	74742900	1.890166701
chrX	74868700	74872700	1.617508272
chrX	75078900	75082900	13.79534581
chrX	75385000	75389000	1.48845131
chrX	75537900	75541900	1.533040459
chrX	75706400	75710400	1.625859306
chrX	75940600	75944600	3.843410181
chrX	76248900	76252900	1.482143465
chrX	76488200	76492200	1.513961732
chrX	76592900	76596900	1.555264337
chrX	76841900	76845900	1.734949242
chrX	77100800	77104800	1.570666212

chrX	77226400	77230400	1.572256155
chrX	77350400	77354400	1.429473413
chrX	77434000	77438000	1.624899786
chrX	77521200	77525200	1.581694911
chrX	77667700	77671700	1.567223302
chrX	77778000	77782000	1.491114164
chrX	77966200	77970200	1.525207701
chrX	78123600	78127600	15.2170509
chrX	78300700	78304700	1.516925867
chrX	78493000	78497000	1.566212573
chrX	78650800	78654800	1.603796439
chrX	78921100	78925100	1.514484439
chrX	79236600	79240600	1.249328878
chrX	79370500	79374500	1.706081723
chrX	79462800	79466800	1.521222785
chrX	79622600	79626600	1.51391143
chrX	79768100	79772100	1.388489182
chrX	80349100	80353100	1.575813945
chrX	80974100	80978100	1.555874311
chrX	81062100	81066100	1.562970333
chrX	81356700	81360700	1.47837519
chrX	81658000	81662000	4.909688998
chrX	81844600	81848600	1.466690149
chrX	82011700	82015700	1.486452059
chrX	82269600	82273600	4.554262726
chrX	82536400	82540400	1.517328632
chrX	82731000	82735000	1.531106078
chrX	82927600	82931600	1.469641906
chrX	83038100	83042100	2.599418227
chrX	83144200	83148200	1.488879009
chrX	83237300	83241300	1.53526771
chrX	83289500	83293500	1.660651094
chrX	83379900	83383900	1.564340952
chrX	83484300	83488300	1.661697848
chrX	83565200	83569200	1.584750709
chrX	83686300	83690300	1.779733606
chrX	83793000	83797000	1.738129445
chrX	83873900	83877900	1.804685081
chrX	83958000	83962000	2.066278818
chrX	84075100	84079100	1.702820313
chrX	84157800	84161800	4.909688998
chrX	84260100	84264100	1.667168869
chrX	84337900	84341900	1.560591032
chrX	84407900	84411900	1.51914347
chrX	84458100	84462100	1.443203611
chrX	84582200	84586200	1.568682036
chrX	84687000	84691000	2.177349528
chrX	84843000	84847000	1.587568155
chrX	84933500	84937500	1.63154255
chrX	85026300	85030300	1.920768733
chrX	85101400	85105400	1.476455046
chrX	85276000	85280000	1.927057001
chrX	85447100	85451100	1.956282292
chrX	85734300	85738300	1.517544174
chrX	86024000	86028000	1.706418953
chrX	86213200	86217200	1.444282841

chrX	86380700	86384700	1.563832335
chrX	86536900	86540900	1.505107277
chrX	86641300	86645300	1.496497525
chrX	86787000	86791000	1.629846758
chrX	86908100	86912100	1.529541977
chrX	86988900	86992900	1.510226461
chrX	87070700	87074700	1.640507762
chrX	87244400	87248400	1.382668526
chrX	87354200	87358200	1.457581679
chrX	87495500	87499500	1.453493583
chrX	87602300	87606300	1.520583589
chrX	87707100	87711100	1.455100162
chrX	87802000	87806000	2.08849296
chrX	87918700	87922700	1.661058526
chrX	88031800	88035800	13.79534581
chrX	88148200	88152200	1.658824686
chrX	88237500	88241500	1.522637242
chrX	88323900	88327900	1.584758967
chrX	88410700	88414700	1.505672517
chrX	88548100	88552100	1.521566194
chrX	88704700	88708700	1.669940168
chrX	88846200	88850200	1.575427602
chrX	89112400	89116400	1.675801857
chrX	89335600	89339600	1.591417806
chrX	89414700	89418700	1.702820313
chrX	89476800	89480800	1.505812315
chrX	89546100	89550100	3.843410181
chrX	89617300	89621300	1.507584354
chrX	89781900	89785900	1.438405169
chrX	89977700	89981700	1.57736666
chrX	90141500	90145500	1.522202022
chrX	90329300	90333300	1.506542885
chrX	90611800	90615800	1.592936627
chrX	90911200	90915200	1.519993506
chrX	91228400	91232400	1.552268918
chrX	91589900	91593900	1.542850509
chrX	91726700	91730700	1.56896867
chrX	91844300	91848300	1.621995977
chrX	91977900	91981900	19.48216617
chrX	92197200	92201200	1.6517817
chrX	92377500	92381500	1.639767291
chrX	92490300	92494300	12.37364072
chrX	92667900	92671900	1.520297667
chrX	92935400	92939400	15.2170509
chrX	93192400	93196400	1.476614874
chrX	93335700	93339700	1.590923435
chrX	93387900	93391900	1.565450888
chrX	93443900	93447900	1.710852545
chrX	93507000	93511000	1.504321062
chrX	93625300	93629300	1.489459076
chrX	93914800	93918800	11.3073619
chrX	94186000	94190000	1.605726465
chrX	94469200	94473200	1.596056482
chrX	94762000	94766000	1.552885313
chrX	94818700	94822700	1.289953012
chrX	94889500	94893500	1.480797092

chrX	95035000	95039000	1.878111968
chrX	95335500	95339500	1.464712467
chrX	95510400	95514400	1.530021635
chrX	95588700	95592700	1.594000072
chrX	95766600	95770600	1.463953379
chrX	96039100	96043100	1.579354353
chrX	96287600	96291600	1.547764181
chrX	96419200	96423200	1.537600827
chrX	96781900	96785900	1.543745287
chrX	97254000	97258000	1.53600575
chrX	97616200	97620200	1.606104752
chrX	97972400	97976400	1.529888559
chrX	98148500	98152500	1.485749239
chrX	98212800	98216800	1.578974924
chrX	98334000	98338000	1.535832032
chrX	98449500	98453500	1.47659432
chrX	98598200	98602200	1.853023054
chrX	98747300	98751300	1.450680514
chrX	99272100	99276100	1.558315436
chrX	99876700	99880700	1.574927252
chrX	100040900	100044900	12.37364072
chrX	100146100	100150100	1.717558701
chrX	100267600	100271600	1.455900131
chrX	100383800	100387800	1.525412751
chrX	100437000	100441000	1.607704361
chrX	100496500	100500500	1.55353272
chrX	100606400	100610400	1.483193887
chrX	100719900	100723900	1.618369178
chrX	100846400	100850400	1.671100923
chrX	101095900	101099900	1.53799014
chrX	101543900	101547900	1.498892607
chrX	102217600	102221600	1.614338419
chrX	102661100	102665100	1.560216128
chrX	102887800	102891800	1.40918823
chrX	103267300	103271300	1.844137397
chrX	103614600	103618600	1.967225594
chrX	103891600	103895600	1.616072206
chrX	104043300	104047300	2.032428697
chrX	104156400	104160400	1.640249458
chrX	104247700	104251700	1.727710708
chrX	104336800	104340800	1.556182762
chrX	104412200	104416200	1.602544014
chrX	104486300	104490300	1.559907073
chrX	104601200	104605200	1.65056823
chrX	104715500	104719500	1.552073332
chrX	104918200	104922200	1.45437568
chrX	105295100	105299100	3.487983908
chrX	105671900	105675900	1.426511527
chrX	105940000	105944000	3.843410181
chrX	106063100	106067100	1.545230651
chrX	106137900	106141900	2.42170509
chrX	106215300	106219300	12.37364072
chrX	106356100	106360100	1.512086285
chrX	106595200	106599200	1.483755985
chrX	106815000	106819000	1.576071071
chrX	107059700	107063700	1.631279499

chrX	107183800	107187800	12.37364072
chrX	107242000	107246000	1.710852545
chrX	107369200	107373200	1.49877499
chrX	107560600	107564600	1.647647411
chrX	107725900	107729900	1.776278146
chrX	107835300	107839300	1.729879648
chrX	107910300	107914300	1.690368827
chrX	108145000	108149000	1.916333359
chrX	108368700	108372700	15.2170509
chrX	108440000	108444000	1.232895455
chrX	108509500	108513500	1.628450782
chrX	108614600	108618600	1.557628986
chrX	108745700	108749700	1.681719244
chrX	108803800	108807800	1.613264407
chrX	108922700	108926700	1.547422895
chrX	109063500	109067500	1.647774463
chrX	109254900	109258900	1.549453344
chrX	109449800	109453800	1.621995977
chrX	109836700	109840700	1.487465752
chrX	110264600	110268600	1.533650372
chrX	110523500	110527500	1.467899981
chrX	110732400	110736400	1.551160242
chrX	110998000	111002000	12.37364072
chrX	111377700	111381700	1.349986075
chrX	111552600	111556600	1.523843645
chrX	111708500	111712500	1.502059533
chrX	111877700	111881700	1.415575334
chrX	112037000	112041000	1.461711299
chrX	112130000	112134000	1.988670538
chrX	112257900	112261900	1.645098685
chrX	112413500	112417500	1.537891097
chrX	112594800	112598800	13.79534581
chrX	112655500	112659500	1.520832405
chrX	112738100	112742100	2.279534581
chrX	112827900	112831900	1.993370864
chrX	112914100	112918100	13.79534581
chrX	112986300	112990300	1.708563165
chrX	113153500	113157500	2.184754242
chrX	113413700	113417700	1.731493448
chrX	113602900	113606900	1.66418418
chrX	113750000	113754000	1.864671478
chrX	114035500	114039500	1.772128303
chrX	114257600	114261600	1.643657528
chrX	114328600	114332600	1.696996945
chrX	114493400	114497400	1.633467613
chrX	114692800	114696800	1.818395011
chrX	114792200	114796200	1.618640857
chrX	114877700	114881700	1.576244297
chrX	114995800	114999800	1.523695716
chrX	115146800	115150800	2.263737858
chrX	115279800	115283800	1.848580226
chrX	115379300	115383300	1.667770573
chrX	115445200	115449200	1.785679129
chrX	115606600	115610600	1.571439654
chrX	115716200	115720200	1.451117961
chrX	115848800	115852800	1.540936907

chrX	115998000	116002000	1.560748726
chrX	116172000	116176000	1.605485647
chrX	116514100	116518100	1.644008434
chrX	116691700	116695700	3.843410181
chrX	116770700	116774700	1.58915768
chrX	116836700	116840700	1.663462375
chrX	117064800	117068800	1.528263646
chrX	117327900	117331900	1.507022451
chrX	117413900	117417900	1.54229988
chrX	117484100	117488100	1.44814617
chrX	117594200	117598200	1.635459093
chrX	117768800	117772800	2.19956367
chrX	117971100	117975100	1.561982902
chrX	118058100	118062100	1.449791469
chrX	118325200	118329200	1.414347205
chrX	118604600	118608600	15.2170509
chrX	118746500	118750500	1.673439253
chrX	119003500	119007500	1.506746369
chrX	119365000	119369000	12.37364072
chrX	119641700	119645700	1.477229658
chrX	119820000	119824000	4.198836453
chrX	119934000	119938000	1.469110411
chrX	120011700	120015700	12.37364072
chrX	120054100	120058100	1.611333189
chrX	120112100	120116100	1.556834494
chrX	120329600	120333600	1.425851293
chrX	120567500	120571500	1.510709596
chrX	120632900	120636900	1.585037935
chrX	120728300	120732300	1.538338181
chrX	120822400	120826400	1.612972677
chrX	120944200	120948200	1.482327751
chrX	121153300	121157300	4.376549589
chrX	121301200	121305200	1.585258426
chrX	121468500	121472500	15.2170509
chrX	121709600	121713600	1.572278611
chrX	121836400	121840400	2.163213256
chrX	122083500	122087500	1.581789385
chrX	122329900	122333900	1.671360737
chrX	122395200	122399200	1.42919399
chrX	122462600	122466600	1.575609137
chrX	122576300	122580300	1.573765055
chrX	122691300	122695300	1.736240136
chrX	122751500	122755500	1.741759178
chrX	122844200	122848200	1.38688745
chrX	122905700	122909700	1.442574061
chrX	123031200	123035200	1.598360728
chrX	123161500	123165500	15.2170509
chrX	123370700	123374700	1.515772879
chrX	123482900	123486900	1.538340769
chrX	123556700	123560700	1.475329112
chrX	123623900	123627900	1.559988156
chrX	123748000	123752000	1.598777175
chrX	123850300	123854300	1.321804868
chrX	123911200	123915200	2.400797662
chrX	123985200	123989200	1.581050599
chrX	124139700	124143700	1.377827088

chrX	126238000	126242000	1.410170089
chrX	126607200	126611200	2.777131363
chrX	126895800	126899800	1.504552055
chrX	127190700	127194700	1.4468216
chrX	127345700	127349700	1.510184795
chrX	127515400	127519400	1.490826757
chrX	127659500	127663500	1.555691837
chrX	127737300	127741300	1.444526283
chrX	127804300	127808300	1.493904041
chrX	127895300	127899300	1.697033483
chrX	128010400	128014400	1.671977797
chrX	128118000	128122000	1.594441153
chrX	128261300	128265300	1.53069157
chrX	128377900	128381900	1.605597555
chrX	128425700	128429700	13.79534581
chrX	128569500	128573500	2.599418227
chrX	128666500	128670500	1.564726128
chrX	128947200	128951200	1.746395172
chrX	129202300	129206300	1.565624606
chrX	129277100	129281100	1.592377121
chrX	129440000	129444000	1.607322415
chrX	129567100	129571100	1.610327943
chrX	129715600	129719600	1.675054216
chrX	129807500	129811500	1.652394277
chrX	129890500	129894500	1.533876044
chrX	129987700	129991700	1.555073776
chrX	130082900	130086900	1.469336969
chrX	130349100	130353100	1.58838526
chrX	130419100	130423100	1.558690685
chrX	130482300	130486300	1.589402843
chrX	130564700	130568700	1.697536863
chrX	130695700	130699700	1.521632803
chrX	130839500	130843500	12.37364072
chrX	131014800	131018800	12.37364072
chrX	131150700	131154700	1.806697832
chrX	131229500	131233500	1.5496555
chrX	131357100	131361100	1.639767291
chrX	131558200	131562200	2.089973903
chrX	131698400	131702400	1.643200385
chrX	131823500	131827500	1.964728454
chrX	131981900	131985900	1.5173804
chrX	132165700	132169700	1.610025158
chrX	132366700	132370700	11.3073619
chrX	132525500	132529500	1.553803727
chrX	132709300	132713300	1.612158861
chrX	132876300	132880300	1.915906164
chrX	132981700	132985700	1.522313757
chrX	133161000	133165000	1.612017432
chrX	133343700	133347700	1.771782763
chrX	133452700	133456700	1.522259013
chrX	133572400	133576400	1.897919004
chrX	133686300	133690300	1.740199669
chrX	133741100	133745100	2.42170509
chrX	133811200	133815200	1.558215496
chrX	134062300	134066300	1.888565681
chrX	134309000	134313000	1.643470719

chrX	134464700	134468700	1.475232881
chrX	134694800	134698800	1.264905724
chrX	134879300	134883300	12.37364072
chrX	135017100	135021100	1.299673132
chrX	135161900	135165900	1.402192887
chrX	135276600	135280600	1.272154974
chrX	135632900	135636900	13.79534581
chrX	135816400	135820400	1.271317765
chrX	136087800	136091800	1.456976636
chrX	136262100	136266100	1.544622412
chrX	136497300	136501300	1.502933594
chrX	136680300	136684300	1.637858962
chrX	136792100	136796100	1.589236809
chrX	136907400	136911400	1.532189071
chrX	137040700	137044700	1.491220363
chrX	137115800	137119800	1.594234999
chrX	137347800	137351800	1.613346223
chrX	137591900	137595900	1.651873513
chrX	137659100	137663100	1.679491403
chrX	137743500	137747500	2.079203409
chrX	137834400	137838400	1.560065642
chrX	137893300	137897300	1.691106641
chrX	137966000	137970000	1.632658765
chrX	138052000	138056000	2.599418227
chrX	138129100	138133100	13.79534581
chrX	138186900	138190900	1.475895274
chrX	138268100	138272100	1.58766503
chrX	138394600	138398600	1.567113979
chrX	138507900	138511900	4.198836453
chrX	138583100	138587100	1.578356361
chrX	138680300	138684300	1.465439166
chrX	138797000	138801000	1.678729471
chrX	138887300	138891300	1.668166547
chrX	138973800	138977800	1.639767291
chrX	139033700	139037700	1.461794719
chrX	139150000	139154000	2.954844499
chrX	139267600	139271600	1.562562114
chrX	139498700	139502700	1.487765842
chrX	139656900	139660900	1.464788203
chrX	139869300	139873300	5.265115271
chrX	140026600	140030600	1.494437437
chrX	140161700	140165700	1.434748874
chrX	140266200	140270200	1.500436749
chrX	140437700	140441700	1.574853425
chrX	140708700	140712700	1.641341134
chrX	140943300	140947300	15.2170509
chrX	141175000	141179000	1.556152621
chrX	141271400	141275400	1.51578461
chrX	141333400	141337400	1.656321391
chrX	141473500	141477500	1.629236142
chrX	141552400	141556400	1.516022563
chrX	141603100	141607100	1.579344824
chrX	141651200	141655200	1.630250412
chrX	141813200	141817200	1.477968764
chrX	142020000	142024000	1.596608386
chrX	142136800	142140800	1.563287173

chrX	142332800	142336800	1.539974529
chrX	142550300	142554300	1.624322065
chrX	142708500	142712500	1.470113238
chrX	142864500	142868500	1.46939448
chrX	143083400	143087400	1.510169684
chrX	143202600	143206600	148.8573294
chrX	143269100	143273100	2.42170509
chrX	143441700	143445700	1.519317276
chrX	143660900	143664900	1.606180083
chrX	143770400	143774400	1.484534107
chrX	143856500	143860500	1.797278387
chrX	143989900	143993900	1.759863119
chrX	144111700	144115700	15.2170509
chrX	144181100	144185100	1.787521803
chrX	144323400	144327400	2.42170509
chrX	144457400	144461400	1.600883049
chrX	144529700	144533700	1.608255271
chrX	144639500	144643500	1.682653436
chrX	144762300	144766300	1.613376733
chrX	144908500	144912500	1.565678434
chrX	145071200	145075200	1.48276274
chrX	145139900	145143900	1.644210119
chrX	145212400	145216400	1.957357863
chrX	145394600	145398600	1.552563194
chrX	145592100	145596100	1.761627727
chrX	145757700	145761700	2.10892997
chrX	145873500	145877500	1.459687151
chrX	146031200	146035200	1.656306929
chrX	146228900	146232900	15.2170509
chrX	146316600	146320600	1.626744038
chrX	146405900	146409900	1.625370277
chrX	146470800	146474800	1.592377121
chrX	146572200	146576200	1.684328196
chrX	146914500	146918500	1.651614833
chrX	147191700	147195700	1.592377121
chrX	147299000	147303000	1.521513316
chrX	147448900	147452900	1.532042414
chrX	147504500	147508500	1.572480485
chrX	147706200	147710200	1.360295126
chrX	147841500	147845500	1.601685904
chrX	147977300	147981300	1.464261298
chrX	148205900	148209900	1.625974629
chrX	148612300	148616300	1.442439343
chrX	148657200	148661200	4.376549589
chrX	148728100	148732100	13.79534581
chrX	148833000	148837000	1.727644338
chrX	148964000	148968000	1.547183608
chrX	149019700	149023700	1.597884992
chrX	149173700	149177700	1.628082043
chrX	149445900	149449900	1.584979631
chrX	149505100	149509100	1.833559234
chrX	149622700	149626700	1.666424261
chrX	149701500	149705500	1.928289794
chrX	149862600	149866600	1.812125752
chrX	150011000	150015000	1.595613014
chrX	150261500	150265500	1.570319316

chrX	150481700	150485700	1.930087442
chrX	150689600	150693600	1.496576419
chrX	150893800	150897800	2.335912542
chrX	151099100	151103100	2.42170509
chrX	151353200	151357200	1.537942467
chrX	151563000	151567000	1.403619665
chrX	151689500	151693500	3.132557635
chrX	151829300	151833300	1.44814617
chrX	151986200	151990200	1.483530441
chrX	152152000	152156000	1.514001071
chrX	152290000	152294000	1.576046725
chrX	152438700	152442700	1.669443659
chrX	152564200	152568200	1.568682036
chrX	152757100	152761100	1.569360213
chrX	153074300	153078300	1.618988524
chrX	153338000	153342000	1.556119556
chrX	153475200	153479200	12.37364072
chrX	153684100	153688100	1.092240781
chrX	153934200	153938200	1.575123418
chrX	154119300	154123300	1.669841821
chrX	154615600	154619600	1.464498885
chrX	155098000	155102000	1.43908202
chrX	155263600	155267600	1.451813058
chrX	155467700	155471700	12.37364072
chrX	155619000	155623000	1.909337347
chrX	155753600	155757600	1.353575094
chrX	155856300	155860300	1.598109803
chrX	155995800	155999800	1.431545198
chrX	156167400	156171400	1.443467643
chrX	156282500	156286500	1.589760944
chrX	156353600	156357600	1.609302182
chrX	156413800	156417800	2.42170509
chrX	156511400	156515400	1.340193718
chrX	156701000	156705000	1.565786391
chrX	156915100	156919100	1.435234783
chrX	157161200	157165200	1.544986951
chrX	157276100	157280100	1.55281364
chrX	157480000	157484000	1.632373386
chrX	157682200	157686200	1.792873993
chrX	157809800	157813800	1.453803187
chrX	157929300	157933300	12.37364072
chrX	158015800	158019800	1.581776688
chrX	158219100	158223100	1.453100668
chrX	158401500	158405500	1.515283065
chrX	158456200	158460200	1.604686256
chrX	158521300	158525300	1.422133843
chrX	158572600	158576600	1.654435676
chrX	158627500	158631500	2.066278818
chrX	158711800	158715800	1.609005251
chrX	158788000	158792000	12.37364072
chrX	158883700	158887700	1.263521854
chrX	158964100	158968100	3.487983908
chrX	159039500	159043500	26.59069163
chrX	159146600	159150600	1.426511527
chrX	159443200	159447200	4.198836453
chrX	159608900	159612900	1.502077801

chrX	159714300	159718300	1.589744334
chrX	160114700	160118700	12.37364072
chrX	160477700	160481700	13.79534581
chrX	160600100	160604100	15.2170509
chrX	160811800	160815800	12.37364072
chrX	161090000	161094000	1.770090257
chrX	161499400	161503400	1.434843865
chrX	161849800	161853800	1.454836686
chrX	162002500	162006500	1.309066324
chrX	162168400	162172400	1.572103252
chrX	162361100	162365100	1.744702666
chrX	162662300	162666300	1.61004705
chrX	162931400	162935400	1.588840541
chrX	163094600	163098600	1.772179671
chrX	163366800	163370800	1.620826812
chrX	163567700	163571700	1.586111594
chrX	163626500	163630500	1.593396703
chrX	163713900	163717900	1.578320715
chrX	163814100	163818100	1.630478115
chrX	164056500	164060500	1.734159186
chrX	164384400	164388400	1.907389874
chrX	164594600	164598600	1.372405235
chrX	164713200	164717200	1.807306515
chrX	164887800	164891800	1.538116991
chrX	165109400	165113400	1.550786448
chrX	165388300	165392300	1.58457335
chrX	165833300	165837300	1.646136201
chrX	166268200	166272200	1.532602511
chrX	166423700	166427700	1.820168525
chrX	166472000	166476000	1.59759302
chrX	166561000	166565000	1.576922689
chrX	166656500	166660500	1.442286064
chrX	166767300	166771300	1.619090168
chrX	166932800	166936800	1.552014752
chrX	167160900	167164900	2.243991954
chrX	167446800	167450800	1.513554696
chrX	167647000	167651000	1.432764397
chrX	167757500	167761500	1.501362888
chrX	167885300	167889300	1.559704775
chrX	168085100	168089100	16.63875599
chrX	168179700	168183700	1.804385775
chrX	168220700	168224700	1.87489544
chrX	168316600	168320600	1.552735154
chrX	168390200	168394200	1.543878409
chrX	168496800	168500800	1.434127804
chrX	168688800	168692800	1.583546655
chrX	168807800	168811800	1.465474575
chrX	168984300	168988300	1.657939461
chrX	169141200	169145200	1.573336428
chrX	169337200	169341200	1.580230587
chrX	169509700	169513700	2.42170509
chrX	169679100	169683100	1.7819378
chrX	169753200	169757200	1.551565535
chrX	169839500	169843500	19.48216617
chrX	169966300	169970300	1.861908711
chrX	170673300	170677300	2.658655939

chrX	170743300	170747300	2.42170509
chrX	170843100	170847100	2.540180514
chrY	158600	162600	1.617319316
chrY	289000	293000	1.611140197
chrY	741300	745300	1.468965221
chrY	872800	876800	1.625647617
chrY	1131200	1135200	1.501022577
chrY	1373900	1377900	1.482261858
chrY	1437400	1441400	1.654033749
chrY	1903400	1907400	2.42170509
chrY	2162400	2166400	1.536318018
chrY	2355200	2359200	1.61060112
chrY	2577100	2581100	1.588291761
chrY	2735700	2739700	1.594499645
chrY	2916700	2920700	1.642087089
chrY	3334900	3338900	1.54988802
chrY	3771500	3775500	1.523612943
chrY	3839000	3843000	1.641090366
chrY	3983900	3987900	1.759319764
chrY	4260100	4264100	1.551330517
chrY	4438500	4442500	1.602313769
chrY	4553700	4557700	1.668066465
chrY	4658600	4662600	2.146423958
chrY	4854800	4858800	1.601845686
chrY	5011400	5015400	1.585720251
chrY	5259200	5263200	1.513974267
chrY	5507600	5511600	2.42170509
chrY	5597400	5601400	1.53662398
chrY	5691900	5695900	1.710852545
chrY	5828200	5832200	1.604504527
chrY	5984100	5988100	1.570817106
chrY	6057100	6061100	1.455216665
chrY	6149700	6153700	1.516983669
chrY	6458500	6462500	1.592099336
chrY	6805400	6809400	1.509095867
chrY	6990100	6994100	1.506092784
chrY	8001900	8005900	1.53517489
chrY	8046900	8050900	1.623521412
chrY	8092500	8096500	13.79534581
chrY	8149200	8153200	1.660077363
chrY	8261100	8265100	1.815495813
chrY	8380600	8384600	13.79534581
chrY	8534200	8538200	1.541291388
chrY	8660100	8664100	1.591780267
chrY	8723100	8727100	1.523633042
chrY	8794000	8798000	1.519469168
chrY	8841300	8845300	1.526587772
chrY	8900700	8904700	1.947803394
chrY	9006600	9010600	1.482535533
chrY	9083500	9087500	1.548299771
chrY	9157400	9161400	13.79534581
chrY	9727600	9731600	12.37364072
chrY	10142000	10146000	1.486853994
chrY	10303500	10307500	1.419741503
chrY	10383600	10387600	1.579690296
chrY	10470000	10474000	1.704429179

chrY	10614300	10618300	1.64903928
chrY	10769300	10773300	1.482815208
chrY	11843200	11847200	1.56483959
chrY	12750800	12754800	1.523995332
chrY	12949900	12953900	1.545641841
chrY	13444300	13448300	12.37364072
chrY	14108400	14112400	1.422621289
chrY	14189300	14193300	1.533139409
chrY	14650300	14654300	1.591562857
chrY	14911500	14915500	4.11617918
chrY	16187100	16191100	2.198735814
chrY	16263300	16267300	2.67637189
chrY	16484500	16488500	1.209820972
chrY	16611800	16615800	1.200893111
chrY	17374200	17378200	1.7000411
chrY	17463300	17467300	1.687790535
chrY	18364900	18368900	1.624129328
chrY	19506200	19510200	1.540544123
chrY	19600100	19604100	1.832508518
chrY	20199500	20203500	1.584243445
chrY	20261700	20265700	2.777131363
chrY	20380800	20384800	1.582564943
chrY	20489700	20493700	1.495266118
chrY	20535900	20539900	1.591784744
chrY	20611300	20615300	1.062969222
chrY	20665300	20669300	1.129595861
chrY	20731800	20735800	20.90387126
chrY	20854900	20858900	1.868819777
chrY	20946700	20950700	1.672409192
chrY	21161700	21165700	1.643020462
chrY	21694900	21698900	1.881195091
chrY	21921900	21925900	1.607186549
chrY	22539300	22543300	1.342004581
chrY	22715100	22719100	1.512740073
chrY	22935500	22939500	1.699005003
chrY	23173700	23177700	1.532325907
chrY	23250500	23254500	1.582504169
chrY	23333500	23337500	1.431082419
chrY	23727300	23731300	1.373325437
chrY	23841900	23845900	1.357860699
chrY	23888900	23892900	1.364367814
chrY	24170900	24174900	1.339972956
chrY	25009500	25013500	1.388946149
chrY	25717300	25721300	1.545131434
chrY	26159700	26163700	1.598006623
chrY	26551500	26555500	1.630934212
chrY	27968500	27972500	4.198836453
chrY	28291900	28295900	3.843410181
chrY	28705900	28709900	2.599418227
chrY	28750900	28754900	8.463951724
chrY	28933100	28937100	13.79534581
chrY	29056800	29060800	1.496541713
chrY	29223900	29227900	1.513927178
chrY	29347700	29351700	4.554262726
chrY	29424400	29428400	1.517550537
chrY	29467900	29471900	2.370929908

chrY	29516500	29520500	3.843410181
chrY	29645100	29649100	1.541341554
chrY	29879300	29883300	1.584701248
chrY	31565300	31569300	6.686820361
chrY	32021500	32025500	1.56464883
chrY	32084900	32088900	1.518411287
chrY	32488700	32492700	1.383678104
chrY	33376000	33380000	3.843410181
chrY	33819300	33823300	1.764771701
chrY	34332700	34336700	1.534971503
chrY	34417000	34421000	1.621335333
chrY	34582500	34586500	8.108525451
chrY	34687100	34691100	2.419202088
chrY	34752900	34756900	2.559926419
chrY	34828700	34832700	29.43410181
chrY	34939800	34943800	1.368044957
chrY	34998100	35002100	1.346918729
chrY	35119400	35123400	4.554262726
chrY	35195400	35199400	23.74728144
chrY	35269700	35273700	1.651614833
chrY	35407200	35411200	1.473901697
chrY	35487200	35491200	12.37364072
chrY	36258300	36262300	2.777131363
chrY	36464400	36468400	1.715882162
chrY	37452800	37456800	2.540180514
chrY	37695700	37699700	1.568682036
chrY	37764100	37768100	12.37364072
chrY	37840100	37844100	7.042246634
chrY	37918200	37922200	2.066278818
chrY	38002700	38006700	4.198836453
chrY	38051700	38055700	16.63875599
chrY	38127500	38131500	1.283320045
chrY	38214600	38218600	2.42170509
chrY	38339600	38343600	2.269379545
chrY	38473500	38477500	3.843410181
chrY	38766100	38770100	3.905223445
chrY	38816700	38820700	1.42477774
chrY	38910800	38914800	1.2468238
chrY	39050500	39054500	3.843410181
chrY	39133900	39137900	2.777131363
chrY	39174500	39178500	5.975967816
chrY	39289500	39293500	4.198836453
chrY	39381600	39385600	3.843410181
chrY	39694500	39698500	4.198836453
chrY	39771400	39775400	2.42170509
chrY	39855000	39859000	13.79534581
chrY	39937900	39941900	3.843410181
chrY	40006400	40010400	4.198836453
chrY	40085100	40089100	4.198836453
chrY	40146900	40150900	1.473901697
chrY	40224100	40228100	15.2170509
chrY	40344100	40348100	1.399854557
chrY	40625900	40629900	13.79534581
chrY	40744100	40748100	3.843410181
chrY	40790100	40794100	2.42170509
chrY	40950300	40954300	12.37364072

chrY	41057300	41061300	4.198836453
chrY	41264100	41268100	12.37364072
chrY	41661400	41665400	3.843410181
chrY	41716100	41720100	2.184754242
chrY	41756800	41760800	1.322253154
chrY	41806900	41810900	1.37959884
chrY	41847300	41851300	1.361296676
chrY	41918200	41922200	12.37364072
chrY	42023300	42027300	1.290803314
chrY	42087300	42091300	12.37364072
chrY	42162700	42166700	13.79534581
chrY	42306100	42310100	1.330038682
chrY	42373300	42377300	26.59069163
chrY	42428600	42432600	3.843410181
chrY	42517200	42521200	2.42170509
chrY	42603600	42607600	12.37364072
chrY	42897700	42901700	12.37364072
chrY	43277900	43281900	1.809582065
chrY	43389300	43393300	12.37364072
chrY	43519900	43523900	13.79534581
chrY	43664300	43668300	1.054237126
chrY	43766300	43770300	2.42170509
chrY	43843900	43847900	1.710852545
chrY	43920900	43924900	1.14770962
chrY	44099800	44103800	1.115421934
chrY	44228300	44232300	1.215409862
chrY	44290900	44294900	13.79534581
chrY	44333900	44337900	1.117861562
chrY	44498600	44502600	1.18458602
chrY	44647300	44651300	3.843410181
chrY	44746000	44750000	1.131507721
chrY	44890100	44894100	1.196330703
chrY	45661100	45665100	2.777131363
chrY	46752100	46756100	2.706046108
chrY	47157100	47161100	1.2101651
chrY	47501100	47505100	3.843410181
chrY	53330700	53334700	1.128029894
chrY	53641900	53645900	2.599418227
chrY	53880100	53884100	1.109699467
chrY	54633900	54637900	3.843410181
chrY	54944000	54948000	2.066278818
chrY	55358300	55362300	2.42170509
chrY	55946100	55950100	1.28726233
chrY	56287900	56291900	1.241507595
chrY	56398300	56402300	3.843410181
chrY	56472200	56476200	12.37364072
chrY	56742500	56746500	3.843410181
chrY	56968800	56972800	1.373970252
chrY	57222700	57226700	1.338185446
chrY	57384400	57388400	2.066278818
chrY	57566500	57570500	1.947803394
chrY	57834300	57838300	1.327730719
chrY	57885100	57889100	3.25103306
chrY	58189100	58193100	2.42170509
chrY	58436600	58440600	1.383302843
chrY	58549300	58553300	1.330848924

chrY	58660100	58664100	2.42170509
chrY	58723700	58727700	1.50095514
chrY	58848500	58852500	2.954844499
chrY	58936600	58940600	12.37364072
chrY	59168700	59172700	4.198836453
chrY	59218700	59222700	1.188721915
chrY	59261700	59265700	16.63875599
chrY	59322700	59326700	4.198836453
chrY	59392300	59396300	1.558527
chrY	59570500	59574500	1.107240686
chrY	59660900	59664900	1.300569485
chrY	59886300	59890300	1.713286972
chrY	60158500	60162500	1.257377646
chrY	60278900	60282900	3.843410181
chrY	60375500	60379500	3.487983908
chrY	60424900	60428900	1.947803394
chrY	68127100	68131100	1.799709113
chrY	69045400	69049400	1.559273694
chrY	69226900	69230900	1.29618856
chrY	69345400	69349400	12.37364072
chrY	69864500	69868500	1.292291343
chrY	70239000	70243000	1.292201407
chrY	70863500	70867500	12.37364072
chrY	70935300	70939300	1.287895281
chrY	71096200	71100200	1.243672858
chrY	71312100	71316100	2.218604363
chrY	72077700	72081700	15.2170509
chrY	72480900	72484900	1.436647998
chrY	72689100	72693100	1.242730137
chrY	73099300	73103300	1.219875676
chrY	73628700	73632700	1.371736465
chrY	74247300	74251300	12.37364072
chrY	74342700	74346700	12.37364072
chrY	74404900	74408900	12.37364072
chrY	74518500	74522500	1.241080019
chrY	74578300	74582300	1.947803394
chrY	74830100	74834100	2.42170509
chrY	75103300	75107300	1.710852545
chrY	75170200	75174200	1.286200807
chrY	75411800	75415800	1.607455811
chrY	75604100	75608100	1.459394502
chrY	75683900	75687900	15.2170509
chrY	75800100	75804100	13.79534581
chrY	76028000	76032000	1.114814667
chrY	76118700	76122700	12.37364072
chrY	76171800	76175800	13.79534581
chrY	76406700	76410700	15.2170509
chrY	76555500	76559500	2.42170509
chrY	77558500	77562500	2.563875599
chrY	78011500	78015500	19.48216617
chrY	78122100	78126100	1.4864773
chrY	78229300	78233300	12.37364072
chrY	78315100	78319100	1.181978252
chrY	78472300	78476300	1.318972296
chrY	78666900	78670900	12.37364072
chrY	78788200	78792200	1.515168418

chrY	78858400	78862400	2.303229666
chrY	78935500	78939500	23.74728144
chrY	79029400	79033400	3.843410181
chrY	79083300	79087300	1.119471016
chrY	79168100	79172100	3.843410181
chrY	79275000	79279000	4.198836453
chrY	79499300	79503300	18.06046108
chrY	79798500	79802500	3.843410181
chrY	80260900	80264900	1.14744758
chrY	80439700	80443700	4.198836453
chrY	81066900	81070900	2.42170509
chrY	81109300	81113300	2.777131363
chrY	81266700	81270700	2.90257593
chrY	81635000	81639000	1.145528868
chrY	81809700	81813700	1.177713136
chrY	81929900	81933900	15.2170509
chrY	82094500	82098500	3.843410181
chrY	82228700	82232700	12.37364072
chrY	82275900	82279900	13.79534581
chrY	82702700	82706700	1.947803394
chrY	82837900	82841900	13.79534581
chrY	83157700	83161700	4.198836453
chrY	83225900	83229900	1.147793886
chrY	83457700	83461700	2.42170509
chrY	83896900	83900900	12.37364072
chrY	84081700	84085700	2.599418227
chrY	84273700	84277700	15.2170509
chrY	84402900	84406900	1.135708213
chrY	84462100	84466100	12.37364072
chrY	84560800	84564800	2.510561658
chrY	84662800	84666800	2.599418227
chrY	84707100	84711100	1.087043169
chrY	85048900	85052900	13.79534581
chrY	85179700	85183700	2.42170509
chrY	85870100	85874100	1.201728425
chrY	85988500	85992500	13.79534581
chrY	86196300	86200300	12.37364072
chrY	86247700	86251700	3.843410181
chrY	86302100	86306100	2.42170509
chrY	86405100	86409100	1.382766755
chrY	86461100	86465100	3.843410181
chrY	86520400	86524400	12.37364072
chrY	86565900	86569900	13.79534581
chrY	86626900	86630900	3.843410181
chrY	86734800	86738800	1.163303963
chrY	86839100	86843100	1.710852545
chrY	86930000	86934000	13.79534581
chrY	87076400	87080400	4.909688998
chrY	87308500	87312500	1.578837072
chrY	87411700	87415700	1.211034349
chrY	87461100	87465100	15.2170509
chrY	87682500	87686500	4.198836453
chrY	87800400	87804400	15.2170509
chrY	87871300	87875300	1.401500049
chrY	87952000	87956000	12.37364072
chrY	88176300	88180300	1.449312458

chrY	88300900	88304900	1.101550364
chrY	88389900	88393900	2.066278818
chrY	88575900	88579900	12.37364072
chrY	88757000	88761000	43.65115271
chrY	88851300	88855300	12.37364072
chrY	88926900	88930900	5.975967816
chrY	89119400	89123400	1.214908909
chrY	89228700	89232700	2.42170509
chrY	89318700	89322700	12.37364072
chrY	89454100	89458100	1.160788076
chrY	89508400	89512400	1.168827479
chrY	89609900	89613900	15.2170509
chrY	89770200	89774200	1.297476337
chrY	89827500	89831500	15.2170509
chrY	89969700	89973700	1.132796629
chrY	90021700	90025700	1.321804868
chrY	90117400	90121400	12.37364072
chrY	90349300	90353300	12.37364072
chrY	90502700	90506700	12.37364072
chrY	90769000	90773000	3.843410181
chrX	466882738	46882899	13.79534581
chrX	70385611	70385785	15.2170509
chrY	2707089	2707178	1.358020625
chr1	97538228	97538304	1.30723288
chr15	51865029	51865206	1.18816685

Annexure 2

Chromosome	Start	End	Fold Change
GL456210.1	82700	86700	1.619387283
GL456211.1	128400	132400	1.742071278
GL456212.1	87200	91200	1.6829958
GL456216.1	27000	31000	3.101996739
GL456221.1	101200	105200	1.506835603
GL456233.1	39400	43400	1.582481024
GL456233.1	91300	95300	1.771154225
GL456233.1	236200	240200	1.511587637
GL456239.1	18100	22100	2.390550695
GL456359.1	8400	12400	1.919256692
GL456360.1	14400	18400	1.805467879
GL456366.1	21800	25800	1.829563798
GL456367.1	11700	15700	1.742301516
GL456368.1	8200	12200	1.404050917
GL456370.1	11300	15300	1.49272596
GL456372.1	12200	16200	1.879563499
GL456378.1	13300	17300	1.675478142
GL456379.1	6300	10300	2.028205634
GL456379.1	66300	70300	13.33846761
GL456381.1	7100	11100	15.10110583
GL456382.1	5100	9100	3.643957344
GL456383.1	17900	21900	1.203805045
GL456385.1	18500	22500	1.739497648
GL456387.1	10300	14300	3.210129718
GL456389.1	10900	14900	1.008015066
GL456390.1	12100	16100	1.158311026
GL456392.1	9900	13900	1.059260584
GL456393.1	25500	29500	1.541314861
GL456394.1	10200	14200	1.984739215
GL456396.1	7900	11900	1.006913632
JH584292.1	6900	10900	1.548513295
JH584297.1	161400	165400	1.089122158
JH584299.1	193700	197700	13.33846761
JH584299.1	338000	342000	1.52587697
JH584299.1	489600	493600	1.136961754
JH584299.1	743500	747500	4.965936016
JH584299.1	818500	822500	2.982968008
JH584299.1	946900	950900	3.643957344
JH584304.1	55200	59200	1.145272275
JH792827.1	9700	13700	1.54637334
JH792828.1	220300	224300	1.490486786
JH792829.1	144300	148300	1.769339745
KB469742.1	16500	20500	29.20221167
KB469742.1	868500	872500	13.33846761
KQ030484.1	11400	15400	1.568758266
KQ030488.1	43200	47200	5.112822535
KQ030489.1	61300	65300	13.33846761
KQ030490.1	75800	79800	2.12612998

KQ030491.1	10400	14400	2.05475655
KQ030492.1	12400	16400	2.100016821
KQ030493.1	3400	7400	3.108870739
KQ030494.1	504000	508000	51.96962213
KV575233.1	210000	214000	1.881319115
KV575236.1	70200	74200	2.249541484
KV575238.1	100400	104400	2.33388839
KV575239.1	20800	24800	2.969197397
KV575242.1	156800	160800	4.34166831
chr1	12578700	12582700	1.74833043
chr1	48964900	48968900	1.866376911
chr1	80231400	80235400	1.833923521
chr1	114419300	114423300	1.892793068
chr1	149783800	149787800	1.829446362
chr1	167154600	167158600	1.914059442
chr1	180666400	180670400	2.283217502
chr1	183244200	183248200	2.183564604
chr1	187646700	187650700	2.063309911
chr1	193737400	193741400	1.872262995
chr10	5300300	5304300	1.817661655
chr10	32716700	32720700	1.803886139
chr10	69984200	69988200	2.188317566
chr10	81820500	81824500	1.199742304
chr10	93052800	93056800	1.890817229
chr10	117395400	117399400	1.875837334
chr11	15470900	15474900	1.870206223
chr11	31230500	31234500	2.013473833
chr11	52938300	52942300	2.021045302
chr11	79634400	79638400	2.328353189
chr11	105152000	105156000	2.335262568
chr12	10789400	10793400	3.147338143
chr12	19114500	19118500	1.765926605
chr12	19829700	19833700	1.83547598
chr12	21078000	21082000	2.041280148
chr12	22179500	22183500	1.288021458
chr12	22328200	22332200	1.231025399
chr12	22457100	22461100	1.307858047
chr12	22565900	22569900	1.232652473
chr12	23016500	23020500	1.666968847
chr12	23431200	23435200	1.252531823
chr12	23558700	23562700	1.315710635
chr12	23655100	23659100	1.318254125
chr12	23775100	23779100	1.885963748
chr12	23902100	23906100	1.401250979
chr12	24136700	24140700	1.488782978
chr12	39724400	39728400	1.794847946
chr12	68632300	68636300	1.873864101
chr12	84852100	84856100	2.436841453
chr12	87760500	87764500	1.844597485
chr12	98590300	98594300	1.938397275
chr12	114858500	114862500	2.037073599

chr13	12946800	12950800	1.753378431
chr13	44522900	44526900	2.02209577
chr13	67039700	67043700	1.737718392
chr13	93740900	93744900	1.845219587
chr13	119782100	119786100	1.702512825
chr13	120168500	120172500	1.631151117
chr14	3080000	3084000	1.686665562
chr14	3263400	3267400	1.307997838
chr14	3543700	3547700	1.991484004
chr14	3719400	3723400	1.046012645
chr14	4406000	4410000	1.463466966
chr14	5078000	5082000	1.247088176
chr14	5247600	5251600	5.99414165
chr14	5366200	5370200	1.243168841
chr14	5480500	5484500	2.982968008
chr14	5587100	5591100	34.49012636
chr14	5716700	5720700	2.65247334
chr14	6257500	6261500	1.779054956
chr14	7164000	7168000	1.774076115
chr14	13535100	13539100	1.781881159
chr14	22064200	22068200	2.04313516
chr14	25292800	25296800	2.633360225
chr14	33910100	33914100	1.909196935
chr14	41662000	41666000	1.390508982
chr14	42373100	42377100	1.348911536
chr14	43193200	43197200	1.658146963
chr14	48143300	48147300	1.814429571
chr14	52972500	52976500	1.058038088
chr14	53087500	53091500	1.464121586
chr14	61298800	61302800	2.094733149
chr14	97245200	97249200	1.753527981
chr15	6100500	6104500	1.844266468
chr15	23998000	24002000	1.799245524
chr15	71398200	71402200	2.012629197
chr15	103826100	103830100	1.686033206
chr16	3014800	3018800	5.186265795
chr16	3127100	3131100	1.373211666
chr16	10607200	10611200	2.073437295
chr16	41871600	41875600	1.846945418
chr16	81700300	81704300	1.799230937
chr17	5235100	5239100	2.027289242
chr17	10385600	10389600	2.116244872
chr17	13446900	13450900	2.137353968
chr17	14311900	14315900	2.157997671
chr17	34867600	34871600	2.10876015
chr17	75315500	75319500	1.899158707
chr18	7117700	7121700	1.926832148
chr18	43965200	43969200	1.881512942
chr18	77204400	77208400	2.399267715
chr18	80050200	80054200	2.016318224
chr18	84996700	85000700	1.8578266

chr18	89216600	89220600	1.638289147
chr19	3544500	3548500	2.722665205
chr19	5220000	5224000	2.993457423
chr19	22006900	22010900	1.875625273
chr19	46990500	46994500	2.053503884
chr19	58929800	58933800	2.064318653
chr2	12735300	12739300	1.801102509
chr2	40796600	40800600	2.005164908
chr2	71532000	71536000	1.866429607
chr2	86596500	86600500	1.72262066
chr2	89705700	89709700	1.685615873
chr2	90276500	90280500	1.773727078
chr2	90618700	90622700	2.312292157
chr2	95747400	95751400	5.974138391
chr2	100610900	100614900	1.881319115
chr2	100703300	100707300	4.084616901
chr2	111670500	111674500	1.910251659
chr2	148947300	148951300	2.078514305
chr2	176752700	176756700	1.609192511
chr2	177321200	177325200	1.524710165
chr2	179868500	179872500	2.439344442
chr3	9301700	9305700	1.746838742
chr3	28249900	28253900	1.82905589
chr3	45703400	45707400	1.708140965
chr3	74634900	74638900	1.884378155
chr3	105929200	105933200	1.953913196
chr3	122450900	122454900	1.798731887
chr3	145700700	145704700	1.785117215
chr4	22451300	22455300	1.757638435
chr4	51529200	51533200	2.011647222
chr4	60505600	60509600	1.359562566
chr4	60637000	60641000	1.353175675
chr4	60740200	60744200	1.418626579
chr4	60830700	60834700	1.763572026
chr4	91666500	91670500	1.850932603
chr4	121891700	121895700	5.406595573
chr4	122085400	122089400	1.210081882
chr4	122192300	122196300	1.346442815
chr4	122400500	122404500	1.985003716
chr4	126417600	126421600	2.583779878
chr4	136982100	136986100	3.016412716
chr4	144738300	144742300	1.719386297
chr4	146164600	146168600	1.465064474
chr4	146539600	146543600	1.635862594
chr4	146727900	146731900	1.794653846
chr4	146932400	146936400	1.478349863
chr4	151634500	151638500	2.600493256
chr4	156330300	156334300	1.596143114
chr5	6989400	6993400	1.768172879
chr5	11044100	11048100	3.203297787
chr5	11085300	11089300	2.468865191

chr5	11198800	11202800	1.679251965
chr5	11430200	11434200	1.350914247
chr5	11634100	11638100	1.771154225
chr5	11741800	11745800	1.183878161
chr5	13448900	13452900	1.648004498
chr5	22959800	22963800	1.934635154
chr5	61917400	61921400	1.855437784
chr5	93565900	93569900	1.537754036
chr5	93635400	93639400	1.157308622
chr5	93737200	93741200	1.562220815
chr5	94185500	94189500	1.257359994
chr5	94267900	94271900	2.175092153
chr5	94367600	94371600	1.392241408
chr5	94648500	94652500	4.525276459
chr5	94723200	94727200	2.707555785
chr5	94968700	94972700	4.525276459
chr5	95303000	95307000	1.179923279
chr5	95450100	95454100	1.282640236
chr5	110213200	110217200	2.348890227
chr5	127249000	127253000	2.278765137
chr5	130583400	130587400	2.157518919
chr5	134879700	134883700	2.401128102
chr5	140540500	140544500	2.566863788
chr5	147801300	147805300	2.223832159
chr6	16897400	16901400	1.741437599
chr6	35880300	35884300	1.99318994
chr6	44340700	44344700	1.683866673
chr6	60015100	60019100	1.860905816
chr6	97217800	97221800	1.910048941
chr6	122089700	122093700	1.706976021
chr6	122797000	122801000	1.978374054
chr6	123492100	123496100	2.028205634
chr6	123545700	123549700	13.33846761
chr6	131646300	131650300	1.912789697
chr6	142866100	142870100	1.97218096
chr6	147827300	147831300	1.964343842
chr7	3494000	3498000	2.020624394
chr7	3641700	3645700	2.57114173
chr7	3799200	3803200	1.286925697
chr7	4772400	4776400	2.021479351
chr7	6785000	6789000	1.85398261
chr7	7814600	7818600	1.13361935
chr7	7915500	7919500	2.542308451
chr7	8064400	8068400	1.235733824
chr7	8388700	8392700	1.506605316
chr7	8707600	8711600	1.219125791
chr7	8799400	8803400	1.211962825
chr7	8892100	8896100	4.525276459
chr7	8935500	8939500	15.10110583
chr7	9173300	9177300	1.335592494
chr7	12531600	12535600	1.699553133

chr7	16404100	16408100	2.113845459
chr7	18847200	18851200	2.182456937
chr7	20265700	20269700	1.11424507
chr7	21092200	21096200	1.361146801
chr7	22136400	22140400	1.098092025
chr7	22274700	22278700	1.137332924
chr7	22397600	22401600	1.069619463
chr7	22537000	22541000	1.084194747
chr7	22669700	22673700	18.62638229
chr7	22809300	22813300	1.736113827
chr7	27893900	27897900	2.217276069
chr7	35854200	35858200	2.200990778
chr7	38817300	38821300	1.574699566
chr7	38995900	38999900	2.542308451
chr7	39174800	39178800	1.853240677
chr7	49554600	49558600	1.870617815
chr7	82894200	82898200	1.912433177
chr7	106086300	106090300	1.32629939
chr7	122568800	122572800	2.108827171
chr7	140525100	140529100	2.399508495
chr7	143563400	143567400	2.559732666
chr8	11400000	11404000	1.930505578
chr8	20029200	20033200	1.490119219
chr8	20347500	20351500	1.289924178
chr8	20597100	20601100	1.506961232
chr8	21152500	21156500	1.480814334
chr8	27770100	27774100	1.902801844
chr8	44581700	44585700	1.794786146
chr8	63008200	63012200	1.776629621
chr8	71717200	71721200	2.421485002
chr8	100970200	100974200	2.08389854
chr9	8160200	8164200	1.993692303
chr9	46906200	46910200	2.083020034
chr9	94609600	94613600	1.913809646
chr9	116411200	116415200	2.177801594
chr9	124040500	124044500	1.669099635
chr9	124255900	124259900	1.34242335
chr9	124482500	124486500	1.893391979
chrM	6000	10000	2.861327609
chrX	3067700	3071700	2.202574147
chrX	3323000	3327000	1.508271094
chrX	3530700	3534700	16.86374406
chrX	3699800	3703800	1.369652804
chrX	3822500	3826500	1.2103472
chrX	3962700	3966700	4.525276459
chrX	4127700	4131700	1.438896919
chrX	4278500	4282500	16.86374406
chrX	4352600	4356600	1.200299799
chrX	4489500	4493500	1.389163449
chrX	4666700	4670700	1.481179976
chrX	4865000	4869000	1.404090299

chrX	4945500	4949500	15.10110583
chrX	5112500	5116500	2.008147601
chrX	5482300	5486300	1.44382882
chrX	5822700	5826700	1.426816849
chrX	5988200	5992200	1.593793738
chrX	6253500	6257500	1.597858792
chrX	6541300	6545300	1.536085522
chrX	6745200	6749200	1.556363463
chrX	7424700	7428700	1.802169941
chrX	8957900	8961900	1.544439781
chrX	10566500	10570500	1.619116852
chrX	12194500	12198500	1.987496766
chrX	13297800	13301800	1.897856008
chrX	13531200	13535200	1.812108896
chrX	13782900	13786900	1.64659227
chrX	13985900	13989900	1.58418867
chrX	14091100	14095100	1.618219438
chrX	14285000	14289000	1.565282316
chrX	14717800	14721800	1.541634006
chrX	15031100	15035100	13.33846761
chrX	15226700	15230700	1.487562136
chrX	15422700	15426700	2.542308451
chrX	15506500	15510500	1.484725513
chrX	15716900	15720900	1.511413345
chrX	16021700	16025700	1.550717387
chrX	16199000	16203000	2.085911052
chrX	16261700	16265700	1.582566872
chrX	16463600	16467600	1.463486516
chrX	17005400	17009400	1.528029721
chrX	17795000	17799000	1.569119687
chrX	18273900	18277900	1.396429788
chrX	18659100	18663100	1.478126137
chrX	19145200	19149200	1.500443306
chrX	19432200	19436200	1.529457453
chrX	19591500	19595500	1.431283822
chrX	19716800	19720800	1.665568939
chrX	19942300	19946300	1.499910217
chrX	21011200	21015200	1.649903719
chrX	21957400	21961400	1.548891729
chrX	22052500	22056500	1.450806323
chrX	22213500	22217500	1.608320863
chrX	22367300	22371300	1.512662753
chrX	22500000	22504000	1.355094595
chrX	22560700	22564700	13.33846761
chrX	22667300	22671300	1.547118594
chrX	22843500	22847500	1.540318258
chrX	23112300	23116300	1.531375667
chrX	23534200	23538200	1.490328128
chrX	23887100	23891100	1.528930478
chrX	24355700	24359700	1.431006108
chrX	24702400	24706400	1.454218313

chrX	25376500	25380500	1.816915026
chrX	25490800	25494800	1.353602425
chrX	25671500	25675500	1.43842837
chrX	25827900	25831900	15.10110583
chrX	25922900	25926900	1.274696867
chrX	26073900	26077900	1.342275306
chrX	26314700	26318700	1.334515284
chrX	26427700	26431700	1.68466113
chrX	26479700	26483700	20.38902052
chrX	26587400	26591400	1.452332658
chrX	26664500	26668500	2.321978672
chrX	26749000	26753000	1.847422226
chrX	26836700	26840700	1.664682014
chrX	27257500	27261500	3.203297787
chrX	28007500	28011500	1.11725705
chrX	28076100	28080100	15.10110583
chrX	28621300	28625300	4.525276459
chrX	28744600	28748600	1.094999333
chrX	29568500	29572500	3.864287123
chrX	29663700	29667700	2.175092153
chrX	30062900	30066900	13.33846761
chrX	30246500	30250500	13.33846761
chrX	30373900	30377900	2.468865191
chrX	31197700	31201700	2.135048854
chrX	31330900	31334900	1.205392167
chrX	31592500	31596500	1.22346243
chrX	31726500	31730500	1.416986584
chrX	31962100	31966100	2.175092153
chrX	32081200	32085200	1.319898045
chrX	32197100	32201100	1.532737674
chrX	32304200	32308200	1.67665259
chrX	32478000	32482000	1.297136852
chrX	32662000	32666000	1.693325794
chrX	32926400	32930400	1.313137499
chrX	33084500	33088500	1.933117257
chrX	33202600	33206600	1.399347724
chrX	33362700	33366700	1.719086243
chrX	33525500	33529500	13.33846761
chrX	33652800	33656800	1.342735211
chrX	33713100	33717100	15.10110583
chrX	33761700	33765700	1.365117919
chrX	33845300	33849300	1.359055936
chrX	33964800	33968800	1.386314651
chrX	34259200	34263200	1.420888809
chrX	34472000	34476000	1.253673454
chrX	34601600	34605600	1.328046559
chrX	35173500	35177500	1.149766647
chrX	35594900	35598900	1.448301053
chrX	35915800	35919800	1.539673682
chrX	36689000	36693000	1.754317857
chrX	37474300	37478300	1.49805639

chrX	37635300	37639300	1.508791459
chrX	38311100	38315100	1.708032342
chrX	38913300	38917300	1.519477993
chrX	39223600	39227600	1.577621312
chrX	39330400	39334400	1.410034569
chrX	39589500	39593500	1.535448395
chrX	39850900	39854900	1.517746216
chrX	39975700	39979700	13.33846761
chrX	40155700	40159700	1.558527032
chrX	40370600	40374600	1.728121065
chrX	40673300	40677300	1.486488151
chrX	40942500	40946500	1.46820078
chrX	41275600	41279600	1.486719877
chrX	41998800	42002800	1.621090188
chrX	42487900	42491900	1.887194575
chrX	42573400	42577400	1.587938821
chrX	42800700	42804700	1.50795385
chrX	43172900	43176900	1.533271619
chrX	43434400	43438400	1.576412868
chrX	43642700	43646700	1.514579279
chrX	43952000	43956000	1.529820246
chrX	44179900	44183900	1.860823321
chrX	44301700	44305700	1.476080421
chrX	44455500	44459500	1.710930752
chrX	44590500	44594500	1.485548477
chrX	44724800	44728800	1.453289927
chrX	44858100	44862100	1.570976561
chrX	45034400	45038400	1.518885886
chrX	45246200	45250200	1.537692208
chrX	45399400	45403400	1.541443008
chrX	45715300	45719300	1.554865244
chrX	46065200	46069200	1.583626352
chrX	46202500	46206500	1.622519057
chrX	46321200	46325200	1.480661794
chrX	46468800	46472800	1.423528084
chrX	46614200	46618200	1.531773376
chrX	46694400	46698400	1.506902497
chrX	46811900	46815900	1.415794755
chrX	46880900	46884900	13.33846761
chrX	46956600	46960600	1.53148252
chrX	47047100	47051100	1.488466962
chrX	47198200	47202200	1.478470388
chrX	47451700	47455700	1.504523261
chrX	47617900	47621900	1.837253159
chrX	47725900	47729900	1.471027591
chrX	48381800	48385800	1.753631936
chrX	49099500	49103500	1.535575634
chrX	49406000	49410000	1.472666378
chrX	49780500	49784500	1.497272872
chrX	50050200	50054200	1.476388711
chrX	50239200	50243200	1.495898932

chrX	50482100	50486100	1.596506255
chrX	50759300	50763300	1.605604573
chrX	51064100	51068100	1.682785668
chrX	51288700	51292700	1.598326738
chrX	51365900	51369900	1.62829524
chrX	51447800	51451800	1.525465736
chrX	51565400	51569400	1.501440186
chrX	51684000	51688000	1.837832974
chrX	52038300	52042300	1.699121843
chrX	52516100	52520100	1.580487014
chrX	52987700	52991700	1.756750483
chrX	53392100	53396100	1.697621182
chrX	53893900	53897900	1.631968821
chrX	54253200	54257200	2.001498994
chrX	54745600	54749600	1.240605525
chrX	55184600	55188600	2.046566449
chrX	55258200	55262200	1.22597926
chrX	55361800	55365800	1.617572602
chrX	55607100	55611100	1.52212064
chrX	56293600	56297600	1.635849309
chrX	57496000	57500000	1.612267763
chrX	58322000	58326000	1.478557086
chrX	58630400	58634400	1.488802481
chrX	58851500	58855500	1.482850366
chrX	58909800	58913800	1.534132797
chrX	59012000	59016000	1.619559805
chrX	59155300	59159300	1.662927721
chrX	59400400	59404400	1.498877737
chrX	59685900	59689900	1.468603822
chrX	60012600	60016600	1.570087767
chrX	61037200	61041200	1.571062552
chrX	61335400	61339400	3.203297787
chrX	61483600	61487600	1.565608479
chrX	61676900	61680900	1.624030792
chrX	61810800	61814800	1.668096748
chrX	61962100	61966100	1.537830639
chrX	62470600	62474600	1.560935879
chrX	62944300	62948300	1.407717047
chrX	63178200	63182200	1.540675745
chrX	63305500	63309500	2.542308451
chrX	63352100	63356100	1.771154225
chrX	63417900	63421900	4.525276459
chrX	63524900	63528900	1.516135848
chrX	63804200	63808200	1.469711351
chrX	64127300	64131300	1.549505824
chrX	64359800	64363800	1.566562288
chrX	64487500	64491500	13.33846761
chrX	64582300	64586300	1.575176685
chrX	64924800	64928800	1.508986877
chrX	65279100	65283100	1.542350224
chrX	65405800	65409800	1.614440791

chrX	65664700	65668700	1.54737711
chrX	65924400	65928400	1.502771571
chrX	66205200	66209200	1.487490533
chrX	66475700	66479700	1.515645743
chrX	66646300	66650300	1.606066551
chrX	66791600	66795600	1.504114534
chrX	67018200	67022200	1.596513269
chrX	67292700	67296700	1.571307366
chrX	67430100	67434100	1.683782072
chrX	67617700	67621700	1.526063731
chrX	67908700	67912700	1.518603518
chrX	68070700	68074700	2.762638229
chrX	68614800	68618800	1.532983378
chrX	69275200	69279200	1.473911427
chrX	69569200	69573200	1.478927361
chrX	69672700	69676700	1.684318371
chrX	69751400	69755400	1.753127243
chrX	69839700	69843700	2.321978672
chrX	69938100	69942100	1.53219362
chrX	70142900	70146900	1.603440513
chrX	70271600	70275600	1.507292814
chrX	70383700	70387700	13.33846761
chrX	70493800	70497800	1.434899302
chrX	70685600	70689600	1.539886596
chrX	71354700	71358700	1.691116061
chrX	72005000	72009000	1.531463973
chrX	72250000	72254000	1.668395379
chrX	72403900	72407900	1.552405761
chrX	72516100	72520100	2.909524748
chrX	72845700	72849700	1.600157281
chrX	73903200	73907200	1.812378719
chrX	74699100	74703100	2.035037565
chrX	74770200	74774200	1.893337103
chrX	74921800	74925800	1.515654435
chrX	75095400	75099400	1.719683744
chrX	75204900	75208900	2.762638229
chrX	75320300	75324300	1.504603846
chrX	75421100	75425100	1.72708827
chrX	75950500	75954500	1.524812498
chrX	77247600	77251600	1.515566652
chrX	78221000	78225000	1.466993794
chrX	78300300	78304300	1.615220348
chrX	78753200	78757200	1.567938274
chrX	79249100	79253100	1.707315084
chrX	79377400	79381400	1.607130946
chrX	79541900	79545900	1.469721461
chrX	79726200	79730200	1.562755103
chrX	80151200	80155200	1.500503923
chrX	80520900	80524900	1.691668166
chrX	80737000	80741000	1.499039932
chrX	80958900	80962900	1.393020686

chrX	81022800	81026800	3.329200517
chrX	81081800	81085800	1.653025609
chrX	81321900	81325900	1.543204462
chrX	81551200	81555200	1.647218725
chrX	81750100	81754100	1.536166018
chrX	82061700	82065700	1.547930448
chrX	82236500	82240500	1.470036861
chrX	82578800	82582800	1.558831419
chrX	83090100	83094100	1.610870007
chrX	83378700	83382700	1.483537334
chrX	83581700	83585700	1.51918134
chrX	83659400	83663400	1.796576892
chrX	83775600	83779600	1.663410542
chrX	83900500	83904500	1.480922867
chrX	84013600	84017600	1.860335326
chrX	84091300	84095300	1.557899256
chrX	84271000	84275000	1.524732762
chrX	84394100	84398100	1.560511748
chrX	84595700	84599700	1.510475989
chrX	84769300	84773300	1.592829764
chrX	84878000	84882000	1.591251929
chrX	85045000	85049000	1.569096562
chrX	85167300	85171300	1.812196047
chrX	85445100	85449100	1.55337436
chrX	85757100	85761100	1.611307131
chrX	86179700	86183700	1.631656142
chrX	86552100	86556100	2.762638229
chrX	86609300	86613300	1.761139235
chrX	86772100	86776100	1.554086733
chrX	86926100	86930100	2.041558954
chrX	86987300	86991300	13.33846761
chrX	87051300	87055300	1.359055936
chrX	87253100	87257100	1.459491162
chrX	87389000	87393000	1.484190917
chrX	87533000	87537000	1.652828974
chrX	87732000	87736000	1.555161647
chrX	88033100	88037100	1.531179659
chrX	88294000	88298000	1.488995158
chrX	88487100	88491100	1.544193162
chrX	88589100	88593100	4.965936016
chrX	88727000	88731000	1.527882892
chrX	88874900	88878900	1.537863871
chrX	88977100	88981100	1.449385489
chrX	89077900	89081900	1.513144028
chrX	89322100	89326100	1.543897912
chrX	89866900	89870900	1.581893276
chrX	90359000	90363000	1.572564303
chrX	90532800	90536800	1.618618225
chrX	90682300	90686300	1.501440186
chrX	90789500	90793500	1.918040744
chrX	90845500	90849500	1.510237382

chrX	90922100	90926100	1.683980269
chrX	91046900	91050900	1.496991295
chrX	91322300	91326300	1.484651783
chrX	91562100	91566100	4.525276459
chrX	91622900	91626900	1.832356942
chrX	91796300	91800300	1.362829513
chrX	92025100	92029100	1.595833448
chrX	92163900	92167900	1.665940567
chrX	92262600	92266600	1.476582891
chrX	92841000	92845000	1.581316699
chrX	93785100	93789100	1.749290515
chrX	94348700	94352700	1.807249664
chrX	94741900	94745900	1.467967379
chrX	95023000	95027000	1.797817022
chrX	95182300	95186300	1.692568728
chrX	95577000	95581000	1.564368716
chrX	96130700	96134700	1.675692091
chrX	96434900	96438900	1.435247949
chrX	96621600	96625600	1.454599578
chrX	96835400	96839400	1.572256773
chrX	96981400	96985400	1.608731632
chrX	97327500	97331500	1.510506156
chrX	97703300	97707300	1.600309412
chrX	97853100	97857100	1.542763601
chrX	97949700	97953700	2.321978672
chrX	98106200	98110200	1.609395799
chrX	98309400	98313400	1.70820286
chrX	98615800	98619800	1.57198049
chrX	99018200	99022200	1.936035157
chrX	99607200	99611200	1.920521784
chrX	101200700	101204700	1.808919417
chrX	102702100	102706100	1.692743849
chrX	103661700	103665700	1.739419185
chrX	104468300	104472300	1.715290469
chrX	104784200	104788200	1.585551192
chrX	105231000	105235000	1.5938993
chrX	105896000	105900000	1.668597771
chrX	106415900	106419900	1.568519325
chrX	106533600	106537600	3.497070825
chrX	106806000	106810000	1.57717368
chrX	107284300	107288300	1.593064934
chrX	107601200	107605200	1.480860078
chrX	107723100	107727100	15.10110583
chrX	107905400	107909400	1.525671192
chrX	108254400	108258400	1.530301223
chrX	108441700	108445700	1.598722225
chrX	108525700	108529700	1.433099222
chrX	108831900	108835900	1.604133262
chrX	109248300	109252300	1.49102065
chrX	109480700	109484700	1.573180647
chrX	109637800	109641800	1.602576325

chrX	109884400	109888400	1.469304094
chrX	110239500	110243500	1.548416471
chrX	110497400	110501400	1.441508612
chrX	110775100	110779100	1.549149238
chrX	111112200	111116200	1.47544847
chrX	111374900	111378900	1.975746163
chrX	111454800	111458800	1.773498159
chrX	111557800	111561800	1.66333327
chrX	112023300	112027300	1.576927774
chrX	112662100	112666100	1.554552439
chrX	113145500	113149500	1.542082925
chrX	113507000	113511000	1.556020904
chrX	113645300	113649300	4.084616901
chrX	113736600	113740600	1.604510435
chrX	113871500	113875500	1.699459615
chrX	114115300	114119300	1.581167005
chrX	114382500	114386500	1.638956358
chrX	114493300	114497300	1.452441898
chrX	114591300	114595300	1.516114961
chrX	114838500	114842500	1.498507787
chrX	115068900	115072900	1.376669391
chrX	115201300	115205300	1.40806454
chrX	115539200	115543200	1.476422205
chrX	116086900	116090900	1.578095772
chrX	116466300	116470300	1.478303841
chrX	116690800	116694800	1.598507757
chrX	116854200	116858200	1.623702758
chrX	117015100	117019100	1.587884525
chrX	117174900	117178900	1.526829868
chrX	117305600	117309600	2.344771408
chrX	117406100	117410100	1.441967152
chrX	117526300	117530300	1.613884349
chrX	117724100	117728100	1.53459861
chrX	117950600	117954600	1.881319115
chrX	118017500	118021500	13.33846761
chrX	118182200	118186200	1.58693848
chrX	118348000	118352000	1.497154372
chrX	118430900	118434900	1.456175739
chrX	118590900	118594900	1.487996785
chrX	118846300	118850300	1.561575326
chrX	119047900	119051900	1.603241612
chrX	119147100	119151100	2.707555785
chrX	119285800	119289800	1.569443865
chrX	119545400	119549400	1.525977783
chrX	119808000	119812000	1.620187525
chrX	119968800	119972800	1.64199539
chrX	120332900	120336900	1.59431504
chrX	120640500	120644500	1.881319115
chrX	120723600	120727600	1.756897593
chrX	120791400	120795400	2.226183116
chrX	120949900	120953900	1.485970314

chrX	121139300	121143300	1.509762988
chrX	121283900	121287900	1.635099266
chrX	121477800	121481800	1.496697189
chrX	121654100	121658100	1.623790802
chrX	121875900	121879900	1.448662455
chrX	122019100	122023100	4.745606237
chrX	122126100	122130100	1.57447687
chrX	122356500	122360500	1.534981335
chrX	122568200	122572200	1.930375265
chrX	122685100	122689100	1.471130697
chrX	122770800	122774800	1.569633086
chrX	122896500	122900500	1.49434397
chrX	123065100	123069100	1.650638273
chrX	123222300	123226300	1.380413133
chrX	123302900	123306900	13.33846761
chrX	123408700	123412700	13.33846761
chrX	123562200	123566200	1.326747563
chrX	123686300	123690300	1.526093553
chrX	123763300	123767300	4.525276459
chrX	123844500	123848500	2.542308451
chrX	123982800	123986800	1.363847341
chrX	124160600	124164600	1.512572749
chrX	125941100	125945100	2.762638229
chrX	125994300	125998300	15.10110583
chrX	126160600	126164600	1.404803609
chrX	126378400	126382400	1.41737267
chrX	126498600	126502600	1.86437067
chrX	126623100	126627100	1.607677731
chrX	126784300	126788300	2.119275276
chrX	126915700	126919700	1.566040592
chrX	127356200	127360200	1.547866282
chrX	127874300	127878300	1.580530923
chrX	128154900	128158900	1.475334408
chrX	128271300	128275300	2.178089837
chrX	128367900	128371900	1.783394769
chrX	128498200	128502200	1.432119643
chrX	128677500	128681500	1.493208397
chrX	129152000	129156000	1.512146382
chrX	129539600	129543600	1.81162296
chrX	129608100	129612100	1.716071781
chrX	129767700	129771700	1.637268532
chrX	129956500	129960500	1.843548295
chrX	130069800	130073800	1.597300259
chrX	130216700	130220700	1.539486432
chrX	130665400	130669400	1.52824568
chrX	131128900	131132900	1.688802645
chrX	131355700	131359700	1.584130111
chrX	131534100	131538100	1.488749353
chrX	131869400	131873400	1.535795577
chrX	132192700	132196700	1.569237275
chrX	132297300	132301300	1.539159929

chrX	132412900	132416900	1.569268342
chrX	132548600	132552600	1.536455113
chrX	132778000	132782000	1.600714276
chrX	133036800	133040800	1.523518619
chrX	134122600	134126600	1.678376057
chrX	135237500	135241500	1.581138275
chrX	135339200	135343200	2.175092153
chrX	135492900	135496900	1.440659557
chrX	135939900	135943900	1.692867879
chrX	136892500	136896500	1.58912119
chrX	137487800	137491800	1.431584189
chrX	137574700	137578700	2.493346278
chrX	137650300	137654300	1.586441667
chrX	138146600	138150600	1.54298613
chrX	138706800	138710800	1.555770625
chrX	138835500	138839500	1.580869416
chrX	139010700	139014700	1.612139462
chrX	139401100	139405100	1.644310057
chrX	139943900	139947900	1.692443311
chrX	140486100	140490100	1.808316956
chrX	140864500	140868500	1.758992022
chrX	141172600	141176600	2.084700449
chrX	141322400	141326400	1.576247113
chrX	141504300	141508300	1.634549763
chrX	141615400	141619400	1.684690149
chrX	141727600	141731600	1.532340405
chrX	141945700	141949700	1.504460573
chrX	142149400	142153400	1.450092637
chrX	142311700	142315700	1.651466241
chrX	142702400	142706400	1.716649724
chrX	143184700	143188700	1.551212156
chrX	143498900	143502900	1.084305288
chrX	143686200	143690200	1.606772061
chrX	143982400	143986400	1.511087551
chrX	144267300	144271300	1.704515433
chrX	144536200	144540200	1.513149008
chrX	145190200	145194200	1.522337044
chrX	145686300	145690300	1.818367749
chrX	145935200	145939200	1.530102677
chrX	146273200	146277200	1.545884317
chrX	146448100	146452100	13.33846761
chrX	146625000	146629000	1.562261263
chrX	146847200	146851200	1.515830894
chrX	146948000	146952000	1.615793484
chrX	147007500	147011500	5.406595573
chrX	147070000	147074000	1.58977163
chrX	147214800	147218800	1.517904586
chrX	147356200	147360200	1.587546076
chrX	147496500	147500500	1.586340677
chrX	147707700	147711700	1.567536767
chrX	147986400	147990400	1.269034256

chrX	148174500	148178500	4.525276459
chrX	148528700	148532700	15.10110583
chrX	148616200	148620200	1.514102817
chrX	148860700	148864700	1.709140877
chrX	148949100	148953100	13.33846761
chrX	149006000	149010000	1.332189512
chrX	149389100	149393100	5.847255131
chrX	149640400	149644400	1.483304031
chrX	149707000	149711000	1.363136117
chrX	149803000	149807000	1.440659557
chrX	149913400	149917400	1.469006079
chrX	150017700	150021700	1.234595736
chrX	150511600	150515600	1.570512982
chrX	151099700	151103700	1.785203398
chrX	151846600	151850600	1.678013882
chrX	152460100	152464100	1.677055049
chrX	152568100	152572100	1.643305601
chrX	153008100	153012100	1.605798977
chrX	153488400	153492400	1.596594959
chrX	153808900	153812900	1.608891654
chrX	154133700	154137700	1.453405908
chrX	154411000	154415000	1.560090652
chrX	154671000	154675000	1.572199724
chrX	154860900	154864900	1.54157396
chrX	155150500	155154500	1.554789083
chrX	155388800	155392800	1.643520735
chrX	155484300	155488300	1.502434262
chrX	155538100	155542100	13.33846761
chrX	155628500	155632500	1.549258121
chrX	155790700	155794700	1.487465365
chrX	156027200	156031200	1.500502213
chrX	156220200	156224200	1.606240724
chrX	156432200	156436200	1.554367269
chrX	156671500	156675500	1.473574677
chrX	156878900	156882900	1.556576027
chrX	157121400	157125400	1.512347739
chrX	157260300	157264300	2.263224064
chrX	157605200	157609200	1.687589854
chrX	157962000	157966000	1.997964292
chrX	158689600	158693600	1.553032996
chrX	159576000	159580000	1.747942706
chrX	160032800	160036800	1.639213552
chrX	160478600	160482600	1.692776852
chrX	160942000	160946000	1.680313186
chrX	161454300	161458300	1.556210286
chrX	162107000	162111000	1.651700924
chrX	162725800	162729800	1.791344048
chrX	163289700	163293700	1.605339031
chrX	164094600	164098600	1.64732261
chrX	164666100	164670100	1.503204785
chrX	165038600	165042600	1.522443553

chrX	165423300	165427300	1.465499442
chrX	165570400	165574400	1.551750202
chrX	165715800	165719800	1.421783446
chrX	165886500	165890500	1.546020264
chrX	166340700	166344700	1.632516325
chrX	167120700	167124700	1.604735996
chrX	167736500	167740500	1.524123165
chrX	167966900	167970900	1.659654004
chrX	168114500	168118500	1.533361272
chrX	168340100	168344100	1.521175131
chrX	168727800	168731800	1.624421822
chrX	169120300	169124300	1.518666114
chrX	169467000	169471000	1.528791469
chrX	169868200	169872200	1.642251613
chrX	170744300	170748300	1.536329066
chrX	170843600	170847600	1.65201038
chrY	243200	247200	1.109667225
chrY	747400	751400	1.546089566
chrY	920500	924500	1.664900516
chrY	1050500	1054500	1.535937299
chrY	1211900	1215900	1.644502074
chrY	1384800	1388800	1.59388382
chrY	1880100	1884100	1.489410687
chrY	2351100	2355100	1.554779478
chrY	2705100	2709100	15.10110583
chrY	2758100	2762100	13.33846761
chrY	2914200	2918200	1.098265546
chrY	3339900	3343900	2.938902052
chrY	3950600	3954600	1.652699701
chrY	4235700	4239700	1.544857182
chrY	4413500	4417500	1.488315156
chrY	4645300	4649300	1.353099467
chrY	4824500	4828500	1.493487165
chrY	4902900	4906900	16.86374406
chrY	5032200	5036200	1.489287518
chrY	5252000	5256000	1.481461368
chrY	5481600	5485600	1.509258275
chrY	5668000	5672000	1.360691093
chrY	5754900	5758900	1.705055292
chrY	5836900	5840900	1.307667709
chrY	5963000	5967000	1.242247401
chrY	6261300	6265300	1.356395504
chrY	6490200	6494200	1.617841421
chrY	6645900	6649900	1.280419718
chrY	6726600	6730600	1.507878812
chrY	6845800	6849800	1.454905017
chrY	6999700	7003700	1.424742197
chrY	8098400	8102400	1.383182224
chrY	8172000	8176000	1.314173944
chrY	8254100	8258100	1.482627134
chrY	8326300	8330300	4.965936016

chrY	8390000	8394000	1.632947364
chrY	8570100	8574100	1.231407812
chrY	8682700	8686700	15.10110583
chrY	8758500	8762500	1.791693442
chrY	8880000	8884000	1.423330249
chrY	8963700	8967700	2.762638229
chrY	9106700	9110700	1.426586597
chrY	9261100	9265100	2.542308451
chrY	9459800	9463800	1.396392387
chrY	9682800	9686800	1.464777288
chrY	9976900	9980900	1.556991014
chrY	10289000	10293000	1.182139284
chrY	10367000	10371000	1.904511723
chrY	10522200	10526200	1.484963707
chrY	10686500	10690500	1.769759733
chrY	10769300	10773300	5.406595573
chrY	11788300	11792300	16.86374406
chrY	11854900	11858900	2.107298375
chrY	12266100	12270100	2.762638229
chrY	12761200	12765200	1.112167887
chrY	13440500	13444500	1.372516327
chrY	14113400	14117400	1.372491228
chrY	16614000	16618000	1.711064286
chrY	17279700	17283700	2.762638229
chrY	17373700	17377700	2.321978672
chrY	19752900	19756900	13.33846761
chrY	20219900	20223900	1.38190495
chrY	20318200	20322200	1.498136891
chrY	20394800	20398800	1.520779477
chrY	20491300	20495300	18.62638229
chrY	20567500	20571500	13.33846761
chrY	20662000	20666000	1.840007281
chrY	20777300	20781300	4.525276459
chrY	20845500	20849500	1.22645005
chrY	20963900	20967900	1.348855483
chrY	21313100	21317100	5.406595573
chrY	21764100	21768100	5.847255131
chrY	21884100	21888100	2.542308451
chrY	22091000	22095000	1.080049267
chrY	22417900	22421900	5.406595573
chrY	22519500	22523500	2.028205634
chrY	22707800	22711800	1.110164889
chrY	22883400	22887400	1.085714328
chrY	23403900	23407900	15.10110583
chrY	23505500	23509500	15.10110583
chrY	23775700	23779700	15.10110583
chrY	24472300	24476300	4.084616901
chrY	25233500	25237500	4.525276459
chrY	28039900	28043900	3.643957344
chrY	28451900	28455900	2.762638229
chrY	28611100	28615100	1.11807146

chrY	28698700	28702700	2.762638229
chrY	28906600	28910600	1.355063816
chrY	29095700	29099700	1.345615339
chrY	29189000	29193000	1.321873068
chrY	29440100	29444100	20.38902052
chrY	29507500	29511500	13.33846761
chrY	29771700	29775700	4.084616901
chrY	33166100	33170100	4.084616901
chrY	33781900	33785900	4.525276459
chrY	33983300	33987300	15.10110583
chrY	34032700	34036700	4.084616901
chrY	34170500	34174500	4.084616901
chrY	34578100	34582100	3.203297787
chrY	35100300	35104300	13.33846761
chrY	35179200	35183200	1.151423554
chrY	35377700	35381700	2.028205634
chrY	35476500	35480500	13.33846761
chrY	35540100	35544100	1.660989336
chrY	35602300	35606300	2.321978672
chrY	35928700	35932700	1.15276198
chrY	36211900	36215900	13.33846761
chrY	36291500	36295500	13.33846761
chrY	36482700	36486700	13.33846761
chrY	37444500	37448500	1.174744307
chrY	37603100	37607100	13.33846761
chrY	38051500	38055500	18.62638229
chrY	38127500	38131500	2.542308451
chrY	38190000	38194000	1.673949911
chrY	38262900	38266900	13.33846761
chrY	38362300	38366300	2.542308451
chrY	38422500	38426500	1.133493925
chrY	38526700	38530700	2.762638229
chrY	38580900	38584900	13.33846761
chrY	38682100	38686100	2.175092153
chrY	38740700	38744700	15.10110583
chrY	38878300	38882300	13.33846761
chrY	38995700	38999700	1.307580371
chrY	39117600	39121600	1.217908572
chrY	39177700	39181700	13.33846761
chrY	39256200	39260200	1.340805667
chrY	39882300	39886300	16.86374406
chrY	39998500	40002500	1.341052967
chrY	40099100	40103100	15.10110583
chrY	40198700	40202700	4.084616901
chrY	40380200	40384200	1.169643585
chrY	40614700	40618700	15.10110583
chrY	40685300	40689300	13.33846761
chrY	40768200	40772200	1.137011795
chrY	40830900	40834900	2.762638229
chrY	41006700	41010700	16.86374406
chrY	41051500	41055500	3.203297787

chrY	41144000	41148000	1.730235838
chrY	41249100	41253100	1.665885553
chrY	41332900	41336900	4.084616901
chrY	41520100	41524100	1.259127753
chrY	41702300	41706300	1.468549403
chrY	41761800	41765800	2.370940845
chrY	41813200	41817200	1.595276946
chrY	41946900	41950900	2.028205634
chrY	42001100	42005100	15.10110583
chrY	42051800	42055800	1.494775643
chrY	42156800	42160800	1.248009399
chrY	42367400	42371400	1.392761779
chrY	42497500	42501500	1.21261395
chrY	42556100	42560100	4.525276459
chrY	43040400	43044400	4.23150342
chrY	43166300	43170300	13.33846761
chrY	43230200	43234200	1.35803589
chrY	43340800	43344800	1.38190495
chrY	43537100	43541100	1.204797392
chrY	43645300	43649300	1.290006717
chrY	43749600	43753600	1.309752325
chrY	43857200	43861200	1.335390885
chrY	43937200	43941200	1.341155786
chrY	44053500	44057500	18.62638229
chrY	44144300	44148300	1.426444733
chrY	44296500	44300500	2.982968008
chrY	44375500	44379500	4.525276459
chrY	44454700	44458700	2.542308451
chrY	44542900	44546900	25.67693521
chrY	44660700	44664700	1.545849258
chrY	44774300	44778300	1.847422226
chrY	46731900	46735900	2.542308451
chrY	47268700	47272700	4.525276459
chrY	47328500	47332500	22.15165875
chrY	53899400	53903400	1.124069196
chrY	54577900	54581900	4.084616901
chrY	54938500	54942500	1.369936419
chrY	55134700	55138700	2.762638229
chrY	55780500	55784500	15.10110583
chrY	55871900	55875900	4.084616901
chrY	55919900	55923900	16.86374406
chrY	56058500	56062500	16.86374406
chrY	56286900	56290900	15.10110583
chrY	56404900	56408900	16.86374406
chrY	56481900	56485900	1.268067897
chrY	56734900	56738900	4.084616901
chrY	57127200	57131200	5.406595573
chrY	57356900	57360900	13.33846761
chrY	57601900	57605900	15.10110583
chrY	57730600	57734600	1.841259155
chrY	57811600	57815600	1.276777904

chrY	58320900	58324900	1.705055292
chrY	58429800	58433800	6.067584909
chrY	58953900	58957900	1.139542193
chrY	59488300	59492300	2.542308451
chrY	59665700	59669700	4.084616901
chrY	59913500	59917500	13.33846761
chrY	60168500	60172500	1.194710037
chrY	60241500	60245500	1.881319115
chrY	60287100	60291100	16.86374406
chrY	60378300	60382300	3.864287123
chrY	67772900	67776900	2.762638229
chrY	68093500	68097500	2.468865191
chrY	69223500	69227500	1.322433822
chrY	69809700	69813700	13.33846761
chrY	71064900	71068900	4.084616901
chrY	71120900	71124900	2.762638229
chrY	71343500	71347500	18.62638229
chrY	71710300	71714300	13.33846761
chrY	71869700	71873700	4.084616901
chrY	72469100	72473100	15.10110583
chrY	72972300	72976300	13.33846761
chrY	73404900	73408900	4.525276459
chrY	73459700	73463700	16.86374406
chrY	74315500	74319500	4.525276459
chrY	74845000	74849000	1.214775246
chrY	75141300	75145300	15.10110583
chrY	75249500	75253500	4.084616901
chrY	75414700	75418700	2.762638229
chrY	75496900	75500900	4.084616901
chrY	75605700	75609700	13.33846761
chrY	75703500	75707500	15.10110583
chrY	75849100	75853100	4.525276459
chrY	75905700	75909700	15.10110583
chrY	76132100	76136100	15.10110583
chrY	78062700	78066700	15.10110583
chrY	78310100	78314100	13.33846761
chrY	78421500	78425500	4.965936016
chrY	78630300	78634300	3.643957344
chrY	78854300	78858300	2.542308451
chrY	78949500	78953500	4.084616901
chrY	79026500	79030500	4.525276459
chrY	79077200	79081200	1.542350224
chrY	79275700	79279700	1.306788299
chrY	79560100	79564100	23.91429698
chrY	80092700	80096700	13.33846761
chrY	80505100	80509100	4.525276459
chrY	80800900	80804900	2.762638229
chrY	81003100	81007100	16.86374406
chrY	81048100	81052100	2.175092153
chrY	81102100	81106100	4.084616901
chrY	81258000	81262000	1.836123263

chrY	81575300	81579300	1.179527968
chrY	81722500	81726500	4.525276459
chrY	81959500	81963500	1.723940701
chrY	82057900	82061900	15.10110583
chrY	82109700	82113700	2.762638229
chrY	82183100	82187100	15.10110583
chrY	82647900	82651900	4.525276459
chrY	82758500	82762500	4.525276459
chrY	82979800	82983800	1.250886463
chrY	83062900	83066900	15.10110583
chrY	83140400	83144400	1.238690594
chrY	83199900	83203900	13.33846761
chrY	83350500	83354500	4.084616901
chrY	83441900	83445900	15.10110583
chrY	83859100	83863100	15.10110583
chrY	84027700	84031700	1.440659557
chrY	84208700	84212700	1.186839652
chrY	84362000	84366000	2.321978672
chrY	84463300	84467300	4.084616901
chrY	84577700	84581700	4.084616901
chrY	84827300	84831300	15.10110583
chrY	85204700	85208700	2.028205634
chrY	85545700	85549700	2.542308451
chrY	85980800	85984800	1.38790454
chrY	86092700	86096700	4.084616901
chrY	86257600	86261600	1.273512829
chrY	86407100	86411100	1.313196049
chrY	86571400	86575400	1.881319115
chrY	86629300	86633300	1.357086193
chrY	86761700	86765700	1.400031371
chrY	86903100	86907100	1.275412223
chrY	86968700	86972700	2.762638229
chrY	87043400	87047400	1.330494668
chrY	87113900	87117900	16.86374406
chrY	87229700	87233700	1.356872177
chrY	87307500	87311500	18.62638229
chrY	87412400	87416400	1.289056499
chrY	87500300	87504300	1.48962173
chrY	87672200	87676200	1.27795449
chrY	87818700	87822700	6.728574245
chrY	87986500	87990500	22.15165875
chrY	88170700	88174700	4.084616901
chrY	88274700	88278700	2.542308451
chrY	88316100	88320100	15.10110583
chrY	88372100	88376100	4.525276459
chrY	88487400	88491400	1.356052922
chrY	88571900	88575900	16.86374406
chrY	88649000	88653000	1.383977208
chrY	88811000	88815000	1.414429822
chrY	88991400	88995400	1.397261268
chrY	89108900	89112900	4.084616901

chrY	89277300	89281300	1.23410039
chrY	89389500	89393500	15.10110583
chrY	89553900	89557900	4.525276459
chrY	89616100	89620100	2.982968008
chrY	89772100	89776100	20.38902052
chrY	89907000	89911000	1.268159375
chrY	90171700	90175700	2.321978672
chrY	90543900	90547900	4.084616901
chrY	90749200	90753200	1.582919729

Annexure 3

Primer Label	Sequence 5'-3'
chrX1 FP	AAAGAAGAGCTTCCAACTGGTTTAAGT
chr X1 RP	CTACAAATTATTTTGACCCTTACCTCA
chrX2 FP	AACCTACTCCTACTTTCATGGGTTTTT
chrX2 RP	GTAATTAAGCAGTAAGCGACATCGAAT
chrY FP	AAAATTTTGAGGGTTTTATGGCTCTTTTAG
chrY RP	CCCTAAAACATTAAAGCAAAAACTAATACC
Auto1 FP	TCCACCTTGAGTTGTGAGGC
Auto1 RP	GGATTTGGGGCCAGGTACTC
Auto2 FP	AACCCTAAATCCTTCCCATCACAA
Auto2 RP	TCTTCACTTTTGCTCGAAAGACAC
Neg Ctrl1 FP	ACTTATCGCCTTTCCTGTAGGG
Neg Ctrl1 RP	TTCTGAGGAATATTGCCTGCCC
Neg Ctrl2 FP	ACGCTGGGGTGTACAAATCT
Neg Ctrl2 RP	TATGCCTTTGAGACGCTCCC
H1t clone FP (HindIII)	ATAGAAGCTTGCAGCTTCAGGCAACGAC
H1t clone RP (NotI)	ATATGCGGCCGCCTTTCTTCCTGCTGCCTTCC

Annexure 4

Gene Symbol	Unique peptides	Total peptides	Sum Intensity	Function
XY body & Meiotic Recombination				
Smarca5	12	21	7.40E+06	Regulator of γH2AX phosphorylation; Gene Expression
Scml2	11	17	3.90E+06	Critical regulator of PCH formation; shown to interact with γH2AX by IP assays
Hp1bp3	10	19	2.10E+07	Identified as interacting protein partner with γH2AX
Parp1	4	7	4.30E+06	Regulator of genome stability
Mre11a	4	4	4.50E+05	Part of MRN complex involved in DNA repair and recombination
Top2a	4	4	4.50E+05	Topoisomerase protein, involved in centromeric heterochromatin formation
H2afx	3	20	2.30E+07	H2A variant; involved in DSB repair and recombination
Baz1a	3	8	9.90E+05	DSB repair and Gene Regulation
Smarca4 (Brg1)	3	3	5.80E+05	Phosphorylation by ATM kinase regulates DSB repair
Hormad1	2	7	5.50E+05	Chromosomal Axes Protein associated with DSB initiation
Baz1b	2	2	8.50E+04	Regulator of γH2AX-Mdc1 signaling
Chd5	2	2	4.00E+05	Chromatin remodeler in the XY body; Associated with PAR region
H2afy2	1	2	1.60E+05	Macro H2A; Involved in sex chromosome inactivation
Heterochromatin Formation in XY body				
Scml2	11	17	3.90E+06	Critical regulator of PCH formation; also associated with sex chromosomes
Hormad1	2	7	5.50E+05	Chromosomal axes Protein involved in silencing of the XY body
Cbx1	2	5	2.40E+05	Heterochromatin protein associated with MSCI
Chd5	2	2	4.00E+05	Involved in sex chromosome inactivation and PCH formation
Transcription				
Smarca5	12	21	7.40E+06	Regulator of γH2AX phosphorylation; Gene Expression
H3f3b	4	10	3.30E+07	H3 variant, Epigenetic regulator of gene expression
Trim28	4	6	5.40E+05	Associated with Brdt to mediate transcrption repression in spermatocytes
Smarcd2	4	6	1.30E+06	Component of SWI/SNF complex
Smarcc1	4	5	7.60E+05	Component of SWI/SNF complex
Smarcb1	3	4	1.00E+06	Component of SWI/SNF complex
Smarca4 (Brg1)	3	3	5.80E+05	Important chromatin remodeling factor in spermatogenesis
Smarcc2	2	7	9.70E+05	Component of SWI/SNF complex
Brd7	2	4	8.70E+04	Transcriptional regulator of DNA damage and repair genes
Smarca2 (Brm)	2	2	1.50E+05	Provides ATPase activity and part of the SWI/SNF complex

H2afz	2	5	8.30E+06	Histone H2AZ
Other Proteins				
Hist1h4b	11	158	3.70E+09	Core histone H4
Sycp3	8	20	1.50E+07	Axial element of the synaptonemal complex
TH2B	6	40	8.20E+07	H2B variant found in spermatocytes and spermatids
Npm1	4	6	2.60E+06	Histone Chaperone
H2afx	3	20	2.30E+07	Core histone H2A
Sycp2	2	4	6.70E+05	Component of the synaptonemal complex
Syce1	2	3	5.10E+05	Component of the synaptonemal complex
Hist3h2ba	1	3	1.30E+06	Core histone H2B

Annexure 5

The H1t ChIP-sequencing peaks are given in the Google link (https://drive.google.com/open?id=1gVjsOOO9tsROol2C6lGGJQCr2ICNqHts)

Annexure 6

Gene Symbol	Unique peptides	Total peptides	Sum Intensity	Functions
Nucleolar Associated Proteins				
Ncl	16	25	1.10E+08	An NPM1 binding protein(ribosome biogenesis); Nucleolar protein; also involved in RNA pol II mediated transcription
Numa1	9	10	1.40E+06	Nucleolar protein
Npm1	3	4	2.10E+06	Histone chaperone & Nucleolar protein; Maintainence of genome stability
Rps9	3	3	1.30E+06	NPM1 binding proteins involved in ribosome biogenesis
Rpl23a	3	5	8.80E+06	NPM1 binding proteins involved in ribosome biogenesis
Rpl5	1	1	5.90E+05	NPM1 binding proteins involved in ribosome biogenesis
H2afy2	1	2	1.60E+05	Macro H2A; is involved in repression of rDNA elements and XY body
Heterochromatin and Repeat-associated Proteins				
Top2a	18	25	1.20E+07	Topoisomerase protein; condensation of centromeric heterochromatin
Scml2	9	20	5.10E+06	Polycomb Protein; associated with γH2AX in the xy body, modulates epigenetic state in XY, Pericentric Heterochromatin
Tdrkh	9	18	6.40E+06	Tdrkh is essential for spermatogenesis and participates in primary piRNA biogenesis in the germline
Fyttd1	7	15	2.10E+07	UAP56 interacting factor; UAP56 couples piRNA biogenesis to retrotransposable elements; DEAD BOX HELICASE
H2afx	6	19	3.80E+07	H2AX protein; Involved in meiotic sex chromosome inactivation (MSCI) of the XY body
H3f3b	5	15	5.80E+07	H3.3 protein; Involved in meiotic sex chromosome inactivation of the XY body
Hormad1	4	6	2.40E+06	Associated with unsynapsed chromosomal axes, regulation of homolog interaction during DSB repair
Chd4	3	4	7.20E+05	Chromatin remodeler in the XY body; also an Interaction protein partner of H3.3
Cenpv	3	4	3.10E+07	Associated with Scml2 for heterochromatin formation during spermiogenesis; Imp for PCH formation
Cbx1	3	3	2.50E+06	HP1β, Heterochromatin protein involved in XY body silencing (Meiotic silencing of sex chromosomes)
Cbx5	2	4	1.70E+06	HP1 Alpha- HP1alpha and beta are involved in heterochromatin formation and XY body
Sin3a	2	2	6.90E+04	Part of corepressor complex, along with HDAC; IMP for transcriptional repression
Piwil1	2	2	3.00E+05	LTR associated MIWI protein; is a small RNA-guided RNase (slicer); is expressed in specific postnatal germ cells
Hspa2	2	2	4.70E+04	Associated with retrotransposon silencing; Interaction protein partner of Mov10L and interacts with MIWI also
Trim28	1	1	6.50E+04	Associated with Brdt and HDAC1, also interacts with SETBP1 to regulate DDR and asynapsis pathways
Hdac1	1	1	2.50E+06	Association with Trim28 and Brdt to regulate gene expression; Repeat associated repression mechanism
Mael	1	1	6.30E+04	RNA binding protein; involved in LINE element repression; mutants have high DNA damage due to LINE activation
Baz2a	1	1	5.90E+04	Involved in silencing and constitutive heterochromatin formation at rDNA, centromeres and telomeres

H2afy2	**1**	**2**	**1.60E +05**	**Macro H2A; is involved in repression of rDNA elements and XY body**
Mre11a	**1**	**1**	**1.20E +05**	**Part of MRN complex**
MIWI Associated proteins				
Myh9	**7**	**9**	**1.40E +06**	
Myh11	**2**	**2**	**1.00E +06**	
Myh10	**2**	**2**	**3.60E +05**	
Other Important Proteins				
Sycp3				
Sycp2	**7**	**17**	**5.30E +06**	**Axial component of synaptonemal complex**
Hist1h1t	**6**	**25**	**1.40E +08**	**H1t histone**
Parp1	**6**	**9**	**6.40E +06**	**Genome Stability**
Syce1	**4**	**7**	**1.90E +06**	**Central Element of the synaptonemal complex**
Smarcc1	**4**	**5**	**1.20E +06**	**Component of SWI SNF complex**
Smarcd2	**4**	**5**	**2.90E +05**	**Component of SWI SNF complex**
Baz1b	**3**	**4**	**2.20E +06**	**Dispensable for H2AX phosphorylation**
Rad50	**3**	**3**	**9.70E +05**	**Part of MRN complex**
Smarca4	**1**	**1**	**1.90E +05**	**Brg1, Necessary for spermatogenesis, involved in pATM regulation of yH2AX formation**

References

Abbott, D.W., Laszczak, M., Lewis, J.D., Su, H., Moore, S.C., Hills, M., Dimitrov, S., and Ausio, J. (2004). Structural characterization of macroH2A containing chromatin. Biochemistry *43*, 1352-1359.

Ahmad, K., and Henikoff, S. (2002). The histone variant H3.3 marks active chromatin by replication-independent nucleosome assembly. Mol Cell *9*, 1191-1200.

Alavattam, K.G., Maezawa, S., Sakashita, A., Khoury, H., Barski, A., Kaplan, N., and Namekawa, S.H. (2019). Attenuated chromatin compartmentalization in meiosis and its maturation in sperm development. Nat Struct Mol Biol *26*, 175-184.

Albig, W., Ebentheuer, J., Klobeck, G., Kunz, J., and Doenecke, D. (1996). A solitary human H3 histone gene on chromosome 1. Hum Genet *97*, 486-491.

Allfrey, V.G., Faulkner, R., and Mirsky, A.E. (1964). Acetylation and Methylation of Histones and Their Possible Role in the Regulation of Rna Synthesis. Proc Natl Acad Sci U S A *51*, 786-794.

Allis, C.D., and Jenuwein, T. (2016). The molecular hallmarks of epigenetic control. Nat Rev Genet *17*, 487-500.

Andersen, J.S., Lam, Y.W., Leung, A.K., Ong, S.E., Lyon, C.E., Lamond, A.I., and Mann, M. (2005). Nucleolar proteome dynamics. Nature *433*, 77-83.

Angelov, D., Molla, A., Perche, P.Y., Hans, F., Cote, J., Khochbin, S., Bouvet, P., and Dimitrov, S. (2003). The histone variant macroH2A interferes with transcription factor binding and SWI/SNF nucleosome remodeling. Mol Cell *11*, 1033-1041.

Aravin, A.A., Sachidanandam, R., Bourc'his, D., Schaefer, C., Pezic, D., Toth, K.F., Bestor, T., and Hannon, G.J. (2008). A piRNA pathway primed by individual transposons is linked to de novo DNA methylation in mice. Mol Cell *31*, 785-799.

Aviles, F.J., Danby, S.E., Chapman, G.E., Crane-Robinson, C., and Bradbury, E.M. (1979). The conformation of histone H5 bound to DNA. Maintenance of the globular structure after binding. Biochim Biophys Acta *578*, 290-296.

Bailey, T.L., Williams, N., Misleh, C., and Li, W.W. (2006). MEME: discovering and analyzing DNA and protein sequence motifs. Nucleic Acids Res *34*, W369-373.

Bannister, A.J., and Kouzarides, T. (2011). Regulation of chromatin by histone modifications. Cell Res *21*, 381-395.

Bao, J., and Bedford, M.T. (2016). Epigenetic regulation of the histone-to-protamine transition during spermiogenesis. Reproduction *151*, R55-70.

Barral, S., Morozumi, Y., Tanaka, H., Montellier, E., Govin, J., de Dieuleveult, M., Charbonnier, G., Coute, Y., Puthier, D., Buchou, T.*, et al.* (2017). Histone Variant H2A.L.2 Guides Transition Protein-Dependent Protamine Assembly in Male Germ Cells. Mol Cell *66*, 89-101 e108.

Barski, A., Cuddapah, S., Cui, K., Roh, T.Y., Schones, D.E., Wang, Z., Wei, G., Chepelev, I., and Zhao, K. (2007). High-resolution profiling of histone methylations in the human genome. Cell *129*, 823-837.

Bastos, H., Lassalle, B., Chicheportiche, A., Riou, L., Testart, J., Allemand, I., and Fouchet, P. (2005). Flow cytometric characterization of viable meiotic and postmeiotic cells by Hoechst 33342 in mouse spermatogenesis. Cytometry A *65*, 40-49.

Baudat, F., Imai, Y., and de Massy, B. (2013). Meiotic recombination in mammals: localization and regulation. Nat Rev Genet *14*, 794-806.

Bednar, J., Garcia-Saez, I., Boopathi, R., Cutter, A.R., Papai, G., Reymer, A., Syed, S.H., Lone, I.N., Tonchev, O., Crucifix, C.*, et al.* (2017). Structure and Dynamics of a 197 bp Nucleosome in Complex with Linker Histone H1. Mol Cell *66*, 384-397 e388.

Beedle, M.T., Topping, T., Hogarth, C., and Griswold, M. (2019). Differential localization of histone variant TH2B during the first round compared with subsequent rounds of spermatogenesis. Dev Dyn *248*, 488-500.

Bell, O., Tiwari, V.K., Thoma, N.H., and Schubeler, D. (2011). Determinants and dynamics of genome accessibility. Nat Rev Genet *12*, 554-564.

Belmont, A.S. (2014). Large-scale chromatin organization: the good, the surprising, and the still perplexing. Curr Opin Cell Biol *26*, 69-78.

Belmont, A.S., Sedat, J.W., and Agard, D.A. (1987). A three-dimensional approach to mitotic chromosome structure: evidence for a complex hierarchical organization. J Cell Biol *105*, 77-92.

Bernstein, E., Muratore-Schroeder, T.L., Diaz, R.L., Chow, J.C., Changolkar, L.N., Shabanowitz, J., Heard, E., Pehrson, J.R., Hunt, D.F., and Allis, C.D. (2008). A phosphorylated subpopulation of the histone variant macroH2A1 is excluded from the inactive X chromosome and enriched during mitosis. Proc Natl Acad Sci U S A *105*, 1533-1538.

Bettegowda, A., and Wilkinson, M.F. (2010). Transcription and post-transcriptional regulation of spermatogenesis. Philosophical Transactions of the Royal Society B-Biological Sciences *365*, 1637-1651.

Bharath, M.M., Chandra, N.R., and Rao, M.R. (2002). Prediction of an HMG-box fold in the C-terminal domain of histone H1: insights into its role in DNA condensation. Proteins *49*, 71-81.

Bharath, M.M., Chandra, N.R., and Rao, M.R. (2003). Molecular modeling of the chromatosome particle. Nucleic Acids Res *31*, 4264-4274.

Bian, Q., and Belmont, A.S. (2012). Revisiting higher-order and large-scale chromatin organization. Curr Opin Cell Biol *24*, 359-366.

Bickmore, W.A. (2013). The spatial organization of the human genome. Annu Rev Genomics Hum Genet *14*, 67-84.

Bickmore, W.A., and van Steensel, B. (2013). Genome architecture: domain organization of interphase chromosomes. Cell *152*, 1270-1284.

Boateng, K.A., Bellani, M.A., Gregoretti, I.V., Pratto, F., and Camerini-Otero, R.D. (2013). Homologous pairing preceding SPO11-mediated double-strand breaks in mice. Dev Cell *24*, 196-205.

Bonev, B., Mendelson Cohen, N., Szabo, Q., Fritsch, L., Papadopoulos, G.L., Lubling, Y., Xu, X., Lv, X., Hugnot, J.P., Tanay, A.*, et al.* (2017). Multiscale 3D Genome Rewiring during Mouse Neural Development. Cell *171*, 557-572 e524.

Boskovic, A., and Torres-Padilla, M.E. (2013). How mammals pack their sperm: a variant matter. Genes & Development *27*, 1635-1639.

Bourc'his, D., and Bestor, T.H. (2004). Meiotic catastrophe and retrotransposon reactivation in male germ cells lacking Dnmt3L. Nature *431*, 96-99.

Bradbury, E.M., Chapman, G.E., Danby, S.E., Hartman, P.G., and Riches, P.L. (1975). Studies on the role and mode of operation of the very-lysine-rich histone H1 (F1) in eukaryote chromatin. The properties of the N-terminal and C-terminal halves of histone H1. Eur J Biochem *57*, 521-528.

Braunschweig, U., Hogan, G.J., Pagie, L., and van Steensel, B. (2009). Histone H1 binding is inhibited by histone variant H3.3. EMBO J *28*, 3635-3645.

Brick, K., Smagulova, F., Khil, P., Camerini-Otero, R.D., and Petukhova, G.V. (2012). Genetic recombination is directed away from functional genomic elements in mice. Nature *485*, 642-645.

Broering, T.J., Alavattam, K.G., Sadreyev, R.I., Ichijima, Y., Kato, Y., Hasegawa, K., Camerini-Otero, R.D., Lee, J.T., Andreassen, P.R., and Namekawa, S.H. (2014). BRCA1

establishes DNA damage signaling and pericentric heterochromatin of the X chromosome in male meiosis. J Cell Biol *205*, 663-675.

Broering, T.J., Wang, Y.L., Pandey, R.N., Hegde, R.S., Wang, S.C., and Namekawa, S.H. (2015). BAZ1B is dispensable for H2AX phosphorylation on Tyrosine 142 during spermatogenesis. Biol Open *4*, 873-884.

Brykczynska, U., Hisano, M., Erkek, S., Ramos, L., Oakeley, E.J., Roloff, T.C., Beisel, C., Schubeler, D., Stadler, M.B., and Peters, A.H. (2010). Repressive and active histone methylation mark distinct promoters in human and mouse spermatozoa. Nat Struct Mol Biol *17*, 679-687.

Bucci, L.R., Brock, W.A., and Meistrich, M.L. (1982). Distribution and synthesis of histone 1 subfractions during spermatogenesis in the rat. Exp Cell Res *140*, 111-118.

Burston, D., Tombs, M.P., Apsey, M.E., and Maclagan, N.F. (1963). The perchloric acid soluble basic and acidic proteins of the cytoplasm: variation in cancer. Br J Cancer *17*, 162-178.

Bustin, M., Catez, F., and Lim, J.H. (2005). The dynamics of histone H1 function in chromatin. Mol Cell *17*, 617-620.

Cao, K., Lailler, N., Zhang, Y., Kumar, A., Uppal, K., Liu, Z., Lee, E.K., Wu, H., Medrzycki, M., Pan, C.*, et al.* (2013). High-resolution mapping of h1 linker histone variants in embryonic stem cells. PLoS Genet *9*, e1003417.

Carmell, M.A., Girard, A., van de Kant, H.J., Bourc'his, D., Bestor, T.H., de Rooij, D.G., and Hannon, G.J. (2007). MIWI2 is essential for spermatogenesis and repression of transposons in the mouse male germline. Dev Cell *12*, 503-514.

Carone, B.R., Hung, J.H., Hainer, S.J., Chou, M.T., Carone, D.M., Weng, Z., Fazzio, T.G., and Rando, O.J. (2014). High-resolution mapping of chromatin packaging in mouse embryonic stem cells and sperm. Dev Cell *30*, 11-22.

Catena, R., Ronfani, L., Sassone-Corsi, P., and Davidson, I. (2006). Changes in intranuclear chromatin architecture induce bipolar nuclear localization of histone variant H1T2 in male haploid spermatids. Dev Biol *296*, 231-238.

Chakravarthy, S., Gundimella, S.K., Caron, C., Perche, P.Y., Pehrson, J.R., Khochbin, S., and Luger, K. (2005). Structural characterization of the histone variant macroH2A. Mol Cell Biol *25*, 7616-7624.

Chakravarthy, S., Patel, A., and Bowman, G.D. (2012). The basic linker of macroH2A stabilizes DNA at the entry/exit site of the nucleosome. Nucleic Acids Res *40*, 8285-8295.

Chen, J., Herlong, F.H., Stroehlein, J.R., and Mishra, L. (2016). Mutations of Chromatin Structure Regulating Genes in Human Malignancies. Curr Protein Pept Sci *17*, 411-437.

Chen, P., Zhao, J., Wang, Y., Wang, M., Long, H., Liang, D., Huang, L., Wen, Z., Li, W., Li, X.*, et al.* (2013). H3.3 actively marks enhancers and primes gene transcription via opening higher-ordered chromatin. Genes Dev *27*, 2109-2124.

Chi, Y.H., Cheng, L.I., Myers, T., Ward, J.M., Williams, E., Su, Q., Faucette, L., Wang, J.Y., and Jeang, K.T. (2009). Requirement for Sun1 in the expression of meiotic reproductive genes and piRNA. Development *136*, 965-973.

Clare, S.E., Fantz, D.A., Kistler, W.S., and Kistler, M.K. (1997a). The testis-specific histone H1t gene is strongly repressed by a G/C-rich region just downstream of the TATA Box. J Biol Chem *272*, 33028-33036.

Clare, S.E., Hatfield, W.R., Fantz, D.A., Kistler, W.S., and Kistler, M.K. (1997b). Characterization of the promoter region of the rat testis-specific histone H1t gene. Biol Reprod *56*, 73-82.

Cloud, V., Chan, Y.L., Grubb, J., Budke, B., and Bishop, D.K. (2012). Rad51 is an accessory factor for Dmc1-mediated joint molecule formation during meiosis. Science *337*, 1222-1225.

Cloutier, J.M., and Turner, J.M. (2010). Meiotic sex chromosome inactivation. Curr Biol *20*, R962-963.

Conerly, M.L., Teves, S.S., Diolaiti, D., Ulrich, M., Eisenman, R.N., and Henikoff, S. (2010). Changes in H2A.Z occupancy and DNA methylation during B-cell lymphomagenesis. Genome Res *20*, 1383-1390.

Cong, R., Das, S., Douet, J., Wong, J., Buschbeck, M., Mongelard, F., and Bouvet, P. (2014). macroH2A1 histone variant represses rDNA transcription. Nucleic Acids Res *42*, 181-192.

Crichton, J.H., Dunican, D.S., Maclennan, M., Meehan, R.R., and Adams, I.R. (2014). Defending the genome from the enemy within: mechanisms of retrotransposon suppression in the mouse germline. Cell Mol Life Sci *71*, 1581-1605.

Cui, B., Liu, Y., and Gorovsky, M.A. (2006). Deposition and function of histone H3 variants in Tetrahymena thermophila. Mol Cell Biol *26*, 7719-7730.

Czornak, K., Chughtai, S., and Chrzanowska, K.H. (2008). Mystery of DNA repair: the role of the MRN complex and ATM kinase in DNA damage repair. J Appl Genet *49*, 383-396.

De Lucia, F., Faraone-Mennella, M.R., D'Erme, M., Quesada, P., Caiafa, P., and Farina, B. (1994). Histone-induced condensation of rat testis chromatin: testis-specific H1t versus somatic H1 variants. Biochem Biophys Res Commun *198*, 32-39.

Dehghani, H., Dellaire, G., and Bazett-Jones, D.P. (2005). Organization of chromatin in the interphase mammalian cell. Micron *36*, 95-108.

Dekker, J. (2008). Mapping in vivo chromatin interactions in yeast suggests an extended chromatin fiber with regional variation in compaction. J Biol Chem *283*, 34532-34540.

Dekker, J., Marti-Renom, M.A., and Mirny, L.A. (2013). Exploring the three-dimensional organization of genomes: interpreting chromatin interaction data. Nat Rev Genet *14*, 390-403.

Delaval, K., Govin, J., Cerqueira, F., Rousseaux, S., Khochbin, S., and Feil, R. (2007). Differential histone modifications mark mouse imprinting control regions during spermatogenesis. EMBO J *26*, 720-729.

Dhar, S., Thota, A., and Rao, M.R. (2012). Insights into role of bromodomain, testis-specific (Brdt) in acetylated histone H4-dependent chromatin remodeling in mammalian spermiogenesis. J Biol Chem *287*, 6387-6405.

Di Giacomo, M., Comazzetto, S., Saini, H., De Fazio, S., Carrieri, C., Morgan, M., Vasiliauskaite, L., Benes, V., Enright, A.J., and O'Carroll, D. (2013). Multiple epigenetic mechanisms and the piRNA pathway enforce LINE1 silencing during adult spermatogenesis. Mol Cell *50*, 601-608.

Dillinger, S., Straub, T., and Nemeth, A. (2017). Nucleolus association of chromosomal domains is largely maintained in cellular senescence despite massive nuclear reorganisation. PLoS One *12*, e0178821.

Dixon, J.R., Jung, I., Selvaraj, S., Shen, Y., Antosiewicz-Bourget, J.E., Lee, A.Y., Ye, Z., Kim, A., Rajagopal, N., Xie, W.*, et al.* (2015). Chromatin architecture reorganization during stem cell differentiation. Nature *518*, 331-336.

Dong, J., Wang, X., Cao, C., Wen, Y., Sakashita, A., Chen, S., Zhang, J., Zhang, Y., Zhou, L., Luo, M.*, et al.* (2019). UHRF1 suppresses retrotransposons and cooperates with PRMT5 and PIWI proteins in male germ cells. Nat Commun *10*, 4705.

Dorigo, B., Schalch, T., Kulangara, A., Duda, S., Schroeder, R.R., and Richmond, T.J. (2004). Nucleosome arrays reveal the two-start organization of the chromatin fiber. Science *306*, 1571-1573.

Drabent, B., Benavente, R., and Hoyer-Fender, S. (2003). Histone H1t is not replaced by H1.1 or H1.2 in pachytene spermatocytes or spermatids of H1t-deficient mice. Cytogenet Genome Res *103*, 307-313.

Drabent, B., Bode, C., Bramlage, B., and Doenecke, D. (1996). Expression of the mouse testicular histone gene H1t during spermatogenesis. Histochem Cell Biol *106*, 247-251.

Drabent, B., Bode, C., Miosge, N., Herken, R., and Doenecke, D. (1998). Expression of the mouse histone gene H1t begins at premeiotic stages of spermatogenesis. Cell Tissue Res *291*, 127-132.

Drabent, B., Kardalinou, E., and Doenecke, D. (1991). Structure and expression of the human gene encoding testicular H1 histone (H1t). Gene *103*, 263-268.

Dunn, K.W., Kamocka, M.M., and McDonald, J.H. (2011). A practical guide to evaluating colocalization in biological microscopy. Am J Physiol Cell Physiol *300*, C723-742.

Eltsov, M., Maclellan, K.M., Maeshima, K., Frangakis, A.S., and Dubochet, J. (2008). Analysis of cryo-electron microscopy images does not support the existence of 30-nm chromatin fibers in mitotic chromosomes in situ. Proc Natl Acad Sci U S A *105*, 19732-19737.

Eng, J.K., McCormack, A.L., and Yates, J.R. (1994). An approach to correlate tandem mass spectral data of peptides with amino acid sequences in a protein database. J Am Soc Mass Spectrom *5*, 976-989.

Erkek, S., Hisano, M., Liang, C.Y., Gill, M., Murr, R., Dieker, J., Schubeler, D., van der Vlag, J., Stadler, M.B., and Peters, A.H. (2013). Molecular determinants of nucleosome retention at CpG-rich sequences in mouse spermatozoa. Nat Struct Mol Biol *20*, 868-875.

Fan, Y., Nikitina, T., Zhao, J., Fleury, T.J., Bhattacharyya, R., Bouhassira, E.E., Stein, A., Woodcock, C.L., and Skoultchi, A.I. (2005). Histone H1 depletion in mammals alters global chromatin structure but causes specific changes in gene regulation. Cell *123*, 1199-1212.

Fantz, D.A., Hatfield, W.R., Horvath, G., Kistler, M.K., and Kistler, W.S. (2001). Mice with a targeted disruption of the H1t gene are fertile and undergo normal changes in structural chromosomal proteins during spermiogenesis. Biol Reprod *64*, 425-431.

Faraone-Mennella, M.R., De Lucia, F., Gentile, N., Quesada, P., and Farina, B. (1999). In vitro poly(ADP-ribosyl)ated histones H1a and H1t modulate rat testis chromatin condensation differently. J Cell Biochem *76*, 20-29.

Feng, J., Liu, T., Qin, B., Zhang, Y., and Liu, X.S. (2012). Identifying ChIP-seq enrichment using MACS. Nat Protoc *7*, 1728-1740.

Fernandez-Capetillo, O., Allis, C.D., and Nussenzweig, A. (2004). Phosphorylation of histone H2B at DNA double-strand breaks. J Exp Med *199*, 1671-1677.

Fernandez-Capetillo, O., Mahadevaiah, S.K., Celeste, A., Romanienko, P.J., Camerini-Otero, R.D., Bonner, W.M., Manova, K., Burgoyne, P., and Nussenzweig, A. (2003). H2AX is required for chromatin remodeling and inactivation of sex chromosomes in male mouse meiosis. Dev Cell *4*, 497-508.

Finch, J.T., and Klug, A. (1976). Solenoidal model for superstructure in chromatin. Proc Natl Acad Sci U S A *73*, 1897-1901.

Franklin, S.G., and Zweidler, A. (1977). Non-allelic variants of histones 2a, 2b and 3 in mammals. Nature *266*, 273-275.

Fussner, E., Ching, R.W., and Bazett-Jones, D.P. (2011). Living without 30 nm chromatin fibers. Trends in Biochemical Sciences *36*, 1-6.

Gaucher, J., Boussouar, F., Montellier, E., Curtet, S., Buchou, T., Bertrand, S., Hery, P., Jounier, S., Depaux, A., Vitte, A.L.*, et al.* (2012). Bromodomain-dependent stage-specific male genome programming by Brdt. EMBO J *31*, 3809-3820.

Getun, I.V., Torres, B., and Bois, P.R. (2011). Flow cytometry purification of mouse meiotic cells. J Vis Exp.

Ghosh, A.K., Hoff, C.M., and Jacob, S.T. (1993). Characterization of the 130-bp repeat enhancer element of the rat ribosomal gene: functional interaction with transcription factor E1BF. Gene *125*, 217-222.

Goudarzi, A., Shiota, H., Rousseaux, S., and Khochbin, S. (2014). Genome-scale acetylation-dependent histone eviction during spermatogenesis. J Mol Biol *426*, 3342-3349.

Goudarzi, A., Zhang, D., Huang, H., Barral, S., Kwon, O.K., Qi, S., Tang, Z., Buchou, T., Vitte, A.L., He, T.*, et al.* (2016). Dynamic Competing Histone H4 K5K8 Acetylation and Butyrylation Are Hallmarks of Highly Active Gene Promoters. Mol Cell *62*, 169-180.

Govin, J., Caron, C., Lestrat, C., Rousseaux, S., and Khochbin, S. (2004). The role of histones in chromatin remodelling during mammalian spermiogenesis. Eur J Biochem *271*, 3459-3469.

Govin, J., Caron, C., Rousseaux, S., and Khochbin, S. (2005). Testis-specific histone H3 expression in somatic cells. Trends Biochem Sci *30*, 357-359.

Govin, J., Escoffier, E., Rousseaux, S., Kuhn, L., Ferro, M., Thevenon, J., Catena, R., Davidson, I., Garin, J., Khochbin, S., *et al.* (2007). Pericentric heterochromatin reprogramming by new histone variants during mouse spermiogenesis. Journal of Cell Biology *176*, 283-294.

Govin, J., Lestrat, C., Caron, C., Pivot-Pajot, C., Rousseaux, S., and Khochbin, S. (2006). Histone acetylation-mediated chromatin compaction during mouse spermatogenesis. Ernst Schering Res Found Workshop, 155-172.

Grewal, S.I., and Jia, S. (2007). Heterochromatin revisited. Nat Rev Genet *8*, 35-46.

Grey, C., Clement, J.A., Buard, J., Leblanc, B., Gut, I., Gut, M., Duret, L., and de Massy, B. (2017). In vivo binding of PRDM9 reveals interactions with noncanonical genomic sites. Genome Res *27*, 580-590.

Grimes, S.R., Prado, S., and Wolfe, S.A. (2005). Transcriptional activation of the testis-specific histone H1t gene by RFX2 may require both proximal promoter X-box elements. J Cell Biochem *94*, 317-326.

Grimes, S.R., Wilkerson, D.C., Noss, K.R., and Wolfe, S.A. (2003). Transcriptional control of the testis-specific histone H1t gene. Gene *304*, 13-21.

Grozdanov, P., Georgiev, O., and Karagyozov, L. (2003). Complete sequence of the 45-kb mouse ribosomal DNA repeat: analysis of the intergenic spacer. Genomics *82*, 637-643.

Guillemette, B., Bataille, A.R., Gevry, N., Adam, M., Blanchette, M., Robert, F., and Gaudreau, L. (2005). Variant histone H2A.Z is globally localized to the promoters of inactive yeast genes and regulates nucleosome positioning. PLoS Biol *3*, e384.

Guillon, H., Baudat, F., Grey, C., Liskay, R.M., and de Massy, B. (2005). Crossover and noncrossover pathways in mouse meiosis. Mol Cell *20*, 563-573.

Guillon, H., and de Massy, B. (2002). An initiation site for meiotic crossing-over and gene conversion in the mouse. Nat Genet *32*, 296-299.

Gupta, N., Madapura, M.P., Bhat, U.A., and Rao, M.R. (2015). Mapping of Post-translational Modifications of Transition Proteins, TP1 and TP2, and Identification of Protein Arginine Methyltransferase 4 and Lysine Methyltransferase 7 as Methyltransferase for TP2. J Biol Chem *290*, 12101-12122.

Gupta, N., Pentakota, S., Mishra, L.N., Jones, R., and Rao, M.R. (2017). Identification of Posttranslational Modifications of Endogenous Chromatin Proteins From Testicular Cells by Mass Spectrometry. Methods Enzymol *586*, 115-142.

Hada, M., Kim, J., Inoue, E., Fukuda, Y., Tanaka, H., Watanabe, Y., and Okada, Y. (2017a). TH2A is phosphorylated at meiotic centromere by Haspin. Chromosoma *126*, 769-780.

Hada, M., Masuda, K., Yamaguchi, K., Shirahige, K., and Okada, Y. (2017b). Identification of a variant-specific phosphorylation of TH2A during spermiogenesis. Sci Rep *7*, 46228.

Hancks, D.C., and Kazazian, H.H., Jr. (2012). Active human retrotransposons: variation and disease. Curr Opin Genet Dev *22*, 191-203.

Handel, M.A. (2004). The XY body: a specialized meiotic chromatin domain. Exp Cell Res *296*, 57-63.

Handel, M.A., and Schimenti, J.C. (2010). Genetics of mammalian meiosis: regulation, dynamics and impact on fertility. Nat Rev Genet *11*, 124-136.

Hartman, P.G., Chapman, G.E., Moss, T., and Bradbury, E.M. (1977). Studies on the role and mode of operation of the very-lysine-rich histone H1 in eukaryote chromatin. The three structural regions of the histone H1 molecule. Eur J Biochem *77*, 45-51.

Hasegawa, K., Sin, H.S., Maezawa, S., Broering, T.J., Kartashov, A.V., Alavattam, K.G., Ichijima, Y., Zhang, F., Bacon, W.C., Greis, K.D., *et al.* (2015). SCML2 establishes the male germline epigenome through regulation of histone H2A ubiquitination. Dev Cell *32*, 574-588.

Hendzel, M.J., Lever, M.A., Crawford, E., and Th'ng, J.P. (2004). The C-terminal domain is the primary determinant of histone H1 binding to chromatin in vivo. J Biol Chem *279*, 20028-20034.

Henikoff, S., Henikoff, J.G., Sakai, A., Loeb, G.B., and Ahmad, K. (2009). Genome-wide profiling of salt fractions maps physical properties of chromatin. Genome Res *19*, 460-469.

Hoghoughi, N., Barral, S., Vargas, A., Rousseaux, S., and Khochbin, S. (2018). Histone variants: essential actors in male genome programming. J Biochem *163*, 97-103.

Horvath, G.C., Kistler, W.S., and Kistler, M.K. (2004). RFX2 is a potential transcriptional regulatory factor for histone H1t and other genes expressed during the meiotic phase of spermatogenesis. Biol Reprod *71*, 1551-1559.

Howman, E.V., Fowler, K.J., Newson, A.J., Redward, S., MacDonald, A.C., Kalitsis, P., and Choo, K.H. (2000). Early disruption of centromeric chromatin organization in centromere protein A (Cenpa) null mice. Proc Natl Acad Sci U S A *97*, 1148-1153.

Hoyer-Fender, S., Costanzi, C., and Pehrson, J.R. (2000). Histone macroH2A1.2 is concentrated in the XY-body by the early pachytene stage of spermatogenesis. Exp Cell Res *258*, 254-260.

Hu, J., Sun, F., and Handel, M.A. (2018). Nuclear localization of EIF4G3 suggests a role for the XY body in translational regulation during spermatogenesis in mice. Biol Reprod *98*, 102-114.

Huh, N.E., Hwang, I., Lim, K., You, K.H., and Chae, C.B. (1991a). PRESENCE OF A BIDIRECTIONAL S-PHASE-SPECIFIC TRANSCRIPTION REGULATORY ELEMENT IN THE PROMOTER SHARED BY TESTIS-SPECIFIC TH2A AND TH2B HISTONE GENES. Nucleic Acids Research *19*, 93-98.

Huh, N.E., Hwang, I.W., Lim, K., You, K.H., and Chae, C.B. (1991b). Presence of a bi-directional S phase-specific transcription regulatory element in the promoter shared by testis-specific TH2A and TH2B histone genes. Nucleic Acids Res *19*, 93-98.

Huynh, L.M., Shinagawa, T., and Ishii, S. (2016a). Two Histone Variants TH2A and TH2B Enhance Human Induced Pluripotent Stem Cell Generation. Stem Cells Dev *25*, 251-258.

Huynh, L.M., Shinagawa, T., and Ishii, S. (2016b). Two Histone Variants TH2A and TH2B Enhance Human Induced Pluripotent Stem Cell Generation. Stem Cells and Development *25*, 251-258.

Iacovoni, J.S., Caron, P., Lassadi, I., Nicolas, E., Massip, L., Trouche, D., and Legube, G. (2010). High-resolution profiling of gammaH2AX around DNA double strand breaks in the mammalian genome. EMBO J *29*, 1446-1457.

Iwasaki, Y.W., Murano, K., Ishizu, H., Shibuya, A., Iyoda, Y., Siomi, M.C., Siomi, H., and Saito, K. (2016). Piwi Modulates Chromatin Accessibility by Regulating Multiple Factors Including Histone H1 to Repress Transposons. Mol Cell *63*, 408-419.

Izzo, A., Kamieniarz-Gdula, K., Ramirez, F., Noureen, N., Kind, J., Manke, T., van Steensel, B., and Schneider, R. (2013). The genomic landscape of the somatic linker histone subtypes H1.1 to H1.5 in human cells. Cell Rep *3*, 2142-2154.

Jin, C., and Felsenfeld, G. (2007). Nucleosome stability mediated by histone variants H3.3 and H2A.Z. Genes Dev *21*, 1519-1529.

Jin, C., Zang, C., Wei, G., Cui, K., Peng, W., Zhao, K., and Felsenfeld, G. (2009). H3.3/H2A.Z double variant-containing nucleosomes mark 'nucleosome-free regions' of active promoters and other regulatory regions. Nat Genet *41*, 941-945.

Johnson, G.D., Jodar, M., Pique-Regi, R., and Krawetz, S.A. (2016). Nuclease Footprints in Sperm Project Past and Future Chromatin Regulatory Events. Sci Rep *6*, 25864.

Joti, Y., Hikima, T., Nishino, Y., Kamada, F., Hihara, S., Takata, H., Ishikawa, T., and Maeshima, K. (2012). Chromosomes without a 30-nm chromatin fiber. Nucleus *3*, 404-410.

Kan, P.Y., Caterino, T.L., and Hayes, J.J. (2009). The H4 tail domain participates in intra- and internucleosome interactions with protein and DNA during folding and oligomerization of nucleosome arrays. Mol Cell Biol *29*, 538-546.

Kauppi, L., Barchi, M., Baudat, F., Romanienko, P.J., Keeney, S., and Jasin, M. (2011). Distinct properties of the XY pseudoautosomal region crucial for male meiosis. Science *331*, 916-920.

Khadake, J.R., and Rao, M.R. (1995). DNA- and chromatin-condensing properties of rat testes H1a and H1t compared to those of rat liver H1bdec; H1t is a poor condenser of chromatin. Biochemistry *34*, 15792-15801.

Khadake, J.R., and Rao, M.R. (1997). Condensation of DNA and chromatin by an SPKK-containing octapeptide repeat motif present in the C-terminus of histone H1. Biochemistry *36*, 1041-1051.

Kimmins, S., and Sassone-Corsi, P. (2005). Chromatin remodelling and epigenetic features of germ cells. Nature *434*, 583-589.

Kireeva, N., Lakonishok, M., Kireev, I., Hirano, T., and Belmont, A.S. (2004). Visualization of early chromosome condensation: a hierarchical folding, axial glue model of chromosome structure. J Cell Biol *166*, 775-785.

Kobayashi, W., Takaku, M., Machida, S., Tachiwana, H., Maehara, K., Ohkawa, Y., and Kurumizaka, H. (2016). Chromatin architecture may dictate the target site for DMC1, but not for RAD51, during homologous pairing. Sci Rep *6*, 24228.

Kojima, K., Kuramochi-Miyagawa, S., Chuma, S., Tanaka, T., Nakatsuji, N., Kimura, T., and Nakano, T. (2009). Associations between PIWI proteins and TDRD1/MTR-1 are critical for integrated subcellular localization in murine male germ cells. Genes Cells *14*, 1155-1165.

Kornberg, R.D. (1974). Chromatin structure: a repeating unit of histones and DNA. Science *184*, 868-871.

Kouzarides, T. (2007). Chromatin modifications and their function. Cell *128*, 693-705.

Krueger, F., and Andrews, S.R. (2011). Bismark: a flexible aligner and methylation caller for Bisulfite-Seq applications. Bioinformatics *27*, 1571-1572.

Kumaroo, K.K., Jahnke, G., and Irvin, J.L. (1975). Changes in basic chromosomal proteins during spermatogenesis in the mature rat. Arch Biochem Biophys *168*, 413-424.

Lai, W.K.M., and Pugh, B.F. (2017). Understanding nucleosome dynamics and their links to gene expression and DNA replication. Nat Rev Mol Cell Biol *18*, 548-562.

Lam, I., and Keeney, S. (2014). Mechanism and regulation of meiotic recombination initiation. Cold Spring Harb Perspect Biol *7*, a016634.

Lange, J., Yamada, S., Tischfield, S.E., Pan, J., Kim, S., Zhu, X., Socci, N.D., Jasin, M., and Keeney, S. (2016). The Landscape of Mouse Meiotic Double-Strand Break Formation, Processing, and Repair. Cell *167*, 695-708 e616.

Langmead, B., and Salzberg, S.L. (2012). Fast gapped-read alignment with Bowtie 2. Nat Methods *9*, 357-359.

Lassalle, B., Ziyyat, A., Testart, J., Finaz, C., and Lefevre, A. (1999). Flow cytometric method to isolate round spermatids from mouse testis. Hum Reprod *14*, 388-394.

Lennox, R.W., and Cohen, L.H. (1984). The alterations in H1 histone complement during mouse spermatogenesis and their significance for H1 subtype function. Dev Biol *103*, 80-84.

Li, A., Maffey, A.H., Abbott, W.D., Conde e Silva, N., Prunell, A., Siino, J., Churikov, D., Zalensky, A.O., and Ausio, J. (2005). Characterization of nucleosomes consisting of the human testis/sperm-specific histone H2B variant (hTSH2B). Biochemistry *44*, 2529-2535.

Li, B., Carey, M., and Workman, J.L. (2007). The role of chromatin during transcription. Cell *128*, 707-719.

Li, G., and Reinberg, D. (2011). Chromatin higher-order structures and gene regulation. Curr Opin Genet Dev *21*, 175-186.

Lin, Q., Sirotkin, A., and Skoultchi, A.I. (2000). Normal spermatogenesis in mice lacking the testis-specific linker histone H1t. Mol Cell Biol *20*, 2122-2128.

Linggi, B.E., Brandt, S.J., Sun, Z.W., and Hiebert, S.W. (2005). Translating the histone code into leukemia. J Cell Biochem *96*, 938-950.

Loury, R., and Sassone-Corsi, P. (2003). Histone phosphorylation: how to proceed. Methods *31*, 40-48.

Loyola, A., Bonaldi, T., Roche, D., Imhof, A., and Almouzni, G. (2006). PTMs on H3 variants before chromatin assembly potentiate their final epigenetic state. Mol Cell *24*, 309-316.

Lu, L.Y., Xiong, Y., Kuang, H., Korakavi, G., and Yu, X. (2013). Regulation of the DNA damage response on male meiotic sex chromosomes. Nat Commun *4*, 2105.

Lu, S., Xie, Y.M., Li, X., Luo, J., Shi, X.Q., Hong, X., Pan, Y.H., and Ma, X. (2009). Mass spectrometry analysis of dynamic post-translational modifications of TH2B during spermatogenesis. Mol Hum Reprod *15*, 373-378.

Luense, L.J., Wang, X., Schon, S.B., Weller, A.H., Lin Shiao, E., Bryant, J.M., Bartolomei, M.S., Coutifaris, C., Garcia, B.A., and Berger, S.L. (2016). Comprehensive analysis of histone post-translational modifications in mouse and human male germ cells. Epigenetics Chromatin *9*, 24.

Luger, K., Mader, A.W., Richmond, R.K., Sargent, D.F., and Richmond, T.J. (1997). Crystal structure of the nucleosome core particle at 2.8 A resolution. Nature *389*, 251-260.

Ma, L., Buchold, G.M., Greenbaum, M.P., Roy, A., Burns, K.H., Zhu, H., Han, D.Y., Harris, R.A., Coarfa, C., Gunaratne, P.H.*, et al.* (2009). GASZ is essential for male meiosis and suppression of retrotransposon expression in the male germline. PLoS Genet *5*, e1000635.

Machida, S., Hayashida, R., Takaku, M., Fukuto, A., Sun, J., Kinomura, A., Tashiro, S., and Kurumizaka, H. (2016). Relaxed Chromatin Formation and Weak Suppression of Homologous Pairing by the Testis-Specific Linker Histone H1T. Biochemistry *55*, 637-646.

Maezawa, S., Hasegawa, K., Alavattam, K.G., Funakoshi, M., Sato, T., Barski, A., and Namekawa, S.H. (2018). SCML2 promotes heterochromatin organization in late spermatogenesis. J Cell Sci *131*.

Mahadevan, I.A., Pentakota, S., Roy, R., Bhaduri, U., and Satyanarayana Rao, M.R. (2019). TH2BS11ph histone mark is enriched in the unsynapsed axes of the XY body and predominantly associates with H3K4me3-containing genomic regions in mammalian spermatocytes. Epigenetics Chromatin *12*, 53.

Maksakova, I.A., Romanish, M.T., Gagnier, L., Dunn, C.A., van de Lagemaat, L.N., and Mager, D.L. (2006). Retroviral elements and their hosts: insertional mutagenesis in the mouse germ line. PLoS Genet *2*, e2.

Malik, H.S., and Henikoff, S. (2003). Phylogenomics of the nucleosome. Nat Struct Biol *10*, 882-891.

Martens, J.H., O'Sullivan, R.J., Braunschweig, U., Opravil, S., Radolf, M., Steinlein, P., and Jenuwein, T. (2005). The profile of repeat-associated histone lysine methylation states in the mouse epigenome. EMBO J *24*, 800-812.

Martianov, I., Brancorsini, S., Catena, R., Gansmuller, A., Kotaja, N., Parvinen, M., Sassone-Corsi, P., and Davidson, I. (2005). Polar nuclear localization of H1T2, a histone H1 variant, required for spermatid elongation and DNA condensation during spermiogenesis. Proc Natl Acad Sci U S A *102*, 2808-2813.

Matzuk, M.M., McKeown, M.R., Filippakopoulos, P., Li, Q., Ma, L., Agno, J.E., Lemieux, M.E., Picaud, S., Yu, R.N., Qi, J.*, et al.* (2012). Small-molecule inhibition of BRDT for male contraception. Cell *150*, 673-684.

Mayor, R., Izquierdo-Bouldstridge, A., Millan-Arino, L., Bustillos, A., Sampaio, C., Luque, N., and Jordan, A. (2015). Genome distribution of replication-independent histone H1 variants shows H1.0 associated with nucleolar domains and H1X associated with RNA polymerase II-enriched regions. J Biol Chem *290*, 7474-7491.

Maze, I., Wenderski, W., Noh, K.M., Bagot, R.C., Tzavaras, N., Purushothaman, I., Elsasser, S.J., Guo, Y., Ionete, C., Hurd, Y.L., *et al.* (2015). Critical Role of Histone Turnover in Neuronal Transcription and Plasticity. Neuron *87*, 77-94.

Meistrich, M.L., Bucci, L.R., Trostle-Weige, P.K., and Brock, W.A. (1985). Histone variants in rat spermatogonia and primary spermatocytes. Dev Biol *112*, 230-240.

Mendiburo, M.J., Padeken, J., Fulop, S., Schepers, A., and Heun, P. (2011). Drosophila CENH3 is sufficient for centromere formation. Science *334*, 686-690.

Metzler-Guillemain, C., Luciani, J., Depetris, D., Guichaoua, M.R., and Mattei, M.G. (2003). HP1beta and HP1gamma, but not HP1alpha, decorate the entire XY body during human male meiosis. Chromosome Res *11*, 73-81.

Meyer-Ficca, M.L., Ihara, M., Lonchar, J.D., Meistrich, M.L., Austin, C.A., Min, W., Wang, Z.Q., and Meyer, R.G. (2011). Poly(ADP-ribose) Metabolism Is Essential for Proper Nucleoprotein Exchange During Mouse Spermiogenesis. Biology of Reproduction *84*, 218-228.

Millan-Arino, L., Islam, A.B., Izquierdo-Bouldstridge, A., Mayor, R., Terme, J.M., Luque, N., Sancho, M., Lopez-Bigas, N., and Jordan, A. (2014). Mapping of six somatic linker histone H1 variants in human breast cancer cells uncovers specific features of H1.2. Nucleic Acids Res *42*, 4474-4493.

Mishra, L.N., Gupta, N., and Rao, S.M. (2015). Mapping of post-translational modifications of spermatid-specific linker histone H1-like protein, HILS1. J Proteomics *128*, 218-230.

Mishra, L.N., Shalini, V., Gupta, N., Ghosh, K., Suthar, N., Bhaduri, U., and Rao, M.R.S. (2018a). Spermatid-specific linker histone HILS1 is a poor condenser of DNA and chromatin and preferentially associates with LINE-1 elements. Epigenetics & Chromatin *11*.

Mishra, L.N., Shalini, V., Gupta, N., Ghosh, K., Suthar, N., Bhaduri, U., and Rao, M.R.S. (2018b). Spermatid-specific linker histone HILS1 is a poor condenser of DNA and chromatin and preferentially associates with LINE-1 elements. Epigenetics Chromatin *11*, 43.

Montellier, E., Boussouar, F., Rousseaux, S., Zhang, K., Buchou, T., Fenaille, F., Shiota, H., Debernardi, A., Hery, P., Curtet, S., *et al.* (2013). Chromatin-to-nucleoprotamine transition is controlled by the histone H2B variant TH2B. Genes & Development *27*, 1680-1692.

Murray, K. (1964). The Occurrence of Epsilon-N-Methyl Lysine in Histones. Biochemistry *3*, 10-15.

Muthurajan, U.M., McBryant, S.J., Lu, X., Hansen, J.C., and Luger, K. (2011). The linker region of macroH2A promotes self-association of nucleosomal arrays. J Biol Chem *286*, 23852-23864.

Nagamori, I., Kobayashi, H., Shiromoto, Y., Nishimura, T., Kuramochi-Miyagawa, S., Kono, T., and Nakano, T. (2015). Comprehensive DNA Methylation Analysis of Retrotransposons in Male Germ Cells. Cell Rep *12*, 1541-1547.

Neale, M.J., and Keeney, S. (2006). Clarifying the mechanics of DNA strand exchange in meiotic recombination. Nature *442*, 153-158.

Neale, M.J., Pan, J., and Keeney, S. (2005). Endonucleolytic processing of covalent protein-linked DNA double-strand breaks. Nature *436*, 1053-1057.

Nemeth, A., Conesa, A., Santoyo-Lopez, J., Medina, I., Montaner, D., Peterfia, B., Solovei, I., Cremer, T., Dopazo, J., and Langst, G. (2010). Initial genomics of the human nucleolus. PLoS Genet *6*, e1000889.

Okamoto, Y., Nakano, M., Ohzeki, J., Larionov, V., and Masumoto, H. (2007). A minimal CENP-A core is required for nucleation and maintenance of a functional human centromere. EMBO J *26*, 1279-1291.

Okuwaki, M., Kato, K., Shimahara, H., Tate, S., and Nagata, K. (2005). Assembly and disassembly of nucleosome core particles containing histone variants by human nucleosome assembly protein I. Mol Cell Biol *25*, 10639-10651.

Ou, H.D., Phan, S., Deerinck, T.J., Thor, A., Ellisman, M.H., and O'Shea, C.C. (2017). ChromEMT: Visualizing 3D chromatin structure and compaction in interphase and mitotic cells. Science *357*.

Ozturk, M.A., Cojocaru, V., and Wade, R.C. (2018). Toward an Ensemble View of Chromatosome Structure: A Paradigm Shift from One to Many. Structure *26*, 1050-1057.

Padavattan, S., Shinagawa, T., Hasegawa, K., Kumasaka, T., Ishii, S., and Kumarevel, T. (2015a). Structural and functional analyses of nucleosome complexes with mouse histone variants TH2a and TH2b, involved in reprogramming. Biochemical and Biophysical Research Communications *464*, 929-935.

Padavattan, S., Shinagawa, T., Hasegawa, K., Kumasaka, T., Ishii, S., and Kumarevel, T. (2015b). Structural and functional analyses of nucleosome complexes with mouse histone variants TH2a and TH2b, involved in reprogramming. Biochem Biophys Res Commun *464*, 929-935.

Padavattan, S., Thiruselvam, V., Shinagawa, T., Hasegawa, K., Kumasaka, T., Ishii, S., and Kumarevel, T. (2017). Structural analyses of the nucleosome complexes with human testis-specific histone variants, hTh2a and hTh2b. Biophysical Chemistry *221*, 41-48.

Parra, M.A., Kerr, D., Fahy, D., Pouchnik, D.J., and Wyrick, J.J. (2006). Deciphering the roles of the histone H2B N-terminal domain in genome-wide transcription. Mol Cell Biol *26*, 3842-3852.

Parvanov, E.D., Tian, H., Billings, T., Saxl, R.L., Spruce, C., Aithal, R., Krejci, L., Paigen, K., and Petkov, P.M. (2017). PRDM9 interactions with other proteins provide a link between recombination hotspots and the chromosomal axis in meiosis. Mol Biol Cell *28*, 488-499.

Pehrson, J.R., Changolkar, L.N., Costanzi, C., and Leu, N.A. (2014). Mice without macroH2A histone variants. Mol Cell Biol *34*, 4523-4533.

Pehrson, J.R., and Fried, V.A. (1992). MacroH2A, a core histone containing a large nonhistone region. Science *257*, 1398-1400.

Peng, J., and Gygi, S.P. (2001). Proteomics: the move to mixtures. J Mass Spectrom *36*, 1083-1091.

Pentakota, S.K., Sandhya, S., A, P.S., Chandra, N., and Satyanarayana Rao, M.R. (2014). Mapping post-translational modifications of mammalian testicular specific histone variant TH2B in tetraploid and haploid germ cells and their implications on the dynamics of nucleosome structure. J Proteome Res *13*, 5603-5617.

Peters, A.H., O'Carroll, D., Scherthan, H., Mechtler, K., Sauer, S., Schofer, C., Weipoltshammer, K., Pagani, M., Lachner, M., Kohlmaier, A.*, et al.* (2001). Loss of the Suv39h histone methyltransferases impairs mammalian heterochromatin and genome stability. Cell *107*, 323-337.

Peters, A.H., Plug, A.W., van Vugt, M.J., and de Boer, P. (1997). A drying-down technique for the spreading of mammalian meiocytes from the male and female germline. Chromosome Res *5*, 66-68.

Peters, A.H., and Schubeler, D. (2005). Methylation of histones: playing memory with DNA. Curr Opin Cell Biol *17*, 230-238.

Pezic, D., Manakov, S.A., Sachidanandam, R., and Aravin, A.A. (2014). piRNA pathway targets active LINE1 elements to establish the repressive H3K9me3 mark in germ cells. Genes Dev *28*, 1410-1428.

Pivot-Pajot, C., Caron, C., Govin, J., Vion, A., Rousseaux, S., and Khochbin, S. (2003). Acetylation-dependent chromatin reorganization by BRDT, a testis-specific bromodomain-containing protein. Mol Cell Biol *23*, 5354-5365.

Pogo, B.G., Allfrey, V.G., and Mirsky, A.E. (1966). RNA synthesis and histone acetylation during the course of gene activation in lymphocytes. Proc Natl Acad Sci U S A *55*, 805-812.

Pombo, A., and Dillon, N. (2015). Three-dimensional genome architecture: players and mechanisms. Nat Rev Mol Cell Biol *16*, 245-257.

Powers, N.R., Parvanov, E.D., Baker, C.L., Walker, M., Petkov, P.M., and Paigen, K. (2016). The Meiotic Recombination Activator PRDM9 Trimethylates Both H3K36 and H3K4 at Recombination Hotspots In Vivo. PLoS Genet *12*, e1006146.

Raisner, R.M., Hartley, P.D., Meneghini, M.D., Bao, M.Z., Liu, C.L., Schreiber, S.L., Rando, O.J., and Madhani, H.D. (2005). Histone variant H2A.Z marks the 5' ends of both active and inactive genes in euchromatin. Cell *123*, 233-248.

Ramesh, S., Bharath, M.M., Chandra, N.R., and Rao, M.R. (2006). A K52Q substitution in the globular domain of histone H1t modulates its nucleosome binding properties. FEBS Lett *580*, 5999-6006.

Rao, B.J., Brahmachari, S.K., and Rao, M.R. (1983). Structural organization of the meiotic prophase chromatin in the rat testis. J Biol Chem *258*, 13478-13485.

Rao, B.J., and Rao, M.R. (1987). DNase I site mapping and micrococcal nuclease digestion of pachytene chromatin reveal novel structural features. J Biol Chem *262*, 4472-4476.

Rattle, H.W., Langan, T.A., Danby, S.E., and Bradbury, E.M. (1977). Studies on the role and mode of operation of the very-lysine-rich histones in eukaryote chromatin. Effect of A and B site phosphorylation on the conformation and interaction of histone H1. Eur J Biochem *81*, 499-505.

Rattner, J.B., and Lin, C.C. (1985). Radial loops and helical coils coexist in metaphase chromosomes. Cell *42*, 291-296.

Rennie, S., Dalby, M., van Duin, L., and Andersson, R. (2018). Transcriptional decomposition reveals active chromatin architectures and cell specific regulatory interactions. Nat Commun *9*, 487.

Reuter, M., Berninger, P., Chuma, S., Shah, H., Hosokawa, M., Funaya, C., Antony, C., Sachidanandam, R., and Pillai, R.S. (2011). Miwi catalysis is required for piRNA amplification-independent LINE1 transposon silencing. Nature *480*, 264-267.

Reuter, M., Chuma, S., Tanaka, T., Franz, T., Stark, A., and Pillai, R.S. (2009). Loss of the Mili-interacting Tudor domain-containing protein-1 activates transposons and alters the Mili-associated small RNA profile. Nat Struct Mol Biol *16*, 639-646.

Richler, C., Dhara, S.K., and Wahrman, J. (2000). Histone macroH2A1.2 is concentrated in the XY compartment of mammalian male meiotic nuclei. Cytogenet Cell Genet *89*, 118-120.

Robinson, P.J., Fairall, L., Huynh, V.A., and Rhodes, D. (2006). EM measurements define the dimensions of the "30-nm" chromatin fiber: evidence for a compact, interdigitated structure. Proc Natl Acad Sci U S A *103*, 6506-6511.

Romer, K.A., de Rooij, D.G., Kojima, M.L., and Page, D.C. (2018). Isolating mitotic and meiotic germ cells from male mice by developmental synchronization, staging, and sorting. Dev Biol *443*, 19-34.

Roque, A., Ponte, I., and Suau, P. (2016). Interplay between histone H1 structure and function. Biochim Biophys Acta *1859*, 444-454.

Roussel, L., Erard, M., Cayrol, C., and Girard, J.P. (2008). Molecular mimicry between IL-33 and KSHV for attachment to chromatin through the H2A-H2B acidic pocket. EMBO Rep *9*, 1006-1012.

Royo, H., Prosser, H., Ruzankina, Y., Mahadevaiah, S.K., Cloutier, J.M., Baumann, M., Fukuda, T., Hoog, C., Toth, A., de Rooij, D.G.*, et al.* (2013). ATR acts stage specifically to regulate multiple aspects of mammalian meiotic silencing. Genes Dev *27*, 1484-1494.

Saitou, M., and Kurimoto, K. (2014). Paternal nucleosomes: are they retained in developmental promoters or gene deserts? Dev Cell *30*, 6-8.

Samans, B., Yang, Y., Krebs, S., Sarode, G.V., Blum, H., Reichenbach, M., Wolf, E., Steger, K., Dansranjavin, T., and Schagdarsurengin, U. (2014). Uniformity of nucleosome preservation pattern in Mammalian sperm and its connection to repetitive DNA elements. Dev Cell *30*, 23-35.

Saxe, J.P., Chen, M., Zhao, H., and Lin, H. (2013). Tdrkh is essential for spermatogenesis and participates in primary piRNA biogenesis in the germline. EMBO J *32*, 1869-1885.

Schalch, T., Duda, S., Sargent, D.F., and Richmond, T.J. (2005). X-ray structure of a tetranucleosome and its implications for the chromatin fibre. Nature *436*, 138-141.

Schneider, R., Bannister, A.J., Myers, F.A., Thorne, A.W., Crane-Robinson, C., and Kouzarides, T. (2004). Histone H3 lysine 4 methylation patterns in higher eukaryotic genes. Nat Cell Biol *6*, 73-77.

Schones, D.E., Cui, K., Cuddapah, S., Roh, T.Y., Barski, A., Wang, Z., Wei, G., and Zhao, K. (2008). Dynamic regulation of nucleosome positioning in the human genome. Cell *132*, 887-898.

Sedat, J., and Manuelidis, L. (1978). A direct approach to the structure of eukaryotic chromosomes. Cold Spring Harb Symp Quant Biol *42 Pt 1*, 331-350.

Sexton, T., and Cavalli, G. (2015). The role of chromosome domains in shaping the functional genome. Cell *160*, 1049-1059.

Shang, E., Nickerson, H.D., Wen, D., Wang, X., and Wolgemuth, D.J. (2007). The first bromodomain of Brdt, a testis-specific member of the BET sub-family of double-bromodomain-containing proteins, is essential for male germ cell differentiation. Development *134*, 3507-3515.

Shechter, D., Dormann, H.L., Allis, C.D., and Hake, S.B. (2007). Extraction, purification and analysis of histones. Nat Protoc *2*, 1445-1457.

Sheikh, B.N. (2014). Crafting the brain - role of histone acetyltransferases in neural development and disease. Cell Tissue Res *356*, 553-573.

Shevchenko, A., Wilm, M., Vorm, O., and Mann, M. (1996). Mass spectrometric sequencing of proteins silver-stained polyacrylamide gels. Anal Chem *68*, 850-858.

Shinagawa, T., Huynh, L.M., Takagi, T., Tsukamoto, D., Tomaru, C., Kwak, H.G., Dohmae, N., Noguchi, J., and Ishii, S. (2015). Disruption of Th2a and Th2b genes causes defects in spermatogenesis. Development *142*, 1287-1292.

Shinagawa, T., Takagi, T., Tsukamoto, D., Tomaru, C., Huynh, L.M., Sivaraman, P., Kumarevel, T., Inoue, K., Nakato, R., Katou, Y.*, et al.* (2014). Histone variants enriched in oocytes enhance reprogramming to induced pluripotent stem cells. Cell Stem Cell *14*, 217-227.

Shoji, M., Tanaka, T., Hosokawa, M., Reuter, M., Stark, A., Kato, Y., Kondoh, G., Okawa, K., Chujo, T., Suzuki, T.*, et al.* (2009). The TDRD9-MIWI2 complex is essential for piRNA-mediated retrotransposon silencing in the mouse male germline. Dev Cell *17*, 775-787.

Shukla, R., Upton, K.R., Munoz-Lopez, M., Gerhardt, D.J., Fisher, M.E., Nguyen, T., Brennan, P.M., Baillie, J.K., Collino, A., Ghisletti, S.*, et al.* (2013). Endogenous retrotransposition activates oncogenic pathways in hepatocellular carcinoma. Cell *153*, 101-111.

Simpson, R.T. (1978). Structure of the chromatosome, a chromatin particle containing 160 base pairs of DNA and all the histones. Biochemistry *17*, 5524-5531.

Sinha, D., and Shogren-Knaak, M.A. (2010). Role of direct interactions between the histone H4 Tail and the H2A core in long range nucleosome contacts. J Biol Chem *285*, 16572-16581.

Sitbon, D., Podsypanina, K., Yadav, T., and Almouzni, G. (2017). Shaping Chromatin in the Nucleus: The Bricks and the Architects. Cold Spring Harb Symp Quant Biol *82*, 1-14.

Soboleva, T.A., Nekrasov, M., Pahwa, A., Williams, R., Huttley, G.A., and Tremethick, D.J. (2011). A unique H2A histone variant occupies the transcriptional start site of active genes. Nat Struct Mol Biol *19*, 25-30.

Somyajit, K., Basavaraju, S., Scully, R., and Nagaraju, G. (2013). ATM- and ATR-mediated phosphorylation of XRCC3 regulates DNA double-strand break-induced checkpoint activation and repair. Mol Cell Biol *33*, 1830-1844.

Song, F., Chen, P., Sun, D., Wang, M., Dong, L., Liang, D., Xu, R.M., Zhu, P., and Li, G. (2014). Cryo-EM study of the chromatin fiber reveals a double helix twisted by tetranucleosomal units. Science *344*, 376-380.

Steger, K., Klonisch, T., Gavenis, K., Drabent, B., Doenecke, D., and Bergmann, M. (1998). Expression of mRNA and protein of nucleoproteins during human spermiogenesis. Mol Hum Reprod *4*, 939-945.

Strahl, B.D., and Allis, C.D. (2000). The language of covalent histone modifications. Nature *403*, 41-45.

Sullivan, K.F. (2001). A solid foundation: functional specialization of centromeric chromatin. Curr Opin Genet Dev *11*, 182-188.

Suzuki, M. (1989). SPKK, a new nucleic acid-binding unit of protein found in histone. EMBO J *8*, 797-804.

Tachibana, M., Nozaki, M., Takeda, N., and Shinkai, Y. (2007). Functional dynamics of H3K9 methylation during meiotic prophase progression. EMBO J *26*, 3346-3359.

Tachiwana, H., Kagawa, W., Osakabe, A., Kawaguchi, K., Shiga, T., Hayashi-Takanaka, Y., Kimura, H., and Kurumizaka, H. (2010). Structural basis of instability of the nucleosome containing a testis-specific histone variant, human H3T. Proceedings of the National Academy of Sciences of the United States of America *107*, 10454-10459.

Tachiwana, H., Osakabe, A., Kimura, H., and Kurumizaka, H. (2008a). Nucleosome formation with the testis-specific histone H3 variant, H3t, by human nucleosome assembly proteins in vitro. Nucleic Acids Res *36*, 2208-2218.

Tachiwana, H., Osakabe, A., Kimura, H., and Kurumizaka, H. (2008b). Nucleosome formation with the testis-specific histone H3 variant, H3t, by human nucleosome assembly proteins in vitro. Nucleic Acids Research *36*, 2208-2218.

Tachiwana, H., Osakabe, A., Shiga, T., Miya, Y., Kimura, H., Kagawa, W., and Kurumizaka, H. (2011). Structures of human nucleosomes containing major histone H3 variants. Acta Crystallographica Section D-Biological Crystallography *67*, 578-583.

Talbert, P.B., Ahmad, K., Almouzni, G., Ausio, J., Berger, F., Bhalla, P.L., Bonner, W.M., Cande, W.Z., Chadwick, B.P., Chan, S.W.*, et al.* (2012). A unified phylogeny-based nomenclature for histone variants. Epigenetics Chromatin *5*, 7.

Tan, M., Luo, H., Lee, S., Jin, F., Yang, J.S., Montellier, E., Buchou, T., Cheng, Z., Rousseaux, S., Rajagopal, N.*, et al.* (2011). Identification of 67 histone marks and histone lysine crotonylation as a new type of histone modification. Cell *146*, 1016-1028.

Tanaka, H., Iguchi, N., Isotani, A., Kitamura, K., Toyama, Y., Matsuoka, Y., Onishi, M., Masai, K., Maekawa, M., Toshimori, K.*, et al.* (2005). HANP1/H1T2, a novel histone H1-like protein involved in nuclear formation and sperm fertility. Mol Cell Biol *25*, 7107-7119.

Tani, R., Hayakawa, K., Tanaka, S., and Shiota, K. (2016). Linker histone variant H1T targets rDNA repeats. Epigenetics *11*, 288-302.

Tardat, M., Brustel, J., Kirsh, O., Lefevbre, C., Callanan, M., Sardet, C., and Julien, E. (2010). The histone H4 Lys 20 methyltransferase PR-Set7 regulates replication origins in mammalian cells. Nat Cell Biol *12*, 1086-1093.

Tarsounas, M., Morita, T., Pearlman, R.E., and Moens, P.B. (1999). RAD51 and DMC1 form mixed complexes associated with mouse meiotic chromosome cores and synaptonemal complexes. J Cell Biol *147*, 207-220.

Thakar, A., Gupta, P., Ishibashi, T., Finn, R., Silva-Moreno, B., Uchiyama, S., Fukui, K., Tomschik, M., Ausio, J., and Zlatanova, J. (2009). H2A.Z and H3.3 histone variants affect nucleosome structure: biochemical and biophysical studies. Biochemistry *48*, 10852-10857.

Trostle-Weige, P.K., Meistrich, M.L., Brock, W.A., Nishioka, K., and Bremer, J.W. (1982). Isolation and characterization of TH2A, a germ cell-specific variant of histone 2A in rat testis. J Biol Chem *257*, 5560-5567.

Turner, J.M., Burgoyne, P.S., and Singh, P.B. (2001). M31 and macroH2A1.2 colocalise at the pseudoautosomal region during mouse meiosis. J Cell Sci *114*, 3367-3375.

Turner, J.M., Mahadevaiah, S.K., Fernandez-Capetillo, O., Nussenzweig, A., Xu, X., Deng, C.X., and Burgoyne, P.S. (2005). Silencing of unsynapsed meiotic chromosomes in the mouse. Nat Genet *37*, 41-47.

Ueda, J., Harada, A., Urahama, T., Machida, S., Maehara, K., Hada, M., Makino, Y., Nogami, J., Horikoshi, N., Osakabe, A.*, et al.* (2017a). Testis-Specific Histone Variant H3t Gene Is Essential for Entry into Spermatogenesis. Cell Rep *18*, 593-600.

Ueda, J., Harada, A., Urahama, T., Machida, S., Maehara, K., Hada, M., Makino, Y., Nogami, J., Horikoshi, N., Osakabe, A.*, et al.* (2017b). Testis-Specific Histone Variant H3t Gene Is Essential for Entry into Spermatogenesis. Cell Reports *18*, 593-600.

van der Heijden, G.W., Derijck, A.A., Posfai, E., Giele, M., Pelczar, P., Ramos, L., Wansink, D.G., van der Vlag, J., Peters, A.H., and de Boer, P. (2007). Chromosome-wide nucleosome replacement and H3.3 incorporation during mammalian meiotic sex chromosome inactivation. Nat Genet *39*, 251-258.

van Koningsbruggen, S., Gierlinski, M., Schofield, P., Martin, D., Barton, G.J., Ariyurek, Y., den Dunnen, J.T., and Lamond, A.I. (2010). High-resolution whole-genome sequencing reveals that specific chromatin domains from most human chromosomes associate with nucleoli. Mol Biol Cell *21*, 3735-3748.

VanWert, J.M., Wolfe, S.A., and Grimes, S.R. (2008). Binding of RFX2 and NF-Y to the testis-specific histone H1t promoter may be required for transcriptional activation in primary spermatocytes. J Cell Biochem *104*, 1087-1101.

Wang, L., Gao, Y., Zheng, X., Liu, C., Dong, S., Li, R., Zhang, G., Wei, Y., Qu, H., Li, Y.*, et al.* (2019). Histone Modifications Regulate Chromatin Compartmentalization by Contributing to a Phase Separation Mechanism. Mol Cell.

Wang, L., and Wolgemuth, D.J. (2016). BET Protein BRDT Complexes With HDAC1, PRMT5, and TRIM28 and Functions in Transcriptional Repression During Spermatogenesis. Journal of Cellular Biochemistry *117*, 1429-1438.

Wang, L., Xu, Z., Khawar, M.B., Liu, C., and Li, W. (2017). The histone codes for meiosis. Reproduction *154*, R65-R79.

Wilkerson, D.C., Wolfe, S.A., and Grimes, S.R. (2002a). H1t/GC-box and H1t/TE1 element are essential for promoter activity of the testis-specific histone H1t gene. Biol Reprod *67*, 1157-1164.

Wilkerson, D.C., Wolfe, S.A., and Grimes, S.R. (2002b). Sp1 and Sp3 activate the testis-specific histone H1t promoter through the H1t/GC-box. J Cell Biochem *86*, 716-725.

Witt, O., Albig, W., and Doenecke, D. (1996). Testis-specific expression of a novel human H3 histone gene. Exp Cell Res *229*, 301-306.

Wolfe, S.A., and Grimes, S.R. (1993). Histone H1t: a tissue-specific model used to study transcriptional control and nuclear function during cellular differentiation. J Cell Biochem *53*, 156-160.

Wolfe, S.A., and Grimes, S.R. (1999). Binding of nuclear proteins to an upstream element involved in transcriptional regulation of the testis-specific histone H1t gene. J Cell Biochem *75*, 555-565.

Wolfe, S.A., van Wert, J.M., and Grimes, S.R. (1995). Expression of the testis-specific histone H1t gene: evidence for involvement of multiple cis-acting promoter elements. Biochemistry *34*, 12461-12469.

Wolfe, S.A., Wilkerson, D.C., Prado, S., and Grimes, S.R. (2004). Regulatory factor X2 (RFX2) binds to the H1t/TE1 promoter element and activates transcription of the testis-specific histone H1t gene. J Cell Biochem *91*, 375-383.

Woodcock, C.L., Skoultchi, A.I., and Fan, Y. (2006). Role of linker histone in chromatin structure and function: H1 stoichiometry and nucleosome repeat length. Chromosome Res *14*, 17-25.

Wu, Q., Zheng, H., Wiggins, L., von Bartheld, C., Zhao, M., Meistrich, M.L., and Yan, W. (2009). Genetic Interaction of Hils1 with Tnp1 Is Essential for Normal Sperm Production and Male Fertility. Biology of Reproduction *81*, 462-462.

Xu, S., Grullon, S., Ge, K., and Peng, W. (2014). Spatial clustering for identification of ChIP-enriched regions (SICER) to map regions of histone methylation patterns in embryonic stem cells. Methods Mol Biol *1150*, 97-111.

Xu, Z., Song, Z., Li, G., Tu, H., Liu, W., Liu, Y., Wang, P., Wang, Y., Cui, X., Liu, C.*, et al.* (2016). H2B ubiquitination regulates meiotic recombination by promoting chromatin relaxation. Nucleic Acids Res *44*, 9681-9697.

Xue, Z., Huang, K., Cai, C., Cai, L., Jiang, C.Y., Feng, Y., Liu, Z., Zeng, Q., Cheng, L., Sun, Y.E.*, et al.* (2013). Genetic programs in human and mouse early embryos revealed by single-cell RNA sequencing. Nature *500*, 593-597.

Yamada, S., Kim, S., Tischfield, S.E., Jasin, M., Lange, J., and Keeney, S. (2017). Genomic and chromatin features shaping meiotic double-strand break formation and repair in mice. Cell Cycle *16*, 1870-1884.

Yan, W., Ma, L., Burns, K.H., and Matzuk, M.M. (2003). HILS1 is a spermatid-specific linker histone H1-like protein implicated in chromatin remodeling during mammalian spermiogenesis. Proc Natl Acad Sci U S A *100*, 10546-10551.

Yu, L., and Gorovsky, M.A. (1997). Constitutive expression, not a particular primary sequence, is the important feature of the H3 replacement variant hv2 in Tetrahymena thermophila. Mol Cell Biol *17*, 6303-6310.

Zamudio, N., and Bourc'his, D. (2010). Transposable elements in the mammalian germline: a comfortable niche or a deadly trap? Heredity (Edinb) *105*, 92-104.

Zentner, G.E., Balow, S.A., and Scacheri, P.C. (2014). Genomic characterization of the mouse ribosomal DNA locus. G3 (Bethesda) *4*, 243-254.

Zhang, H., Roberts, D.N., and Cairns, B.R. (2005). Genome-wide dynamics of Htz1, a histone H2A variant that poises repressed/basal promoters for activation through histone loss. Cell *123*, 219-231.

Zhou, B.R., Jiang, J., Feng, H., Ghirlando, R., Xiao, T.S., and Bai, Y. (2015). Structural Mechanisms of Nucleosome Recognition by Linker Histones. Mol Cell *59*, 628-638.

Zilberman, D., Coleman-Derr, D., Ballinger, T., and Henikoff, S. (2008). Histone H2A.Z and DNA methylation are mutually antagonistic chromatin marks. Nature *456*, 125-129.

Zink, L.M., and Hake, S.B. (2016). Histone variants: nuclear function and disease. Curr Opin Genet Dev *37*, 82-89.

Zovkic, I.B., and Sweatt, J.D. (2015). Memory-Associated Dynamic Regulation of the "Stable" Core of the Chromatin Particle. Neuron *87*, 1-4.

List of publications

Iyer Aditya Mahadevan*, Satyakrishna Pentakota*, Raktim Roy, Utsa Bhaduri, Satyanarayana MR Rao, TH2BS11ph histone mark is enriched in the unsynapsed axes of the XY body and predominantly associates with H3K4me3-containing genomic regions in mammalian spermatocytes; **Epigenetics and Chromatin**, (2019). *-equal contribution

Iyer Aditya Mahadevan, Sanjeev Kumar, Satyanarayana MR Rao, Linker histone variant H1t is closely associated with repeat-element chromatin domains in pachytene spermatocytes; **Manuscript under peer review**, (2020).

Vasantha Shalini, **Iyer Aditya Mahadevan**, Satyanarayana MR Rao, Germ cell specific linker histone variants: Chromatin organization and function. **Review Article**, **Under preparation**, (2020).

Epigenetics & Chromatin

RESEARCH

Open Access

TH2BS11ph histone mark is enriched in the unsynapsed axes of the XY body and predominantly associates with H3K4me3-containing genomic regions in mammalian spermatocytes

Iyer Aditya Mahadevan[1†], Satyakrishna Pentakota[2†], Raktim Roy[3], Utsa Bhaduri[1] and Manchanahalli R. Satyanarayana Rao[1*]

Abstract

Background: TH2B is a major histone variant that replaces about 80–85% of somatic H2B in mammalian spermatocytes and spermatids. The post-translational modifications (PTMs) on TH2B have been well characterised in spermatocytes and spermatids. However, the biological function(s) of these PTMs on TH2B have not been deciphered in great detail. In our attempt to decipher the unique function(s) of histone variant TH2B, we detected the modification in the N-terminal tail, Serine 11 phosphorylation on TH2B (TH2BS11ph) in spermatocytes.

Results: The current study is aimed at understanding the function of the TH2BS11ph modification in the context of processes that occur during meiotic prophase I. Immunofluorescence studies with the highly specific antibodies revealed that TH2BS11ph histone mark is enriched in the unsynapsed axes of the sex body and is associated with XY body-associated proteins like Scp3, γH2AX, pATM, ATR, etc. Genome-wide occupancy studies as determined by ChIP sequencing experiments in P20 C57BL6 mouse testicular cells revealed that TH2BS11ph is enriched in X and Y chromosomes confirming the immunofluorescence staining pattern in the pachytene spermatocytes. Apart from the localisation of this modification in the XY body, TH2BS11ph is majorly associated with H3K4me3-containing genomic regions like gene promoters, etc. These data were also found to corroborate with the ChIP sequencing data of TH2BS11ph histone mark carried out in P12 C57BL6 mouse testicular cells, wherein we found the predominant localisation of this modification at H3K4me3-containing genomic regions. Mass spectrometry analysis of proteins that associate with TH2BS11ph-containing mononucleosomes revealed key proteins linked with the functions of XY body, pericentric heterochromatin and transcription.

Conclusions: TH2BS11ph modification is densely localised in the unsynapsed axes of the XY body of the pachytene spermatocyte. By ChIP sequencing studies in mouse P12 and P20 testicular cells, we demonstrate that TH2BS11ph is predominantly associated with H3K4me3 positive genomic regions like gene promoters, etc. We propose that TH2BS11ph modification could act alone or in concert with other histone modifications to recruit the appropriate transcription or XY body recombination protein machinery at specific genomic loci.

*Correspondence: mrsrao@jncasr.ac.in
†Iyer Aditya Mahadevan and Satyakrishna Pentakota contributed equally to this work
[1] Molecular Biology and Genetics Unit, Jawaharlal Nehru Centre for Advanced Scientific Research, Jakkur PO., Bangalore 560064, India
Full list of author information is available at the end of the article

Keywords: TH2B serine 11 phosphorylation, Spermatocytes, TH2B, Immunofluorescence, Coimmunoprecipitation, H3K4me3 co-association

Background

Mammalian spermatogenesis offers an excellent model system to study chromatin remodelling by histone variants as the testis is known to express a large number of core and linker histone variants in a stage-specific manner [1–6]. It is hypothesised that chromatin locus-specific histone replacement with histone variants could be a possible basis for genome reprogramming in germ cells. Testis-specific histone variants play critical roles during the germ cell development. H3t (testis-specific histone variant of H3) is essential for the process of spermatogonial differentiation and ensures entry into meiosis [7]. The loss of TH2A and TH2B leads to male sterility with defects in cohesin release during interkinesis and histone to protamine replacement, suggesting an essential role of the testis-specific histone variants during critical periods of male germ development [8].

TH2B, a synonym of germ cell-specific H2B.1 (or TS H2B.1) [9] was one of the earliest histone variants discovered in mammalian testis [10, 11]. To date, it is the only testis-specific histone variant known to replace a core histone on a genome-wide scale replacing 80–85% of H2B in spermatocytes and spermatids [12]. The pachytene nucleosome core particle harbouring the TH2B molecule was shown to be less compact compared to H2B-containing nucleosome core particle [13, 14]. hTSH2B (human TH2B)-reconstituted histone octamer was found to be less stable than the H2B-reconstituted histone octamer in vitro [15]. On the other hand, the loss of mouse TH2B is compensated for upregulation of H2B and compensatory histone modifications on the core histones H2B, H3 and H4 in germ cells. However, the expression of tagged-TH2B protein created a dominant negative phenotype, resulting in a defective histone to protamine replacement that led to male sterility [12]. TH2B shares 85% sequence similarity with canonical histone H2B with majority of the differences being at its N-terminus. We surmised that these differences or the post-translational modifications acquired by some of the residues could contribute to unique functions of TH2B. In this direction, Pentakota et al. [16] characterised the repertoire of post-translational modifications (PTMs) on histone variant TH2B isolated from spermatocytes and spermatid stages. By computational analysis, it was also shown that the amino acid differences and the post-translational modifications acquired by some of the residues cause the destabilisation of TH2B-containing nucleosomes. Histone PTMs are key molecular players in epigenomic functions [17, 18]. Recently, various studies have focussed on understanding the post-translational modifications on testis-specific histone variants like TH2B [16, 19], TP1 (Transition Protein 1) [20], TP2 (Transition Protein 2) [20], HILS1 (Histone Linker H1 Spermatid specific 1) [21], etc.

During prophase I of meiosis, the homologous chromosomes synapse and undergo recombination at non-randomly selected loci. The exchange of genetic material is critical for the generation of diversity in the offspring. During leptotene interval, the global induction of Spo11-mediated DSBs occurs throughout the genome triggering the DNA damage response (DDR) [22, 23]. Subsequently, MRN (Mre11-Rad50-Nbs1) complex recruits ATM kinase, and catalyses the first level of H2AX phosphorylation to form γH2AX [24–26]. The end resection and strand invasion mediated by MRN complex, RAD51, DMC1 and other proteins are characteristic of the next stage, the zygotene interval. During the pachytene stage, BRCA1 senses asynapsis and recruits ATR kinase for amplification of DDR signals along the unsynapsed axes for the establishment of the γH2AX domain in the XY body [27–29]. The region of homology between the X and the Y chromosomes termed as pseudo-autosomal region (PAR) is limited in size (~800 kb in mice) and is largely unsynapsed during meiosis. Therefore, to ensure chromosome segregation with at least one crossover in PAR, a higher crossover density and increased DSB occurrence are observed in the PAR compared to that of autosomes [30]. The increase in DSB sites is caused by specialised chromatin configuration in PAR where DNA is organised on a longer axis with shorter chromatin loops compared to autosomes [31, 32]. The non-PAR regions of the X and Y chromosomes are transcriptionally silenced during meiotic prophase by a process termed as meiotic sex

Table 1 List of datasets used for computational data analyses

Dataset	Geo accession IDs
DSB hotspots	GSE93955
TSS (of mouse)	GENCODE
H3K4me3	GSE35498
H3K4me3 common	GSE93955
H3K4me3 (B6 specific)	GSE93955
TH2B	GSE45915

chromosome inactivation (MSCI) [33, 34]. The crossover products are generated at the end of pachytene [35]. The completion of meiosis I yields secondary spermatocytes which undergo meiotic II division to produce haploid round spermatids.

In our efforts to gain insight into the unique functions of TH2B particularly during meiotic prophase I, we detected a post-translational modification in the amino terminal end that was already reported in another study in round spermatid TH2B [36], Serine 11 phosphorylation on TH2B (TH2BS11ph according to Brno nomenclature for histone modifications [37]). Histone phosphorylation is linked to diverse biological processes like DNA damage and repair (DDR) [38], apoptosis [39], etc. In this study, we show that TH2BS11ph modification is a histone mark associated with unsynapsed axes of the XY body in pachytene spermatocytes of rodents. ChIP-sequencing studies further reveal that majority of TH2BS11ph-containing genomic regions were not hotspot-related but associated with other H3K4me3-containing regions like gene promoters, enhancers, etc (Table 1). Additionally, this histone mark is also associated with important proteins and histone marks linked to functions of gene regulation and XY body, as revealed by mass spectrometry studies. This is the first report documenting the role of a post-translational modification of a germ cell-specific core histone variant in meiotic prophase I-related events.

Results

TH2B serine 11 phosphorylation (TH2BS11ph) is a novel histone modification detected in mammalian spermatocytes

TH2B is the major histone variant in spermatocytes and spermatids [12] (Fig. 1a). As mentioned earlier, TH2B differs from H2B protein with majority of amino acid residues differing in the solvent exposed amino terminal tail (Fig. 1b, c). In an attempt to decipher various PTMs on TH2B, we purified in vivo TH2B from 30-day rat testicular cells by the reverse-phase HPLC technique. By employing a different set of procedures that includes enzyme digestion and post-mass spectrometry analyses of various PTMs obtained on in vivo TH2B, we detected the modification TH2BS11ph (TH2B serine 11 phosphorylation) in spermatocytes. This modification was already detected in TH2B from round spermatids by Luense et al. but not in spermatocytes [36]. We show for the first time the occurrence of this modification on TH2B isolated from spermatocytes. The representative MS/MS plot is shown in Fig. 1d. The corresponding fragmentation table has been given in Additional file 1: Fig. S1A. The somatic H2BS14ph modification has been shown to be involved in DNA repair processes in somatic cells [40]. Therefore, we were interested to ascertain the function of the testis-specific H2B variant TH2B serine 11 phosphorylation in the context of DNA repair and meiotic recombination associated events in spermatocytes. For this purpose, polyclonal antibodies specific to this modification were generated in rabbits.

The specificity of the antibody was determined by ELISA and western blot assays. ELISA assays were carried out with the TH2BS11ph antibody, wherein the antibody showed high reactivity towards the TH2B serine 11 phosphopeptide but not with the TH2B and H2B backbone peptides (Fig. 1e). The antibody showed reactivity towards testis nuclear lysates (Fig. 1f, Lane 'Testis nuclear lysate') but did not cross-react with the H2B containing liver nuclear lysate and also the recombinant TH2B protein by western blotting (Fig. 1f, lanes 'Liver nuclear lysate' and 'rTH2B'). Further, the reactivity of the antibody was abolished by the TH2B serine 11 phosphopeptide (Fig. 1g, lane 2) but not by the TH2B unmodified peptide (Fig. 1g, lane 3). The combination of mass

(See figure on next page.)

Fig. 1 Identification of TH2BS11ph modification by mass spectrometry and characterization of the TH2BS11ph antibody. **a** Genome-wide replacement of H2B by TH2B histone variant in mammalian spermatocytes and spermatids [12]. **b** Model of the TH2B-containing nucleosome highlighting the exposed serine 11 residue. **c** Alignment of protein sequences of TH2B from rat and mouse. H2B sequence of rat has been given for reference. The boxed region in black represents the peptide sequence used for generation of the polyclonal antibody in rabbits. **d** Identification of TH2BS11ph modification by LC–MS/MS technique. The *y*-axis indicates the relative intensity of MS/MS spectra and the *x*-axis indicates the mass–charge ratio. The phosphorylated serine residue of TH2B-containing peptide fragment is highlighted in red. **e** ELISA assay—TH2B antibody reacts with both TH2B serine 11 phospho- and non-phosphopeptides, whereas the TH2BS11ph antibody specifically reacts with the TH2B serine 11 phosphopeptide. ELISA was carried out with the Pre-bleed immune sera, Immune sera, TH2BS11ph sera and the TH2BS11ph purified antibody; white bars represent reactivity of the mentioned sera or antibody with TH2B backbone peptide, black bars represent reactivity with H2B peptide and the orange bars represent reactivity with the TH2B serine 11 phosphopeptide. **f** Immunoblotting of affinity purified TH2BS11ph antibody shows reactivity with only TH2B-containing nuclear lysate. Western blotting was performed with anti-TH2BS11ph antibody against liver nuclear lysates, testes nuclear lysates and recombinant TH2B (rTH2B). Coomassie stained gel is given for reference on the left. **g** Peptide competition assay—first lane represents no peptide control, second lane TH2BS11ph antibody pre-incubated with TH2B serine 11 phosphopeptide, third lane TH2BS11ph antibody pre-incubated with TH2B backbone peptide. Western blot was carried out with the antibodies indicated as alpha alongside the blot

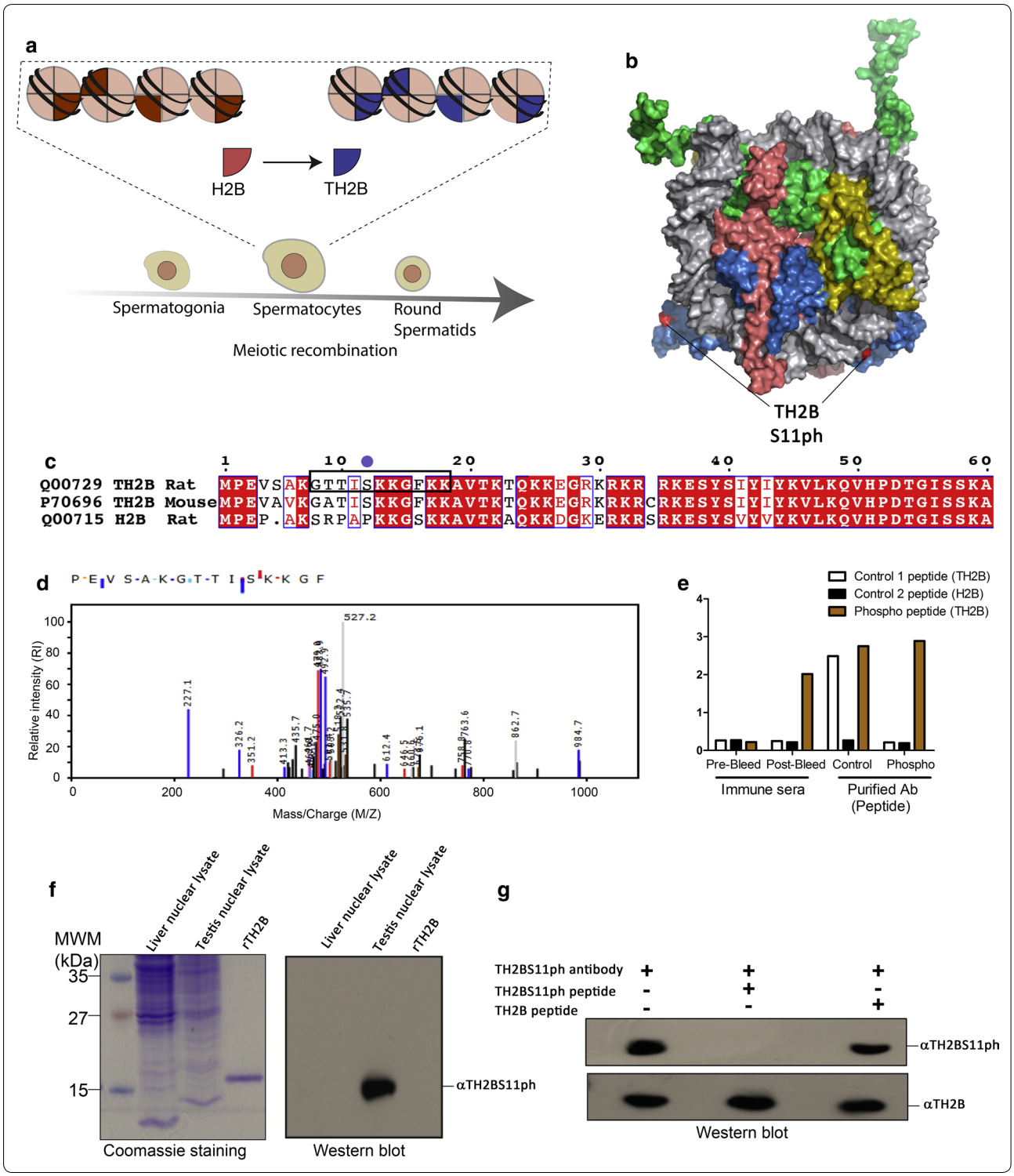
a
H2B
TH2B
Spermatogonia
Spermatocytes
Round Spermatids
Meiotic recombination
b
TH2B S11ph
c
Q00729 TH2B Rat MPEVSAKGTTISKKGFKKAVTKTQKKEGRKRKR RKESYSIYIYKVLKQVHPDTGISSKA
P70696 TH2B Mouse MPEVAVKGATISKKGFKKAVTKTQKKEGRKRKRC RKESYSIYIYKVLKQVHPDTGISSKA
Q00715 H2B Rat MPEP.AKSRPAPKKGSKKAVTKAQKKDGKERKRS RKESYSVYVYKVLKQVHPDTGISSKA
d
Relative intensity (RI)
Mass/Charge (M/Z)
527.2
227.1
e
Control 1 peptide (TH2B)
Control 2 peptide (H2B)
Phospho peptide (TH2B)
Pre-Bleed
Post-Bleed
Control
Phospho
Immune sera
Purified Ab (Peptide)
f
MWM (kDa)
35
27
15
Liver nuclear lysate
Testis nuclear lysate
rTH2B
αTH2BS11ph
Coomassie staining
Western blot
g
TH2BS11ph antibody
TH2BS11ph peptide
TH2B peptide
αTH2BS11ph
αTH2B
Western blot

spectrometry and Western blotting analysis, thus, establishes that the TH2BS11ph modification is physiological.

TH2BS11ph modification is densely localised in the axes of the XY body during the pachytene stage of meiosis prophase I

After establishing the high specificity of the TH2BS11ph antibody, we carried out immunofluorescence studies with the TH2BS11ph antibody to examine the staining pattern during meiotic prophase I. TH2B begins to express in preleptotene spermatocytes and continues to be present till the late stages of spermiogenesis [12]. Keeping this in mind, we carried out immunofluorescence staining of meiotic spreads of mouse testicular germ cells to examine whether the TH2BS11ph modification has any role in the events that are characteristic of meiotic prophase I. We have used Scp3 (Synaptonemal Complex Protein 3) and γH2AX as markers to distinguish various stages of meiotic prophase I in mouse [41] (Table 2). We observe that TH2BS11ph is detectable during the stages leptotene, zygotene and pachytene intervals as indicated in Fig. 2b. It is interesting to note that the backbone TH2B is detected all over the nucleus (Fig. 2a), while TH2BS11ph signal was more distributed as specific foci, suggesting a locus-dependent function. An important observation that is apparent in the staining pattern in pachytene spermatocytes is that TH2BS11ph modification was found to be highly enriched at the axes of the XY body-like structure (Fig. 2b, pachytene). This was further corroborated by colocalization analysis as represented in Fig. 2f (Scp3) which revealed that TH2BS11ph signal colocalizes with Scp3 in the XY body (Fig. 2f, pachytene without rotation and XY body without rotation). We found a higher colocalization percentage of TH2BS11ph and Scp3 of about 47% in the XY body compared to 14% in the whole pachytene spermatocyte (Fig. 2f pachytene without rotation, XY body without rotation). To evaluate the specificity of colocalization and to ensure that the observed signal is not a result of random overlap, we performed colocalization analyses after rotating images captured in the red channel by 90° in the anticlockwise direction. A significant decrease in colocalization percentages with usage of rotated images in comparison to non-rotated images would mean specific colocalization between the two channels. On rotation of the TH2BS11ph images captured in the red channel, we found that the colocalization percentage of TH2BS11ph and Scp3 decreased significantly in the XY body (Fig. 2f, Scp3, XY body with rotation) and in pachytene spermatocyte (Fig. 2f, Scp3, pachytene with rotation) in comparison with the non-rotated images. This indicates that TH2BS11ph is highly enriched in the axes of the XY body of the pachytene spermatocyte. We, therefore, conjectured that this modification may have a XY body-specific function in spermatocytes. This was also confirmed in meiotic spreads of rat testicular cells where we observed increased enrichment of TH2BS11ph signal in the XY body-like structure (Additional file 2: Fig. S2A, pachytene). Apart from the XY body of pachytene cells, we observed many foci outside the sex body suggesting the role of TH2BS11ph may not be just restricted to XY body-specific functions.

H2AX is required for chromatin remodelling and sex chromosome inactivation in male meiosis [42]. We confirmed the enrichment and localization of this TH2B modification in the XY body of the pachytene nucleus using the sex body-specific marker γH2AX. As can be seen in Fig. 2c (pachytene), TH2BS11ph colocalizes with γH2AX corresponding to the axes of the XY body in the pachytene spermatocytes. The degree of colocalization of TH2BS11ph with γH2AX in the XY body was found to be 21% in the XY body as opposed to colocalization in the whole pachytene spermatocyte (~11%) as indicated in Fig. 2f (γH2AX, Pachytene without rotation, XY body without rotation). It is to be noted that γH2AX has a different staining pattern where it stains the axes and loops of the XY body, whereas TH2BS11ph stains only the axes; this might be the reason for lower colocalization

(See figure on next page.)

Fig. 2 TH2BS11ph modification is densely localised in the axes of the XY body. **a** Immunofluorescence studies of backbone TH2B and Scp3 in leptotene (1st panel), zygotene (2nd panel) and pachytene stages (3rd panel) of meiotic prophase I. **b** Colocalization studies of TH2BS11ph modification with synaptonemal complex protein Scp3 across leptotene (1st panel), zygotene (2nd panel) and pachytene stages (3rd panel) of meiotic prophase I. The inset in the pachytene image represents the XY body. **c** Colocalization studies of TH2BS11ph with γH2AX in leptotene (1st panel), zygotene (2nd panel) and pachytene spermatocytes (3rd panel). The inset in the pachytene image shows the XY body. Immunofluorescence studies of TH2BS11ph with **d** pATM and **e** ATR kinases in pachytene spermatocytes. The insets in **d**, **e** show the XY body. Data information in (**a**–**e**); All data were confirmed with at least three independent mice (C57BL6 species). Nuclei were visualised by DAPI staining, Scale bars, 10 µm. **f** Quantitation of colocalization percentages of TH2BS11ph with Scp3, γH2AX, pATM and ATR in the whole pachytene spermatocyte and XY body. The colocalization percentages were calculated with (with rotation) and without (without rotation) image rotation. For calculation of colocalization percentages upon image rotation, the TH2BS11ph images captured in the red channel were rotated by 90° in the anticlockwise direction in the XY plane. The number of nuclei analysed are Scp3 ($n = 10$), γH2AX ($n = 15$), pATM ($n = 15$) and pATR ($n = 15$). The data are plotted in terms of mean ± SD ***$P \leq 0.0005$, **$P \leq 0.005$, *$P \leq 0.05$ (*t*-test). *w rotation* with rotation, *wo rotation* without rotation

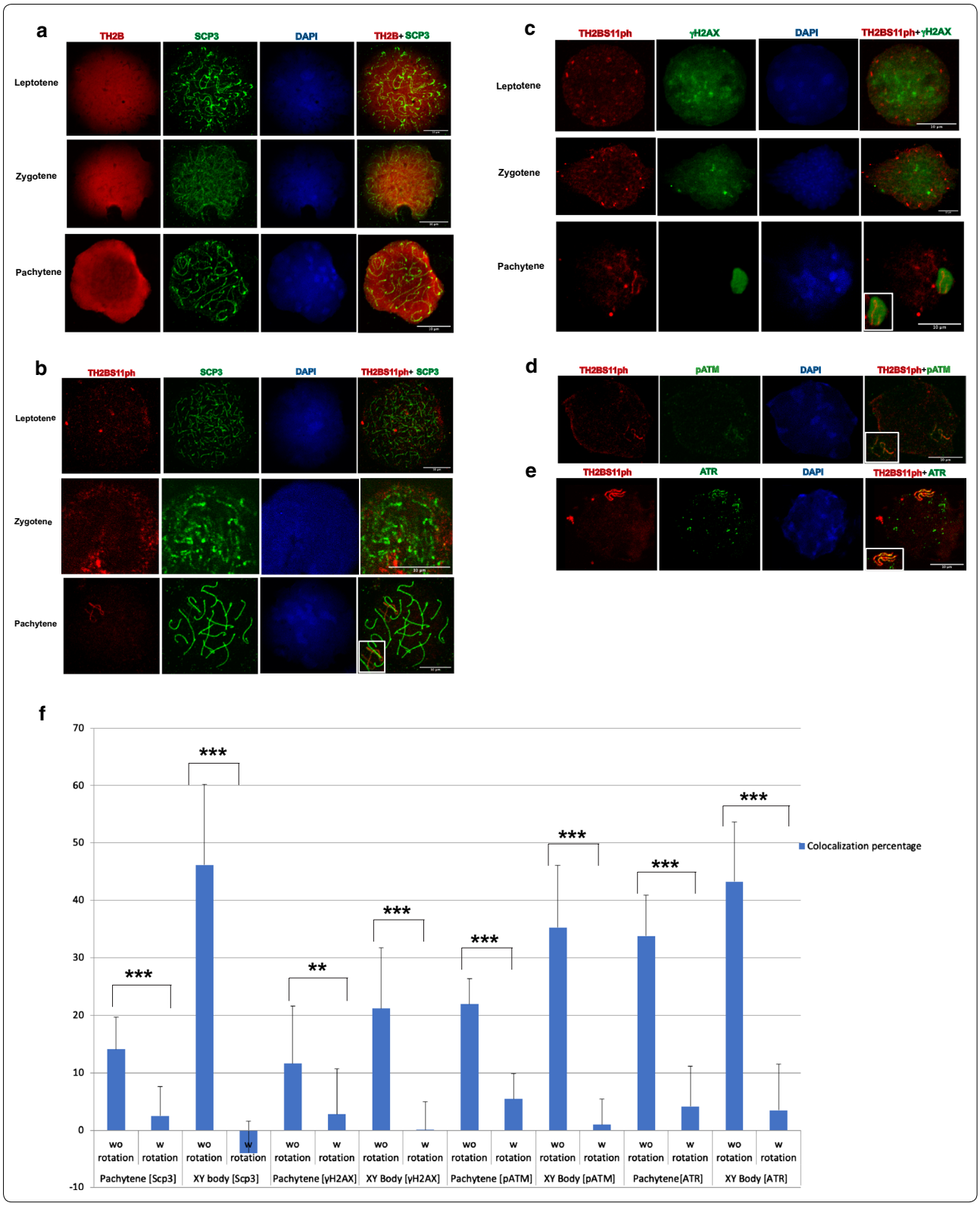
a
TH2B
SCP3
DAPI
TH2B+ SCP3
Leptotene
Zygotene
Pachytene
b
TH2BS11ph
SCP3
DAPI
TH2BS11ph+ SCP3
Leptotene
Zygotene
Pachytene
c
TH2BS11ph
γH2AX
DAPI
TH2BS11ph+γH2AX
Leptotene
Zygotene
Pachytene
d
TH2BS11ph
pATM
DAPI
TH2BS11ph+pATM
e
TH2BS11ph
ATR
DAPI
TH2BS11ph+ATR
f
70
60
50
40
30
20
10
0
-10
***
**
Colocalization percentage
wo rotation
w rotation
Pachytene [Scp3]
XY body [Scp3]
Pachytene [γH2AX]
XY Body [γH2AX]
Pachytene [pATM]
XY Body [pATM]
Pachytene[ATR]
XY Body [ATR]

Table 2 List of antibodies used in the present study

Reagents				
Antibodies	**Host**	**Company name**	**Cat number**	**Application**
Scp3	Mouse	Abcam	ab97672	IF
γH2AX	Mouse	Upstate (Millipore)	05-636	IF, ChIP, WB
H2BS14ph	Rabbit	Scbt	sc31671	WB
pATM	Mouse	Upstate (Millipore)	05-740	IF
ATR	Mouse	Abcam	ab54793	IF
H3K4me3	Mouse	Abcam	ab12209	ChIP, WB
TH2B	Rabbit	Generated in house		IF, WB
Rad51	Mouse	Abcam	ab1837	IF
Spo11	Goat	Santa Cruz	sc22476	IF

IF immunofluorescence, *ChIP* chromatin immunoprecipitation, *WB* western blotting

percentages for γH2AX in the XY body. On rotation of TH2BS11ph images captured in the red channel, we found colocalization percentages to decrease significantly as shown in Fig. 2f (γH2AX, pachytene with rotation and XY body with rotation) in comparison with the non-rotated images. On the basis of colocalization observed with Scp3 and γH2AX in the axes of the sex body, we conclude that TH2BS11ph is densely localised to the axes of the XY body.

In a previous study, H2BS14ph was shown to stain the XY body of pachytene spermatocytes in mouse [40]. Since, our data also showed that TH2BS11ph localizes to XY axes, we wondered whether the TH2BS11ph antibody did crossreact with H2B or its posttranslational modifications in spermatocytes. However, on re-examination of the published data, we found that the same H2BS14ph commercial antibody cross-reacts also with in vivo TH2B (Additional file 1: Fig. S1C, in vivo TH2B). The antibody has been withdrawn and no more available. Therefore, we generated a H2B-specific antibody, validated its reactivity by dot-blot assay and western blotting with liver and testicular histones as shown in Additional file 1: Fig. S1D. We carried out staging of the H2B antibody with Scp3 to obtain the staining pattern at various stages of meiotic prophase I. The staining of backbone H2B was found to be not intense contrary to that previously reported for H2BS14ph modification in all the stages of meiotic prophase I (Additional file 1: Fig. S1E). Furthermore, H2B staining did not coincide with the XY body of the pachytene spermatocyte (Additional file 1: Fig. S1E, pachytene). This also supports the report wherein H2B levels were found to decrease completely at 18 dpp mouse testes that coincide with onset of differentiation of pachytene cells [12]. Nevertheless, the combination of Western Blotting with peptide competition, and ELISA assays prove that the TH2BS11ph antibody did not cross-react with H2B, further negating the previous report where H2BS14ph was shown to localise to the XY body suggesting that the reported staining pattern was a result of cross-reactivity with TH2B.

TH2BS11ph modification is enriched in the unsynapsed axes and associated with recombination-related kinases like pATM and ATR in the XY body of the pachytene spermatocyte

From mid-zygotene interval, unsynapsed chromosomes are marked by ATR, where the latter carries out the second level of H2AX phosphorylation [27, 29]. pATM and ATR are the markers of the unsynapsed axes of the XY body [43]. To test the enrichment of TH2BS11ph in the axes of the XY body, we next sought to perform colocalization studies with pATM and ATR kinases. We observe colocalization with pATM in axes of the XY body as can be seen in Fig. 2d. Upon further quantitative analyses, we observe colocalization with pATM of about 35% corresponding to the axes of the XY body as indicated in Fig. 2f (pATM, XY body without rotation). On rotation of the TH2BS11ph images captured in the red channel, the colocalization percentage dipped to about 1%, suggesting the specific overlap of TH2BS11ph and pATM in the axes of the XY body in the non-rotated images (Fig. 2f, pATM, XY body with rotation).

To determine the association of XY body-specific kinase ATR and TH2BS11ph, colocalization studies were also carried out of TH2BS11ph and ATR. There was a distinct colocalization seen specifically in the axes of the XY body as seen in Fig. 2e. We also quantified the colocalization percentages between TH2BS11ph and ATR, where we found a high colocalization percentage of about 43% in the XY body (Fig. 2f, ATR, XY body without rotation). We found colocalization percentage of 33.8% in the whole pachytene spermatocyte (Fig. 2f, ATR, pachytene without rotation). The colocalization percentages decreased significantly on rotation of the TH2BS11ph images captured in the red channel (Fig. 2f, ATR, pachytene with rotation, XY body with rotation). On the basis of colocalization of TH2BS11ph with ATR and pATM in the XY axes during the pachytene interval, we conclude that this modification is densely localised to the unsynapsed axes of the XY body.

XY body harbours various proteins related to recombination and heterochromatin formation. DDR proteins that accumulate in the XY body, have different and distinct localisation patterns. Proteins like γH2AX are spread over the entire sex chromosomes (axes + loops), whereas ATR, pATM, Rad51 are localised in the unsynapsed axes [43]. This suggests that unsynapsed axes are different from other chromosomal regions of the sex

body in terms of distinct localisation patterns of various DDR related proteins. Since pATM and ATR are marker proteins of the unsynapsed axes and colocalize with TH2BS11ph [43], we conclude that TH2BS11ph histone mark is enriched in the unsynapsed axes of the XY body of pachytene spermatocyte. Taken together, the immunofluorescence studies reveal that the TH2BS11ph modification is associated with the proteins γH2AX, pATM and ATR that are related to DNA recombination and repair processes in the XY body. Some of the key observations of the immunofluorescence data in mouse meiotic spreads were also shown to be true for rat testicular cells as shown in the Additional file 2: Fig. S2.

TH2BS11ph modification is predominantly associated with H3K4me3-containing genomic regions in spermatocytes

ATR kinase, not pATM, has been shown to be involved in XY body-specific phosphorylation of H2AX [29]. Therefore, we went ahead to examine whether TH2BS11ph is associated with the known sex body-specific marker, γH2AX. To verify the immunofluorescence studies further, we, therefore, carried out immunoprecipitation reactions with mononucleosomes to determine the coexistence of sex body-associated histone mark γH2AX in a single nucleosome core particle. We employed MNase digestion followed by immunoprecipitation to address whether TH2BS11ph is associated with γH2AX in the context of mononucleosomes. The profile of MNase digestion with respect to time of digestion has been given in Additional file 5: Fig. S5A. By IP assays, we demonstrate that TH2BS11ph pulled down γH2AX protein (Fig. 3a, TH2BS11ph). Conversely, TH2BS11P is also found in γH2AX elute fraction (Fig. 3b, γH2AX). These experiments suggest that TH2BS11ph and γH2AX co-associate possibly to recruit similar set of proteins in turn to regulate DSB processes in the XY body.

Since meiotic recombination is a non-random event and occurs at specific loci termed as meiotic recombination hotspots, we were curious to examine the possible presence of TH2BS11ph at these hotspot loci. Since the genetics of homologous recombination and hotspot genomic regions are well characterised in C57BL6 mouse species, and also many of the colocalization experiments were reproduced in both rat and mouse testicular cells, we were interested to determine the genome-wide occupancy of this modification in pachytene cells (P20 testicular cells) and in leptotene (P12 testicular cells). Immunofluorescence studies revealed the predominant localisation of TH2BS11ph in the unsynapsed axes of the XY body, also the localisation of this modification revealed many foci outside the XY body. Therefore, the localization of this modification in the context of binding sites on the pachytene genome had to be determined.

In this direction, ChIP-sequencing analyses of genome-wide distribution of TH2BS11ph was carried out to obtain a comprehensive picture of the association of TH2BS11ph with genomic regions in P20 mouse testicular cells enriched in pachytene cells. The workflow of the ChIP sequencing protocol and computational analyses is given in Fig. 3c. We used the already published TH2B ChIP-seq data for comparison that was carried out in elutriation-purified spermatocyte populations that usually is representative of TH2B occupancy in pachytene cells [12]. The important question was to determine the unique regions that are enriched for TH2BS11ph compared to backbone TH2B. To address this, we performed peak calling of TH2BS11ph ChIP seq data against the published TH2B dataset to obtain the unique peaks of TH2BS11ph occupancy. We observed high number of peaks in chromosomes X and Y (Fig. 3d, chrX and chrY). As can be seen in Fig. 3e, we also observe higher number of reads of TH2BS11ph IP in the X-chromosome in comparison to the backbone TH2B occupancy. This validated our immunofluorescence studies, wherein TH2BS11ph modification was found to be enriched in the XY body.

(See figure on next page.)

Fig. 3 TH2BS11ph histone mark is predominantly associated with genomic regions containing the histone mark H3K4me3. TH2BS11ph-containing mononucleosomes associate with sex body-specific histone mark γH2AX-Mononucleosome IP studies determining the coexistence of histone marks TH2BS11ph with γH2AX, **a** γH2AX is associated with TH2BS11ph-containing mononucleosomes. IP was carried out using the anti-TH2BS11ph antibody where the TH2BS11ph, γH2AX and TH2B were probed by western blotting. **b** TH2BS11ph is associated with γH2AX-containing mononucleosomes. IP was carried out with the γH2AX antibody, and scored for TH2BS11ph, γH2AX, and TH2B by western blotting. The antibodies used for western blotting are indicated to the side of the blot. Ponceau stained blots have been given for reference. Data information in **a**, **b** The numbers represent molecular weight in kilodaltons. The first lane in all the blots represents the input fraction, 2nd lane IgG elute fraction and 3rd lane immunoprecipitation with the mentioned antibodies. **c** Workflow of ChIP sequencing analysis for TH2BS11ph histone mark carried out in mouse P20 testicular cells. **d** Chromosome wise distribution of TH2BS11ph peaks across chromosomes of mouse-majority of the TH2BS11ph peaks were found in chromosomes X and Y. **e** Distribution of TH2BS11ph and TH2B reads across the X-chromosome. For both TH2BS11ph and TH2B sections, the upper track represents the peaks, whereas the bottom track represents the read distributions as observed in IGV Genome Browser. TH2B ChIP sequencing data were taken from Gene Expression Omnibus (GSE45915) [12]

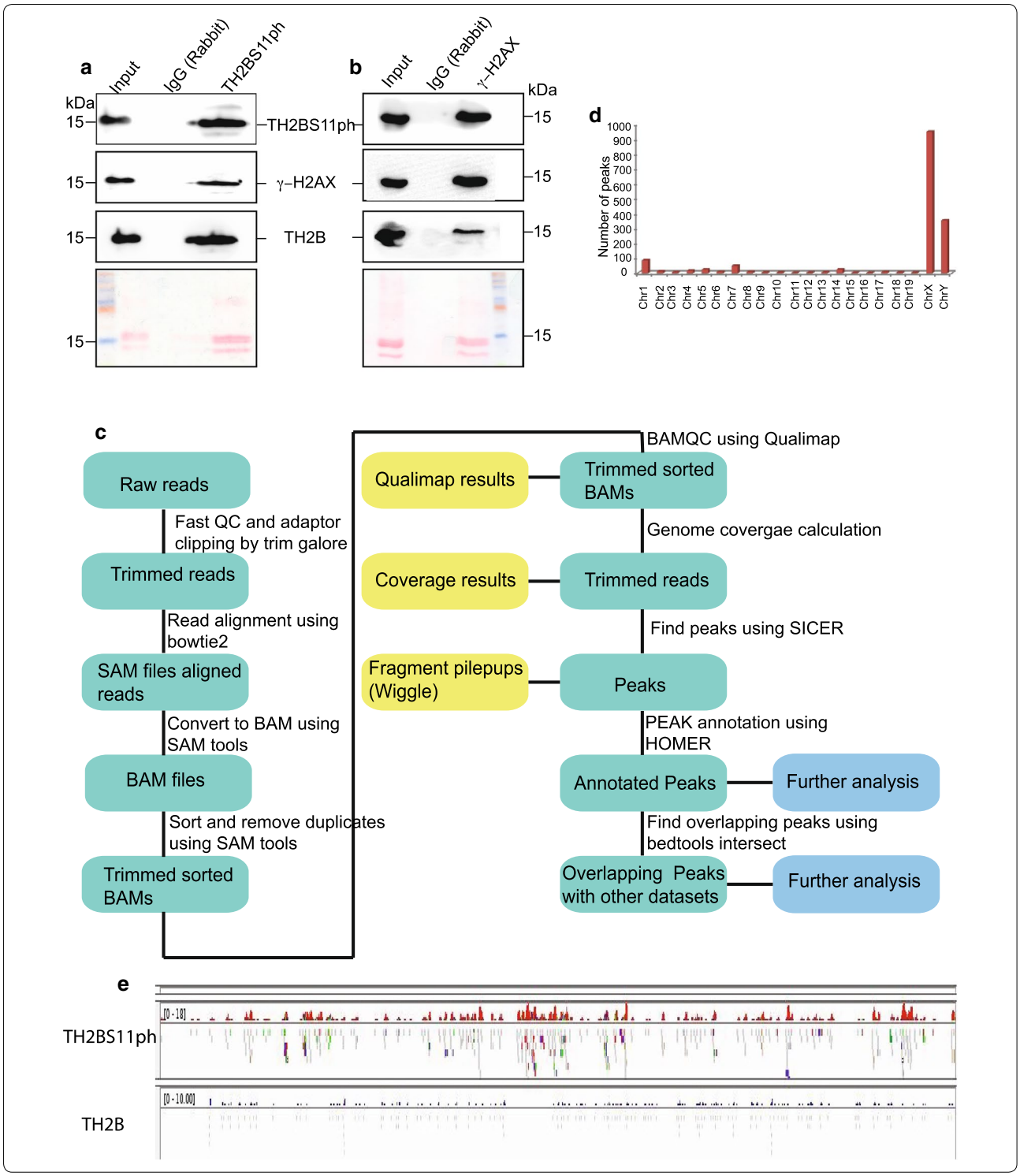

To identify the characteristic features of the genomic regions bound by TH2BS11ph histone mark, we were interested to check their overlap with meiotic recombination and transcription-related histone H3K4me3 ChIP-seq datasets [44]. To address this, we generated aggregation plots to determine the localisation of TH2BS11ph reads with respect to the centre of binding sites of total H3K4me3 marks, DSB hotspots and

transcription-associated H3K4me3 mark [common H3K4me3], etc. All the analyses of overlap of TH2BS11ph with particular histone mark ChIP-seq datasets have been carried out in comparison with TH2B control dataset. We have generated two kinds of data to determine the overlap of TH2BS11ph with TSS or recombination hotspot-specific histone marks. Aggregation plot shows the concentration of read counts in respective genomic coordinates, i.e., TSS, etc. Heatmap are also generated for the corresponding aggregation plot to address the spatial distribution of reads within the proximity of the region of interest.

Aggregation plot as given in Fig. 4a demonstrates that majority of the reads were concentrated within 1 kb from the centre of occupancy of H3K4me3 mark (Fig. 4a, first panel). We also find secondary peaks further away from the centre of H3K4me3 mark, which might be due to the interaction of promoters with distal regulatory elements like enhancers, etc. The heat map representation corroborates with the fact the majority of TH2BS11ph reads lie at the centre of H3K4me3 peaks (Fig. 4a, second panel). The important thing to be kept in mind is that TSS and recombination hotspots also have similar histone mark profile consisting of H3K4me3, H3K36me3 marks, etc. Therefore, we were interested to delineate whether TH2BS11ph is linked to either TSS-specific or hotspot-specific histone mark H3K4me3. With respect to DSB hotspots, represented by occupancy of hotspot-specific H3K4me3 marks genome wide, we did not find significant overlap of TH2BS11ph at recombination hotspots as shown by aggregation plot given in Fig. 4b, (first panel). There were no reads concentrated at the centre of the DSB hotspots (Fig. 4b, first and second panels). We further looked at the association of TH2BS11ph with common H3K4me3 peaks representing the H3K4me3 marks present at gene regulatory regions like promoters, enhancers, etc. On further analysis, we found close association of TH2BS11ph with TSS (Transcription Start Sites) containing-H3K4me3 (Fig. 4c). Aggregation plot supports the conclusion wherein majority of the reads were concentrated within the centre of TSS-specific H3K4me3 (Fig. 4c, first and second panels). As the distance from H3K4me3 increases, the overlap of both these two histone marks also decreases. Therefore, the overlap of TH2BS11ph was specific to TSS-associated H3K4me3 but not hotspot-specific H3K4me3. We also generated Aggregation plot and heat map using available dataset of TSS of mouse. As can be seen in Fig. 4d, we observe specific localisation of TH2BS11ph reads at the centre of the transcription start sites further supporting the fact the specific association of this histone mark towards TSS (Fig. 4d, first and second panels). The presence of H3K4me3 is linked to high DSB activity in the PAR of the X-chromosome [45]. Furthermore, since we had found out that majority of TH2BS11ph peaks were in the X-chromosome, it became important to check the association with X-chromosome-specific H3K4me3 marks. We observed that TH2BS11ph-containing genomic regions were indeed positive for H3K4me3 mark in the X-chromosome (Fig. 4e, first and second panels). We have also plotted the read distribution of TH2BS11ph occupancy with respect to these datasets in Additional file 3: Fig. S3, wherein we observed the maximum overlap of TH2BS11ph reads at the centre of TSS and TSS-specific H3K4me3 marks (Additional file 3: Fig. S3C, D).

To determine the localisation and dynamics of localisation of the TH2BS11ph modification, we also performed ChIP-sequencing studies in mouse P12 testicular cells representative of leptotene/zygotene cells. Since various datasets for H3K4me3 and DSB hotspots are available for P12 mouse testicular cells, we wanted to compare the localisation and overlap of TH2BS11ph with these datasets in leptotene/zygotene cells. Aggregation plot for P12 TH2BS11ph ChIP sequencing data showed the predominant localisation with respect to total H3K4me3 marks (Additional file 4: Fig. S4A). Furthermore, the localisation was specific to transcription-specific H3K4me3 (common H3K4me3) but not recombination hotspot-specific H3K4me3 [B6 specific H3K4me3] as can be seen in Additional file 4: Fig. S4B, C, respectively. Even in leptotene cells, we observed specific association of TH2BS11ph towards TSS-associated H3K4me3 marks (Additional file 4: Fig. S4C). The defining factor of TH2BS11ph occupancy in leptotene and pachytene cells, therefore, also demonstrates association with TSS-associated H3K4me3 nucleosomes.

Open chromatin regions like transcription start sites are initiation for meiotic recombination in yeast [46]. However, hotspots and TSS are distinctly located in the mouse genome [47]. Aggregation plots and heat maps had showed strong association of TH2BS11ph with histone mark H3K4me3. To verify the ChIP sequencing results further, we were interested in carrying out immunoprecipitation reactions with mononucleosomes to determine the coexistence of histone mark H3K4me3 in a single nucleosome core particle. Therefore, we performed IP assays with mononucleosomes to prove the association of TH2BS11ph and H3K4me3 in the context of mononucleosomes. This interaction was also proved by IP assays, where co-IP with H3K4me3 antibody pulled down TH2BS11ph protein (Fig. 4f, H3K4me3 IP). Reciprocal IP also proves the association of H3K4me3 with TH2BS11ph-containing mononucleosomes (Fig. 4f, TH2BS11ph IP). Thus, we conclude that H3K4me3 is associated with TH2BS11ph-containing mononucleosomes.

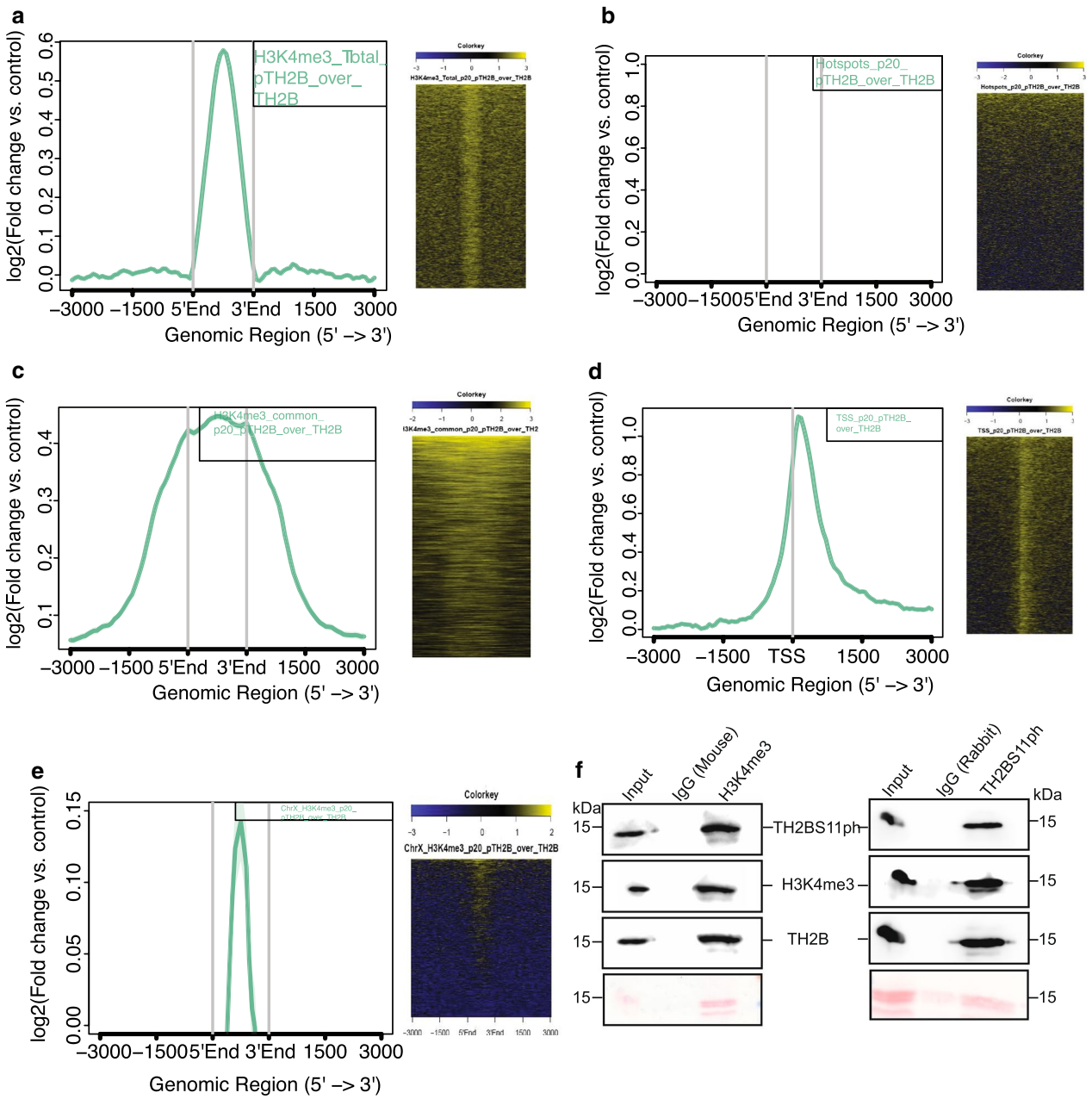

Fig. 4 Localisation of TH2BS11ph at TSS and recombination hotspots with respect to TH2B. **a** Analysis of overlap of TH2BS11ph with Total H3K4me3. **b** Analysis of overlap of TH2BS11ph with DSB hotspots. **c** Overlap of TH2BS11ph with H3K4me3 common peaks representing the TSS-associated H3K4me3 marks. **d** Localisation of TH2BS11ph at TSS. **e** Overlap of TH2BS11ph with Chromosome X-associated H3K4me3 marks. The aggregation plots in **a**–**e** show the read coverage of unique TH2BS11ph reads (compared against TH2B) at ± 3 kb from the centre of the particular histone or protein marks as indicated in the boxes in the top right corner. *Y*-axis represents log2(fold change of TH2BS11ph versus TH2B control), *X*-axis represents distance in terms of kilobases. The heat map in **a**–**e** is the corresponding representation of the read coverage at ± 3 kb from the centre of occupancy of candidate histone/protein marks. **f** Association of H3K4me3 and TH2BS11ph in mononucleosomes. Mononucleosome IP studies to determine the coexistence of TSS-related histone mark H3K4me3 with TH2BS11ph histone modification by forward (1st panel) and reverse IP reactions (2nd panel). Ponceau stained blots have been given for reference. The first lane in all the blots represents the Input, second lane immunoprecipitation with the Mouse IgG antibody, third lane refers to the IP using the specific antibody (anti-H3K4me3 or anti-TH2BS11ph). The antibodies labelled alongside the blot refer to the antibodies that were used for western blotting

TH2B is depleted from active TSS and present at background levels at recombination hotspots in mouse spermatocytes

TH2B replaces H2B on a genome-wide scale in spermatocytes and spermatids. Further, TH2B was previously reported to be depleted from transcriptionally active H2AZ-containing nucleosomes [12]. Since we have extensively proven the association of TH2BS11ph in the XY body and with TSS-associated H3K4me3, it became important to determine the level of backbone TH2B at those characteristic genomic loci like TSS and recombination hotspots. We observed that TH2B was present at background levels with respect to total H3K4me3 marks (Fig. 5a, first and second panels). We did not observe any specific enrichment of TH2B at recombination hotspots (Fig. 5b, first and second panels). Furthermore, the occupancy of TH2B reads was plotted against H3K4me3 common dataset, representing the TSS-related H3K4me3 marks; we did not find significant enrichment of TH2B in the proximity of TSS-specific H3K4me3 (Fig. 5c, first and second panels). We, therefore, reconfirmed the published dataset wherein we observe the depletion of TH2B at TSS regions; there was no preferential enrichment observed for TH2B at centre of known TSS genomic regions (Fig. 5d, first panel). Heat map also showed a characteristic depletion of TH2B reads at TSS regions (Fig. 5d, second panel). The important point to be noted is the read count per million mapped reads were plotted on the same scale as the observed TH2BS11ph levels at TSS and recombination hotspots. Taken together, we observe the specific enrichment of TH2BS11ph over TH2B at the H3K4me3-associated TSS regions. These analyses show that TH2BS11ph is preferentially enriched over TH2B in the XY body and H3K4me3-containing TSS regions.

Validation of the ChIP sequencing dataset by ChIP-PCR

For confirmation of the ChIP-sequencing dataset at selected loci, we designed primers for various chromosomal loci across the mouse genome. The genomic regions were determined for TH2BS11ph occupancy as can be in Fig. 6, in comparison to occupancy of backbone TH2B. The genomic regions with the TH2BS11ph and TH2B IP tracks that have been selected for experimental validation are shown in Fig. 6a. We have chosen two peaks from Chromosome X, one from Chromosome Y and two from autosomal regions for experimental validation (i–vii). By ChIP-PCR in P20 mouse testicular cells, we show the occupancy of TH2BS11ph at all the

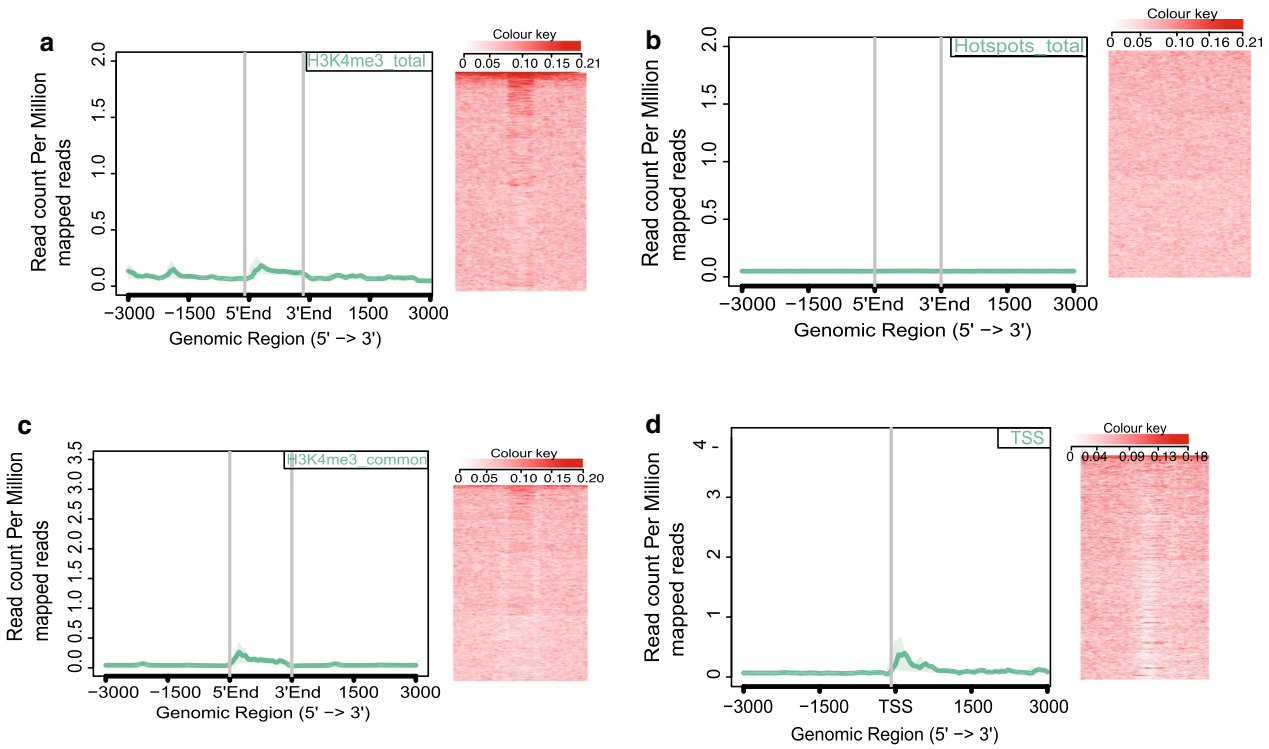

Fig. 5 Localisation of backbone TH2B at TSS and recombination hotspots. Analysis of overlap between backbone TH2B with **a** total H3K4me3, **b** DSB hotspots, **c** H3K4me3 common representing the TSS-specific H3K4me3 marks. TH2B does not display preferential localization towards H3K4me3 (total), DSB hotspots and TSS-associated H3K4me3 histone marks. **d** Analysis of overlap of backbone TH2B with TSS of mouse. TH2B was observed to be depleted at TSS regions [12]. In each figure from **a**–**d**; the overlap has been determined using Aggregation plots and heat maps

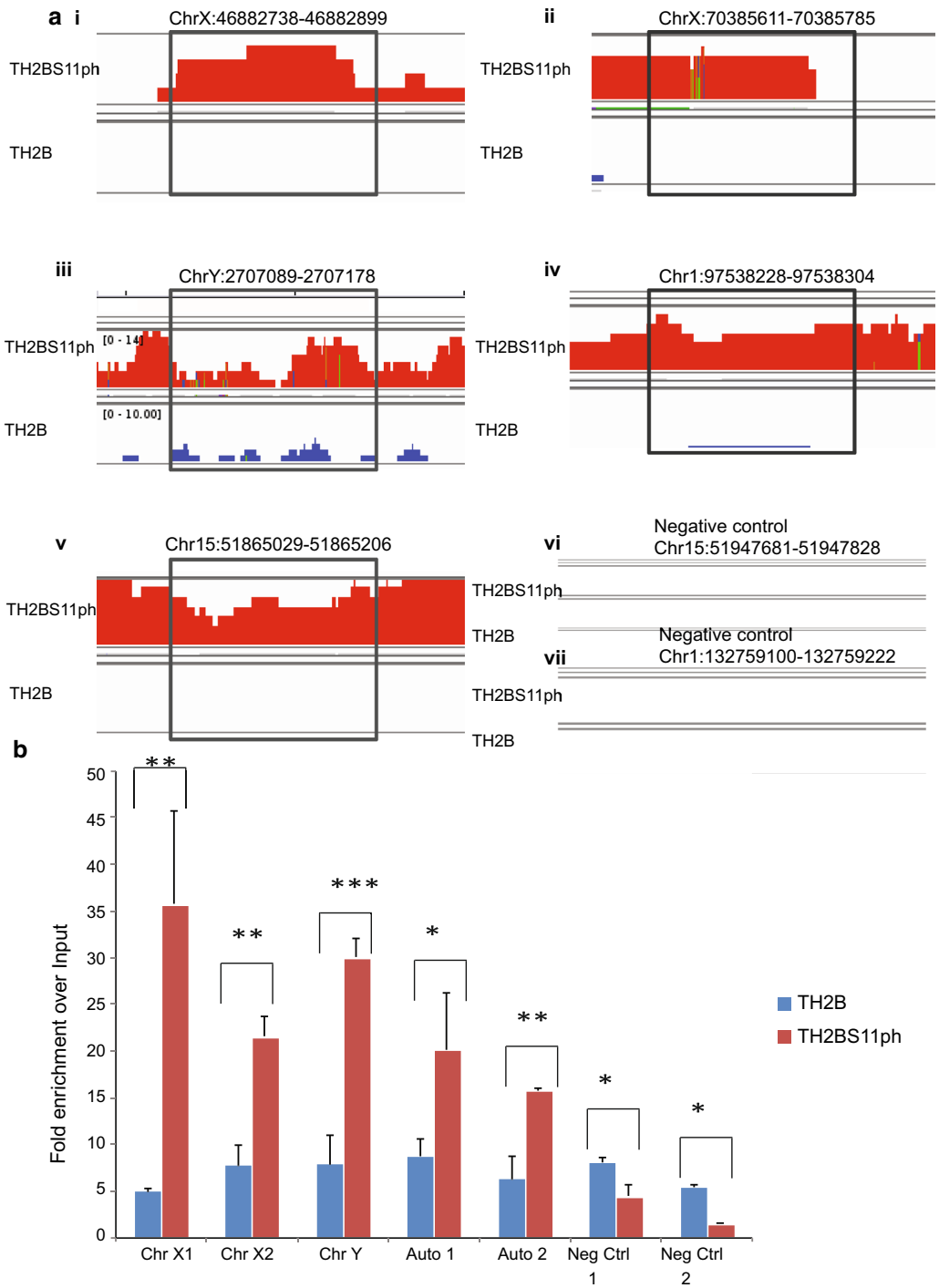

Fig. 6 Validation of the ChIP sequencing dataset of TH2BS11ph in mouse P20 testicular cells. **a** Genomic regions used for designing primers required to confirm the ChIP-sequencing dataset by ChIP-PCR studies. Every top lane in all the panels from (i)–(vii) is TH2BS11ph IP, bottom panel-TH2B IP. **b** Validation of TH2BS11ph genome-wide occupancy data using ChIP-PCR technique using TH2B and TH2BS11ph antibodies. ChIP-PCR shows the enrichment of TH2BS11ph histone mark at the selected genomic regions associated with Chromosome X (2 regions), Chromosome Y and autosomes (2 regions) over TH2B IP and input control (i–v). A specific region in chromosome 15 and chromosome 1 were used as negative controls for this study (vi and vii). The fold enrichment values of TH2B and TH2BS11ph IPs were plotted against input control. ChIP-PCR experiments were done for three biological replicates including technical duplicates for a single biological replicate. The data are plotted in terms of mean ± SD, $^{***}P \leq 0.0005$, $^{**}P \leq 0.005$, $^{*}P \leq 0.05$ (*t*-test)

selected genomic regions, further validating the ChIP-seq results (Fig. 6b, ChrX1, ChrX2, ChrY, Auto1 and Auto2). Our main aim was to determine unique peaks of TH2BS11ph occupancy by comparing against the occupancy of backbone TH2B. TH2B ChIP was used as additional control to determine the occupancy of backbone TH2B at these genomic regions. We observe the specific enrichment of TH2BS11ph over TH2B as well as input control at all the selected genomic regions (Fig. 6b, ChrX1, ChrX2, ChrY, Auto1 and Auto2). There was no significant enrichment of TH2BS11ph over TH2B control in the selected regions of chromosomes 15 and 1 that were used as negative controls (Fig. 6b, Neg Ctrl 1 and Neg Ctrl 2).

TH2BS11ph modification is associated with key proteins related to XY body and transcription

Since TH2BS11ph is a nucleosomal histone protein, we were interested to determine the proteins that are associated with TH2BS11ph-containing mononucleosomes. To address this question, we performed mass spectrometry of the immunoprecipitated mononucleosomes using TH2BS11ph antibodies. We have again validated the specificity of the TH2BS11ph antibody, where we demonstrate that the TH2B Serine 11 phosphopeptide competes with the antibody in the immunoprecipitation (Additional file 5: Fig. S5B). The proteins were identified on the basis of enrichment of immunoprecipitated proteins with respect to those in non-specific pre-immune IgG lane (Fig. 7a). Mass spectrometric analyses revealed key proteins associated with the functions of XY body and transcription as shown in Fig. 7b further revalidating the ChIP-seq results where we observed the predominant association of TH2BS11ph with important genomic regions related to XY body and transcription.

Smarca5 is known to regulate Tyr142 phosphorylation on H2AX. It also associates with Cer2 to regulate gene expression. It was identified as the interacting protein partner of γH2AX [48]. Scml2, a germline specific subunit of Polycomb complex, is involved in epigenetic reprogramming of sex chromosomes [49]. Scml2 also promotes heterochromatin organisation in post-meiotic spermatids, by regulating the localization of CENP-V at pericentric heterochromatin [50]. Remodelling of the sex chromosomes is brought about by replacement of H3 by H3.3 wherein DSB proteins and chromatin remodelers act in sync to bring about MSCI induced nucleosome replacement [51]. Mre11 is a part of MRN complex associated with DSB events in the XY body [52]. Consistent with the localization of TH2BS11ph in the XY body, many proteins associated with the XY body functions like Scml2 [49, 50], Cbx1 [53], macroH2A [54], H2AX [42], H3.3 [51] were identified in the mass spectrometric analyses. Apart from this, chromosomal axes proteins like HORMAD1 that are involved in checkpoint surveillance required for meiotic progression [55] is also associated with TH2BS11ph mark. HORMAD1 preferentially is localised to unsynapsed chromosomes during the prophase I of meiosis [56]. It is also known that Cbx1/HP1β and macroH2A are co-associated with the PAR region of the XY body during male meiosis [57]. This reconfirms the association of TH2BS11ph with the XY body as both these proteins also shown to interact with TH2BS11ph-containing mononucleosomes.

H2AZ-containing nucleosomes are sites of transcription activation [58]. The fact that TH2BS11ph associates with proteins like SWI/SNF complex members, Trim28, H3.3, H2AZ, etc. establishes the fact that the TH2BS11ph-containing nucleosomes are also TSS associated. Synaptonemal complex proteins like Scp1, Scp2 and Scp3 were found to be associated with TH2BS11ph mononucleosomes [59–65]. Synaptonemal complex proteins are implicated in proper crossover formation and completion of meiosis [66]. Trim28 is known to associate with Brdt to mediate transcriptional repression in spermatogenic cells [67]. Npm1 is a known histone chaperone. In this list, we also obtained core nucleosomal histones, thus serving as internal control for the isolation of mononucleosomes.

In comparison to the proteins that were shown to be associated with γH2AX-containing nucleosomes in

(See figure on next page.)

Fig. 7 Determination of interacting protein partners of TH2BS11ph-containing mononucleosomes in rat testicular cells. **a** Silver-stained image of the TH2BS11ph ChIP-Input lane refers to 5% input; IgG lane refers to non-specific IgG control; TH2BS11ph refers to TH2BS11ph IP lane. **b** List of interacting proteins of TH2BS11ph-containing mononucleosomes as determined by mass spectrometry in rat testicular cells. The associated proteins are classified into three different categories based on their known functions: XY body, Transcription and other important proteins. The first row is the gene/protein name; the second row refers to the sum intensity that refers to the peak intensity values for all the peptides matched to a particular protein. The proteins highlighted in red refer to common proteins identified between TH2BS11ph IP and γH2AX IP (as reported by Broering et al. [48]). **c** Model of TH2BS11ph-containing nucleosomes showing the association with XY body-related histone marks. TH2BS11ph could function along with γH2AX and H3K4me3 histone marks to mediate DNA repair in the XY body. **d** Model of TH2BS11ph-containing nucleosomes showing the association of this histone mark with transcription start sites. TH2BS11P could associate with H3K4me3, H2AZ and transcription-associated H4 acetylated marks to mediate transcription in pachytene cells. TH2BS11ph could function in association with specific repertoire of histone marks to mediate chromatin-templated events like DNA repair in the XY body or TSS activation

a

b

List of proteins identified	Sum Intensity
XY body associated	
Smarca5	7,40E+06
Scml2	3.90E+06
HP1BP3	2.10E+07
H3F3b	3.30E+07
Parp1	4.30E+06
Mre11a	4.50E+05
H2afx	2.30E+07
Hormad1	5.50E+05
Cbx1	2.40E+05
Chd5	4.00E+05
Baz1b	8.50E+04
H2afy2	1.60E+05
Transcription	
Trim28	5.40E+05
Smarcd2	5.40E+05
Smarcc1	7.60E+05
Smarcb1	1.00E+06
Smarca4	5.80E+05
Smarcc2	9.70E+05
Brd7	8.70E+04
Smarca2	1.50E+05
H2afZ	8.30E+06
Other proteins	
Hist1h4b	3.70E+09
Sycp3	1.50E+07
Glyr1	4.10E+06
TH2B	8.20E+07
Npm1	2.60E+06
Top2a	4.50E+05
Baz1a	9.90E+05
Sycp2	6.70E+05
Syce1	5.10E+05
Chd5	4.00E+05
Hist3h2ba	1.30E+06
Trip12	1.30E+06

c

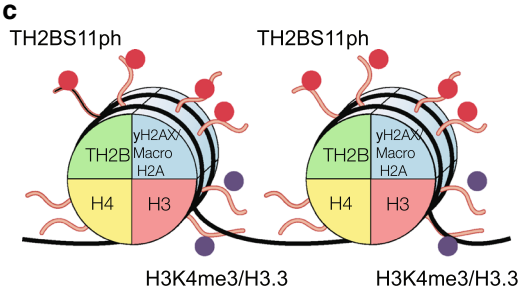

DNA repair associated chromatin domains in the XY body.

d

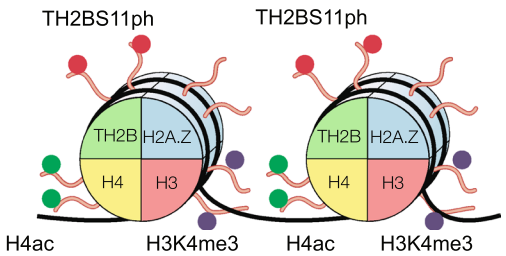

TSS associated chromatin domains.

- Phosphorylation
- Acetylation
- Methylation

another report [48], we find that many proteins (highlighted in red) were common and also associated with TH2BS11ph-containing mononucleosomes (Fig. 7b). This suggests that both these histone marks associate with similar set of protein players in spermatocytes. The important point we would like to stress here is that TH2BS11ph histone mark also associates with proteins related to transcriptional regulation as shown by mass spectrometry. This indicates that TH2BS11ph associates with different set of protein machineries in turn regulating different loci in a context-dependent manner. Taken together, a recurrent theme that emerges from our study is that the histone mark TH2B Serine 11 phosphorylation is densely localised in the unsynapsed axes of the XY body, predominantly associate with H3K4me3-containing genomic regions and also associate with protein players involved in processes of XY body and transcription-related processes.

Discussion

TH2B, a testis-specific histone variant, globally replaces somatic histone H2B in mammalian spermatocytes and spermatids [12]. Although, the biological function of TH2B has been delineated in spermatids in the context of histone to protamine transition, very little is known about its role in spermatocytes. The major differences between TH2B and its somatic counterpart H2B, is the sequence variation in the N-terminus tail. Histone tails do not exhibit specific structures in high-resolution crystal structures. However, they contribute to stabilisation of chromatin through contacts with DNA backbone and acidic patch of adjacent nucleosomes. Tail domains also provide the stabilisation effect by suppressing the accessibility of the DNA and regulating nucleosome mobility [68, 69]. The present study was initiated to explore the possible biological function(s) of the N-terminus of TH2B and associated histone modifications particularly with respect to the biological functions in spermatocytes. We have recently described the complete repertoire of TH2B PTMs from pachytene spermatocytes and round spermatids [16]. Our revisit to the mass spectrometric analysis of TH2B PTMs using a modified procedure of enzyme procedure and processing of peptides revealed Serine 11 phosphorylation on TH2B. This TH2BS11ph histone mark was reported by Luense et al. [36] only in round spermatids, but not in spermatocytes. This serine is highly conserved in TH2B of most of the mammals suggesting possible role(s) in germ cells. Our present study describes our detailed analysis of TH2BS11ph modification towards our understanding the biological function in the context of processes characteristic of meiotic prophase I in rodent spermatocytes.

TH2BS11ph and the XY body

One of the major observations of the present study is the enrichment of TH2BS11ph in the axes of the XY body in pachytene spermatocytes as evidenced by both immunostaining pattern as well as ChIP-seq analysis. The key biological events that occur in the XY body are late DSB repair and heterochromatin formation. Based on the observation that TH2BS11ph is co-associated with γH2AX as demonstrated by immunolocalization as well as pull down experiments, we would like to believe that TH2BS11ph is associated with chromatin domains undergoing DSB repair in the XY body. This conclusion is also supported by the fact that somatic H2BS14ph has been shown to be associated with DNA repair chromatin domains in somatic cells [40]. The intense staining in the axes of the XY body could be due to increased DSB density that occurs in the PAR (Pseudo-Autosomal Region) of the XY body as compared to autosomal DSBs [31]. Importantly, a specialised chromatin configuration is found in the XY body wherein chromatin is organised into larger axes and shorter loops promoting higher DSB density. The fact that TH2BS11ph associated proteins also share similar protein interactome with γH2AX proteins [48] provides further support for our hypothesis that TH2BS11ph is associated with DNA repair domains within the XY body. It is also interesting to note that we also observed that several proteins associated with heterochromatinization were also present in the TH2BS11ph associated mononucleosomes like Scml2, macroH2A, HP1β, HP1γ, etc. Our studies also show the association of TH2BS11ph with X-chromosome-specific H3K4me3 marks. It is known that H3K4me3 catalysed in the PAR of the XY body is PRDM9 independent. This raises the question as to which kinase(s) is(are) responsible for the formation of TH2BS11ph-associated H3K4me3 mark. Taken together, these results strongly suggest that TH2BS11ph is an important histone mark associated with XY body-specific DSB repair and subsequent heterochromatinization. TH2BS11ph along with specific histone marks like H3K4me3, γH2AX, macroH2A could contribute to these specialised chromatin structure in the XY body, thus contributing to recombinational repair and heterochromatinization in the XY body (Fig. 7c).

TH2BS11ph and transcription

Another major observation made in the present study is the association of TH2BS11ph with H3K4me3 mark. H3K4me3 has strong association with promoters, enhancers and meiotic recombination hotspots. The factors that determine selection of hotspots versus transcription start sites are the specific enzymes that catalyse the creation of H3K4me3 marks. PRDM9

catalyses H3K4me3 and H3K36me3 formation at recombination hotspots, whereas the enzyme(s) responsible for H3K4 trimethylation at transcription start sites in spermatocytes is(are) speculated to be SET/MLL enzymes [70].

Genomic-occupancy overlap studies using aggregation plots and heat maps obtained from ChIP-seq experiments in P20 testicular cells (pachytene) demonstrated the specific association of TH2BS11ph reads with TSS-specific H3K4me3 marks, but not the hotspot-related H3K4me3 marks. This was also proved by forward and reciprocal IP assays where we show the co-association of TH2BS11ph with H3K4me3 mark in vivo. This co-association with H3K4me3-positive TSS-associated genomic regions were also found to be true in P12 testicular cells (leptotene). It is quite likely that punctuate staining of TH2BS11ph observed outside the XY body in pachytene nuclei might correspond to transcriptional active chromatin domains. The association of TH2BS11ph with H3K4me3 marks within TSS is further demonstrated by the association of transcription-associated proteins like H2AZ, H3.3, SWI SNF complex members with the TH2BS11ph immunoprecipitated mononucleosomes as revealed by our mass spectrometric analysis. Taken together, we have demonstrated the strong association of TH2BS11ph with TSS-specific chromatin domains and histone mark H3K4me3 in vivo in pachytene spermatocytes.

As mentioned earlier, the N-terminal domain of H2B is involved in stabilisation and mobilisation of nucleosomes. In addition to the N-terminal tail, the HBR (Histone H2B Repression) domain in H2B (30–37 amino acid residues) is also involved in transcriptional repression. Acetylation of the lysine residues within HBR domain is shown to relieve the repression phenomenon and also facilitate transcription [71]. Our present study shows for the first time that phosphorylation of serine 11 in TH2B to be strongly associated with TSS mononucleosomes in pachytene spermatocytes. It remains to be seen whether serine 14 phosphorylation in somatic histone H2B is also associated with transcription in somatic cells. This is quite possible since the N-terminal is not structured and hence serine 11 phosphorylation in TH2B and serine 14 may have similar functions. Alternatively, the function of TH2B serine 11 phosphorylation may be unique to spermatocyte transcription.

In conclusion, we have demonstrated that TH2BS11ph is associated with two important chromatin functions in spermatocytes—(i) TH2BS11ph is associated with DNA repair domains in the XY body as evidenced by association of TH2BS11ph with repair proteins and histone marks of the XY body (Fig. 7c), (ii) TH2BS11ph could function with H3K.4me3-mediated recruitment of effector proteins and chromatin modellers in regulation of transcription at TSS (Fig. 7d). We would like to point out that the mass spectrometric analysis of proteins associated with TH2BS11ph-containing mononucleosomes and co-existence of H3K4me3, γH2AX by IP assays reflects the average picture of the protein complexes associated with all the TH2BS11ph-containing chromatin domains. Loci-specific recruitment of particular effector molecules, and therefore reprogramming could occur to fine-tune chromatin structure and function at those loci. TH2BS11ph could, therefore, play an important role in creation of chromatin environment along with other histone mark signatures to create platform for XY body and transcription-related functions.

Conclusions

By immunofluorescence assays with the highly specific antibodies, we demonstrate that TH2BS11ph histone mark is densely localised in the unsynapsed axes of the XY body in pachytene spermatocytes. Genome-wide occupancy of TH2BS11ph histone mark as determined by ChIP sequencing assays further confirmed the localisation of this modification in the X and Y chromosomes. Apart from this, TH2BS11ph is also associated with H3K4me3-containing TSS-associated chromatin domains in P20 (pachytene) and P12 (leptotene) mouse testicular cells. Mass spectrometric analysis of proteins revealed various key proteins linked to functions of the XY body and transcription associated with TH2BS11ph-containing mononucleosomes.

Materials and methods

Materials

All fine chemicals were obtained from Sigma Chemicals (USA) unless mentioned otherwise. Synthetic peptides were outsourced from Stork Bio Laboratories (Estonia). The secondary antibodies Donkey anti-mouse, Goat anti-rabbit, Goat anti-rabbit conjugated to Alexa dyes were obtained from Invitrogen (USA). Male Wistar rats and C57BL6 mice were obtained from the Animal Facility, JNCASR. All procedures for handling animals have been approved by the animal ethics committee of the Centre.

Generation of TH2B-containing nucleosome model

The nucleosome models have been taken from the previous work of our lab by Pentakota et al. [16].

Purification of in vivo TH2B protein

Histones were isolated from 30- to 35-day-old rat testes by acid extraction method. In vivo TH2B were purified by RP-HPLC technique using the published protocol [16].

Mass spectrometry for identification of posttranslational modifications on TH2B

In-gel digestion

Gel bands were cut into one-mm^3 pieces and washed twice with MilliQ water. The gel was destained using 1:1 methanol: 50-mM ammonium bicarbonate for 1 min, twice. The gel pieces were dehydrated for 5 min using 1:1 acetonitrile: 50-mM ammonium bicarbonate followed by acetonitrile for 30 s. The gel pieces were dried in a speed-vac (Thermo Savant) for 10 min. The gel pieces were rehydrated in 25-mM dithiothreitol, 50-mM ammonium bicarbonate and incubated at 56 °C for 20 min. After discarding the supernatant, the gel pieces were incubated in 55-mM iodoacetamide at RT for 20 min in the dark and subsequently were washed twice with water, dehydrated and dried as before. The dried gel pieces were rehydrated in 50-mM ammonium bicarbonate containing 250 ng of mass spectrometry grade trypsin (Promega) and incubated overnight at 37 °C. Following digestion, the reaction mixture was acidified with 1% acetic acid and dried in a speed-vac to reduce the volume to 5 µl, to which 10 µl of mobile phase A was added for direct loading for LC–MS/MS analysis.

Liquid chromatography–tandem mass spectrometry

Each reaction mixture was analysed by LC–MS/MS. LC was performed on a Easy nanoLC II HPLC system (Thermo Fisher Scientific). Mobile phase A was 94.5% MilliQ water, 5% acetonitrile, 0.5% acetic acid. Mobile phase B was 80% acetonitrile, 19.5% MilliQ water, 0.5% acetic acid. The 120-min LC gradient ran from 2% B to 35% B over 90 min, with the remaining time used for sample loading and column regeneration. Samples were loaded to a 2 cm × 100 µm I.D. trap column positioned on an actuated valve (Rheodyne). The column was 13 cm × 100 µm I.D. fused silica with a pulled tip emitter. Both trap and analytical columns were packed with 3.5 µm C18 resin (Zorbax SB, Agilent). The LC was interfaced to a dual pressure linear ion-trap mass spectrometer (LTQ Velos, Thermo Fisher) via nano-electrospray ionisation. An electrospray voltage of 1.8 kV was applied to a pre-column tee. The mass spectrometer was programmed to acquire, by data-dependent acquisition, tandem mass spectra from the top 15 ions in the full scan from 400 to 1400 m/z. Dynamic exclusion was set to 30 s.

Data processing and library searching

Mass spectrometer RAW data files were converted into MGF format using msconvert. Detailed search parameters are printed in the search output XML files. Briefly, all searches required strict tryptic cleavage, 0 or 1 missed cleavages, fixed modification of cysteine alkylation, variable modification of methionine oxidation and expectation value scores of 0.01 or lower. MGF files were searched using X! Hunter against the latest library available on the GPM at the time. Other searches used the cRAP contaminant library from the GPM and libraries constructed from the most recent ENSEMBL release available at the time. MGF files were searched using X!! Tandem using both the native and k-score5 scoring algorithms and by OMSSA. All searches were performed on Amazon Web Services-based cluster compute instances using the Proteome Cluster interface. XML output files were parsed, and non-redundant protein sets determined using in-house scripts. Proteins were required to have 2 or unique peptides with *E*-value scores of 0.01 or less, 0.001 for X!Hunter and protein *E*-value scores of 0.0001 or less.

Alignment of the amino acid sequences

Multiple sequence alignment (MSA) was performed for TH2B of selected mammals to elucidate the sequence conservation across species.

Antibody generation

Peptides corresponding to TH2BS11ph modification (CKGTTI(pS)KKGFK), H2B(KSRPAPKKGSK) were injected into rabbits, and the 14-day cycle of antibody generation was followed. Immunoglobulins were purified by caprylic acid based purification. Peptide-affinity-based purification with the Sulfolink columns containing immobilised peptides was used to purify the TH2BS11ph- and H2B-specific antibodies. The TH2B-S11ph antibody was outsourced from Abgenex company.

Preparation of nuclear lysates

Nuclear lysates were prepared by the method described previously with modifications [72]. Briefly, testes were dissected in cytoplasmic lysis buffer (10-mM HEPES pH 7.5, 50-mM NaCl, 0.5-M sucrose, 0.5% Triton-X-100, 0.1-mM EDTA, 1-mM DTT, protease inhibitor cocktail), incubated on ice for 15 min and centrifuged at 1500*g* for 7 min. The nuclear pellet was resuspended in Buffer B1 (10-mM HEPES pH 7.5, 500-mM NaCl, 0.1-mM EDTA, 1-mM DTT, 0.5% NP-40, protease inhibitor cocktail) to obtain nuclear lysates or Buffer B2 (10-mM HEPES, 200-mM NaCl, 1-mM EDTA, 0.5% NP-40, protease inhibitor cocktail) for isolation of chromatin. The nuclear lysates were clarified by centrifugation at 15,100×*g* for 10 min.

ELISA

Peptides were used at 200 ng per well. The pre-bleed and immune sera were used at 1:5000 dilution. Goat anti-rabbit HRP were used as the secondary antibody at 1:5000

dilution. TMB (3,3′,5,5′-tetramethylbenzidine) was used as the substrate for the reaction. After 3 min of enzyme–substrate reaction, the plate was read at 450 nm.

Preparation of meiotic spreads

Meiotic spreads were prepared using the published protocol [73]. Briefly, testes were decapsulated and chopped in PBS solution (pH 7.4). The cell pellet was resuspended in hypotonic buffer (30-mM Tris, 17-mM sodium citrate, 50-mM sucrose, 5-mM EDTA, 0.5-mM DTT, protease inhibitor cocktail) and incubated for 30 min. The pellet was resuspended in 100-mM sucrose solution, and the nuclei were spread onto PFA-coated slides. The slides were kept for drying at room temperature for 2 h and proceeded for immunofluorescence studies.

Immunofluorescence

The slides were kept in blocking solution (3% BSA solution in PBS) for 1 h at room temperature; then treated with primary antibody overnight in the cold room, washed with 0.1% PBST solution and then incubated with secondary antibody for 1 h at room temperature. Next, washes were given with PBST solution and the smears were mounted using DAPI solution. Images were acquired by Zeiss confocal laser scanning microscope (LSM880 or LSM510). Zen software was used for image analysis. Pearson Correlation Coefficient was computed to determine the overlap between the two channels. To evaluate specific colocalization, using ImageJ (Fiji) software, we rotated the red channel in the images by 90° in the anticlockwise direction in the XY plane. Pearson Correlation Coefficient was computed to evaluate colocalization percentages upon rotation of images captured in the red channel [74, 75]. Colocalization percentages were calculated multiplying the Pearson Correlation Coefficient by 100. All data were confirmed with at least three independent mice and rats.

Isolation of mononucleosomes

Immunoprecipitation using mononucleosomes was carried out as described [12]. Briefly, mouse testes were dissected and homogenised in lysis buffer (60-mM KCl, 15-mM NaCl, 15-mM Tris–HCl, 0.03% Triton-X-100, 0.34-M Sucrose, 2-mM EDTA, 0.5-mM EGTA, 0.65-mM spermidine, 1-mM DTT, 1% glycerol, protease and phosphatase inhibitor cocktail), centrifuged at 650×*g* for 10 min at 4 °C. The pellet was washed with wash buffer containing 60-mM KCl, 15-mM NaCl, 15-mM Tris–HCl, 0.34-M Sucrose, 0.5-mM EGTA, 1-mM DTT, 0.5-mM PMSF and protease and phosphatase inhibitor cocktail. The pellet was resuspended in MNase buffer (10-mM Tris–HCl, 10-mM KCl, and 2-mM $CaCl_2$). The nucleosome fraction was isolated by centrifugation at 650×*g* for 10 min at 4 °C, mixed with LSDB250 buffer (20% glycerol, 50-mM HEPES, 3-mM $MgCl_2$, 250-mM KCl, protease and phosphatase inhibitor cocktail) and proceeded with the immunoprecipitation protocol.

ChIP sequencing of TH2BS11ph modification-associated chromatin in P20 and P12 mouse testicular cells

DNA was isolated from TH2BS11ph immunoprecipitated mononucleosomes by phenol–chloroform method. The quality control of the DNA samples was done using the Qubit and Tapestation methods. The libraries were subjected for 40 million depth paired-end (100 bp × 2) sequencing that was carried using Illumina HiSeq 2500. FASTQ files were obtained and data analyses were carried out further.

Data analysis

FASTQ files were aligned to mm10 genome assembly using Bowtie2 [76]. While aligning, unpaired and discordant reads were removed. The aligned files were sorted and indexed accordingly, and also made free from PCR duplicates. On average for all samples, read-alignment rate appeared to be higher than 70%. Principal Component Analysis (PCA) was performed to evaluate the correlation between the aligned samples of each condition. The sorted aligned replicates of background TH2B and antibody-treated (IP) TH2BS11ph were merged, respectively, using Samtools Merge [70]. Unique peaks were obtained by performing the peak calling of TH2BS11ph data against the published backbone TH2B ChIP seq data. The peaks were called between the control and IP files using SICER 1.1 Version [77] with the following parameters—Redundancy threshold: 1; Window size: 200 bp; Fragment size: 150 bp; Gap size: 600 bp; FDR: 0.01. The final peaks were shortlisted giving the cutoff of > 1.5 fold change.

Aggregation plot (NGS plot)

ngs.plot.r [78] was used to plot read count per million mapped reads for each ChIP samples (P20 TH2BS11ph, background TH2B, P12 TH2BS11ph)individually against the genome-wide coordinates of the following datasets—total H3K4me3, common H3K4me3, transcription-specific H3K4me3, TSS, and Total hotspots. Furthermore, ngs.plot.r was also used to plot log2(Fold change vs. Control) of in-house ChIP-seq sample (P20 TH2BS11ph) over the background TH2B dataset for each of the following genome-wide coordinates of Total H3K4me3, common H3K4me3, transcription-specific H3K4me3 (H3K4me3 common), TSS, and Total DSB hotspots.

Primer design for ChIP-PCR studies

Peak summits corresponding to high TH2BS11ph occupancy were chosen for experimental validation using ChIP-PCR. To maintain the rigour of primer design, primers were designed using the Primer BLAST and primer 3 tools and were also verified computationally using NCBI Primer Blast and UCSC In-silico PCR. Verification of primer-dimer formation was also considered during the design (Additional file 6: Table S1).

Immunoprecipitation and quantitative PCR

The mononucleosome fraction was incubated with either anti-γH2AX (Upsate, 05-636) or anti-H3K4me3 (Abcam, ab12209) or anti-TH2BS11ph for overnight at 4 °C. Protein A or Protein G dynabeads were added the next day. LSDB250 buffer was used as the wash buffer for immunoprecipitation studies with mononucleosomes. After the washes, the beads were either proceeded with DNA extraction for PCR analysis or boiled in 5× SDS dye for western blotting. After washing of beads, DNA was eluted from the beads as follows—210 µl of the elution buffer was added, incubated at 65 °C overnight for de-crosslinking. 200 µl of TE buffer was added the next day, subjected for RNase (final; 40 µg/ml) and proteinase K (Final; 100 µg/ml) treatment and DNA were extracted by phenol–chloroform method. DNA that was purified from TH2BS11ph ChIP was proceeded for ChIP-seq analyses. SYBR kit from TAKARA was used to set up quantitative PCR reactions. PCR was carried out for 40 cycles and was followed by melt curve analyses before recording the raw Ct values. The fold enrichment values were calculated over input taking the percentage of input used for the ChIP procedure and the Ct values obtained for the target genomic region from Input and ChIP DNA. PCR was carried out in duplicates for each of the three biological replicates.

$$\text{Fold Enrichment over Input} = \%\ \text{of Input} \times 2^{[\text{Ct(Input)} - \text{Ct(ChIP)}]}$$

Mass spectrometric identification of interacting protein partners of TH2BS11ph-containing mononucleosomes

Immunoprecipitation of TH2BS11ph-containing proteins were carried out and the proteins were extracted from the beads using the elution buffer of the Pierce co-IP kit. The eluted proteins were resolved on 15% SDS gel and the gel was subjected to Coomassie staining. The stained wells corresponding to the IgG and IP lanes were outsourced for mass spectrometry to identify the interacting proteins.

Methods for protein sequence analysis by LC–MS/MS

Excised gel bands were cut into approximately 1-mm^3 pieces. Gel pieces were then subjected to a modified in-gel trypsin digestion procedure [79]. Gel pieces were washed and dehydrated with acetonitrile for 10 min. followed by removal of acetonitrile. Pieces were then completely dried in a speed-vac. Rehydration of the gel pieces was with 50-mM ammonium bicarbonate solution containing 12.5 ng/µl modified sequencing-grade trypsin (Promega, Madison, WI) at 4 °C. After 45 min., the excess trypsin solution was removed and replaced with 50-mM ammonium bicarbonate solution to just cover the gel pieces. Samples were then placed in a 37 °C room overnight. Peptides were later extracted by removing the ammonium bicarbonate solution, followed by one wash with a solution containing 50% acetonitrile and 1% formic acid. The extracts were then dried in a speed-vac (~1 h). The samples were then stored at 4 °C until analysis.

On the day of analysis the samples were reconstituted in 5–10 µl of HPLC solvent A (2.5% acetonitrile, 0.1% formic acid). A nano-scale reverse-phase HPLC capillary column was created by packing 2.6 µm C18 spherical silica beads into a fused silica capillary (100 µm inner diameter × ~30 cm length) with a flame-drawn tip [80]. After equilibrating the column, each sample was loaded via a Famos auto sampler (LC Packings, San Francisco CA) onto the column. A gradient was formed and peptides were eluted with increasing concentrations of solvent B (97.5% acetonitrile, 0.1% formic acid).

As peptides eluted, they were subjected to electrospray ionisation and then entered into an LTQ Orbitrap Velos Pro ion-trap mass spectrometer (Thermo Fisher Scientific, Waltham, MA). Peptides were detected, isolated, and fragmented to produce a tandem mass spectrum of specific fragment ions for each peptide. Peptide sequences (and hence protein identity) were determined by matching protein databases with the acquired fragmentation pattern by the software programme, Sequest (Thermo Fisher Scientific, Waltham, MA) [81]. All databases include a reversed version of all the sequences and the data was filtered to between a one and two percent peptide false discovery rate along with filter to being set to at least 1 unique peptide per protein (Additional file 7: Table S2).

Dot-blot analysis

Two µg of peptides corresponding to TH2B (CKGTTISKKGFK), TH2BS11ph (CKGTTI(pS)KKGFK),H2B(KSRPAPKKGSK),H2BS14ph(SRPAPKKG(pS)KKC) was applied as separate spots on the nitrocellulose membrane. After drying, the blot was subjected to steps of western blotting with the TH2BS11ph antibody.

Western blot analysis

For western blot, proteins were resolved by SDS-PAGE gel electrophoresis and then transferred onto

a nitrocellulose membrane using the semi-dry transfer technique. The membrane was blocked using 5% skimmed milk or 3% BSA (diluted in TBS) for 1 h at room temperature, then incubated with the specific primary antibody for 1 h at room temperature or overnight at 4 °C. The blots were given multiple washes with 0.1% PBST or TBST for 10 min each. Next, the blot was incubated with the secondary antibody (anti-rabbit/anti-mouse) for 1 h at room temperature. Membranes were washed extensively with 0.1% PBST or TBST and developed using the ECL kit (Thermo Scientific). For the peptide competition assay, 50-fold molar excess of the modified and unmodified peptides were added to the antibody solution and mixed for 3 h at 4 °C before the addition to the blot.

Supplementary information

Supplementary information accompanies this paper at https://doi.org/10.1186/s13072-019-0300-y.

Additional file 1: Figure S1. Validation of H2B-specific antibody. H2B antibody was successfully generated in rabbits and the staining pattern was found to not coincide with the XY body in the pachytene spermatocyte. **A** Fragmentation table for the PTM serine 11 phosphorylation obtained on TH2B. **B** Dot-blot assay demonstrating the specificity of TH2BS11ph antibody wherein we show the specificity of the antibody towards the serine 11 phosphopeptide but does not cross-react with backbone TH2B, backbone H2B or H2B Serine 14 phospho peptide. **C** Specificity of the commercial H2BS14ph antibody as shown by immunoblotting against liver histones, testis histones and HPLC-purified in vivo TH2B (labelled 'in vivo TH2B'). This antibody cross-reacts with TH2B as can be seen by its reactivity towards testis nuclear lysates and in vivo TH2B. **D** Validation of H2B antibody by dot-blot [first panel]; the first lane represents reactivity of the H2B with the non-phosphorylated H2B peptide, second lane represents reactivity with the serine 14 phosphorylated H2B peptide. Immunoblotting of H2B antibody against liver histones, testis histones and in vivo TH2B [Second panel]. **E** Immunostaining of anti-H2B and anti-Scp3 antibodies across the three stages of meiotic prophase I-leptotene, zygotene and pachytene intervals. Nuclei were visualised by DAPI staining, Scale bars, 10 µm.

Additional file 2: Figure S2. Colocalization studies of TH2BS11ph with Scp3, γH2AX, Rad51, pATM and Spo11 in rat pachytene spermatocytes. TH2BS11ph colocalizes with Scp3, γH2AX, Spo11, Rad51 and pATM in rat pachytene spermatocytes, a clear colocalization seen in axes of the XY body. **A** Colocalization studies of TH2BS11ph with Scp3 across leptotene (1st panel), zygotene (2nd panel) and pachytene (3rd panel) intervals in meiotic spreads in rats. **B** Colocalization studies of TH2BS11ph with γH2AX in rat spermatocytes in pachytene spermatocytes in rat meiotic spreads. **C** Colocalization studies of TH2BS11ph with Rad51 in pachytene stage of rat spermatocytes. **D** Immunofluorescence studies of TH2BS11ph with pATM in pachytene spermatocyte of rat. **E** Immunofluorescence studies of TH2BS11ph with Spo11 in pachytene spermatocyte of rat. The inset in all the figures shows the XY body in all the pachytene cells. All data were confirmed with at least three independent rats. Nuclei were visualised by DAPI staining, Scale bars, 10 µm.

Additional file 3: Figure S3. Read distribution of TH2BS11ph histone mark at TSS and recombination hotspots in mouse P20 testicular cells. Read Profile of TH2BS11ph at TSS and recombination hotspots in P20 testicular cells. Read distribution of TH2BS11ph at **A** Centre of total H3K4me3 marks; **B** DSB hotspots; **C** TSS-associated H3K4me3, **D** Total TSS of mouse obtained from UCSC; **E** Chromosome X-specific H3K4me3;. The read distribution was plotted in terms of aggregation plots (first panels in Fig (**A**–**D**) and heat maps (second panels in Fig (**A**–**D**). *X*-axis in all the aggregation plots represents read count per million mapped reads whereas *Y*-axis represents the distance from the centre of the reference peak in kilobase pairs (kb).

Additional file 4: Figure S4. Read distribution of TH2BS11ph histone mark at TSS and recombination hotspots in mouse P12 testicular cells. Genome-wide occupancy of TH2BS11ph modification in P12 testicular cells. **A** Aggregation plot and Heat map for analysis of overlap of TH2BS11ph with Total H3K4me3; **B** Aggregation plot and Heat map for determining localisation of TH2BS11ph at DSB hotspots; **C** Aggregation plot and Heat map for analysis of overlap of TH2BS11ph at H3K4me3 associated TSS, **D** Aggregation plot and Heat map for analysis of association of TH2BS11ph at Transcription Start Sites (TSS) of mouse. *X*-axis in all the aggregation plots represents read count per million mapped reads whereas *Y*-axis represents the distance from the centre of the reference peak in kilobase pairs (kb).

Additional file 5: Figure S5. Pattern of digestion of DNA fragments obtained after MNase digestion of chromatin of mouse testicular cells. **A** Profile of chromatin fragments obtained after MNase digestion for various time points in mouse testes; **B** Specificity of TH2BS11ph antibody in the immunoprecipitation reaction—the first lane refers to input fraction, the second lane refers to IP with non-specific rabbit IgG; the third lane refers to the TH2BS11ph containing ChIP fraction whereas the fourth lane refers to TH2BS11ph IP carried out along with the addition of competing TH2B serine 11 phosphopeptide.

Additional file 6: Table S1. Table of primer sequences.

Additional file 7: Table S2. Table of Mass spectrometry dataset.

Additional file 8: Table S2. ChIP-seq dataset [P20]. TH2BS11ph ChIP sequencing peaks (called over TH2B dataset) in P20 mouse testicular cells.

Additional file 9: Table S3. ChIP-seq dataset [P12]. TH2BS11ph ChIP sequencing peaks (called over TH2B dataset) in P12 mouse testicular cells.

Abbreviations

DDR: DNA damage response; ATM: ataxia-telangiectasia-mutated; ATR: ataxia telangiectasia and Rad3-related; PRDM9: PR domain-containing protein 9; Smarca5: SWI/SNF-related, matrix-associated, actin-dependent regulator of chromatin, subfamily A, member 5; Scml2: sex comb on midleg-like protein 2; Mre11: meiotic recombination 11; Cbx1: chromobox protein homolog 1; HORMAD1: HORMA (Hop1, Rev7 and Mad2) domain-containing protein 1; Brdt: bromodomain, testis-specific.

Acknowledgements

We thank Dr. Brian Balgely of Bioproximity for mass spectrometry. We acknowledge Dr. R.G Prakash of the Animal Facility and Suma B.S with Sunil Kumar of the Confocal Imaging Facility at JNCASR. We also thank members of the Imgenex facility for carrying out the antibody generation project. We also thank Tomaino Ross of TAPLIN Mass spectrometry facility at Harvard for mass spectrometry-based identification of interacting proteins.

Authors' contributions

IAM, SP, RR performed the experiments. IAM, SP and MRS designed the experiments and wrote the manuscript. UB performed the computational data analysis associated with the ChIP seq datasets. All authors discussed the results. All authors read and approved the final manuscript.

Funding

M.R.S. Rao thanks Department of Science and Technology, Government of India for SERB Distinguished Fellowship and this work was financially supported by Department of Biotechnology, Govt. of India (Grant Numbers: BT/01/COE/07/09 and DBT/INF/22/SP27679/2018).

Availability of data and materials

The ChIP-sequencing dataset containing the raw and processed files have been deposited in the Gene Expression Omnibus (Accession Number—GSE135209) (Additional file 8: Table S3 and Additional file 9: Table S4).

Ethics approval and consent to participate
This work was approved by the Animal Ethics Committee of JNCASR, Bangalore, India.

Consent for publication
Not applicable.

Competing interests
The authors declare that they have no competing interests.

Author details
[1] Molecular Biology and Genetics Unit, Jawaharlal Nehru Centre for Advanced Scientific Research, Jakkur PO., Bangalore 560064, India. [2] Novo Nordisk Foundation Center for Protein Research, Faculty of Health and Medical Sciences, University of Copenhagen, Blegdamsvej 3B, 2200 Copenhagen, Denmark. [3] The Graduate School of the Stowers Institute for Medical Research, 1000E. 50th St., Kansas City, MO 64110, USA.

Received: 26 May 2019 Accepted: 22 August 2019
Published online: 07 September 2019

References

1. Rao MRS, Rao BJ, Ganguly J. Localization of testis-variant histones in rat testis chromatin. Biochem J. 1982;205:15–21.
2. Sassone-corsi P. Unique chromatin remodeling and transcriptional regulation in spermatogenesis. Science. 2002;296:2176–8.
3. Govin J, Caron C, Lestrat C, Rousseaux S, Khochbin S. The role of histones in chromatin remodelling during mammalian spermiogenesis. Eur J Biochem. 2004;271:3459–69.
4. Pradeepa MM, Rao MR. Chromatin remodeling during mammalian spermatogenesis: role of testis specific histone variants and transition proteins. Soc Reprod Fertil Suppl. 2007;63:1–10.
5. Kwak H, Dohmae N. Proteomic characterization of histone variants in the mouse testis by mass spectrometry-based top-down analysis. BioSci Trends. 2016;10:357–64.
6. Hoghoughi N, Barral S, Varghas A, Rousseaux S, Khochbin S. Histone variants: essential actors in male genome programming. J Biochem. 2018;163:97–103.
7. Ueda J, Harada A, Urahama T, Machida S, Maehara K, Hada M, Makino Y, Nogami J, Horikoshi N, Osakabe A, et al. Testis-specific histone variant H3t gene is essential for entry into spermatogenesis. Cell Rep. 2017;18:593–600.
8. Shinagawa T, Huynh LM, Takagi T, Tsukamoto D, Tomaru C, Kwag HG, Dohmae N, Noguchi J, Ishii S. Disruption of Th2a and Th2b genes causes defects in spermatogenesis. Development. 2015;142:1287–92.
9. Talbert PB, Ahmad K, Almouzni G, Ausio J, Berger F, Bhalla PL, Bonner WM, Cande WZ, Chadwick BP, et al. A unified phylogeny-based nomenclature for histone variants. Epigenet Chromatin. 2012;5:7.
10. Kumaroo KK, Jahnke G, Irvin JL. Changes in basic chromosomal proteins during spermatogenesis in the mature rat. Arch Biochem Biophys. 1975;168:413–24.
11. Meistrich ML, Bucci LR, Trostle-Weige PK, Brock WA. Histone variants in rat spermatogonia and primary spermatocytes. Dev Biol. 1985;112:230–40.
12. Montellier E, Boussouar F, Rousseaux S, Montellier E, Rousseaux S, Zhang K, Buchou T, et al. Chromatin-to-nucleoprotamine transition is controlled by the histone H2B variant TH2B. Genes Dev. 2013;27:1680–92.
13. Rao BJ, Brahmachari SK, Rao MR. Structural organization of the meiotic prophase chromatin in the rat testis. J Biol Chem. 1983;258:13478–85.
14. Rao BJ, Rao MRS. DNase I site mapping and micrococcal nuclease digestion of pachytene chromatin reveal novel structural features. J Biol Chem. 1987;262:4472–6.
15. Li A, Maffey AH, Abbott WD, Conde e Silva N, Prunell A, Siino J, Churikov D, Zalensky AO, Ausio J. Characterization of nucleosomes consisting of the human testis/sperm-specific histone H2B variant (hTSH2B). Biochemistry. 2005;44:2529–35.
16. Pentakota SK, Sandhya S, Sikarwar AP, Chandra N, Rao MRS. Mapping post-translational modifications of mammalian testicular specific histone variant TH2B in tetraploid and haploid germ cells and their implications on the dynamics of nucleosome structure. J Proteome Res. 2014;13:5603–17.
17. Strahl BD, Allis CD. The language of covalent histone modifications. Nature. 2000;403:41–5.
18. Kouzarides T. Chromatin modifications and their function. Cell. 2007;128:693–705.
19. Lu S, Xie YM, Li X, Luo J, Shi XQ, Hong X, Pan YH, Ma X. Mass spectrometry analysis of dynamic post-translational modifications of TH2B during spermatogenesis. Mol Hum Reprod. 2009;15:373–8.
20. Gupta N, Madapura MP, Bhat UA, Rao MR. Mapping of post-translational modifications of transition proteins TP1 and TP2 and identification of protein arginine methyltransferase 4 and lysine methyltransferase 7 as methyltransferase for TP2. J Biol Chem. 2015;290:12101–22.
21. Mishra LN, Gupta N, Rao SM. Mapping of post-translational modifications of spermatid-specific linker histone H1-like protein, HILS1. J Proteomics. 2015;128:218–30.
22. Neale MJ, Pan J, Keeney S. Endonucleolytic processing of covalent protein-linked DNA double-strand breaks. Nature. 2005;436:1053–7.
23. Boateng KA, Bellani MA, Gregoretti IV, Pratto F, Camerini-Otero RD. Homologous pairing preceding SPO11 mediated double-strand breaks in mice. Dev Cell. 2013;24:196–205.
24. Chen BP, Murphy M, Kurimasa A, Chen DJ. ATM phosphorylates histone H2AX in response to DNA double-strand breaks. J Biol Chem. 2001;276:42462–7.
25. Lange J, Pan J, Cole F, Thelen MP, Jasin M, Keeney S. ATM controls meiotic double-strand-break formation. Nature. 2011;479:237–40.
26. Bellani MA, Romanienko PJ, Cairatti DA, Camerini-Otero RD. SPO11 is required for sex-body formation, and Spo11 heterozygosity rescues the prophase arrest of Atm−/− spermatocytes. J Cell Sci. 2005;118:3233–45.
27. Broering TJ, Alavattam KG, Sadreyev RI, Ichijima Y, Kato Y, Hasegawa K, Camerini-Otero RD, Lee JT, Andreassen PR, Namekawa SH. BRCA1 establishes DNA damage signaling and pericentric heterochromatin of the X chromosome in male meiosis. J Cell Biol. 2014;205:663–75.
28. Turner JMA, Aprelikova O, Xu X, Wang R, Kim S, Chandramouli GVR, Barrett JC, Burgoyne PS, Deng C. Male meiotic sex chromosome inactivation. Curr Biol. 2004;14:2135–42.
29. Royo H, Prosser H, Ruzankina Y, Mahadevaiah SK, Cloutier JM, Baumann M, Fukuda T, Hoog C, Toth A, de Rooji DG, Bradley A, Brown EJ, Turner JM. ATR acts stage specifically to regulate multiple aspects of mammalian meiotic silencing. Genes Dev. 2013;27:1484–94.
30. Baudat F, Imai Y, de Massy B. Meiotic recombination in mammals: localization and regulation. Nat Rev Genet. 2013;14:794–806.
31. Kauppi L, Barchi M, Baudat F, Romanienko JP, Keeney S, Jasin M. Distinct properties of the XY pseudoautosomal region crucial for male meiosis. Science. 2011;331:916–20.
32. Lange J, Yamada S, Tischfield SE, Pan J, Kim S, Zhu X, Socci ND, Jasin M, Keeney S. The landscape of mouse meiotic double-strand break formation, processing, and repair. Cell. 2016;167:695–708.
33. Turner JMA, Mahadevaiah SK, Fernandez-Capetillo O, Nussenzweig A, Xu X, Deng CX, Burgoyne PS. Silencing of unsynapsed meiotic chromosomes in the mouse. Nat Genet. 2005;37:41–7.
34. Turner JMA. Meiotic sex chromosome inactivation. Development. 2007;134:1823–31.
35. Guillon H, de Massy B. An initiation site for meiotic crossing-over and gene conversion in the mouse. Nat Genet. 2002;32:296–9.
36. Luense LJ, Wang X, Schon SB, Weller AH, Lin Shiao E, Bryant JM, Bartolomei MS, Coutifaris C, Garcia BA, Berger SL. Comprehensive analysis of histone post-translational modifications in mouse and human male germ cells. Epigenet Chromatin. 2016;9:24.
37. Turner BM. Reading signals on the nucleosome with a new nomenclature for modified histones. Nat Struct Mol Biol. 2005;12:110–2.
38. Paull TT, Rogakou EP, Yamazaki V, Kirchgessner CU, Gellert M, Bonner WM. A critical role for histone H2AX in recruitment of repair factors to nuclear foci after DNA damage. Curr Biol. 2000;10:886–95.
39. Park C, Kim K. Apoptotic phosphorylation of histone H3 on Ser-10 by protein kinase Cδ. PLoS ONE. 2012. https://doi.org/10.1371/journal.pone.0044307.
40. Fernandez-Capetillo O, Allis CD, Nussenzweig A. Phosphorylation of histone H2B at DNA double-strand breaks. J Exp Med. 2004;199:1671–7.

41. Chi YH, Cheng LI, Myers T, Ward JM, Williams E, Su Q, Faucette L, Wang JY, Jeang KT. Requirement for Sun1 in the expression of meiotic reproductive genes and piRNA. Development. 2009;136:965–73.
42. Fernandez-Capetillo O, Mahadevaiah SK, Celeste A, Romanienko PJ, Camerini-Otero RD, Bonner WM, Manova K, Burgoyne P, Nussenzweig A. H2AX is required for chromatin remodeling and inactivation of sex chromosomes in male mouse meiosis. Dev Cell. 2003;4:497–508.
43. Lu LY, Xiong Y, Kuang H, Korakavi G, Yu X. Regulation of the DNA damage response on male meiotic sex chromosomes. Nat Commun. 2013. https://doi.org/10.1038/ncomms3105.
44. Grey C, Clément JA, Buard J, Leblanc B, Gut I, Gut M, Duret L, de Massy B. In vivo binding of PRDM9 reveals interactions with noncanonical genomic sites. Genome Res. 2017;27:580–90.
45. Brick K, Smalgulova F, Khil P, Camerini-Otero RD, Petukhova GV. Genetic recombination is directed away from functional genomic elements in mice. Nature. 2012;485:642–5.
46. Tischfield SE, Keeney S. Scale matters: the spatial correlation of yeast meiotic DNA breaks with histone H3 trimethylation is driven largely by independent colocalization at promoters. Cell Cycle. 2012;11:1496–503.
47. Smagulova F, Gregoretti IV, Brick K, Khil P, Camerini-Otero RD, Petukhova GV. Genome-wide analysis reveals features of mouse recombination hotspots. Nature. 2011;472:375–8.
48. Broering TJ, Wang YL, Pandey RN, Hegde RS, Wang SC, Namekawa SH. BAZ1B is dispensable for H2AX phosphorylation on tyrosine 142 during spermatogenesis. Biol Open. 2015;4:873–84.
49. Hasegawa K, Sin HS, Maezawa S, Broering TJ, Kartashov AV, Alavattam KG, Ichijima Y, Zhang F, Bacon WC, Greis KD, Andreassen PR, Barski A, Namekawa SH. SCML2 establishes the male germline epigenome through regulation of histone H2A ubiquitination. Dev Cell. 2015;32:574–88.
50. Maezawa S, Hasegawa K, Alavattam KG, Funakoshi M, Sato T, Barski A, Namekawa SH. SCML2 promotes heterochromatin organization in late spermatogenesis. J Cell Sci. 2018. https://doi.org/10.1242/jcs.217125.
51. van der Heijden GW, Derijck AA, Posfai E, Giele M, Pelczar P, Ramos L, Wansink DG, van der Vlag J, Peters AH, de Boer P. Chromosome-wide nucleosome replacement and H3.3 incorporation during mammalian meiotic sex chromosome inactivation. Nat Genet. 2007;39:251–8.
52. Handel MA. The XY body: a specialized meiotic chromatin domain. Exp Cell Res. 2004;296:57–63.
53. Metzler-Guillemain C, Luciani J, Depetris D, Guichaoua MR, Mattei MG. HP1beta and HP1gamma, but not HP1alpha, decorate the entire XY body during human male meiosis. Chromosome Res. 2003;11:73–81.
54. Richler C, Dhara SK, Wahrman J. Histone macroH2A1.2 is concentrated in the XY compartment of mammalian male meiotic nuclei. Cytogenet Cell Genet. 2000;89:118–20.
55. Shin YH, Choi Y, Erdin SU, Yatsenko SA, Kloc M, Yang F, Wang PJ, Meistrich ML, Rajkovic A. Hormad1 mutation disrupts synaptonemal complex formation, recombination, and chromosome segregation in mammalian meiosis. PLoS Genet. 2010. https://doi.org/10.1371/journal.pgen.1001190.
56. Fukuda T, Daniel K, Wojtasz L, Toth A, Hoog C. A novel mammalian HORMA domain-containing protein, HORMAD1, preferentially associates with unsynapsed meiotic chromosomes. Exp Cell Res. 2010;316:158–71.
57. Turner JM, Burgoyne PS, Singh PB. M31 and macroH2A1.2 colocalise at the pseudoautosomal region during mouse meiosis. J Cell Sci. 2001;114:3367–75.
58. Soboleva TA, Nekrasov M, Pahwa A, Williams R, Huttley GA, Tremethick DJ. A unique H2A histone variant occupies the transcriptional start site of active genes. Nat Struct Mol Biol. 2011;19:25–30.
59. Ollinger R, Alsheimer M, Benavente R. Mammalian protein SCP1 forms synaptonemal complex-like structures in the absence of meiotic chromosomes. Mol Biol Cell. 2005;16:212–7.
60. Meuwissen RLJ, Offenberg HH, Dietrich AJ, Riesewijk A, van Iersel M, Heyting C. A coiled-coil related protein specific for synapsed regions of meiotic prophase chromosomes. EMBO J. 1992;1:5091–100.
61. Offenberg HH, Schalk JA, Meuwissen RL, van Aalderen M, Kester HA, Dietrich AJ, Heyting C. SCP2: a major protein component of the axial elements of synaptonemal complexes of the rat. Nucleic Acids Res. 1998;26:2572–9.
62. Schramm S, Fraune J, Naumann R, Hernandez-Hernandez A, Hoog C, Cooke HJ, Alsheimer M, Benavente R. A novel mouse synaptonemal complex protein is essential for loading of central element proteins, recombination, and fertility. PLoS Genet. 2011. https://doi.org/10.1371/journal.pgen.1002088.
63. Winkel K, Alsheimer M, Öllinger R, Benavente R. Protein SYCP2 provides a link between transverse filaments and lateral elements of mammalian synaptonemal complexes. Chromosoma. 2009;118:259–67.
64. Yang F, De La Fuente R, Leu NA, Baumann C, Mclaughlin KJ, Wang PJ. Mouse SYCP2 is required for synaptonemal complex assembly and chromosomal synapsis during male meiosis. J Cell Biol. 2006;173:497–507.
65. Yuan L, Pelttari J, Brundell E, Bjorkroth B, Zhao J, Liu JG, Brismar H, Daneholt B, Hoog C. The synaptonemal complex protein SCP3 can form multistranded, cross-striated fibers in vivo. J Cell Biol. 1998;142:331–9.
66. Kobayashi W, Hosoya N, Machida S, Miyagawa K, Kurumizaka H. SYCP3 regulates strand invasion activities of RAD51 and DMC1. Genes Cells. 2017;22:799–809.
67. Wang L, Wolgemuth DJ. BET protein BRDT complexes with HDAC1, PRMT5 and TRIM28 and functions in transcriptional repression during spermatogenesis. J Cell Biochem. 2016;117:1429–38.
68. Ausio J, Dong F, van Holde KE. Use of selectively trypsinized nucleosome core particles to analyze the role of the histone 'tails' in the stabilization of the nucleosome. J Mol Biol. 1989;206:451–63.
69. Polach KJ, Lowary PT, Widom J. Effects of core histone tail domains on the equilibrium constants for dynamic DNA site accessibility in nucleosomes. J Mol Biol. 2000;298:211–23.
70. Powers NR, Parvanov ED, Baker CL, Walker M, Petkov PM, Paigen K. The meiotic recombination activator PRDM9 trimethylates both H3K36 and H3K4 at recombination hotspots in vivo. PLoS Genet. 2016;12:1–24.
71. Parra MA, Kerr D, Fahy D, Pouchnik DJ, Wyrick JJ. Deciphering the roles of the histone H2B N-terminal domain in genome-wide transcription. Mol Cell Biol. 2006;26:3842–52.
72. Somyajit K, Basavaraju S, Scully R, Nagaraju G. ATM- and ATR-mediated phosphorylation of XRCC3 regulates DNA double-strand break-induced checkpoint activation and repair. Mol Cell Biol. 2013;33:1830–44.
73. Peters AH, Plug AW, van Vugt MJ, de Boer P. A drying-down technique for the spreading of mammalian meiocytes from the male and female germline. Chromosome Res. 1997;5:66–8.
74. Parvanov ED, Tian H, Billings T, Saxl RL, Spruce C, Aithal R, Krejci L, Paigen K, Petkov PM. PRDM9 interactions with other proteins provide a link between recombination hotspots and the chromosomal axis in meiosis. Mol Biol Cell. 2017;28:488–99.
75. Dunn KW, Kamocka MM, McDonald JH. A practical guide to evaluating colocalization in biological microscopy. Am J Physiol Cell Physiol. 2011;300:723-742
76. Langmead B, Salzberg SL. Fast gapped-read alignment with Bowtie2. Nat Methods. 2012;9:357–60.
77. Xu S, Grullon S, Ge K, Peng W. Spatial clustering of identification of ChIP-enriched regions (SICER) to map regions of histone methylation patterns in embryonic stem cells. Methods Mol Biol. 2014;1150:97–111.
78. Shen L, Shao N, Liu X, Nestler E. ngs.plot: quick mining and visualization of next-generation sequencing data by integrating genomic databases. BMC Genomics. 2014;15:284.
79. Shevchenko A, Wilm M, Vorm O, Mann M. Mass spectrometric sequencing of proteins from silver-stained polyacrylamide gels. Anal Chem. 1996;68:850–8.
80. Peng J, Gygi SP. Proteomics: the move to mixtures. J Mass Spectrom. 2001;36:1083–91.
81. Eng JK, McCormack AL, Yates JR. An approach to correlate tandem mass spectral data of peptides with amino acid sequences in a protein database. J Am Soc Mass Spectrom. 1994;5:976–89.

Publisher's Note